NEW MATERIALS FOR IMPROVED COMPETITIVENESS OF FB PLANTS USING RENEWABLE FUELS

RAPPORT 2023:931

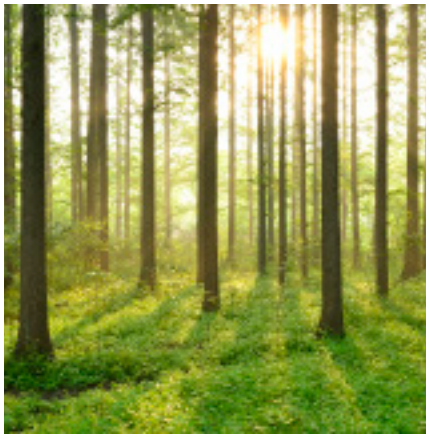

KME
CONSORTIUM MATERIALS TECHNOLOGY
for thermal energy processes

Energiforsk

New materials and Oxygen Carrier Aided Combustion for improved competitiveness of FB plants using renewable fuels

HAMPUS LINDMARK, FREDRIK LIND, JESPER LISKE, MARIA DOLORES PAZ, LAURA RIOJA-MONLLOR, BERTIL WAHLUND, ANNA JONASSON, JOHANNA NOCKERT, MATTI HAUTAKANGAS, HANS LARSSON, KYÖSTI VÄNSKÄ & VESNA BARISIC

ISBN 978-91-7673-931-0 | © Energiforsk March 2023
Energiforsk AB | Phone: 08-677 25 30 | E-mail: kontakt@energiforsk.se | www.energiforsk.se

Foreword

The project has been performed within the framework of the materials technology research programme KME, Consortium materials technology for thermal energy processes, period 2018-2023. The consortium is at the forefront of developing material technology to create maximum efficiency for energy conversion of renewable fuels and waste.

KME was established 1997 and is a multi-cliental group of companies over the entire value chain, including stakeholders from the material producers, manufacturers of systems and components for energy conversion and energy industry (utilities), that are interested in materials technology research. The consortium is managed by Energiforsk.

The program activities are characterized by long term industry and demand driven research and contribute to the development of thermal energy processes for efficient utilization of renewable fuels and waste in power and heat production. The KME goals are to bring about cost-effective materials solutions for increased availability and power production, improved fuel flexibility and improved operating flexibility, with low environmental impact.

The specific project has focused on corrosion and erosion of heat exchangers and water walls in biomass and waste fired boilers; two problems that today limits boilers availability and fuel flexibility. The project aims to decrease the corrosion attack of the water walls and the fluidized bed heat exchangers in waste fired CFB boilers through improved corrosion resistance of the materials and mitigation of the corrosive/erosive environment by changing the bed material or by optimized boiler design. Maria Dolores Paz, Chalmers, has been the project leader. Hampus Lindmark, Fredrik Lind, Jesper Liske & Maria Dolores Paz, Chalmers, Laura Rioja-Monllor, Alleima, Bertil Wahlund, Energiforsk, Anna Jonasson, E.ON, Johanna Nockert, Kanthal, Matti Huhtakangas, MH Engineering, Hans Larsson, Stockholm Exergi, and Kyösti Vänskä & Vesna Barisic, Sumitomo SHI FW Energia have been project members and co-authors of the report. The industry has participated in the project through own investment (60 %) and the Swedish Energy Agency has financed the academic partners (40 %).

Energiforsk would like to thank all the participants for a well performed project.

Bertil Wahlund, Energiforsk

These are the results and conclusions of a project, which is part of a research programme run by Energiforsk. The authors are responsible for the content.

Summary

The use of biomass and waste as fuel for power plants as well as combined heat and power plants (so called CHPs) has steadily been increasing in the last decades. The reason for this increase is primarily environmental, the net emission of CO_2 is considerably less for renewable fuels, such as biomass and waste, compared to fossil fuels, such as e.g., coal. In Sweden, the increase in the use of renewable fuels was achieved by the introduction of a CO_2-tax targeting the combustion of fossil fuels. As consequence, the share of renewable fuels in heat and power production is much higher in Sweden compared to the rest of the world. In fact, the share of renewable fuels in heat and power production is about 65-70% in Sweden. However, despite the positive effects on decreasing CO_2 emissions by renewable fuels, the use of fossil fuels in these plants is still indisputably the primary fuel choice worldwide.

Thus, to increase the share of renewable fuels, at the expense of fossil fuels, the competitiveness needs to increase for power plants and CHPs using renewable fuels. Without using (governmental, EU, etc.) substitutes, there is in practice only three different routes towards obtaining this goal:

- Increase the revenue by increasing the efficiency of heat and power production (e.g., increased electrical efficiency).
- Decrease the costs by using cheaper (but usually more corrosive) fuels.
- Decrease the costs by minimizing maintenance of the plant.

Furthermore, these three routes are usually interlinked and will affect each other. Today renewable fuels may compete in the second route (i.e., fuel costs), depending of course on the quality of the fuel. However, if comparing the other two routes affecting the overall plant economy, using renewable fuels instead of fossil fuels, the more climate neutral fuels come out short. The state of the art of coal fired boilers has today an electrical efficiency up to 45 % whereas the best biomass fired boiler is up to 40 % (using virgin and clean biomass).

In CHPs, the total efficiency is high, around 90 %, this is since the heat produced is used and should also be taken into account. However, in countries where the need for heat is low, electrical efficiency is of greater importance. In addition to a decrease in electrical efficiency, the plants using renewable fuels also exhibit higher maintenance costs compared to fossil fueled plants. One of the reasons for this is the much higher corrosion rate of e.g., superheater tubes and water walls in plants using renewable fuels. This leads to both planned and unplanned revision stops where these tubes need to be replaced. These stops are very costly as it leads not only to an increase in direct costs (e.g., replacing tubes, building scaffolding, etc.) but also to the loss of revenue. This is particularly devastating if the plant owner is forced to stop the boiler during cold periods, when the demand for heat and power is normally at its highest.

This project addresses two problem areas related to material wastage that today limits availability and fuel flexibility of biomass and waste fired power plants, corrosion/erosion of heat exchangers and water walls. The overall goal of the project is to improve the economy of CHP plants using renewable fuels and thereby increase the competitiveness towards fossil fueled plants by targeting these two problem areas in the (fluidized bed) boilers. The project will utilize a two-pronged approach towards decreasing the extent of the corrosion attack of the water walls and the fluidized bed heat exchangers (FBHE) in waste fired CFB boilers:

1. Improving the corrosion resistance of the materials
2. Mitigating the corrosive/erosive environment by changing the bed material or by optimized boiler design.

The project has successfully conducted several corrosion tests in two commercially operated boilers; the waste-fired P15 boiler at Händelö and the waste-fired P6 boiler in Högdalen. The corrosion tests were carried out at two different positions in the boiler; the water wall region and the fluidized bed heat exchanger region. The water wall tests were carried out in the P6 boiler in Högdalen and lasted for 1 week while the fluidized bed heat exchanger tests were carried out both in Högdalen and Händelö with an exposure time ranging from 6 to 24 months. A wide range of materials, ranging from low alloyed steels, austenitic stainless steels, Ni-base alloys, FeCrAl alloys and different coating techniques including overlay weld materials has been investigated. The following conclusions can be made from the findings:

Water wall exposures:

- Oxide formation was only observed for the low alloyed steel (16Mo3) after 1 week of exposure in the water wall region of the waste fired P6 boiler in Högdalen. High concentration of chlorine was observed close to the metal/oxide interface suggesting the formation of metal chlorides which is attributed to the rapid oxidation of the material.
- Neither Ni-base steel nor stainless steel showed any indication of material degradation, and no accumulation of Cl was observed at the metal/deposit interface for these samples.
- Both conventional and newly developed FeCrAl alloy showed promising results as their performance was on par with the Ni-base and stainless-steel samples.

Fluidized bed heat exchangers:

- The newly developed FeCrAl EF101 showed the most promising results after 12 and 24 months of exposure in Händelö and Högdalen, respectively, obtaining a material loss significantly lower than conventional stainless steels and Ni-base alloys.
- Nitridation zones were observed on all FeCrAl alloys regardless of boiler type with the following severity ranked: APMT > EF100 > EF101. It is not known how nitridation affects corrosion behavior. In the present project the material presented an increase of thickness of the nitridated zone without an increase in the material loss, so it is unclear how nitridation affects corrosion in this particular application or if it affects at all.
- EF101 WOL is the most promising material from the overlay weld samples at Händelö. It performs better than all the other coatings exposed for 6 months. It performs better than the EF101 bulk material for the same exposure time. No sample could be recovered from the P15 boiler in Händelö after 12-month exposure.
- The most promising material from the austenitic stainless-steel block is the alloy SX. It experienced the lowest material loss regardless of boiler type and time. A Si-rich/Cr-rich oxide was observed in the grain boundaries at the corrosion front of the material. It is suggested that Si oxide may improve the resistance towards both corrosion and erosion mechanisms.
- Both HVAF and CorEr coating failed after 12 months of exposure regardless of boiler type. The oxide formation on the underlaying bulk material indicates that the failure occurred at an early stage of the exposure.

Goal fulfillment

This project addresses two problem areas related to material wastage that today limits availability and fuel flexibility of biomass and waste fired power plants, namely corrosion/erosion of heat exchangers and water walls. Below the different goals are specified in detail and if the goal has been reached or not.

- **Reduce the total cost of water walls and/or fluidized bed superheaters by enabling new materials and/or by mitigating the corrosive environment by changing bed material or optimized design. The total cost can be reduced by improving the material lifetime or by lowering the cost.**

This project aimed at improving the plant economy for plants using renewable fuels and thereby increasing the competitiveness towards fossil fueled plants by targeting areas in the plants where material issues are of concern. A key parameter in increasing the plant economy is to decrease the maintenance cost. The replacement of failing heat exchanger materials inside the plant is a larger contributor to the maintenance costs. By optimizing the materials, in such a way that the most cost-effective materials are used, the overall maintenance can be decreased. We have performed a substantial number of material testing campaigns

including a wide palette of materials for two positions in the boiler, which has high degradation rates when burning challenging fuels, namely water walls and fluidized bed superheaters. From a material perspective, almost 20 types of material including low alloyed steels, stainless steels, nickel-based alloys and FeCrAl alloys have been investigated. Furthermore, the material selection has included both commercial alloys and newly developed alloys, in the form of bulk material as well as weld overlay coatings and metallic spray coatings.

The main aim of this goal has been to provide reliable data on the material performance of the abovementioned materials and thereby enable more accurate cost calculations to be done by the industry. As such, the material selection of boiler components can be optimized, and the maintenance cost be decreased. The exact cost of the materials is unfortunately not open to the public and furthermore, the material cost is changing constantly due to the price of alloying elements, etc. However, in order to provide an estimate about the cost difference between different materials (which is fairly stable over time), Table 15 and Table 16 was provided in chapter 5 "Analysis of the results". Hereby, the reader can get a rough idea about the material cost, which can be combined with their performance.

This goal is considered as fulfilled.

- **Increase the knowledge of material degradation mechanisms and environmental parameters at play in fluidized bed superheaters.**

Overall, the large exposure matrix together with a wide and in-depth microstructural analysis had provided the material community with valuable information relevant for corrosion performance. This for two positions in the power plants that today are subject to high material wastage rates.

For the FBHE tubes, there was a special interest in deducing if the material wastage was primarily driven by erosion or by corrosion. The collective analysis of all the clamp samples that have been exposed on top of the tubes within the FBHE section indicates that it is a combination of erosive and corrosive forces that causes the degradation. In many cases, the samples were covered by a deposit, which suggests that erosive forces have been mild. In other cases, the deposit layer was minimal or non-existent leading to the conclusion that erosive forces were at play. Furthermore, it is probable that corrosion and erosion influence each other synergistically, leading to higher material wastages. The results showed signs of steel grain boundary attacks (on several occasions in combination with the presence of Cl) and it is expected that a material suffering from steel GB attack is also more susceptible to erosion.

This goal is considered as fulfilled.

- **Investigate the properties of newly developed alloys together with commercially available materials for water walls. Both thermal spray coating and overlay welding will be investigated.**

As above, the material matrix executed in the exposures has been wide, covering both materials that are used today and newly developed steels, FeCrAls and coatings. The corrosion analysis has primarily been performed by means of

material loss determination and cross-sectional SEM/EDX analysis. Special focus has been put towards the newly developed materials (EF100 and EF101) in order to investigate their potential use for both water walls and for tubes to be used as FBHE material. The results show that the newly developed FeCrAl alloys (EF100 and EF101) are potential candidates as boiler materials, taking a corrosion/erosion perspective. However, both these types of materials suffered from nitridation, which needs to be further studied. It is not clear how the nitridation process affects the corrosion performance on a longer perspective than one year. Furthermore, as these materials are not classed as pressure bearing materials, they cannot be used as monotubes. Instead, their initial use would be as corrosion/erosion resistant coatings and/or co-extruded tubes. The new insights in the performance of these alloys were presented in a journal article.

This goal is considered as fulfilled.

- **Publish 1 scientific article, present the results at two conferences and complete two academic theses within the project.**

Within this project the following have been achieved within the sub-goals:

Publish 1 scientific article

- **A material degradation study of novel FeCrAl alloys, stainless steels and nickel base alloy in fluidized bed heat exchangers of a waste fired CFB boiler**
  Hampus Lindmark, Julien Phother, Maria Dolores Paz Olausson, Johanna Nockert, Fredrik Lind, Anna Jonasson, Vesna Barišić, Kyösti Vänskä, Laura Rioja-Monllor and Jesper Liske

  Fuel 338, 127299, 2023

Present the results at two conferences

- **Investigating the performance of novel FeCrAl alloys in a fluidized bed heat exchanger application of a waste fired CFB boiler**
  Hampus Lindmark, Julien Phother, Maria Dolores Paz Olausson, Johanna Nockert, Fredrik Lind, Anna Jonasson, Vesna Barišić, Kyösti Vänskä, Laura Rioja-Monllor and Jesper Liske

  Oral presentation at the 24th Fluidized bed conversion conference, FBC-24, May 2022, Gothenburg Sweden

- **HTC/KME conference 2019**
  KME 803: New materials and Oxygen Carrier Aided Combustion for improved competitiveness of FB plants using renewable fuels

  Oral presentation by Julien Phother and Jesper Liske, Gothenburg 12-13 March 2019

- **HTC/KME conference 2020**
  KME 803: New materials and Oxygen Carrier Aided Combustion for improved competitiveness of FB plants using renewable fuels

Oral presentation by Julien Phother and Jesper Liske, Digital conference, 4-5 November 2020

- **KME conference/workshop (planned 6th March 2023)**
  KME 803: New materials and Oxygen Carrier Aided Combustion for improved competitiveness of FB plants using renewable fuels

  Oral presentation by Hampus Lindmark and Maria Dolores Paz

Complete two academic theses

- **Julien Phother Ph.D. thesis**
  High Temperature Corrosion Behavior in Biomass- and Waste-Fired Boilers - Insights into catastrophic corrosion and corrosion mitigation techniques
  Ph. D. thesis, Chalmers, 2020

- **Hampus Lindmark, Licentiate thesis**
  Title to be decided
  Lic. Thesis planned for fall 2023

This goal is considered as fulfilled. This includes a planned licentiate thesis to be presented in the fall 2023, based on the results and conclusions obtained within this project. The other subgoals (publishing one journal article and two conference presentations) are reached within the project's timeframe.

Keywords

New materials, EF100, EF101, Biomass and Waste combustion, High Temperature corrosion, Water wall corrosion and FBHE corrosion.

Sammanfattning

Användningen av biomassa och avfall som bränsle, framför fossil olja och kol, för kraftverk och kraftvärmeverk (så kallade CHP) har stadigt ökat de senaste decennierna. Anledningen till denna ökning är främst miljömässig, nettoutsläppet av CO_2 är betydligt lägre för förnybara bränslen, som biomassa och avfall, jämfört med fossila bränslen, såsom kol. Trots de positiva effekterna på minskande CO_2-utsläpp från förnybara bränslen är användningen av fossila bränslen i dessa anläggningar fortfarande det primära bränslevalet, sett globalt.

För att öka andelen förnybara bränslen, på bekostnad av fossila bränslen, måste konkurrenskraften öka för kraftverk och kraftvärmeverk som använder förnybara bränslen. I praktiken, kan detta nås genom någon av följande tre spår:

- Öka intäkterna genom att öka effektiviteten i värme- och kraftproduktionen (t.ex. ökad elproduktion).
- Minska kostnaderna genom att använda billigare (men vanligtvis mer korrosiva) bränslen.
- Minska kostnaderna genom att minimera underhållskostnaden av anläggningen.

Detta projekt adresserar två problemområden relaterade till materialslitage som idag begränsar tillgängligheten och bränsleflexibiliteten för biomassabaserade och avfallsvärmeverk: korrosion/erosion av värmeväxlare och vattenväggar. Det övergripande målet med projektet är att förbättra ekonomin i kraftvärmeverk som använder förnybara bränslen och därigenom öka konkurrenskraften gentemot anläggningar som använder fossila bränslen genom att ta itu med dessa två problemområden i (fluidiserade) pannor. Projektet kommer att använda en tvådelad strategi för att minska omfattningen av korrosionsattacken på vattenväggarna och sandlåsvärmeväxlarna i avfallseldade FB-pannor:

1. Förbättra korrosionsbeständigheten hos materialen.
2. Minska den korrosiva/erosiva miljön genom att ändra bäddmaterialet eller genom optimerad pannkonstruktion.

Projektet har framgångsrikt genomfört flera korrosionstester i två kommersiella pannor; den avfallseldade P15-pannan i Händelö och den avfallseldade P6-pannan i Högdalen. Korrosionstesterna utfördes på två olika positioner i pannan; vattenväggar och sandlåsöverhettare. Ett brett spektrum av material, från låglegerade stål, austenitiska rostfria stål, Ni-baslegeringar, FeCrAl-legeringar och olika beläggningstekniker inklusive påläggssvetsade material har undersökts. Följande slutsatser kan dras från resultaten:

Vattenväggsexponeringar:

- Oxidbildning observerades endast för det låglegerade stålet (16Mo3) efter 1 veckas exponering i vattenmantelområdet i den avfallseldade P6-pannan i Högdalen. Höga halter av klor observerades nära metall/oxidgränssnittet vilket antyder bildning av metallklorider som tillskrivs den snabba oxidationen av materialet.
- Varken Ni-bas legeringar eller rostfritt stål visade någon indikation på materialavvverkning, och ingen ansamling av Cl observerades vid metall/beläggningsgränssnittet för dessa prover.
- Både konventionella samt nyutvecklade FeCrAl-legeringar visade lovande resultat eftersom deras prestanda var i paritet med Ni-bas och rostfria stålprover.

Exponeringar i sandlåsöverhettare:

- Det nyutvecklade FeCrAl EF101 visade de mest lovande resultaten efter 12 och 24 månaders exponering i Händelö respektive Högdalen, och erhöll en materilavverkning som var betydligt lägre än konventionella rostfria stål och Ni-baserade legeringar.
- Nitrideringszoner observerades på alla FeCrAl-legeringar oavsett pannans typ, med följande allvarlighetsgrad: APMT > EF100 > EF101. Det är okänt hur nitrideringen påverkar korrosionsbeteendet. I detta projekt ökade tjockleken på nitrideringszonen utan att det uppstod någon ökning av materialförlusten, så det är oklart hur nitrideringen påverkar korrosionen i denna specifika tillämpning eller om den alls påverkar.
- EF101 WOL är det mest lovande materialet av de påläggssvetsade proverna i Händelö. Det presterade bättre än alla andra beläggningar som exponerades i 6 månader och bättre än EF101 som bulkmaterial vid samma exponeringstid.
- Det mest lovande materialet från den austenitiska rostfria stålklassen är legeringen SX. Den hade den lägsta materialförlusten oavsett panntyp och exponeringstid. En Si-rik/Cr-rik oxid observerades i korngränserna vid materialets korrosionsfront. Det föreslås att Si-oxid kan förbättra motståndet mot både korrosions- och erosionsmekanismer.
- Både HVAF- och CorEr-beläggningarna försvann efter 12 månaders exponering oavsett pannans typ. Oxidbildning på det underliggande bulkmaterialet indikerar att beläggningarna försvann i en tidig fas av exponeringen.

List of content

1 Introduction 14
1.1 Motivation 14
1.2 Background 14
1.3 Aim of the project 16
1.4 Project plan 17
1.5 Project organisation 19
2 Description of the plants 20
2.1 P6 Högdalen 20
2.1.1 Design 20
2.1.2 Fuel 21
2.1.3 Steam system 23
2.2 P15 Händelöverket 24
2.2.1 Design 24
2.2.2 Fuel 26
2.2.3 Water/steam system 27
3 Materials 28
3.1 Description of materials 28
3.2 Description of the exposures 31
3.2.1 Clamp samples on FBHE in Händelö P15 and Högdalen P6 31
3.2.2 Furnace water wall probe samples in Högdalen P6 37
3.2.3 Thermal sprayed coatings on the water walls in Händelö P15 38
3.3 Analytical techniques 40
3.3.1 Material loss 40
3.3.2 Scanning Electron Microscopy/Energy Dispersive X-Rays (SEM/EDX) 40
4 Results 41
4.1 Water wall exposures Högdalen P6 waste-fired boiler 41
4.2 Metal sprayed coatings on water walls in Händelö P15 45
4.3 Material loss and microstructural analysis on FBHE 46
4.3.1 Clamp exposures on FBHE - Högdalen P6 46
4.3.2 Clamp exposures on FBHE - Händelö P15 72
5 Analysis of the results 94
5.1 WP1- Water wall corrosion testing 95
5.2 WP2- Material performance in fluidized bed heat exchangers 97
5.3 Review of potential corrosion issues using OCAC 107
6 Goal fulfillment 110
7 Summary and conclusions 113
8 References 115
9 Appendix: LITERATURE Review 119

1 Introduction

1.1 MOTIVATION

This project addresses the corrosion and erosion of fluidized bed heat exchangers (FBHE) and water-wall tube panels that currently limit the availability and fuel flexibility of biomass and waste fired power plants. As the fuel quality shifts from clean, virgin biomass towards cheaper and "dirtier" biomass fractions and waste-derived fuels, the material wastage of boiler tubes becomes increasingly severe, requiring more expensive design and operational solutions.

Even though the fluidized bed heat exchangers are constructed of highly alloyed steels, the corrosion rate with waste-derived fuels causes frequent tube replacements. Simultaneously, mitigating material wastage of evaporative surfaces requires several boiler tube protection options, such as coatings, weld overlays and the use of extended lining of critical components by refractories. By addressing these material issues, we help increase the fuel flexibility, availability, and reliability of these plants, thereby making plants firing green fuels and waste more competitive, compared to e.g., boilers using fossil fuel.

This approach may also be used to increase the steam data and thereby also the electrical efficiency of these types of plants. The two-pronged approach is consisting of both, seeking solutions towards mitigating the material degradation by development of more corrosion resistant materials and decreasing the corrosiveness of the loop seal environment through e.g., new boiler designs and/or operating solutions, e.g., changing the bed material. Regardless of method, both will be based on a knowledge driven approach. The work needed within the project in order to reach the project goals will be divided into several work packages (WPs).

1.2 BACKGROUND

The use of biomass and waste as fuel for power plants as well as combined heat and power plants (so called CHPs) has steadily been increasing in the last decades. The reason for this increase is primarily environmental, the net emission of CO2 is considerably less for renewable fuels, such as biomass and waste, compared to fossil fuels, such as e.g., coal. In Sweden, the increase in the use of renewable fuels was achieved by the introduction of a CO2-tax targeting the combustion of fossil fuels. As consequence, the share of renewable fuels in heat and power production is much higher in Sweden compared to the rest of the world. In fact, the share of renewable fuels in heat and power production is about 65-70% in Sweden. However, despite the positive effects on decreasing CO2 emissions by renewable fuels, the use of fossil fuels in these plants is still indisputably the primary fuel choice worldwide. The share of fossil fuels in heat and power production in the world is about 70-75%. The reason for this is primarily economical, it is today cheaper to produce power and heat using fossil fuels rather than with renewable fuels.

Thus, to increase the share of renewable fuels, at the expense of fossil fuels, the competitiveness needs to increase for power plants and CHPs using renewable fuels. Without using (governmental, EU, etc.) substitutes, there is in practice only three different routes towards obtaining this goal:

- Increase the revenue by increasing the efficiency of heat and power production (e.g., increased electrical efficiency).
- Decrease the costs by using cheaper (but usually more corrosive) fuels.
- Decrease the costs by minimizing maintenance of the plant.

Furthermore, these three routes are usually interlinked and will affect each other. For instance, by decreasing the fuel costs the maintenance costs are usually increased due to increased corrosion rates and other fuel related problems. Hence, if the use of renewable fuels in heat and power production should increase globally the sum of all three routes needs to become a more competitive option compared to the sum of these three routes using fossil fuels.

Today renewable fuels may compete in the second route (i.e., fuel costs), depending of course on the quality of the fuel. For example, virgin (clean) biomass is rather expensive compared to waste (which even could have a negative cost) and ditto for different qualities of coal. However, if comparing the other two routes affecting the overall plant economy, using renewable fuels instead of fossil fuels, the more climate neutral fuels come out short. The state of the art of coal fired boilers has today an electrical efficiency up to 45 % whereas the best biomass fired boiler is up to 40 % (using virgin and clean biomass).

However, if using cheaper biomass sources (e.g., agricultural residues) or waste as fuel the electrical efficiency is only around 30-35 %. In CHPs the total efficiency is high, around 90 %, this since the heat produced is used and should also be taken into account. However, in countries where the need for heat is low, electrical efficiency is of greater importance. In addition to a decrease in electrical efficiency, the plants using renewable fuels also exhibit higher maintenance costs compared to fossil fueled plants. One of the reasons for this is the much higher corrosion rate of e.g., superheater tubes and water walls in plants using renewable fuels. This leads to both planned and unplanned revision stops where these tubes need to be replaced. These stops are very costly as it leads not only to an increase in direct costs (e.g., replacing tubes, building scaffolding, etc.) but also to the loss of revenue. This is particularly devastating if the plant owner is forced to stop the boiler during cold periods, when the demand for heat and power is normally at its highest.

In order to decrease the corrosion rate of the SH tubes in the boilers using renewable fuels, the steam temperature, and thereby also the superheater material temperature, has been decreased. The consequence of this decrease is that the electrical efficiency is lower for boilers using renewable fuels compared to fossil fueled plants. An attempt to increase the electrical efficiency and/or to reduce maintenance costs in fluidized bed boilers using renewable fuels has been to move the final superheating of the steam from the corrosive flue gas to the loop seal of the return leg of the cyclones. By installing a FBHE the aim is to increase the steam

temperature without having the correlated corrosion attack associated with the corrosive flue gas environment. Modern waste/biomass fired CFB boilers are equipped with fluidized bed heat exchangers. However, for some fractions of waste fuels, the corrosion rate is much higher than anticipated. The use of more highly alloyed steels has not seemed to decrease the extent of the problem, the material wastage rate is still unacceptably high. The fluidized bed heat exchangers are in some cases replaced every second year.

The combinatory effect of both corrosion and erosion is particularly detrimental and today's material is not suited to withstand that type of attack. Hence, there is a need for the development of new materials that exhibit improved resilience towards this type of environment. This becomes especially true with the current trend of an increased diversity in the fuel mix, towards more corrosive (cheaper) fuels. The improvement of the materials may be in the form of coatings, weld overlays as well as newly developed alloys, which can be in the form of mono- or compound tubes.

Another area of interest, having potential positive economical outcome, is the water walls of boilers using renewable fuels. Today, a common practice to maintain the availability of the boilers is to coat or overlay weld large water wall areas with nickel base alloys. This type of material has become standard in industry today and it is not unusual that several hundred square meters of water walls with weld overlay are installed in a boiler. However, nickel base materials are usually associated with a high cost, leading to high capital and maintenance costs. If less expensive materials or materials with a higher corrosion resistance can be deployed instead of these nickel-based alloys, the overall plant economy of boilers burning renewable fuels can be improved.

1.3 AIM OF THE PROJECT

The overall goal of the project is to improve the plant economy of power plants and CHPs using renewable fuels and thereby increase the competitiveness towards fossil fueled power plants and CHPs. This is done by targeting two problem areas in the (fluidized bed) boilers: water wall corrosion and fluidized bed heat exchanger corrosion/erosion. The project aimed at utilizing a two-pronged approach towards decreasing the extent of the corrosion attack of the water walls and the fluidized bed heat exchangers in waste fired CFB boilers:

- Improving the corrosion resistance of the materials used.
- Mitigating the corrosive/erosive environment by changing the bed material or optimized design.

The main focus in the project has been topic (1) by deploying a wide range of investigated materials together with newly developed alloys. Due to commercial considerations outside the scope of this project, (2) has mainly been focused on theoretical considerations rather than experimental testing. This, as the planned change of bed material (from sand to Ilmenite) in these boilers was postponed.

Project goals:

The overall project goal, to improve plant economy of power plants and CHPs using renewable fuels, was divided into several individual topics aiming at generating new knowledge and industrial experience:

- Decrease the overall cost of water walls and/or fluidized bed heat exchangers by enabling new materials and/or by mitigating the corrosive environment by changing the bed material or optimized design. The overall cost can be decreased either by improving the material lifetime or by decreasing the material cost.
- Increase the knowledge of what type of material degradation mechanisms as well as environmental parameters are at play in fluidized bed heat exchangers.
- Investigate the performance of newly developed steels and alloys together with commercially available materials for water walls.
- This project will collaborate with other biokraft project(s) in order to facilitate synergistic effects between the projects.
- Academic goals: 2 academic theses; 1 journal article and 2 conference proceedings

1.4 PROJECT PLAN

The project consisted of two major work packages, one directed towards water wall corrosion and the other directed towards FBHE corrosion/erosion. In both work packages (WP1 and WP2), exposures have been performed in two boilers. In addition, a separate work package (WP0) was initiated towards the methodology development and planning of the full-scale tests. Within this WP, the development of procedures and experimental techniques has been discussed and investigated for both FBHE exposures as well as water wall probe exposures. Below, these three work packages are presented in a more detailed manner.

WP0 – Methodology development work package

This WP is aimed at methodology development and planning of full-scale tests. In the two work packages directed towards water walls (WP1) and fluidized bed heat exchangers (WP2), respectively, some methodology development was needed in order for the exposures to proceed in a safe manner. The fluidized bed heat exchanger is, as compared to more "traditional" superheaters situated in the flue gas stream, much less investigated. The environment for the FBHE in the loop seal area is also fundamentally different compared to the environment in the flue gas stream. Within this WP, different exposures techniques (e.g., probes, tube exchange and clamps) have been assessed by the project group and discussed with safety and risk in mind. Furthermore, this WP have also spent time and resources in order to investigate the possibility to change the bed material from silica sand to a bed material with oxygen carrier capabilities (e.g., ilmenite). Since these types of

tests are very costly and, as with everything new, deemed risky, the planned test with OCAC needed to be performed on commercial grounds. Discussions and planning have also been performed in collaboration with other Biokraft-projects. Unfortunately, the planned OCAC exposures were not performed, due to delays from the covid pandemic which resulted in a change in commercial plans. Instead, the focus of the OCAC related work within this project (and this WP) shifted towards a performing a literature study focusing on OCAC in general and its potential effect on material performance of construction materials in the plant.

WP1 – Water wall corrosion work package

This WP has been directed towards investigations of material performance of water walls in waste fired boilers. Within WP0, the planning has been performed whereas within WP1, the actual exposures, analysis and evaluations have been executed. The water wall corrosion tests have been performed in two different boilers. In the P6 boiler at Högdalen, newly developed water wall corrosion probes have been exposed in short term corrosion tests. The current material installed is overlay welding of Inconel625. The aim is to test commercially available materials as well as newly developed alloys and coatings. For the P15 boiler at Händelö, a test section of the water wall in the empty pass was installed with thermal spray coatings.

WP2 – Fluidized bed heat exchanger corrosion work package

In this work package the corrosion/erosion of the fluidized bed heat exchangers have been investigated. This WP was also deployed in the two boilers mentioned above. Both these boilers are constructed by Sumitomo SHI FW and the FBHE's are similar. The material wastage of the tubes has been especially high at the top tubes of the superheater bundle. Within this WP, a wide range of materials have been exposed as clamp samples sitting on top of the FBHE tubes for up to 2 years. The material performance has been investigated both quantitatively in the form of material loss (mm/year) and qualitatively in the form of cross-sectional SEM/EDX analysis (primarily). The exposure matrix includes a great number of samples and the tested materials included low alloyed steels, stainless steels, nickel-based alloys and FeCrAl alloys. Furthermore, the material selection has included both commercial alloys and newly developed alloys, as well as in the form of bulk material, weld overlay coatings and metallic spray coatings. The main aim with the long-term tests was to map out the extent and reasons behind current material degradation, e.g., if the attack primarily was driven by corrosion or erosion.

1.5 PROJECT ORGANISATION

The project is jointly performed by Energiforsk AB, E.ON Värme Sverige AB/E.ON Energiinfrastruktur AB, Kanthal AB, MH Engineering AB, Alleima , Stockholm Exergi AB, Sumitomo SHI FW Energia Oy and HTC at Chalmers University of Technology. The distribution of work was:

Table 1. Participating partners in the project.

Part	Participants role in the project
Energiforsk AB	Responsible for results dissemination, collaboration and continuous knowledge exchange between the academia and the industry stakeholders.
E.ON Energiinfrastruktur AB	Responsible for boiler operation, fuel & gas analysis and collecting other operational data
Kanthal AB	Providing materials, including newly developed model alloys
MH Engineering AB	Providing coating materials
Alleima	Providing materials, including newly developed model alloys
Stockholm Exergi AB	Responsible for boiler operation, fuel & gas analysis and collecting other operational data
Sumitomo SHI FW Energia Oy	Responsible for sample installations, corrosion probe exposures and will also perform some corrosion evaluation and analysis
Chalmers University Technology AB HTC	Project leader. Responsible for corrosion evaluation and analysis. Responsible for communication/collaboration with other projects.
Chalmers University Technology AB Energy Technology	Responsible for evaluation environmental parameters, especially for OCAC.

The project was financed by the Swedish Energy Agency together with cash and in-kind contributions from the company members of the project. The total project budget was 13 704 kSEK and the project time was 2018-2022.

2 Description of the plants

2.1 P6 HÖGDALEN

2.1.1 Design

Högdalen P6 CFB boiler has been in operation since 2000. It features a compact design with FBHE superheaters. The boiler was designed for the following main steam parameters: 32 kg/s of steam at 60 bar(g) and 480 °C. This gives the plant a capacity of 30 MWe, 90 MWth with steam flow of 115 t/h. The design fuels include RDF, woody biomass, and demolition wood. In addition to the boiler, the plant consists of fuel preparation, steam turbine and a flue gas cleaning. The boiler produces steam, primarily used for production of electricity, industrial process steam and district heating.

The boiler is made up of a water-cooled furnace with two integrated water-cooled separators and two loop seals, followed by FBHE chambers containing the final superheaters. On the gas side the separators are followed by a single pass radiation cavity (middle pass) and a vertical back pass with superheater banks and boiler banks. Finally, before entering the flue gas treatment system the flue gas meets the economizer banks.

The two separators are hot gas separators, which are used for separation of the bed material entrained by the flue gas as it is leaving the furnace at the furnace top. The separated material is returned to the lower part of the furnace via the loop seal and FBHE chamber. Loop seal is designed to prevent flue gas from the furnace entering the separators through the bed material return leg. The FBHE chamber contains a bubbling fluidized bed and is equipped with several air nozzles to ensure material transport. The final superheater is in the FBHE chamber.

The separators are followed by the overall layout of the boiler.

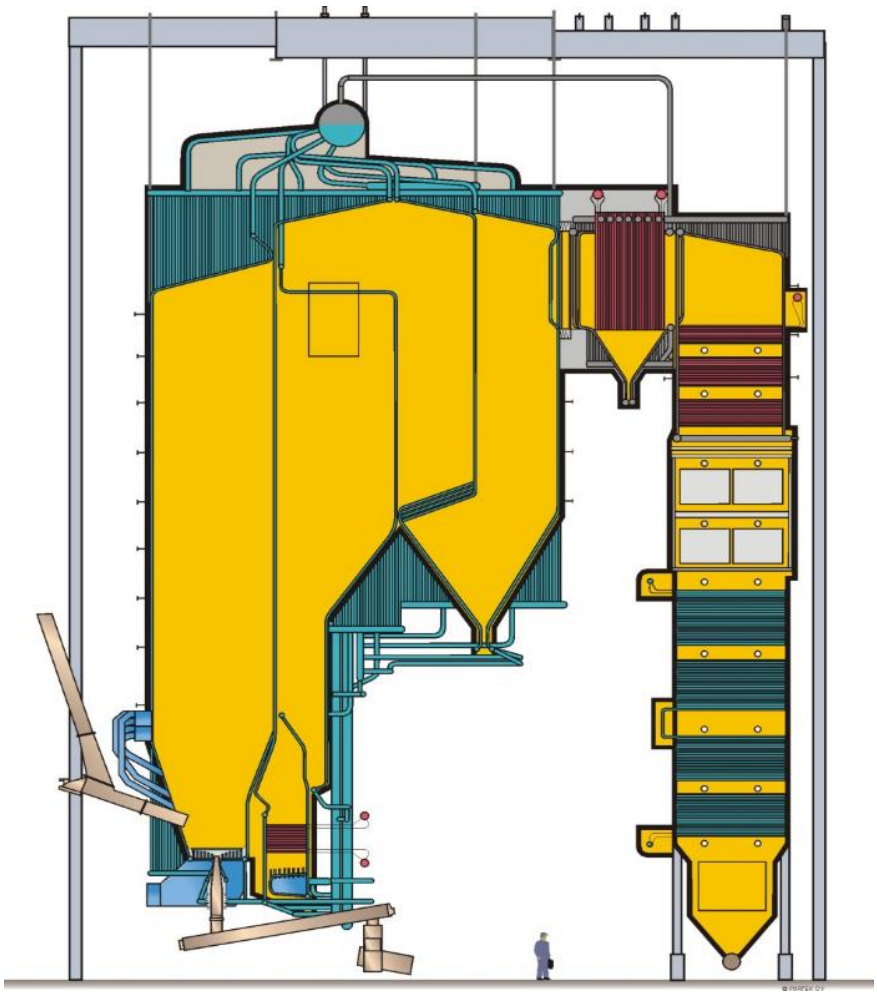

Figure 1. General lay-out of Högdalen P6 boiler.

2.1.2 Fuel

The boiler was originally designed to burn RDF (returbränsle), wood chips, saw dust, bark, wood shavings, wood pellets and briquettes, willow, and rubber chips. The fuel can be fired as a mix of fuels with the maximum fraction of the fuels as shown in Table 2. Fuel specifications are given in Table 3.

Table 2. Design fuel mix for Högdalen P6 boiler

Fuel	RDF	Wood chips	Sawdust	Plywood	Bark	Wood shavings	Pellets	Willow	Rubber chips
Maximum fraction	100 %	100%	40 %	10%	40 %	40%	40%	5%	10%

Table 3. Design fuel properties for Högdalen P6 boiler

Fuel		RDF	Wood chips	Saw dust	Bark	Wood shavings	Pellets
LHV	MJ/kg	13	8.9	8.1	8.6	15.9	17.3
Density	kg/m3	200	250	300	300	110	600
Particle size		100% < 100mm 80% < 80mm 80% > 5 mm	90% < 22 mm	90% < 7 mm	90% < 45 mm	*)	φ6x10-12x30 mm
			50% < 7 mm	50% < 3 mm	50% < 22 mm		
Moisture	%	22	45	50	50	15	8
Ash content	%	10	5	0.5	1	0.5	0.5
C	%	38.8	25	24.8	26.3	42.2	46
H	%	3.9	3	2.9	3.1	5.1	5.4
O	%	24	22	21.7	19.4	37.1	40
N	%	0.5	0.01	0.01	0.1	0.02	0.02
S	%	0.3	0.05	0.05	0.04	0.1	0.1
Cl		0.5**)	-	-	-	-	-

*) Composition can vary based on source; **) Max 0.8%

RDF is further defined in Table 4 and it contains max 0.35% PVC.

Table 4. Description of RDF for Högdalen P6 boiler

Composition	mass-%
Paper *)	< 90
Wood	< 90
Plastic	< 20
Rubber	< 5
Textile	< 5
Other combustible	< 5
Metals	< 5
Other non-combustible	< 10**)
Aluminum, metallic	< 0.25

*) up to 90% of the paper fraction can be made up of paper laminate (plastic coated paper)

**) normally the total non-combustible fraction is below 10% in the fuel

2.1.3 Steam system

The steam system comprises the following equipment:

Superheaters:

Superheater 1, in the flue gas duct before the economizer

Superheater 2, in the flue gas duct before SH1.

Superheater 3A, under the separator

Superheater 3B, next to SH 3A

Steam coolers:

between SH1 and SH2, Steam cooler 1

between SH2 and SH 3A, Steam cooler 2

between SH3A and SH 3B, Steam cooler 3

Superheaters 1 and 2 are in the back-pass while superheaters 3A and 3B are FBHE superheaters.

2.2 P15 HÄNDELÖVERKET

2.2.1 Design

The Händelö P15 CFB boiler is a Waste-to-Energy boiler designed to burn a wide range of fuels, in commercial operation since 2011. It is of a compact design with FBHE super heaters. The boiler was designed for the following main steam parameters: 31 kg/s of steam at 66 bar(g) and 450 °C. This gives the plant a capacity of 30 MWe, 85 MW_{th} with steam flow of 112 t/h. The design fuels include sorted household and industrial waste with biomass, and recycled wood as secondary fuels. In addition to the boiler, the plant consists of fuel preparation, steam turbine and a flue gas cleaning. The boiler produces steam, primarily used for production of electricity, industrial process steam and district heating.

The boiler is made of a water-cooled, refractory lined, furnace with two integrated water-cooled separators and two FBHE superheaters. On the gas side the separators are followed by a single pass radiation cavity (empty pass) and a horizontal convection pass with evaporator and superheater banks. Finally, before entering the flue gas treatment system the flue gas meets the economizer banks.

The two separators are used for separation of the bed material from the flue gas at the furnace top. The separated material is discharged via loop seals into FBHE superheater units and thereafter returned to the lower part of the furnace via FBHE lift legs. Loop seal prevents that flue gas from the furnace enters the separators. The loop seal is a bubbling fluidized bed and is equipped with several air nozzles to ensure material transport.

On the flue gas side, the separators are followed by an empty pass for lowering the flue gas temperature to a temperature, which makes the ash ”dry” and non-sticky to the back pass tube banks. This is to minimize deposit formation and corrosion attacks. The bottom of the empty pass and the horizontal pass are equipped with an ash extraction conveyor system.

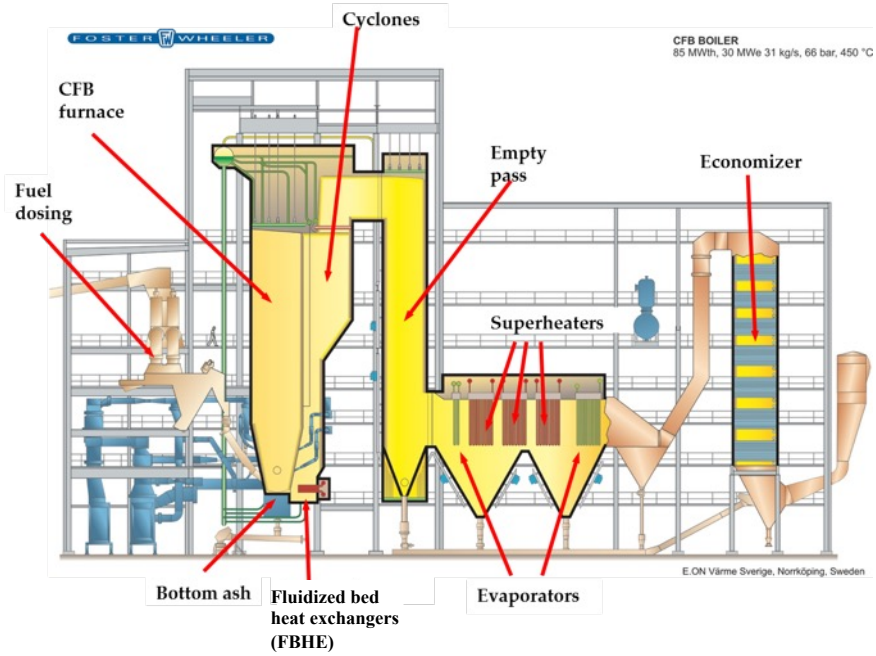

Figure 2. General layout of Händelö P15 boiler.

2.2.2 Fuel

The boiler is designed to burn fuels with specifications given in Table 5, according to ratios given in

Table 6. Table 5

Table 5. Design fuel properties for Händelö P15 (a.r.=as received)

Fuel		Guarantee fuel mixture	Range for guarantee and design fuel mixtures
LHV	MJ/kg	12.9	10.5-16.4
Density	kg/m3	226	150-300
Particle size	90%	-	<100 mm
Moisture	%, a.r.	27	12-37.5
Ash content	%, a.r.	14.3	6.4-16.8
C	%, a.r.	45	35-55
H	%, a.r.	6.1	4-9
0	%, a.r.	28.2	25-45
N	%, a.r.	0.8	0.3-1.2
S	%, a.r.	0.3	0.5
Cl	%, ds	< 0.9	1.0
$Alkali_{total}$	%, ds		<2.0
$Alkali_{weak\ acid\ soluble}$	%, ds		<0.6
Zn	mg/kg, ds	<500	1000
Pb	mg/kg, ds	<90	500

Table 6. Design fuel mix for Händelö P15

Fuel	Sorted and pretreated industrial waste	Sorted and pretreated household waste	Recycled wood
Guarantee Fuel Mixture	60 wt-%	40 wt-%	0 wt-%
Design Fuel Mixture Range	30-100 wt-%	0-70 wt-%	0-20 wt-%

2.2.3 Water/steam system

The water/steam system comprises the following equipment:

1. Water walls
2. Evaporative tube bundle
3. Super heaters:
    a. Superheater 1 (SH1), in the horizontal pass
    b. Superheater 2 (SH2), left FBHE.
    c. Superheater 3 (SH3), right FBHE

3 Materials

3.1 DESCRIPTION OF MATERIALS

A wide material testing matrix has been performed in two boilers designed with a horizontal pass superheater region. The material matrix has included conventional steels used today as well as newly developed stainless steels and FeCrAls and two different types of thermally sprayed coatings, HVOF and HVAF sprayed coatings. Below a short description of the use and benefits of each material type is presented. The complete material matrix of the clamp, tube and probe exposures is presented in 3.2.

The chosen materials are typical for superheaters, carbon steels, low alloyed ferritic steel, austenitic steels and nickel-based alloys. The choice of materials for the superheater depends on the quality of the fuel, placement of the superheater (dependent on the flue gas temperature), material temperature (dependent on the steam temperature), material cost etc. Chromium is often used to increase the corrosion resistance of the steel. Steels with more than 13 % chromium are often referred to as stainless steels. Nickel alloys are also commonly used in order to improve the corrosion resistance of the superheater. The price of low alloy steels may be up to 8 times cheaper than high nickel-based alloys. In Table 15, a rough estimation between the materials and their costs (as well as other information) is shown. The aim is to provide the reader with an estimation of the material costs, although the exact cost of a certain material will vary over time.

The alloys used within this project can be described as:

- **16Mo3, EN10028**

16Mo3 is a pressure vessel grade low alloyed steel for use at elevated working temperatures. The material is used as a weldable steel in boilers as well as steel pressurized vessels found in the oil, gas and chemical industry.

- **316Ti, EN1.4571**

316 is the second most common austenitic stainless steel used in the world with nominal composition 16-chromium, 10-nickel and 2-molybdenum. 316Ti variant is a titanium stabilized version of the high carbon variant 316H, both commonly used in superheaters and reheaters in steam powerplants.

- **347H and 347HFG, EN1.4912 (Alleima® 6R44)**

This is a niobium stabilized austenitic stainless steel, 18-chromium and 10-nickel, used in superheaters in steam powerplants up to 600 °C - 620 °C. The grade also exists in a fine-grained mode, i.e., 347HFG. The fine-grained microstructure is facilitating an increased transport of Cr to the oxide and thereby improves the corrosion properties of the steel.

- **Alleima® Esshete1250, EN1.4982**

This is an austenitic stainless chromium-nickel-manganese 15-9.5-6 steel used in superheaters and reheaters in coal and biomass powerplants. It's allowed for use at metal temperatures up to 650 °C. This alloy is verified in large installations in the UK coal fired power fleet operating at 568 °C superheat and reheat temperatures since the early 70's. Successfully used also in biomass fired boilers delivering superheat and reheat steam at 568 °C. The alloy can be bent to a tight radius as allowed by BS1113 without need for post bend heat treatment. This feature saves significant fabricator costs.

- **310HCbN, EN1.4952**

This is a niobium stabilized nitrogen alloyed austenitic stainless 25 % chromium 20 % nickel type steel. By niobium and nitrogen alloying to high carbon variant 310H, elevated temperature strength and creep resistance is achieved. It is designed for superheater and reheater boiler tubes and suitable in coal fired power stations at 620°C steam temperatures but also suitable to be used in corrosive conditions at metal temperatures up to 525 °C - 540 °C.

- **Alleima® SX**

The SX grade is a high silicon containing austenitic stainless steel, originally developed for use in concentrated sulfuric acid. The grade is characterized by an excellent corrosion resistance in concentrated sulfuric acid, excellent corrosion resistance in high concentrated nitric acid, good mechanical properties and ductility, and good weldability. It is not approved as pressure vessel at the operating temperature of the boiler.

- **Alleima® Sanicro® 28, EN1.4563**

This is an austenitic high alloyed Cr/Ni/Mo (27/31/3.5) very corrosion resistant steel. It was initially developed for wet corrosion applications. It's limited for use at metal temperatures up to 550 °C (VdTUV 483) and 450 °C (ASME Code Case1325-18). To facilitate fabrication/welding, reduce thermal elongation, and increase thermal transfer, it can be co-extruded with a load carrier boiler tube, type 10Cr/T22, X10Cr/T91, to so called composite tubes. Such tubes are used both in superheaters and waterwalls when more corrosive fuels are used.

- **Alleima® Sanicro® 35**

Sanicro® 35 is an alloy combining the best features of a super austenitic stainless steel and a nickel alloy for wet corrosion applications. The grade has excellent corrosion resistance, for service in sea-water applications and other highly corrosive environments. It's limited for use at metal temperatures up to 450 °C, Pre-approval for Particular Material Appraisal (PMA) TÜV file 1326W043219, and ASME Code Case 2982. Boiler and Pressure Vessel Code, Section VIII, Division I and II.

- **Alloy 27Cr33Ni3Mo**

This is a new austenitic heat resistant stainless steel development. It exhibits both high creep strength and high corrosion resistance. This allows the material to be used in environments with high temperature and high pressure at metal temperatures up to 650 °C. The material is not yet approved by any international standard. The grade is targeted for use in superheaters/reheaters in boilers in which more corrosive fuels are used.

- **Kanthal® APMT**

FeCrAl-alloys forms, depending on environment and temperature, a protective layer containing Al_2O_3. The FeCrAl-alloy Kanthal® APMT is an advanced powder metallurgical, dispersion strengthened, ferritic iron-chromium-aluminum alloy. Typical applications for Kanthal® APMT are as radiant tubes in electrically or gas fired furnaces. Kanthal® APMT has also been tested in environments related to biomass and waste fired boilers with good results, which makes FeCrAl alloys interesting for superheater applications, though they are not pressure vessel grades.

- **Kanthal® EF100**

Kanthal® EF is a newly developed group of FeCrAl alloys with a leaner composition than traditional FeCrAls, the baseline being Cr (10%), Al (4%). The aim for this leaner composition is to optimise the alloys for use at lower temperatures by avoiding the 475 °C embrittlement, while retaining their excellent corrosion properties.

- **Kanthal® EF101**

This alloy is an adjustment of EF100 by adding Si (2%) and RE, to improve the corrosion resistance in aggressive environments such as those relevant in boiler applications. As for all the FeCrAl alloys, the material would be used as corrosion protection in the form of overlay welding or tubes co-extruded with a load bearing alloy.

- **Alloy 625**

This is a nickel base alloy containing both chromium and molybdenum for corrosion protection. The alloy exhibits generally good corrosion resistance in chloride containing environments and is today used to a large extent in boilers, primarily as overlay welded and thermal spray coated load carrying tubes.

- **Alleima® Sanicro® 69 (Alloy690)**

This is an austenitic nickel-chromium-iron alloy with high resistance to oxidation, carburization and nitridation, and cracking resistance. This alloy is widely used in black liquor recovery boilers as composite tubes. The corrosion properties and resistance to stress corrosion cracking have been verified in both extensive laboratory testing and in boilers.

- **CorEr thermally sprayed coating**

MH Engineering has developed a nickel-based alloy, with a similar composition to the Inconel625 alloy. However, micro-additives have been added in order to promote precipitation hardening. This hardening process starts when the boiler is started up and after about 3 weeks at 300 °C material temperature the coating is fully hardened. This process increases the hardness to about 800 (HV300) as compared to traditional Inconel625, which has a corresponding hardness of about 300. This increase in hardness is especially useful in CFB boilers burning difficult fuels and where corrosion and erosion is problematic. This coating has both been sprayed on to samples with the HVOF technique (High Velocity Oxy-Fuel) and the newer HVAF technique (High Velocity Air Fuel). The later coating technique is expected to produce more dense coatings and thereby higher corrosion resistance.

3.2 DESCRIPTION OF THE EXPOSURES

3.2.1 Clamp samples on FBHE in Händelö P15 and Högdalen P6

During boiler shutdowns clamp samples were installed on, and removed from, the top and bottom most tube rows of the FBHE tube bundles. Two halfmoon shaped clamp sample halves were mounted around the superheater tubes. Clamping tools were used to hold the clamp halves tightly around the heat exchanger tubes while they were TIG-welded together by using Alloy-625 wire. Three sample batches were installed in Händelö P15 (Apr. 2019, Apr. 2020 and Sep. 2021) and one batch in Högdalen P6 (Aug. 2019). In 2019, all the samples were installed by using method-1 (schematic image in the top of Figure 3. In 2020 and 2021, sample installation was made by using method-2 (schematic image in the bottom of Figure 3. This change was made to reduce the risk of harming the heat exchanger tubes while removing the samples. In Table 7 -

Table 13 the installation locations, together with estimated metal surface temperatures, sample identification names (upward (U) facing on the left and downward (D) facing in the right column) and exposure period / failure by color coding are shown. In the tables, 197 and 198 were the EF101 and EF100 sample respectively. In addition, the "In 625" sample was "alloy 625" sample and "San33" was "27Cr33Ni3Mo alloy".

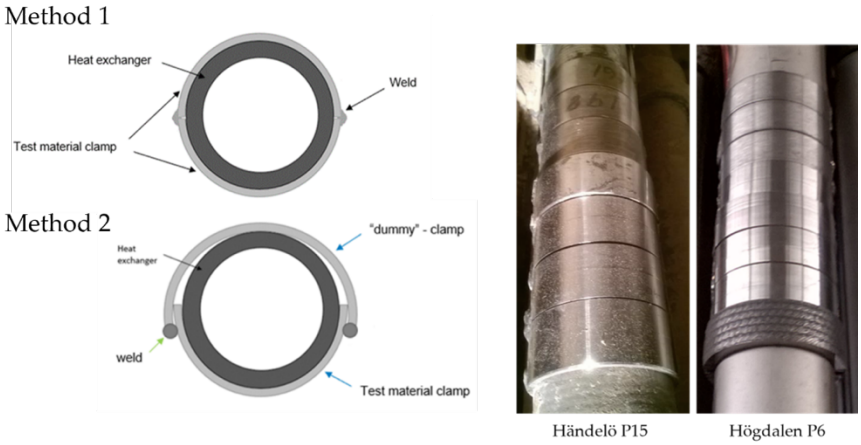

Figure 3. Description of clamp installation. The top left image shows a schematic of the clamp installation according to method 1. The bottom left image shows a schematic of the clamp installation according to method 2.

Table 7. Color describing the dates of exposure in boiler P6, Högdalen positioned in FBHE SH3b row 1 and 8.

	Installed	Removed
	Aug. 2019	Sep. 2020
	Aug. 2019	Sep. 2021
		Not recovered

Table 8. Boiler P6, Högdalen positioned in FBHE SH3b clamp samples installed in Aug. 2019 (shield between the heat exchanger tube and clamp sample on row 1).

SH4, Row 1, Coil 4 (T~600-625 °C)

197'-1U	197'-1D
198'-1U	198'-1D
APMT'-1U	APMT'-1D
316'-1U	316'-1D
K92'-1U	K92'-1D
12RM80'-1U	12RM80'-1D
San69'-1U	San69'-1D
IN625'-1U	IN625'-1D

SH4, Row 1, Coil 6 (T~600-625 °C)

16Mo3'-1U	16Mo3'-1D
San28'-1U	San28'-1D

SH4, Row 1, Coil 8 (T~600-625 °C)

197'-2U	197'-2D
198'-2U	198'-2D
APMT'-2U	APMT'-2D
316'-2U	316'-2D
K92'-2U	K92'-2D
12RM80'-2U	12RM80'-2D
San69'-2U	San69'-2D
IN625'-2U	IN625'-2D

SH4, Row 1, Coil 10 (T~600-625 °C)

16Mo3'-2U	16Mo3'-2D
San28'-2U	San28'-2D

SH4, Row 8, Coil 5 (T~525-550 °C)

197-1U	197-1D
198-1U	198-1D
APMT-1U	APMT-1D
316-1U	316-1D
K92-1U	K92-1D
12RM80-1U	12RM80-1D
San69-1U	San69-1D
IN625-1U	IN625-1D

SH4, Row 8, Coil 7 (T~525-550 °C)

16Mo3-1U	16Mo3-1D
CE-1	CE-2
APMT20C-1	APMT-20C-2
APMT-50C-1	APMT50C-2

SH4, Row 8, Coil 9 (T~525-550 °C)

197-2U	197-2D
198-2U	198-2D
APMT-2U	APMT-2D
316-2U	316-2D
K92-2U	K92-2D
12RM80-2U	12RM80-2D
San69-2U	San69-2D
IN625-2U	IN625-2D

SH4, Row 8, Coil 11 (T~525-550 °C)

16Mo3-2U	16Mo3-2U
CE-3	CE-4
CE-5	APMT-20C-3
CE-6	APMT50C-3

Table 9. Color describing the dates of exposure in boiler P15, Händelö positioned in FBHE SH2 and SH3 region.

	Installed	Removed
	Apr. 2019	Jun. 2019
	Apr. 2019	Sep. 2019
	Apr. 2019	Mar. 2020
	Apr. 2020	Mar. 2021
	Sep. 2021	Mar. 2022
		Not recovered

Table 10. Händelö P15 FBHE SH2 clamp samples installed in Apr. 2019.

SH2, Row 1, Coil 4 (T~500-525 °C)

197-1U	197-1D
198-1U	198-1D
APMT-1U	APMT-1D
316-1U	316-1D
K92-1U	K92-1D
12RM80-1U	12RM80-1D
San69-1U	San69-1D

SH2, Row 1, Coil 6 (T~500-525 °C)

IN625 (WOL)-1U	IN625 (WOL)-1D
"dummy"	APMT (WOL)-1D
"dummy"	197 (WOL) -1D
"dummy"	198 (WOL) -1D
"dummy"	CE-1D
"dummy"	APMT C50-1D

SH2, Row 1, Coil 8 (T~500-525 °C)

197-2U	197-2D
198-2U	198-2D
APMT-2U	APMT-2D
316-2U	316-2D
K92-2U	K92-2D
12RM80-2U	12RM80-2D
San69-2U	San69-2D

SH2, Row 1, Coil 10 (T~500-525 °C)

IN625 (WOL)-2U	IN625 (WOL)-2D
"dummy"	APMT (WOL)-2D
"dummy"	197 (WOL) -2D
"dummy"	198 (WOL) -2D
"dummy"	CE-2D
"dummy"	APMT C20-2D

SH2, Row 1, Coil 12 (T~500-525 °C)

197-3U	197-3D
198-3U	198-3D
APMT-3U	APMT-3D
316-3U	316-3D

SH2, Row 1, Coil 14 (T~500-525 °C)

IN625 (WOL)-3U	IN625 (WOL)-3D
"dummy"	APMT (WOL)-3D
"dummy"	197 (WOL) -3D
"dummy"	198 (WOL) -3D
"dummy"	CE-3D
"dummy"	APMT C50-3D

SH2, Row 6, Coil 3 (T~525-550 °C)

16Mo3-1U	16Mo3-1D

Table 11. Händelö P15 FBHE SH3 clamp samples installed in Apr. 2019.

SH3, Row 1, Coil 4 (T~525-550 °C)

197-4U	197-4D
198-4U	198-4D
APMT-4U	APMT-4D
316-4U	316-4D
K92-3U	K92-3D
12RM80-3U	12RM80-3D
San69-3U	San69-3D

SH3, Row 1, Coil 6 (T~525-550 °C)

IN625 (WOL)-4U	IN625 (WOL)-4D
"dummy"	APMT (WOL)-4D
"dummy"	197 (WOL) -4D
"dummy"	198 (WOL) -4D
"dummy"	CE-4D
"dummy"	APMT C50-4D

SH3, Row 1, Coil 8 (T~525-550 °C)

197-5U	197-5D
198-5U	198-5D
APMT-5U	APMT-5D
316-5U	316-5D
K92-4U	K92-4D
12RM80-4U	12RM80-4D
San69-4U	San69-4D

SH3, Row 1, Coil 10 (T~525-550 °C)

IN625 (WOL)-5U	IN625 (WOL)-5D
"dummy"	APMT (WOL)-5D
"dummy"	197 (WOL) -5D
"dummy"	198 (WOL) -5D
"dummy"	CE-5D
"dummy"	APMT C20-5D

SH3, Row 6, Coil 3 (T~550-575 °C)

197-6U	197-6D
198-6U	198-6D
APMT-6U	APMT-6D
316-6U	316-6D
K92-5U	K92-5D
12RM80-5U	12RM80-5D
San69-5U	San69-5D
16Mo3-2U	16Mo3-2D

SH3, Row 6, Coil 5 (T~550-575 °C)

IN625 (WOL)-6U	IN625 (WOL)-6D
"dummy"	APMT (WOL)-6D
"dummy"	197 (WOL) -6D
"dummy"	198 (WOL) -6D
"dummy"	CE-6D
"dummy"	APMT C20-6D

Table 12. Händelö P15 FBHE SH3 clamp samples installed in Apr. 2020.

SH3, Row 1, Coil 4 (T~525-550 °C)		SH3, Row 1, Coil 18 (T~525-550 °C)	
197-8U	197-8D	197-7U	197-7D
APMT-8U	APMT-8D	APMT-7U	APMT-7D
San69-7U	San69-7D	San69-6U	San69-6D
San33-2U	San33-2D	San33-1U	San33-1D
"dummy"	San59-1D	"dummy"	San59-1U

Table 13. Händelö P15 FBHE SH3 clamp samples installed in Sep. 2021.

SH3, Row 1, Coil 4 (T~525-550 °C)			SH3, Row 1, Coil 18 (T~525-550 °C)	
197-10U	197-10D		197-9U	197-9D
APMT-10U	APMT-10D		AMPT-9U	APMT-9D
San69-9U	San69-9D		San69-8U	San69-8D
San33-4U	San33-4D		San33-3U	San33-3D
"dummy"	San59-3D		"dummy"	San59-3U
197-12U	197-12D		197-11U	197-11D
APMT-12U	APMT-12D		APMT-11U	APMT-11D
San33-6U	San33-6D		San33-5U	San33-5D
"dummy"	San59-4D		"dummy"	San59-4U

3.2.2 Furnace water wall probe samples in Högdalen P6

Högdalen P6 furnace water wall material tests were conducted by using three small sized air-cooled probes. Each probe comprised one sample which was inserted into the furnace via openings made to the membrane panel wall fin (front wall, elevation +17m). The openings were equipped with a double valve system, including pressurized air feeding, allowing safe probe installation and removal. A thermocouple was connected to each sample to verify the exposure temperature. The control unit and mass flow controllers were used to control the air feeding rate required to hold the samples at set temperatures. To reach higher exposure temperatures, insulation material was used between the sample and panel wall fin. The exposure time was one week, and target metal temperatures were 300 and 350 °C. The test matrix is given in Table 14. The tests were started in Nov. 2022.

Furnace wall probe equipment:

- Probe openings
- Air cooled probes
- Samples
- Thermocouples with K-type compensation cables
- Air hoses for cooling air
- Mass flow controllers
- Control unit box

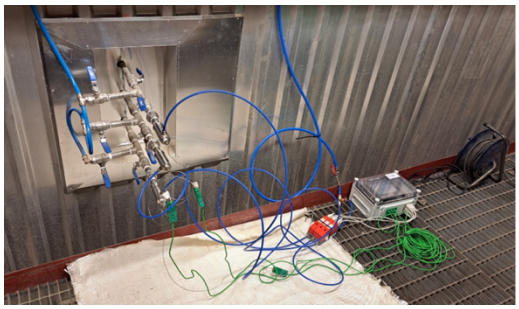

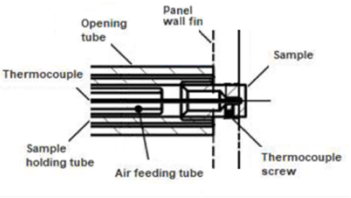

Figure 4. Furnace wall probe set-up (left). Schematic drawing of the probe instrument (left).

Table 14. Högdalen P6 furnace water wall test matrix.

Set	T, °C	Probe-1	Probe-2	Probe-3
1	300	16Mo3	310HCbN	Alloy 625
2	300	EF101	EF100	APMT
3	300	San28	27Cr33Ni3Mo	San35
4	350	16Mo3	310HCbN	Alloy 625
5	350	EF101	EF100	APMT
6	350	San28	27Cr33Ni3Mo	San35

3.2.3 Thermal sprayed coatings on the water walls in Händelö P15

In Händelö P15 a section of the water wall in the empty pass was coated using HVOF, a metallic spray process. This was performed in 2019. In total, four water

wall tubes were sprayed. Two of them were coated with APMT and two of them were coated by CorEr. The thickness of the metal spray coatings was measured twice, in 2020 and 2021, in order to elucidate the material wastage.

3.3 ANALYTICAL TECHNIQUES

The exposed samples were investigated by means of quantitative as well as qualitative analytical techniques. The quantitative measures have involved material loss determination and the qualitative analysis has primarily involved cross-sectional SEM/EDX analysis. All the analyses were performed by HTC/Chalmers.

3.3.1 Material loss

The samples were evaluated by means of metal loss determination, performed with an Olympus 38DL Plus ultrasonic thickness gage with a 0.01 mm resolution. Complementary material loss determinations were performed by OM and SEM measurements. Internal oxidation and nitridation zones were not defined as material loss in this report and were thus not included as material loss when conducting thickness measurements after exposure.

3.3.2 Scanning Electron Microscopy/Energy Dispersive X-Rays (SEM/EDX)

After exposure, some selected samples were prepared for cross-sectional SEM/EDX analysis. These samples were cast in epoxy, cut, and polished prior to the SEM/EDX investigation. The samples were cast in the epoxy resin by putting them into a mold which were subjected to a 10-bar pressure to avoid the formation of bubbles during the hardening of the resin. The hardening time was fixed at 24 hours. After the hardening of the epoxy resin was complete, the samples were cut using a silicon carbide disc and a lubricant without any water due to the delicate corrosion products. The samples were then polished dry with Silicon Carbide P4000. The cross-section was coated with gold to avoid charging in the SEM. The polished cross-sections of the samples were subsequently investigated by scanning electron microscopy, SEM. In addition, an Energy Dispersive X-rays (EDX) system was used to analyze the sample's elemental composition in the SEM image. The resolution and depth of focus in an SEM are much higher than in an optical microscope, revealing more details of the corrosion attack. The samples were examined with an FEI Quanta 200 FEG ESEM. The SEM has a field emission electron gun (FEG) and is equipped with an Oxford Inca energy dispersive X-ray (EDX) system. SEM/EDX was used for elemental mapping and quantification. For imaging and EDX analysis, an accelerating voltage of 20 kV was used.

4 Results

4.1 WATER WALL EXPOSURES HÖGDALEN P6 WASTE-FIRED BOILER

The temperature profile of the three different sets of materials evaluated in the water wall in Högdalen P6 waste-fired boiler is shown in Figure 5-7. A couple of noticeable trends should be addressed. For instance, in Set#1 the 16Mo3 sample achieved an approximately 20 °C higher temperature than 310HCbN and Alloy 625 throughout the exposure (see Figure 5) In set 2, the temperature profile shows that EF101 obtained a temperature between 290-300 °C, while EF100 and APMT had an average temperature around 275 and 270 °C, respectively (see Figure 6). The sudden temperature drop observed in set #3 was due to a sudden boiler shut down, hence the exposure was only carried out for approximately six days. In addition, the 27Cr33Ni3Mo sample was not retrieved.

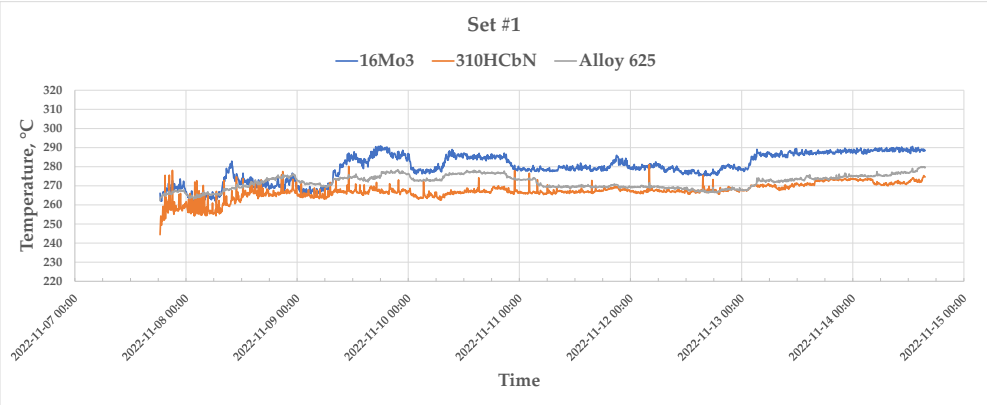

Figure 5. Temperature profile for Set #1.

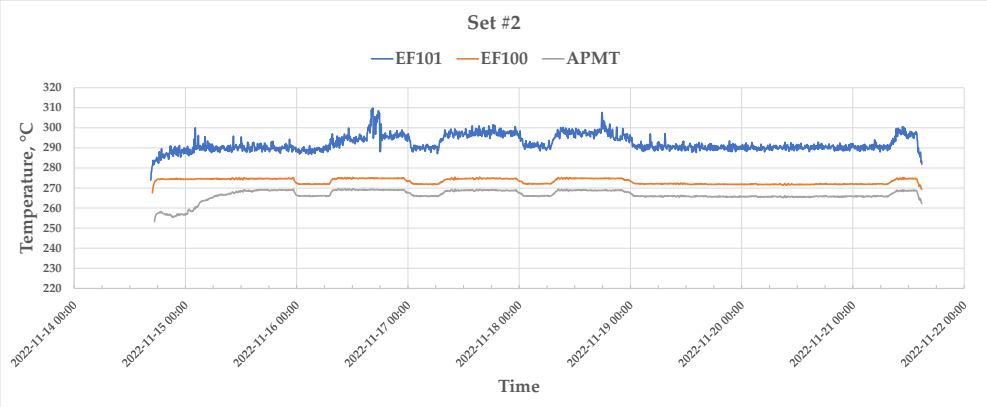

Figure 6. Temperature profile for Set #2.

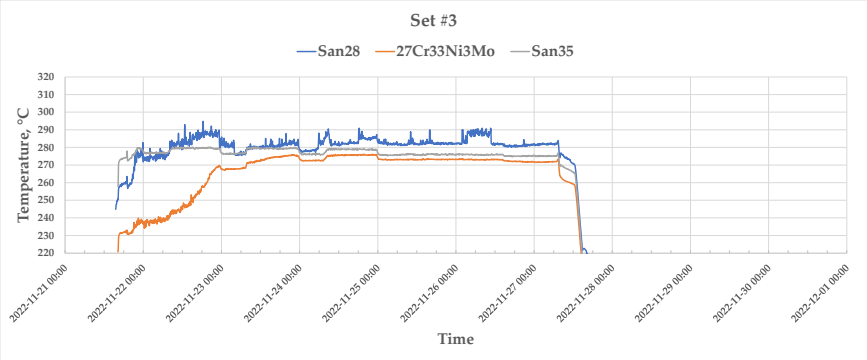

Figure 7. Temperature profile for Set #3.

A SEM cross section overview of all samples tested in the water wall region is shown in Figure 8. As is shown the only sample displaying high oxidation rate was the low alloyed steel 16Mo3. The 310HCbN and Alloy 625 sample from Set #1 showed no indication of significant material loss or oxidation, e.g., a homogenous surface and no alloy element depletion close to the metal/atmosphere interface was observed with SEM/EDX analysis.

A more detailed microstructure investigation of 16Mo3 is shown in Figure 9. A roughly 20 micrometer thick Fe-rich oxide was observed, adherent to the metal substrate. On top of the oxide an adherent deposit with various thickness was covering the oxide surface. The deposit contained mainly Cu, S, O, Na, K, Ca and traces of heavy metals such as Zn and Pb. The bright areas displayed in the deposit and, in some cases the Fe-oxide, were confirmed via EDX point analysis to consist of a mixture of both high concentrations of Cu/O and a mixture of Pb/K/Na/O (see Figure 9). The oxide formed was divided into two regions, where the darker area closest to the metal/oxide interface was confirmed via EDX point analysis to consist of a high concentration of Cl. From the EDX mapping it is evident the Cl ions have migrated from the deposit layer and separated from potential initial cations such as Na, K, Pb and Ca. The overlap between the L series peak of Pb and the Kα peak of S makes it very challenging to distinguish these two elements in EDX mapping and point analysis, which is observed in the EDX mapping. Thus, the quantity of these elements should be considered with caution.

For the FeCrAl alloys exposed in Set #2 the APMT and EF100 sample remained intact with no indication of heavy oxidation nor material losses. Furthermore, none of the FeCrAl samples showed any indication of nitridation close to the metal/deposit interface. For the EF101 sample, a 40 µm thick deposit was observed on the sample after 1 week of exposure. A SEM cross section and EDX analysis were conducted on this sample and is shown in Figure 10. Similar deposit composition was observed as with the 16Mo3 sample. However, as is shown in the EDX mapping and point analysis, it is evident that the Cl ions have not migrated from the deposit layer towards the metal/deposit interface and are thus still in the vicinity of their initial counter ions. Below the deposit a thin Fe,Cr,Al oxide was observed in patch wise fashion with a thickness of roughly 2 µm (see point analysis “b” in Figure 10).

Lastly the Sanicro 28 and 35 sample in Set #3 displayed no indication of heavy oxidation nor material losses. EDX analysis confirmed that the deposit observed on the Sanicro 28 sample had similar composition as the previous mentioned samples. As with the EF101 sample, the Cl remained well distributed over the deposit layer and had not migrated to the metal/deposit interface. In addition, from EDX analysis no indication of internal or outward growing oxide was seen.

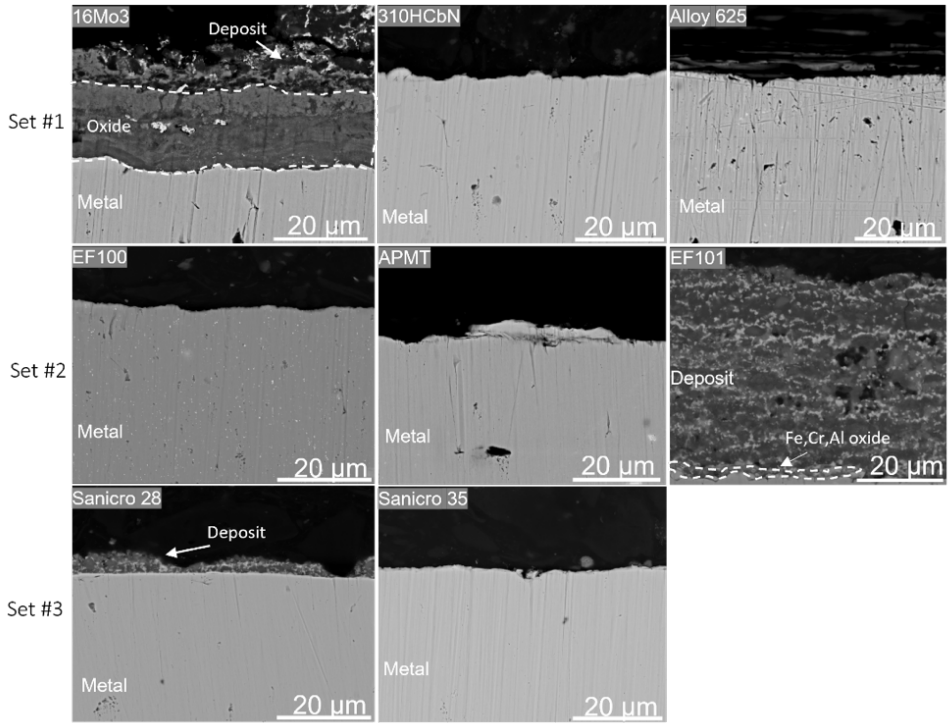

Figure 8. SEM cross section overview of material tested in the water wall region for 1 week at approximately 300 °C in Boiler P6, Högdalen.

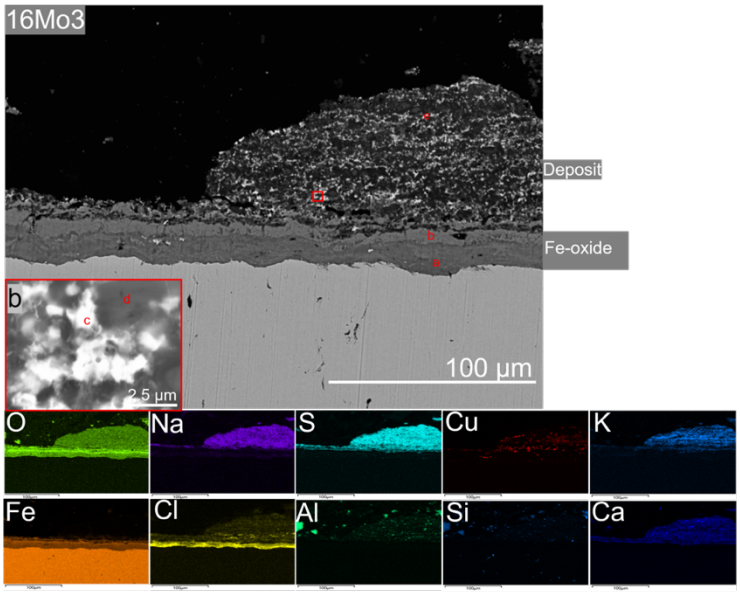

at%	Fe	O	Si	S	Zn	Ca	K	Na	Cl	Cu	Pb
Spectrum a	35.5	47.9	0.2	0.5	1.4	0	0.5	0.6	13.4	0	0
Spectrum b	39.2	55.7	0.5	0.4	0.2	0.1	0.3	1.4	2	0	0
Spectrum c	3	26.1	1.5	4.6	0.2	1.5	0.6	6	0.6	55.7	0.7
Spectrum d	1	54.4	1.6	14.4	0.6	5.4	7.5	11.2	1.3	2.5	0.8
Spectrum e	0	57.6	0	13.8	0.6	2.2	7.7	8.18	3	0	6.8

Figure 9. SEM cross section and EDX analysis of 16Mo3 exposed for 1 week at approximately 300°C in Boiler 6, Högdalen.

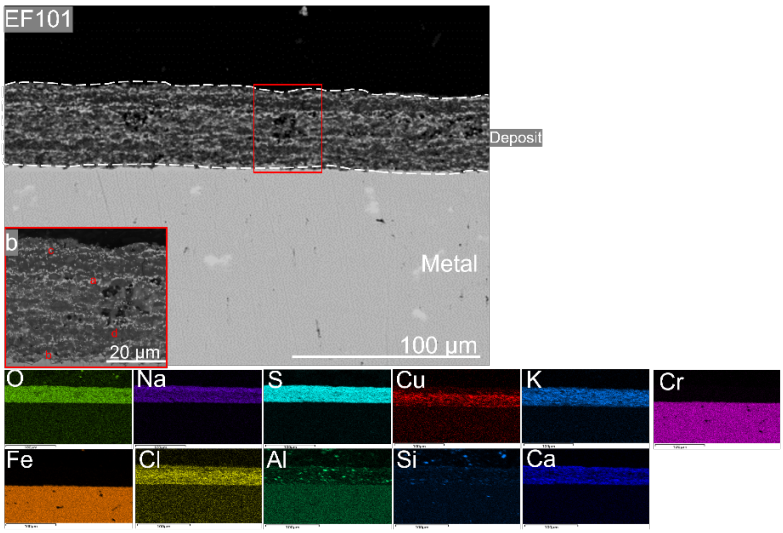

at%	Fe	O	Al	Si	S	Zn	Ca	K	Na	Cl	Cu	Pb
Spectrum a	1	50	1	1	15.8	2	4.5	4.9	7	2	11	1
Spectrum b	46	25	5.6	2	2	2	1	1	1	3	0	0
Spectrum c	0	50.6	1	1	13.8	0.6	2	7.5	8	8	0	8
Spectrum d	0.5	58.1	2	3.3	13.5	1.5	7.1	3	6.4	2	0.9	1

Figure 10. SEM cross section and EDX analysis of EF101 exposed in the water wall region for 1 week at approximately 300 °C in boiler P6, Högdalen.

4.2 METAL SPRAYED COATINGS ON WATER WALLS IN HÄNDELÖ P15

Two test areas, about 1.2 meter in height and about two tubes wide, were HVOF sprayed with APMT and CorEr, respectively. The number 3 and 4 tubes were metallized APMT and the number 7 and 8 tubes were metallized with material CorEr™, see Figure 13. Both materials had been coated in the spring 2019.

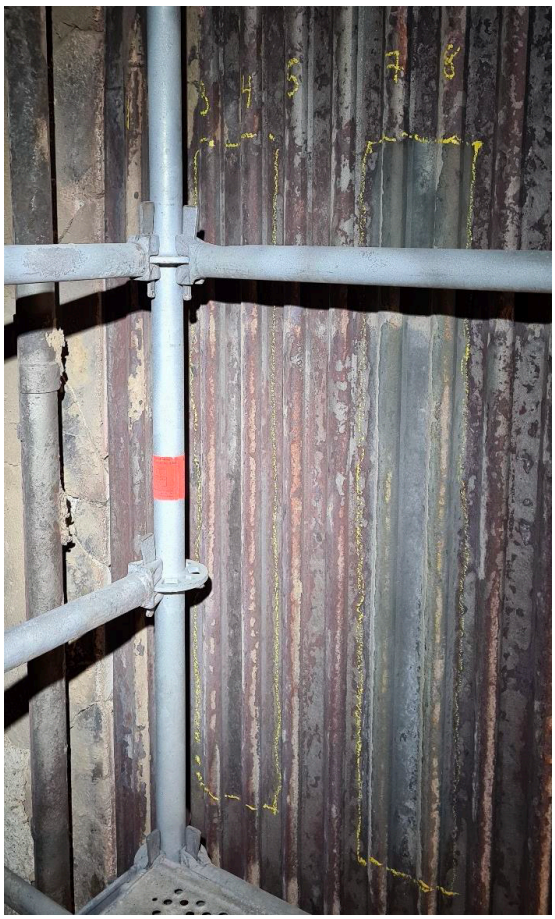

Figure 11. The two areas HVOF sprayed. Tubes 3-4 are metallized with AMPT and tubes 7-8 are metallized with CorEr. The image is taken during the first revision, about 1 year of exposure.

Already at the time of the first inspection, on 2020-03-25, it was noted that only tubes number 7 and 8 (with CorEr) had any metallization left on the tubes. For tubes 3 and 4 (with APMT), only small remnants of metal left in the junction between the tube and the fin could be seen.

At the second inspection (2021-03-25), after about two years of exposure, there was no APMT coating left on the tubes number 3 and 4. For the CorEr coating on tubes number 7 and 8, the metallization was still visibile. The nominal layer thickness of material CorEr™ was approx. 400 ± 50 µm, see Figure 12. The variation depends primarily on manual application. Thus, there has been no appreciable stripping of the metallization on tubes number 7 and 8, after two operating seasons.

Figure 12. Thickness measurement of the HVOF sprayed CorEr coating at the 2021 revision in the P15 boiler in Händelö.

4.3 MATERIAL LOSS AND MICROSTRUCTURAL ANALYSIS ON FBHE

4.3.1 Clamp exposures on FBHE - Högdalen P6

Clamp exposures were conducted on fluidized bed heat exchangers in the P6 waste-fired boiler in Högdalen in continuous mode during two periods: 12 and 24 months. In this exposure times the planned shutdowns of the boiler are counted. The material loss calculations are presented in mm/year to be able to compare with P15 Händelö exposures as well as previous or future research studies. The samples were mounted as two half-moon rings on the top and bottom-most rows of the fluidized bed heat exchanger bundle. The first batch samples, exposed 12 months, were placed in rows 1 and 8, respectively. The second batch samples, exposed 24 months, were placed in row 9.

Material loss

Figure 13 shows the material loss rate for each sample expressed as mm/y. The filled circle for each data set represents the arithmetic mean value of the material loss.

An increase in material loss rate in row 1 compared to row 8 was observed for all materials exposed for 12 months, except for the SX and Sanicro 69 samples.

All three FeCrAl alloys sustained low material loss throughout the exposure ranging from approximately 0-0.35 mm/year, expressed as maximum material loss rate. The Novel FeCrAl alloy EF101 achieved the lowest material loss rate of the FeCrAl alloys, obtaining a material loss close to zero regardless of position and with a maximum material loss rate of 0.09 mm/year observed in row 1. In addition, the spread of the material loss values for EF101 were very low throughout the cross section, indicating that a homogenous surface remained on the sample. This behavior is consistent with the material loss results after the 24 months exposure. The EF101 FeCrAl material presents negligible material loss, while a larger spread in material loss values was observed for the EF100 alloy. After 24 months exposure this alloy obtained an average material loss of 0.36 mm/year, the maximum material loss being 0.55 mm/year. The surface of the EF101 alloy is smoother and it presents less nitridation than the EF100 alloy. This aspect is discussed in the section below.

The APMT bulk sample presents an average material loss of 0.27 mm/year after 24 months exposure with a high grade of nitridation.

The nitridated material has not been considered in the material loss calculation as it is unclear if it affects the corrosion behavior or increases the material loss. This behavior has been observed in several samples and more corrosion experiments are needed to determine if it is a factor affecting corrosion.

The austenitic conventional stainless steel, 316Ti, and Esshete 1250 exhibited high material loss after 12 months exposure, compared to the previously mentioned FeCrAl alloys. An increase in material loss was observed for 316Ti compared to Esshete 1250 in row 1 and row 8. These samples obtained an average material loss rate ranging from 0.33-0.92 mm/year at the two different positions. After 24 months exposure the 316Ti was not recovered. The Esshete 1250 presents higher material loss than after 12 months exposure, with an average value of 0.87 mm/year and a maximum of 1.07 mm/year.

The high Si-containing austenitic steel SX performed significantly better than the previously mentioned austenitic steels both after 12- and 24-months exposure. The average material loss rate for this sample was between 0.02-0.06 mm/year after 12 months exposure for row 1 and 9. The material loss value did not increase after 24 months exposure, with an average of 0.05 mm/year. In addition, the maximum material loss was close to the calculated average value, suggesting that a homogenous surface remained on this sample in both exposures.

The highest material loss was observed for the low alloyed steel, 16Mo3, which obtained an average material loss rate of 1.18 mm/year and a maximum rate of 1.4 mm/year after 12 months.

The high alloyed steel material of the Sanicro series displayed quite different performances, where Sanicro 28 achieved approximately a maximum material loss of 0.55 mm/year and an average value of 0.34 mm/y in row 1 after 12 months exposure. Meanwhile, no noticeable material loss was detected on the Sanicro 69 sample after 12 months, regardless of position. After 24 months exposure, Sanicro 69 still presents negligible material loss.

Finally, as is shown in Figure 13, the coated material of APMT50C, APMT20C and CorEr achieved high material losses, with an average value of 0.55-0.85 mm/year. However, it was later observed during microstructure analysis that these coatings had failed as no coating material remained on the bulk material after exposure (see "microstructure analysis" sector).

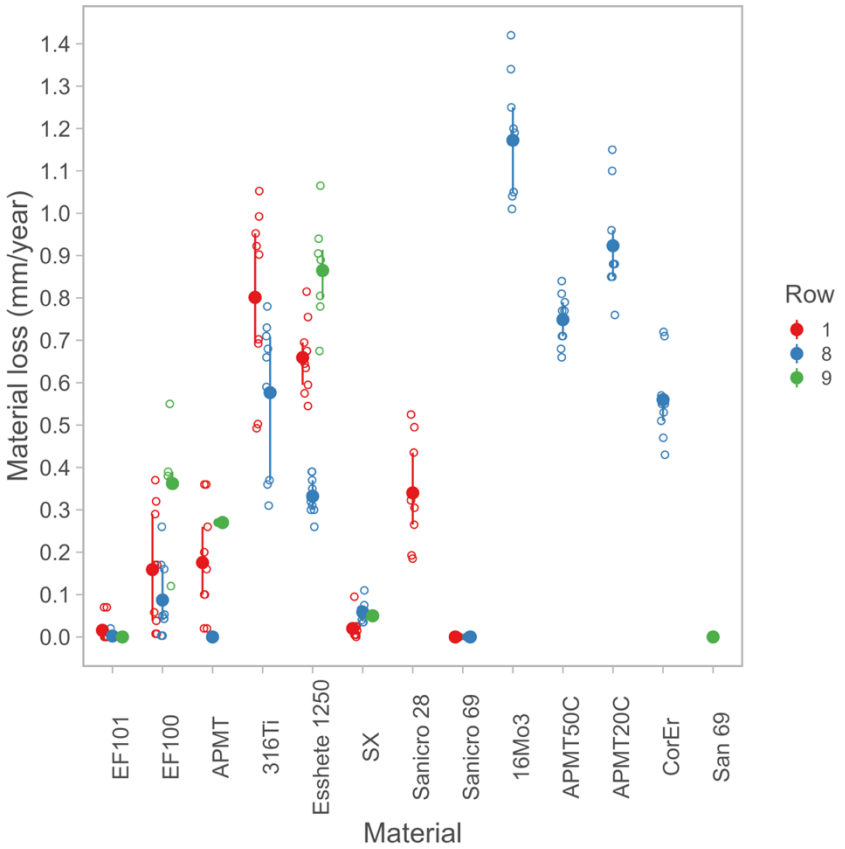

Figure 13. Material loss of the tested clamps exposed in row 1 and 8 for 12 months and row 9 for 24 months in the fluidized bed heat exchanger in P6 boiler, Högdalen.

Microstructure analysis

SEM/EDX analysis were carried out on each exposed sample for microstructure analysis. The results are described below. In many samples, the microstructure contained similar features and chemical composition after 6 and 12 months of exposure, and thus only EDX mapping for 12 month is presented.

Figure 14 presents the SEM cross-section of EF101 positioned in row 1 after 12 months of exposure. A deposited layer of approximately 25 µm of thickness was observed and located on top of a roughly 30 µm Fe-rich oxide. The deposit consisted mainly of Ca, S, Mg, O, and Al (see EDX map analysis below cross-section image). Below the Fe-rich oxide, a Cr/Al-rich oxide was detected at the metal/oxide interface. Compared to the stainless-steel samples of Esshete 1250, 316Ti and SX, there were no indications that the material had been subjected to internal oxidation. However, the EDX analysis confirmed the formation of Al nitrides precipitates below the oxide layer, embedded in a Fe-rich alloy matrix (see EDX point analysis in Figure 14). The thickness of the nitridation region varied

greatly throughout the cross section (between 0-280 µm) and was observed in a patch wise fashion.

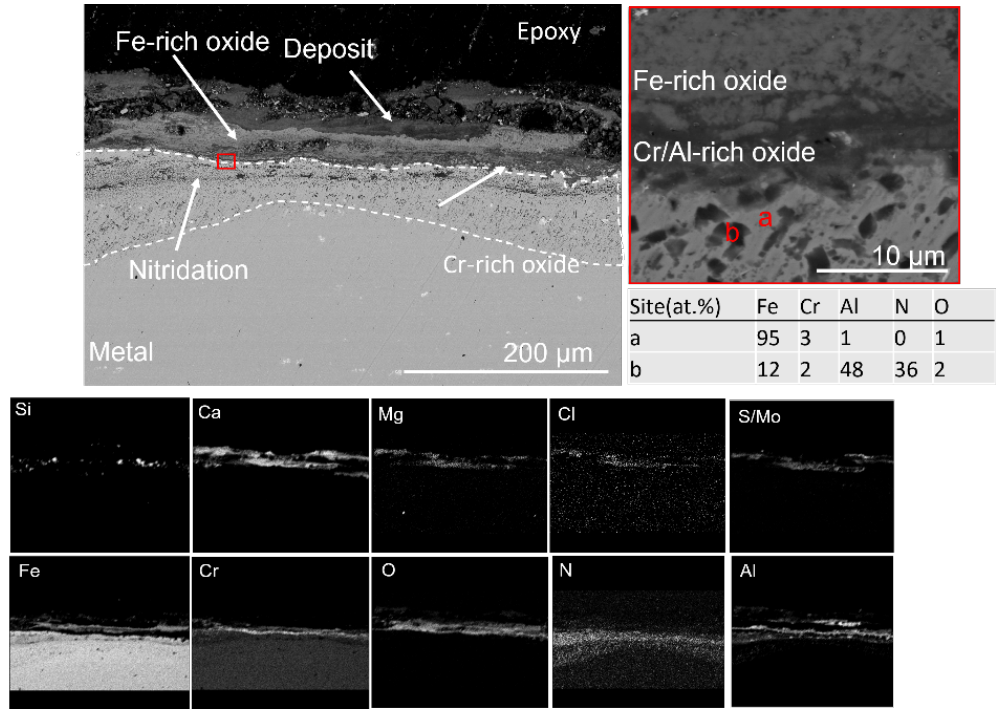

Site(at.%)	Fe	Cr	Al	N	O
a	95	3	1	0	1
b	12	2	48	36	2

Figure 14. Cross-section and EDX analysis of EF101 after 12 months of exposure positioned in row 1. EDX point analysis of highlighted red area (right).

The EF101 sample in row 8 displayed similar features as the previously mentioned sample. An adherent Fe-rich oxide of roughly 40 µm was detected below a 40 µm Ca, S, and Al-rich deposit layer. At the metal/oxide interface, a thin Al/Cr-rich oxide was also observed. Compared to the sample positioned at row 1, a less pronounced nitridation zone was observed. The nitridation was identified throughout the cross section in a patch-wise fashion, with a thickness ranging from 0-150 µm. However, as shown in the figure below, most of the nitridation zones were within the range of 0-10 µm.

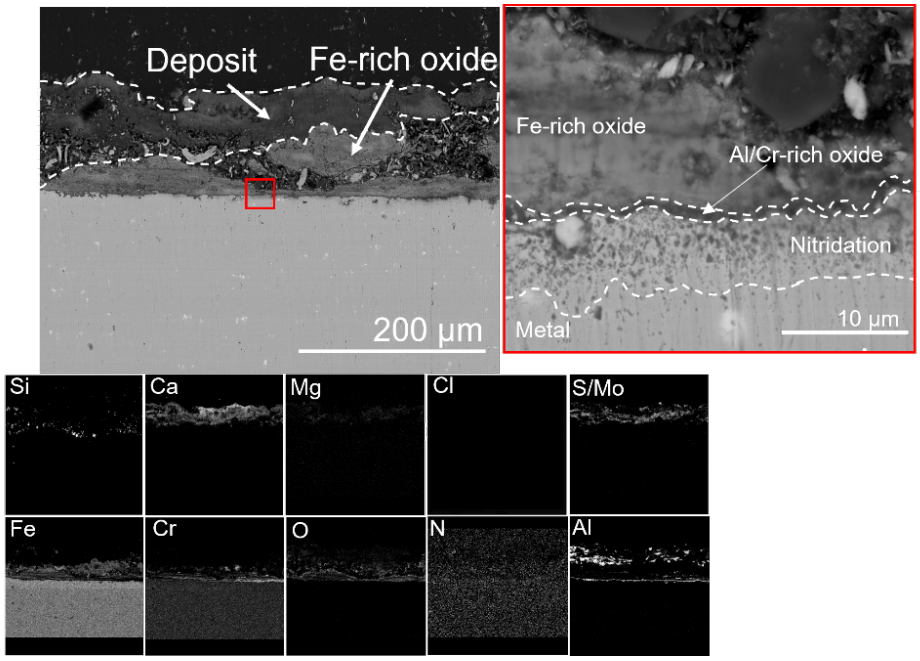

Figure 15. Cross-section and EDX analysis of EF101 after 12 months of exposure positioned in row 8. EDX point analysis of highlighted red area (right).

Figure 16 presents the SEM cross-section and EDX analysis of the EF101 sample after 24 months exposure. The oxide scale is the same as for the 12-month exposed samples presented above. A Cr-rich oxide is formed in contact with the bulk material followed by a thicker Fe-rich oxide. The nitridation zone is over 500 µm thick and it is present all over the sample. However, this value does not seem to affect the material loss, which was still negligible after 24 months exposure (). Some traces of Ca deposit were detected on the top of the oxide scale.

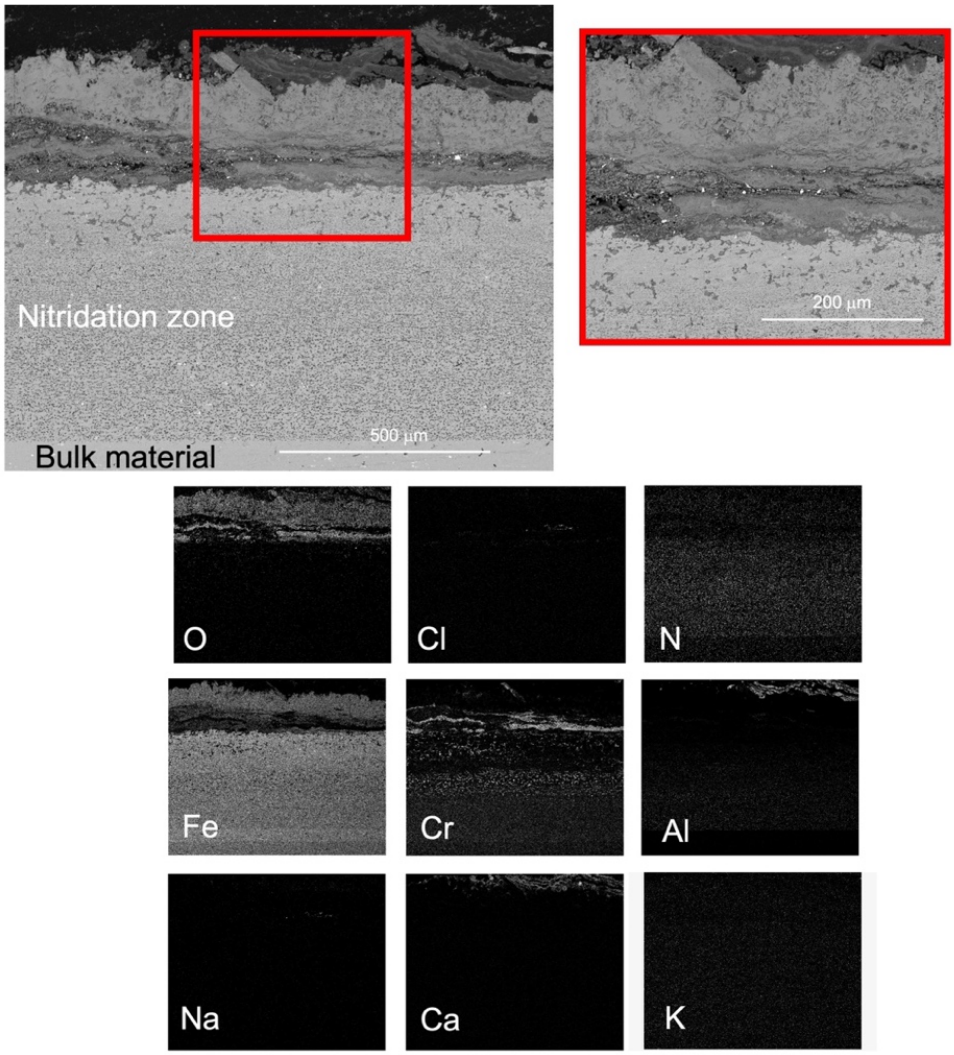

Figure 16. Cross-section and EDX analysis of EF101 after 24 months exposure situated in row 9.

The SEM/EDX cross-section of the EF100 sample situated in row 1 and exposed for 12 months is seen in Figure 17. A thick and adherent deposit layer was observed on the sample containing Ca, S, and Al. In addition, Cl was detected in the deposit. Below, a 140 µm thick, adherent Fe-rich oxide had been formed with elements of void formation, and at the metal/oxide interface, a thin continuous Cr/Al-rich oxide was detected.

Like the EF101 samples, EF100 also developed a nitridation zone below the metal/oxide interface. However, for this sample, a more severe nitration zone was observed, ranging from 75-350 µm thickness, and was seen throughout the cross section in a homogenous fashion.

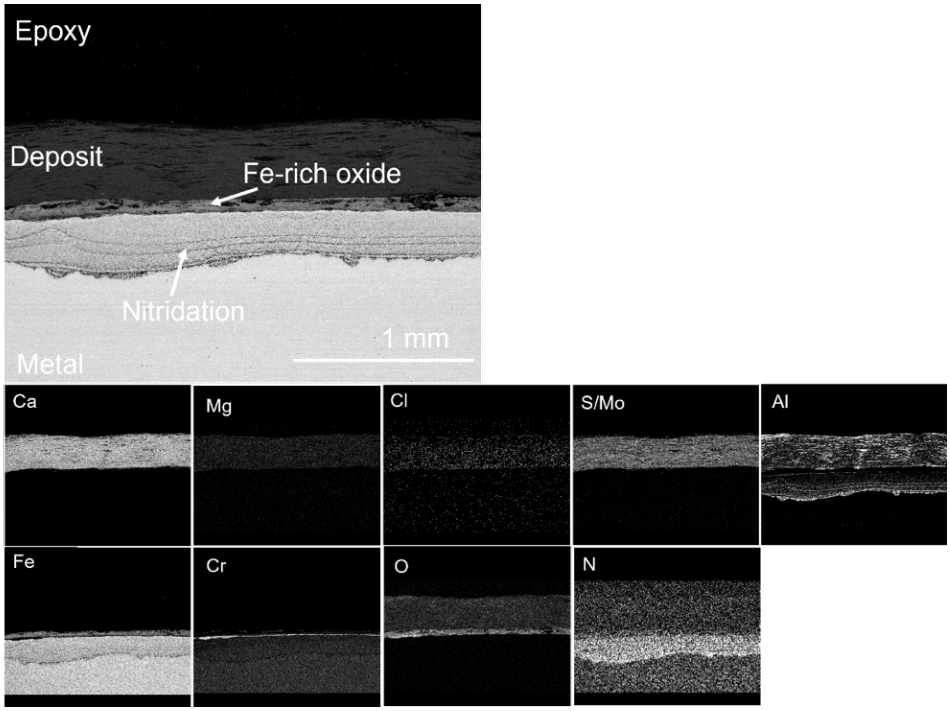

Figure 17. Cross-section and EDX analysis of EF100 after 12 months of exposure positioned in row 1.

The EF100 sample in row 8 displayed similar features as the one in row 1 (see Figure 17). However, no Cl was detected in the deposit. The nitridation zone was less prominent for this sample ranging from 20-200 μm throughout the cross-section. As shown in the material loss figure (Figure 13) described in the previous section, the material loss values varied significantly unlike for the EF101 material. In Figure 18, the image to the right shows a highlighted area of the sample where a more rough and uneven surface was observed, with maximum material losses detected around the middle of the image.

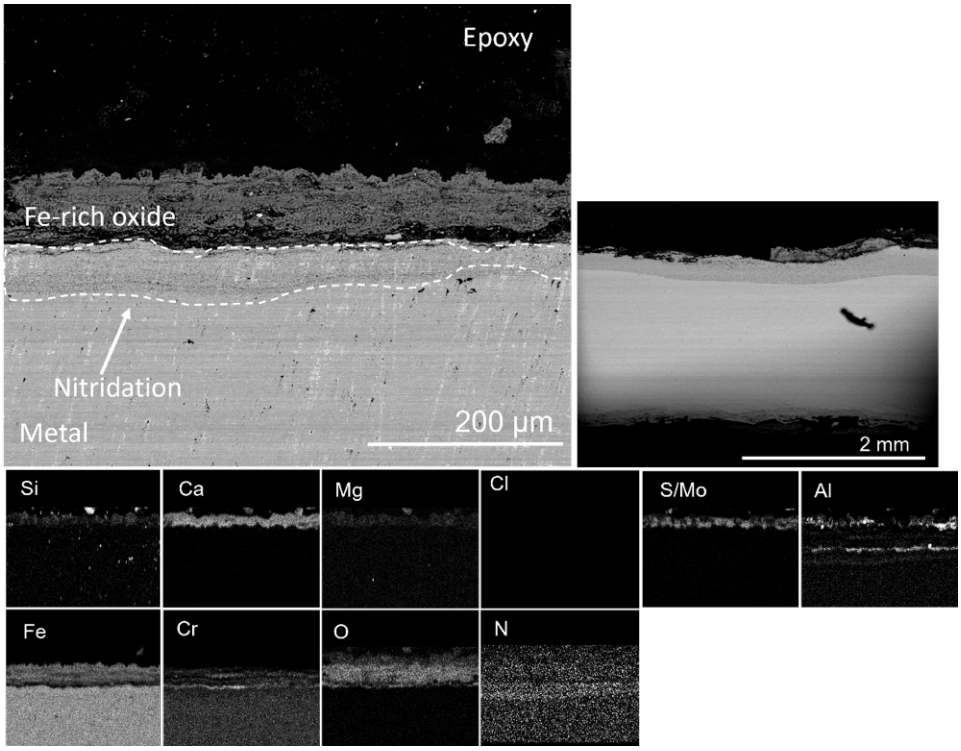

Figure 18. Cross-section and EDX analysis of EF100 after 12 months of exposure positioned in row 8. Cross-section of EF100 positioned in row 8 at lower magnification (right).

Figure 19 presents the SEM cross-section and EDX analysis of the EF100 sample after 24 months exposure. The Fe-rich oxide is thicker than in the 12 months exposure sample (200 µm vs 140 µm thick) and it presents the same void formation. The nitridation zone is also thicker (around 300 µm) and it is present over the whole sample. Regarding the material loss presented in Figure 13, it is still quite low after 24 months, the average value being 0.36 mm/year, but higher than after 12 months (less than 0.2 mm/year).

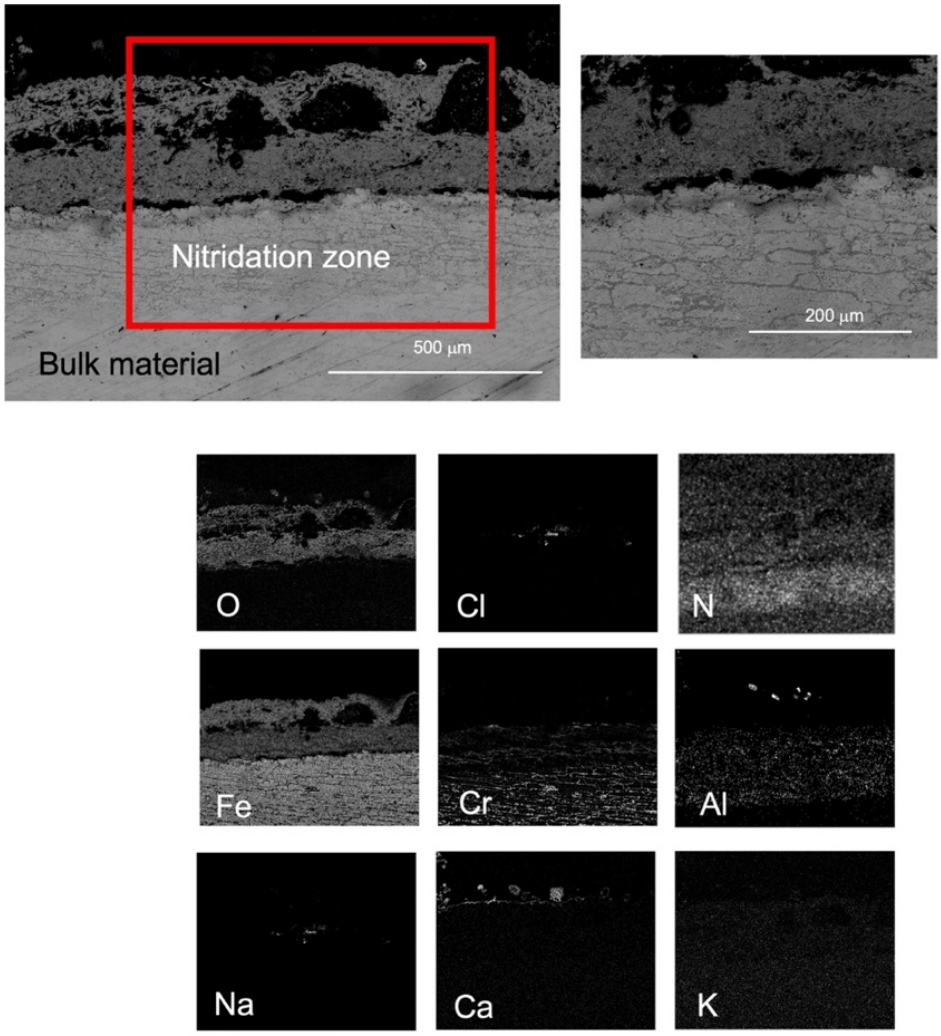

Figure 19. Cross-section and EDX analysis of EF100 after 24 months of exposure positioned in row 9.

To achieve a deeper understanding of the severity of the degradation rate of the newly developed FeCrAl alloys discussed above, a cross-section SEM/EDX analysis was carried out on the corresponding commercial FeCrAl alloy Kanthal APMT in row 1 and row 8 (Figure 20 and Figure 21, respectively).

For the APMT sample positioned in row 1, the deposit layer and oxide had mostly spalled off, which is shown in the EDX mapping. The remaining oxide displayed to the right in the SEM image consisted mainly of a mixture of Cr and Fe, and minor detection of Ca, Si, Mg, and Cl was observed on top of the oxide. The APMT sample suffered from severe nitridation. The thickness of the nitridation zone was measured to roughly 500 µm in row 1 throughout the cross-section with a homogenous structure.

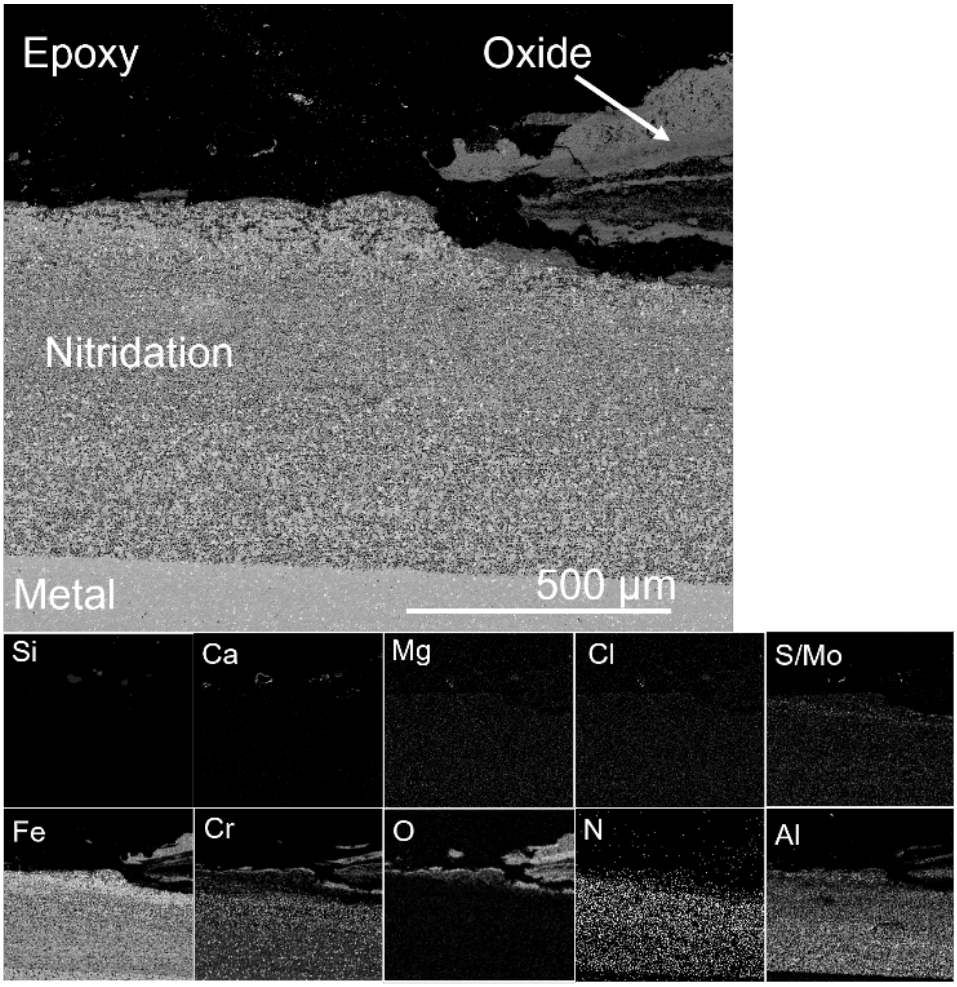

Figure 20. Cross-section and EDX analysis of APMT after 12 months of exposure positioned in row 1.

The APMT sample situated in row 8 displayed less material loss compared to row 1 (see Figure 21). The SEM/EDX image reveals the formation of a Ca, S, Al and O rich deposit with the formation of a Fe-rich oxide below. As for previous FeCrAl alloys, at the metal/oxide interface a Cr/Al-rich oxide was formed. The nitridation zone was significantly thinner for this sample compared to the sample mounted on row 1.

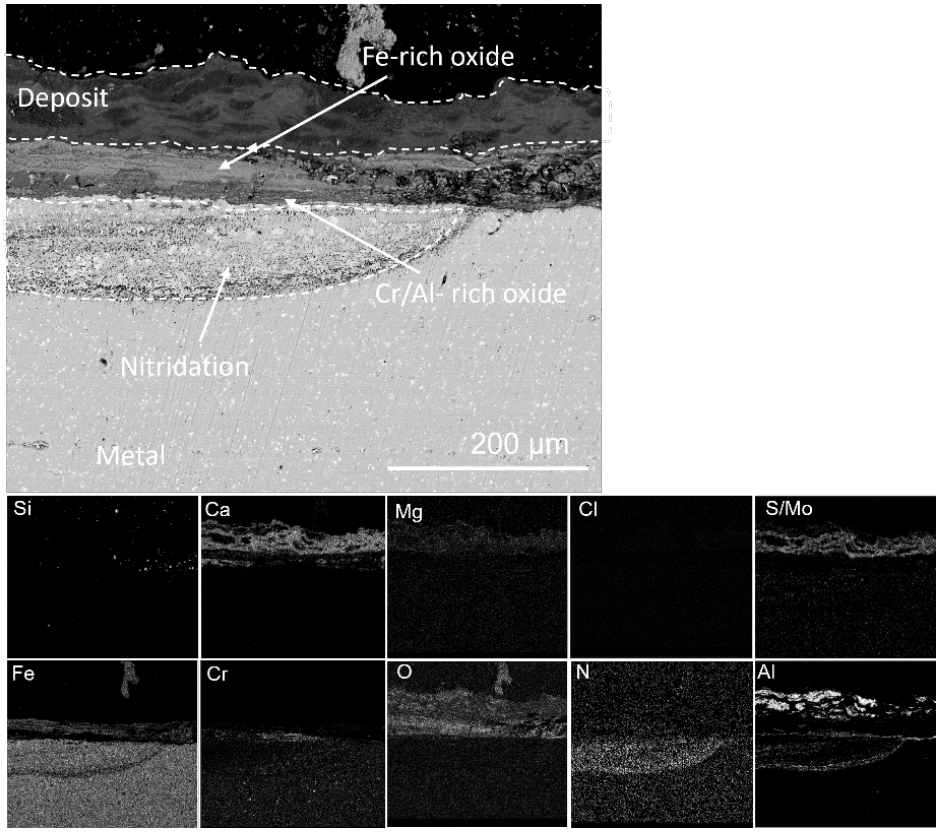

Figure 21. Cross-section and EDX analysis of APMT after 12 months of exposure positioned in row 8.

Figure 22 shows the SEM cross-section and EDX analysis of the APMT sample after 24 months exposure. No traces of deposits were detected. The Fe-rich oxide on the top of the sample reaches a thickness of 300 µm. The sample presents almost a total nitridation of the bulk material but, regardless of that, the material loss after 24 months exposure is still low, with an average value of 0.27 mm/year. As it was explained above, the nitridation zone has not been considered in the material loss calculation.

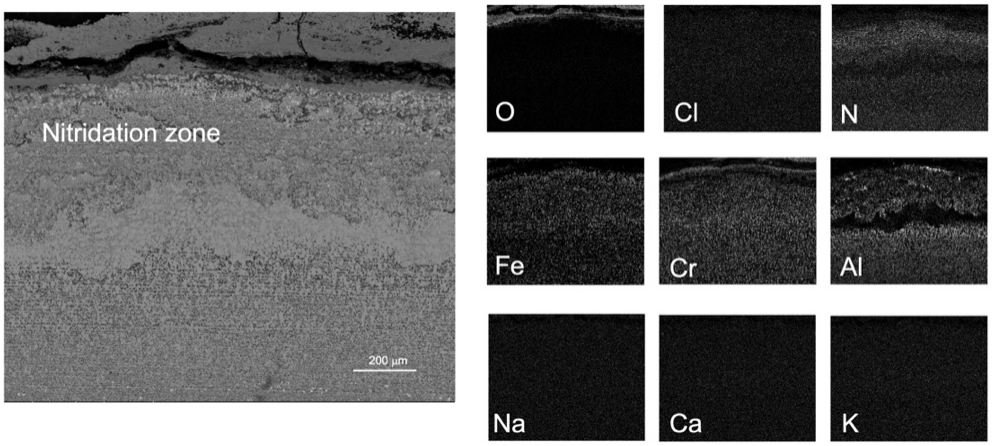

Figure 22. Cross-section and EDX analysis of APMT after 24 months of exposure positioned in row 9.

Figure 23 and Figure 24 show the SEM cross-section image of SX positioned in rows 1 and 8, respectively after 12 months exposure. The material loss analysis concluded that SX showed good resistance toward degradation in the described environment regardless of position (see Figure 11). The highlighted red area in Figure 23 represents the area of interest for the chemical EDX mapping of the sample positioned in row 1. SEM/EDX analysis showed that Ca and Si, together with small traces of S were present on top of the sample, most likely originating from the deposit layer. The corrosion product observed in the cross-section indicates that an internal oxide had been formed that propagated through the sample via grain boundaries to a maximum depth of roughly 70 µm for the sample situated in row 1. Upon detailed EDX point analysis of the internal growing oxide, it was concluded that the oxide mainly consisted of Cr and Si (see Figure 18 to the right). Close to the metal/oxide interface, it was shown that this area was primarily depleted in Cr. At the same time, Ni and Fe remained the main alloy elements in the material matrix. Below the oxide/metal interface, at a depth of roughly 70 µm, small dark precipitates could be observed that were confirmed via EDX point analysis to be Fe-depleted regions.

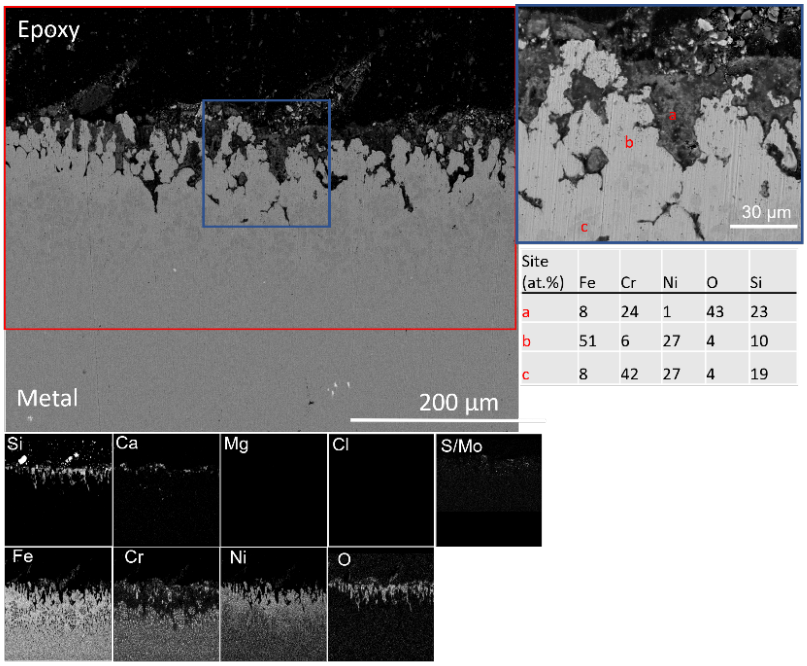

Figure 23. Cross-section and EDX analysis of SX after 12 months of exposure positioned in row 1.

EDX point analysis in highlighted blue area (right) and EDX mapping in highlighted red area. Similar features were observed for the sample in row 8, which aligns well with the material loss results (see Figure 24). A Ca-rich deposit was detected on top of the sample containing traces of Al, S, and Mg.

A Si and Ca-rich oxide was observed at the corrosion front propagating inwards into the bulk material via grain boundaries. A Cr-depletion and Ni enrichment were observed at the metal surface close to the metal/oxide interface.

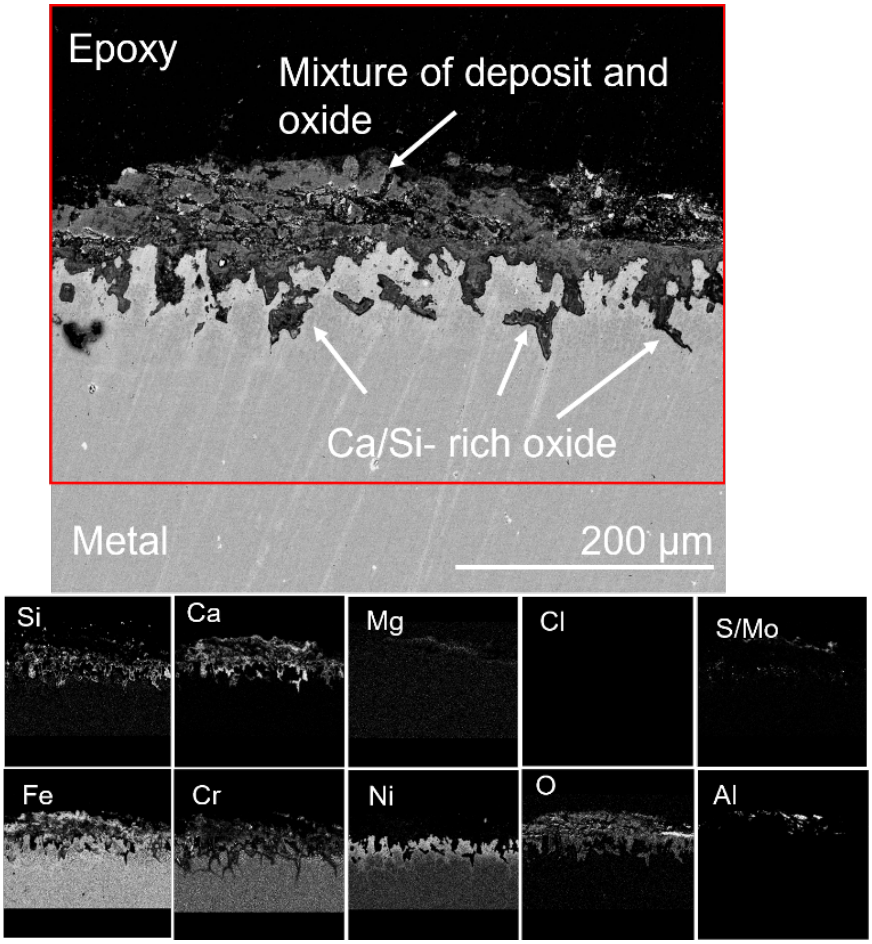

Figure 24. Cross-section and EDX analysis of SX after 12 months of exposure positioned in row 8.

Figure 25 shows the SEM cross-section image and the EDX analysis of the SX positioned in row 9 after 24 months exposure. The Si-rich oxide is still present on the top of the sample after 24 months and the grain boundary attack is around 200 µm thick, in comparison with the 70 µm after the 12 months exposure. This difference in thickness of the grain boundary attack does not seem to affect the material loss, which still was very low (0.05 mm/year) after 24 months and not presenting significant difference compared with this value at 12 months (Figure 13). Some traces of Ca deposit were detected on the top of the oxide scale.

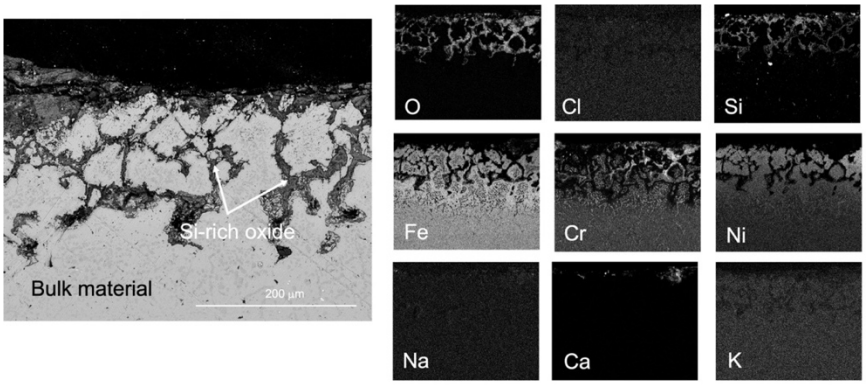

Figure 25. Cross-section and EDX analysis of SX after 24 months of exposure positioned in row 9.

Figure 26 shows the results from the Sanicro 69 sample positioned in row 1. No oxide or deposit was detected on the sample, and only minor material losses were observed. Below the metal/gas interface, a Cr-depleted zone enriched in Ni and Fe was observed, reaching a depth of approximately 150 µm. Further into the material, the alloy composition changed. Cr enrichment was observed at the grain boundaries, while Fe and Ni remained in the bulk matrix. Lastly, as shown in Figure 26 (right), traces of metal chlorides were detected below the Cr-depleted zone. According to EDX analysis, the metal chlorides are suggested to consist of chromium chlorides.

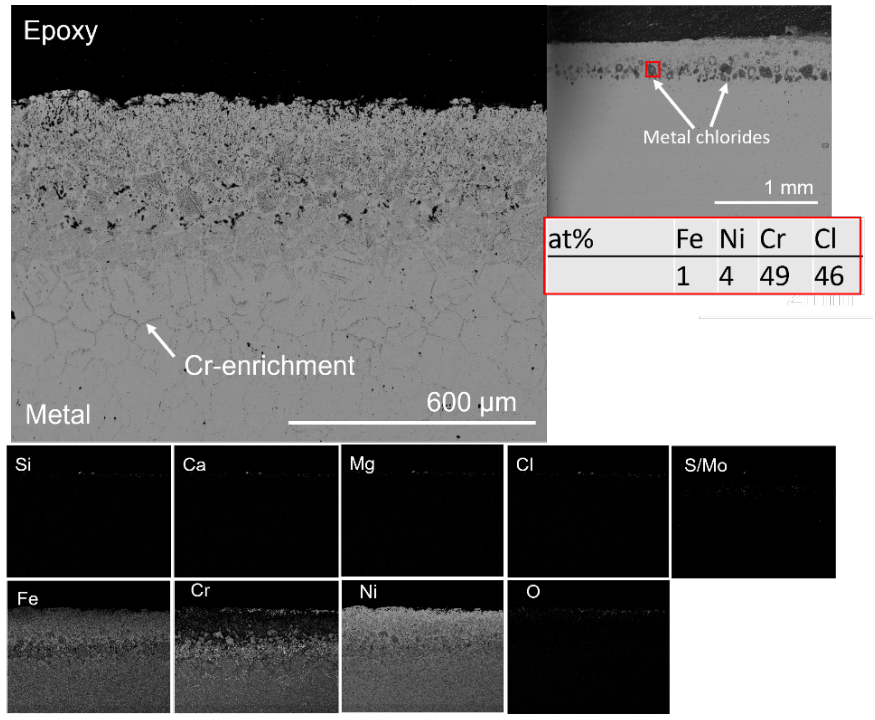

Figure 26. Cross-section of Sanicro 69 after 12 months of exposure positioned in row 1. EDX point analysis of the highlighted red area (right).

The Sanicro 69 sample in row 8 exhibited a roughly 20 µm thin adherent Cr-rich oxide at the material surface (see Figure 27). Similar Cr-depleted zones below the

metal/oxide interface were present as with the sample positioned in row 1. However, compared to the previous sample, a significant increase in metal chlorides was observed below the Cr-depleted zone throughout the cross-section. EDX analysis suggests that the metal chlorides consisted of chromium chlorides.

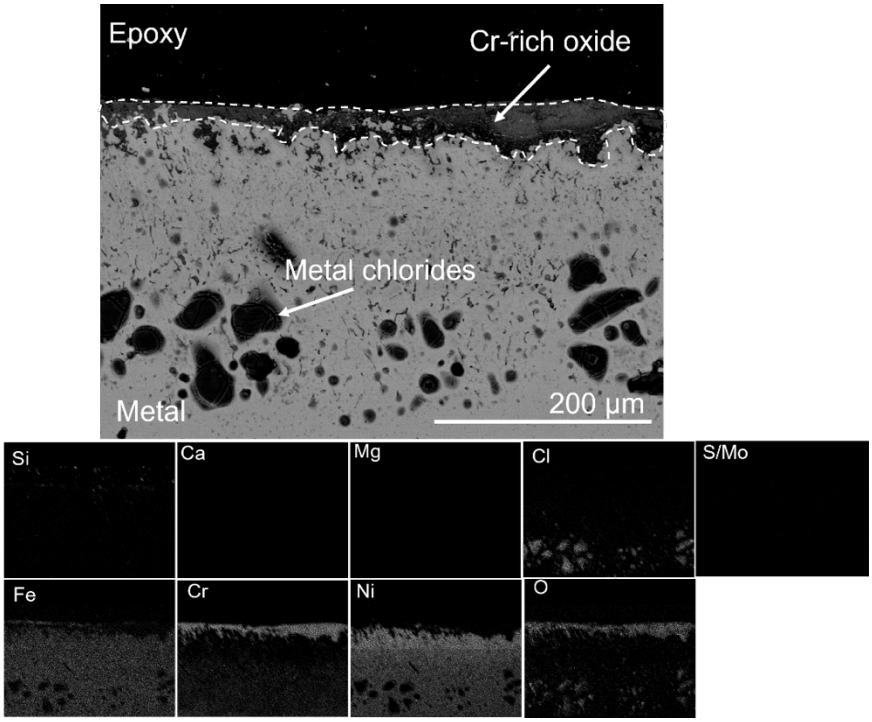

Figure 27. Cross-section and EDX analysis of Sanicro 69 after 12 months of exposure positioned in row 8.

Figure 28 presents the SEM cross-section and EDX analysis of the Sanicro 69 sample after 24 months exposure. The Cr-rich oxide scale is as deep as after 12 months exposure, but no metal chlorides were detected after 24 months. The material loss is still negligible (Figure 13) and some deposit is still detectable on the top of the sample indicating that no oxide scale has been lost during the handling of the samples.

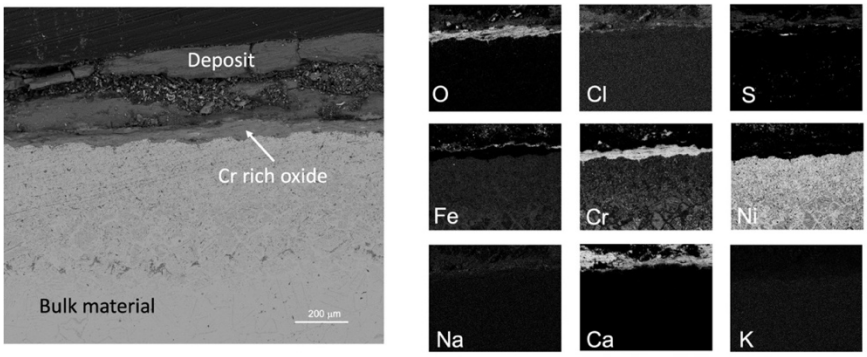

Figure 28. Cross-section and EDX analysis of Sanicro69 after 24 months of exposure positioned in row9.

Figure 29 shows the cross-section SEM image and EDX map analysis for the Esshete 1250 sample situated in row 1 after 12 months exposure. An internal oxide, containing both Cr and Fe, propagating in the grain boundaries of the material, approximately 100 µm deep was observed. No deposit or chlorine compound was detected on the sample as is clearly shown in the EDX map analysis. The remaining alloy elements, such as Ni, tend to stay in the bulk material forming a Ni-rich composition at the corrosion front. Furthermore, below the internal oxide region, a Cr-depleted zone in the grain boundaries was detected propagating in the material.

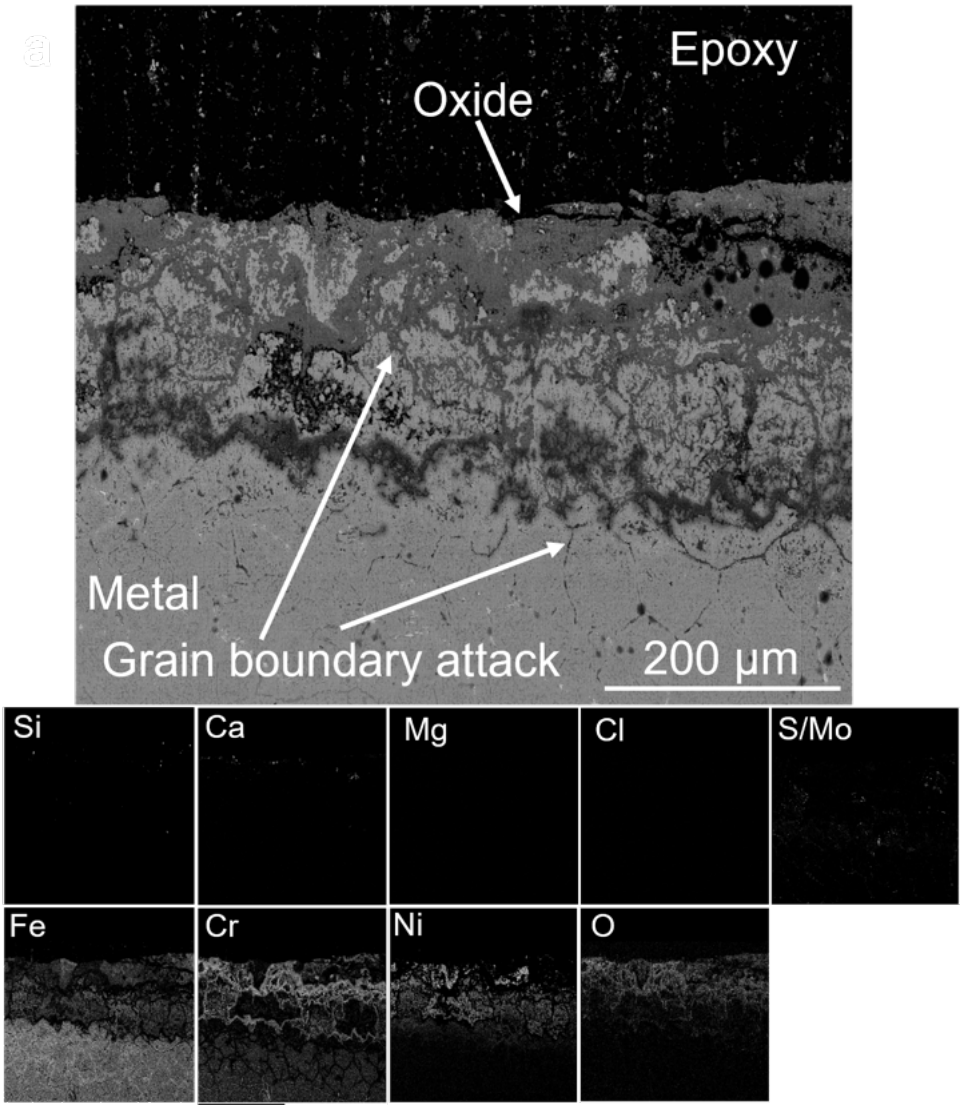

Figure 29. Cross-section and EDX analysis of Esshete 1250 after 12 months of exposure positioned in row 1.

Figure 30 shows the SEM image and EDX mapping of Esshete 1250 positioned in row 8. The degradation mechanism is the same as for the 6 months exposed sample, i.e., internal oxidation propagating within grain boundaries. No deposit was detected on this sample and only minor traces of outward growing oxide remained on the sample. According to EDX analysis the outward growing oxide contained both Fe and Cr. Considering that no adherent outward growing oxide or deposit was detected on the Esshete 1250 sample regardless of position, it is possible that this material is more sensitive to erosion.

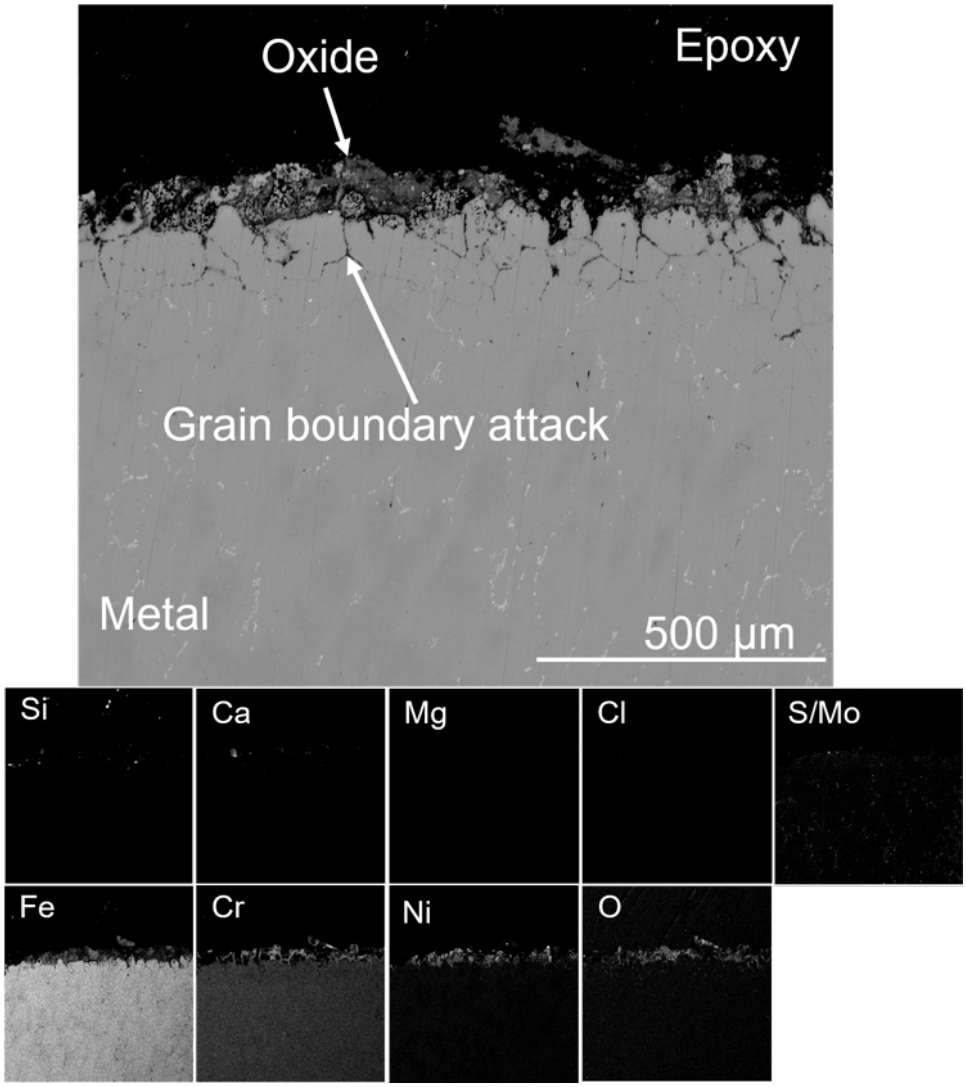

Figure 30. Cross-section and EDX analysis of Esshete 1250 after 12 months of exposure positioned in row 8.

Figure 31 shows the SEM cross-section BSE image of Esshete 1250 after 24 months exposure. The corrosion mechanism is the same as for the previous samples, presenting a clear grain boundary attack on the top of the sample. The depth of the attack is higher this time, around 300 µm. The same occurs with the Cr depleted zone that in this case is around 100 µm thick. No traces of deposit were detected meaning that it was lost during the handling of the samples.

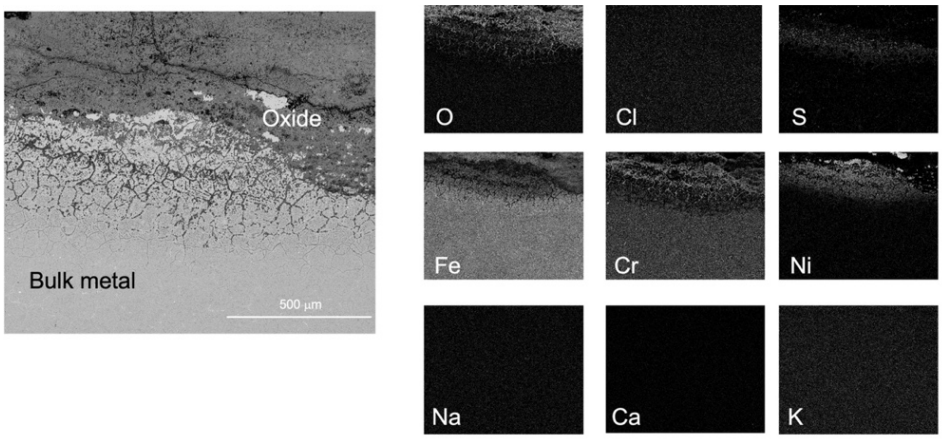

Figure 31. Cross-section and EDX analysis of Esshete 1250 after 24 months of exposure positioned in row 9.

The SEM/EDX cross section of the Sanicro 28 sample is seen in Figure 32. A non-adhesive oxide containing Fe, Cr and Ni was observed on top of the material. No sign of internal oxidation was observed. However, below the metal/oxide interface a roughly 100 µm thick Cr-depleted region was detected in the grain boundaries, leaving a Ni-rich material matrix. At approximately 300 µm in depth the chemical composition changed, and a Cr-enrichment was observed in the grain boundaries.

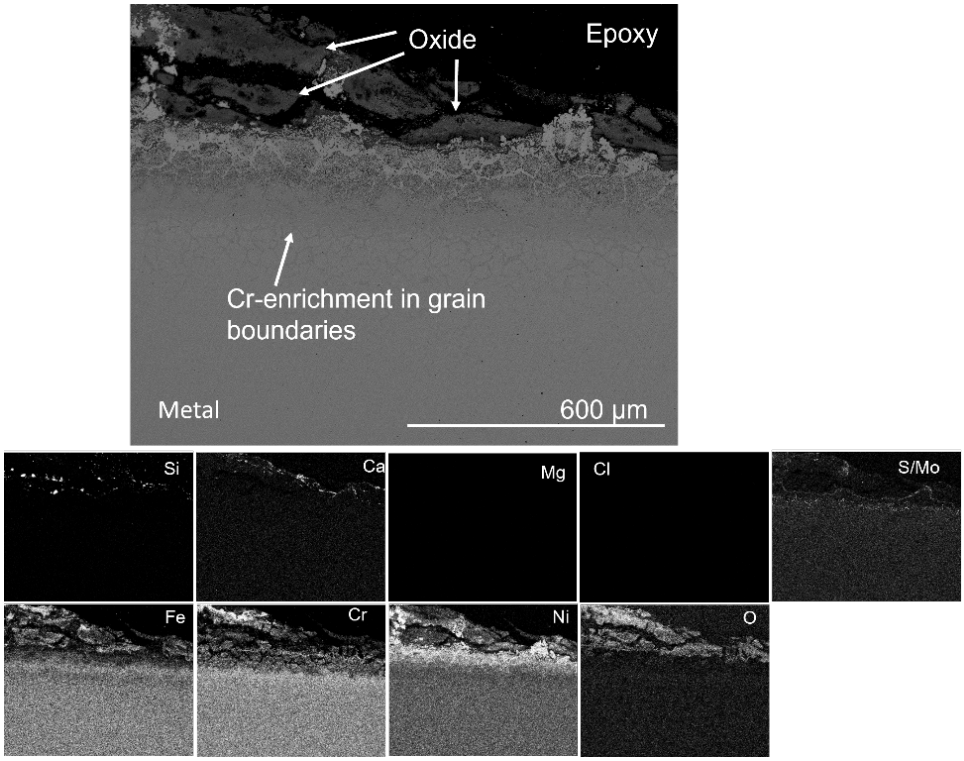

Figure 32. Cross-section and EDX analysis of Sanicro 28 after 12months of exposure positioned in row 8.

Figure 33 and Figure 34 show the SEM cross-section image of 316Ti positioned in row 1 and 8, respectively, after 12 months of exposure. Similar features were observed for both samples. A small amount of remaining outward growing Cr-rich oxide was observed on the sample exposed in row 1. Traces of both Ca and S were observed on top of the material as deposit. The overlap between the L series peak of Mo and the Kα peak of S makes it very challenging to distinguish these elements in EDX mapping. Thus, the signal observed on top of the material should be considered as S and the signal observed in the metal should be regarded as Mo. Both samples suffered from internal oxidation propagating via grain boundaries through the material to a maximum depth of roughly 200 µm and 100 µm, respectively. The remaining material close to the corrosion product consisted of a Ni-enriched region, as is shown in the EDX map for each sample. The chemical composition of the grain boundaries changed drastically after a certain depth through the metal (roughly 50 µm in depth at row 1 and 20 µm in depth at row 8), where initially a Cr-rich oxide was observed close to the metal/oxide interface and at increased depth, a Cr-depletion zone was observed in the grain boundaries leading to an increased concentration of Fe. None of the samples showed traces of deposits on top of the material suggesting that the material is prone to erode in this environment.

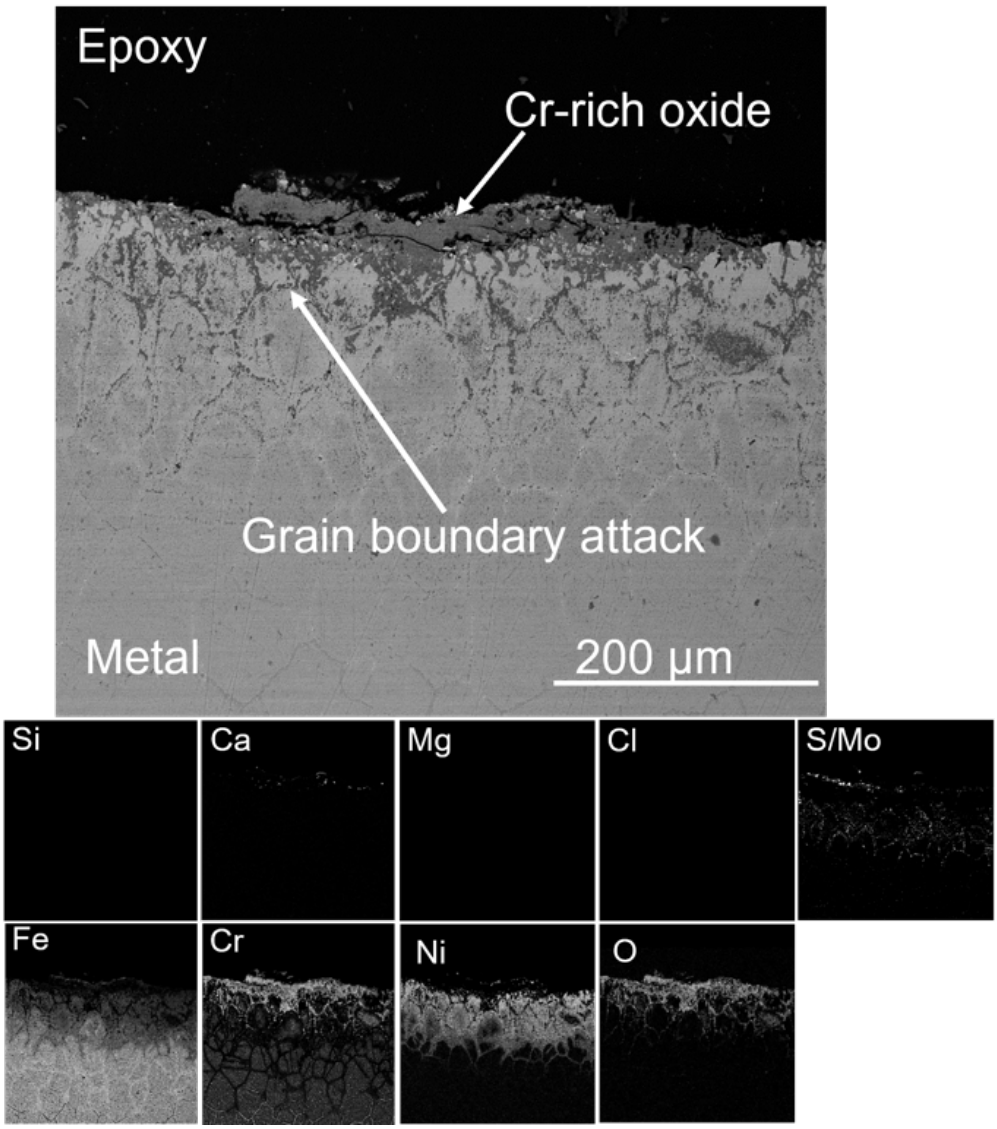

Figure 33. Cross-section and EDX analysis of 316Ti after 12 months of exposure positioned in row 1.

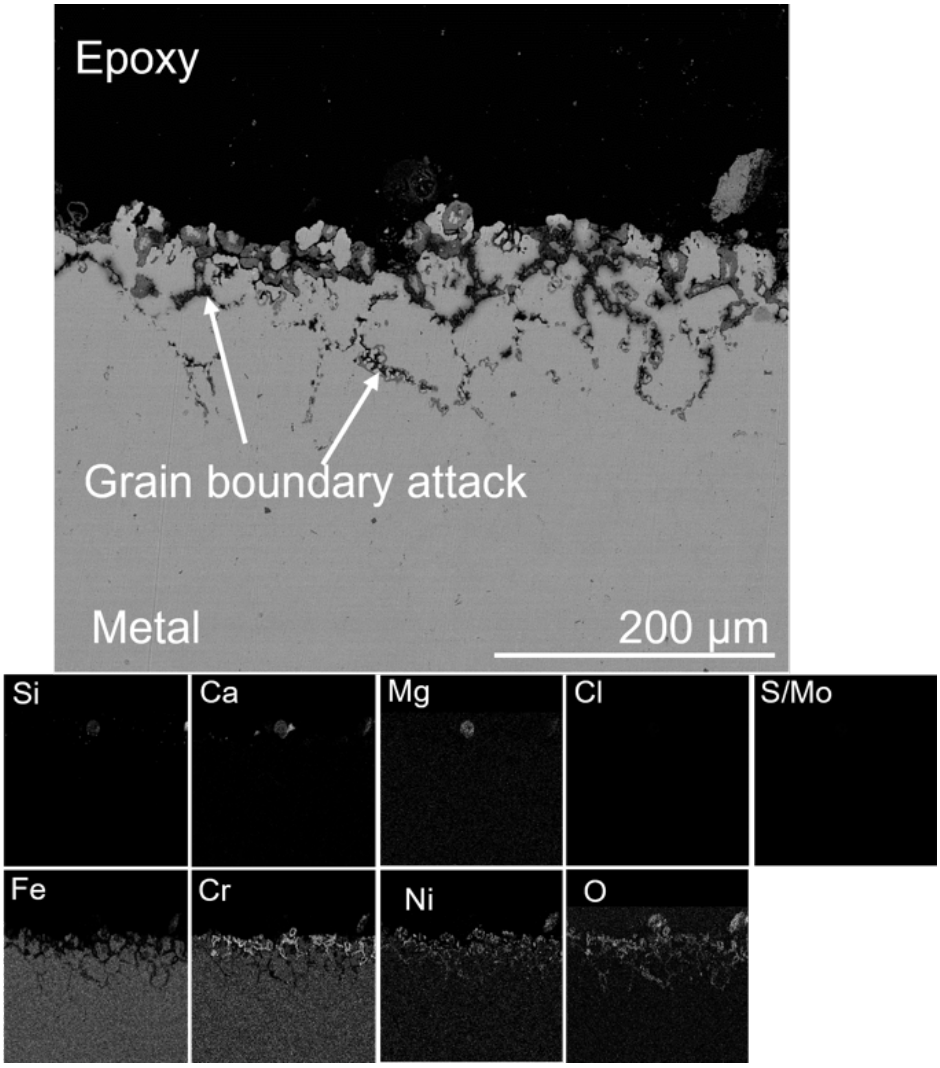

Figure 34. Cross-section and EDX analysis of 316Ti after 12 months of exposure positioned in row 8.

Figure 35 shows the SEM image and EDX mapping of the low alloyed steel 16Mo3 after 12 months of exposure positioned in row 8. The 16Mo3 sample exposed for 24 months was lost during the exposure. As mentioned in the section above, this material suffered from severe material loss. As is shown in Figure 35 and the EDX map below, a slightly undulating surface with minor corrosion products remained adhered to the metal surface. The corrosion product consisted of a Fe-rich oxide poorly adhesive to the material with visible cracks and voids. No signs of deposits nor chloride compounds were observed throughout the cross-section of the sample. However, it is possible that part of the corrosion product and deposit had spalled off during the outtake from the boiler.

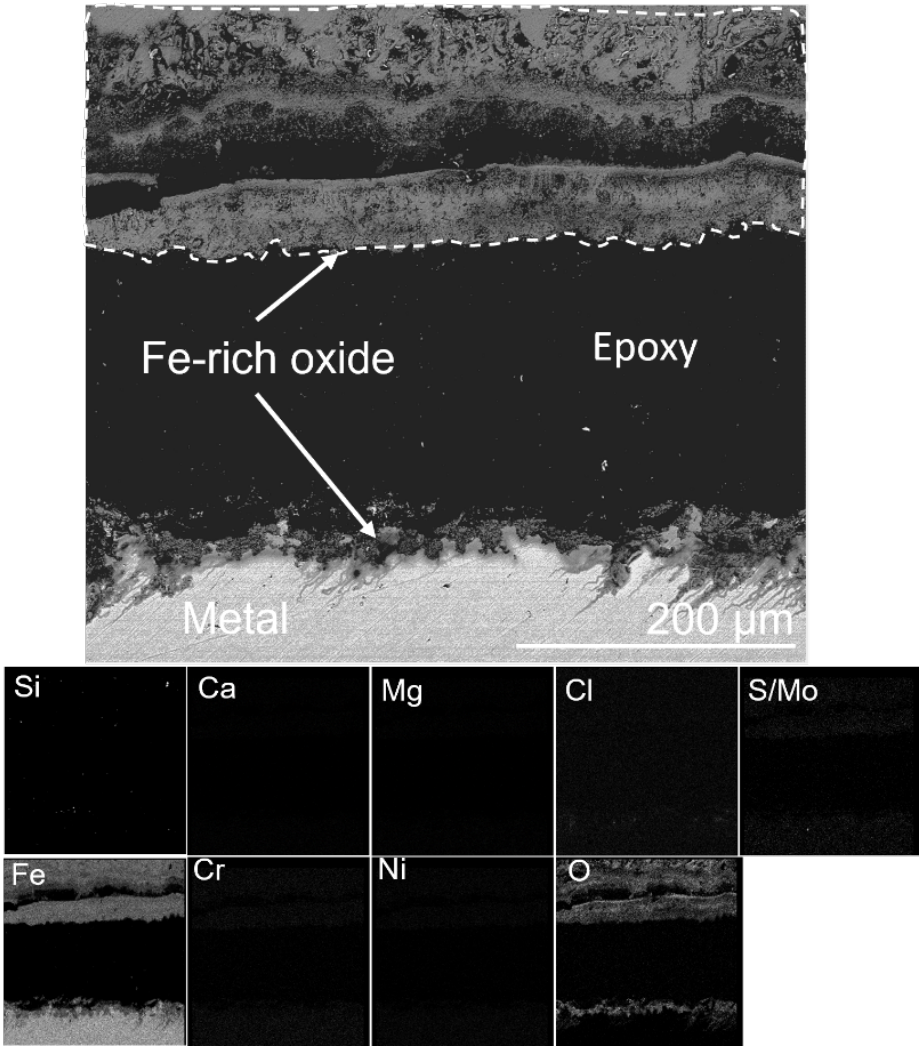

Figure 35. Cross-section and EDX analysis of 16Mo3 after 12 months of exposure positioned in row8.

Figure 36 and Figure 37 show the cross sections of the overlay welded sample Alloy 625 in row 1 and 8, respectively. The welded structure has a characteristic heterogenous surface, which makes accurate material loss measurements challenging. Thus, no material loss measurements were conducted for these samples.

In the case of the overlay welded Alloy 625 sample positioned in row 1, the EDX mapping suggests that a deposit layer containing Ca, Mg, S, O and traces of Cl and Si had been formed on top of a Cr-rich oxide. Traces of internal oxidation were observed below the metal/oxide interface. The internal oxide consisted mainly of Cr-rich oxide and from the EDX mapping analysis it is shown that the remaining material is mostly depleted of Cr, while nickel remains as the main alloy element close to the corrosion front.

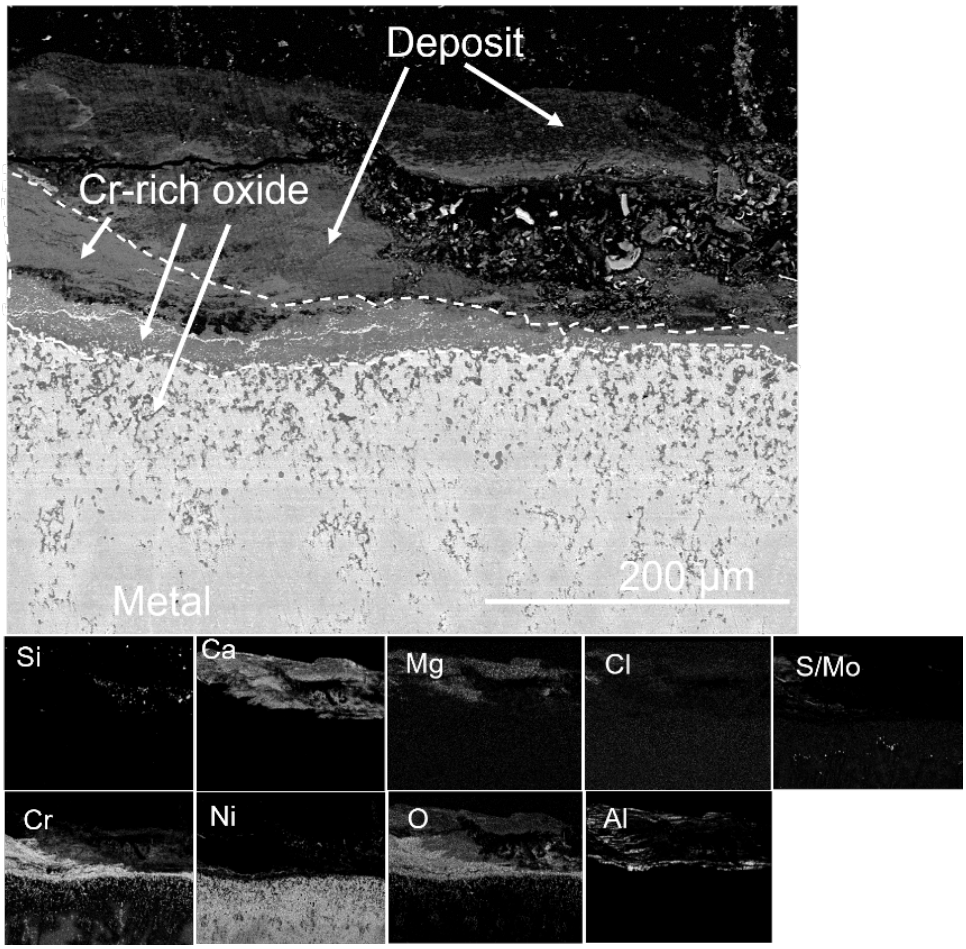

Figure 36. Cross-section and EDX analysis of Alloy 625 overlay weld after 12 months of exposure positioned in row 1.

The SEM/EDX analysis of the weld overlay Alloy 625 positioned in row 8 is shown in Figure 37. A Ca and S rich deposit was observed on the sample and an outward growing oxide containing Ni and Cr rich oxide was detected. Below the metal/oxide interface a roughly 70 µm large Cr-depleted zone was observed.

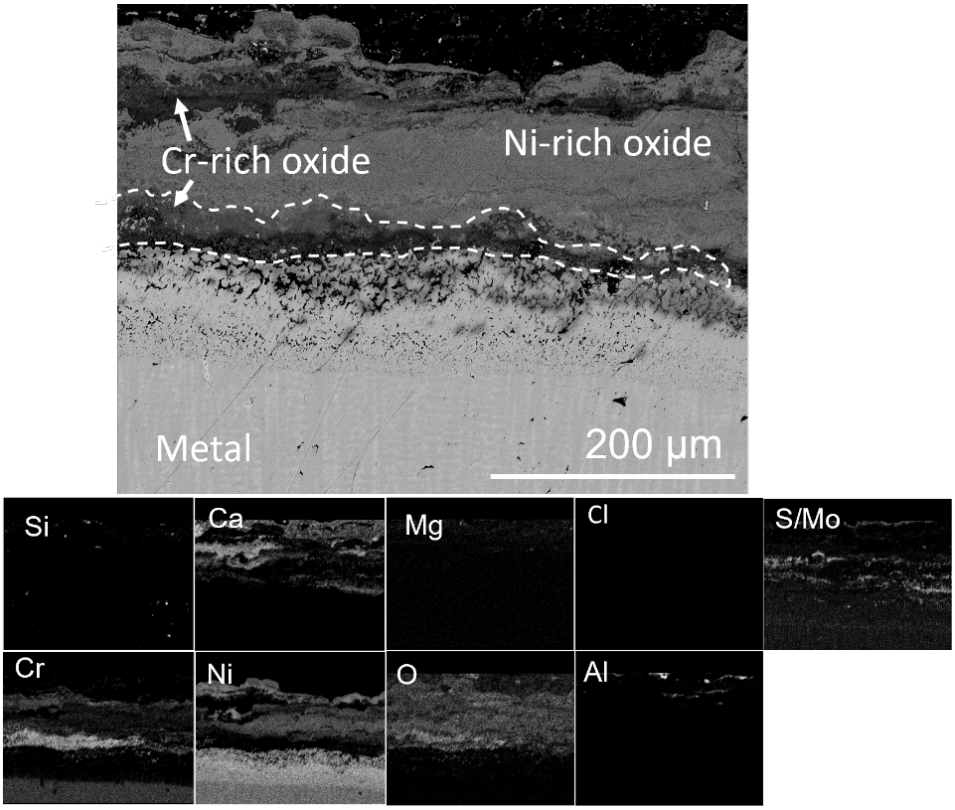

Figure 37. Cross-section and EDX analysis of Alloy 625 weld overlay after 12months of exposure positioned in row 8.

Figure 38 presents the SEM cross-section and EDX analysis of the Alloy 625 overlay weld sample after 24 months exposure. A layer of deposits containing Cl is still present on the top of the sample. The Cr-rich oxide scale is around 100 µm thick. This value is not higher than after the 12-month exposure, indicating a good corrosion behavior.

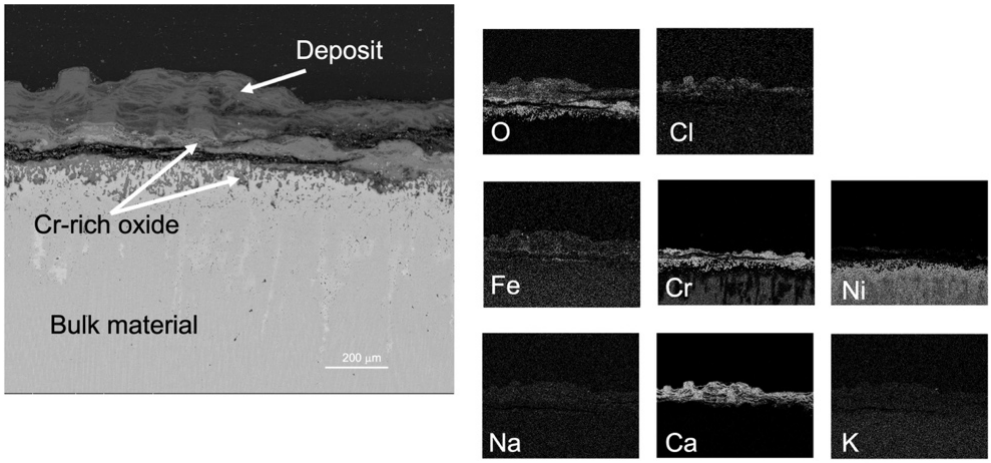

Figure 38. Cross-section and EDX analysis of Alloy 625 weld overlay after 24 months of exposure positioned in row 9.

Exposures were conducted on three different coated materials in row 8. The SEM/EDX analyses of the two APMT-coated materials, APMT20c and APMT50c, are shown in Figure 39 and Figure 40. The results reveal inferior performance for both coatings, as none of the coated material remained attached to the base material after exposure (see EDX map and point analysis in each Figure). In addition, both samples observed corrosion features such as internal growing oxide, indicating that the coating failure might have occurred at an early stage of exposure.

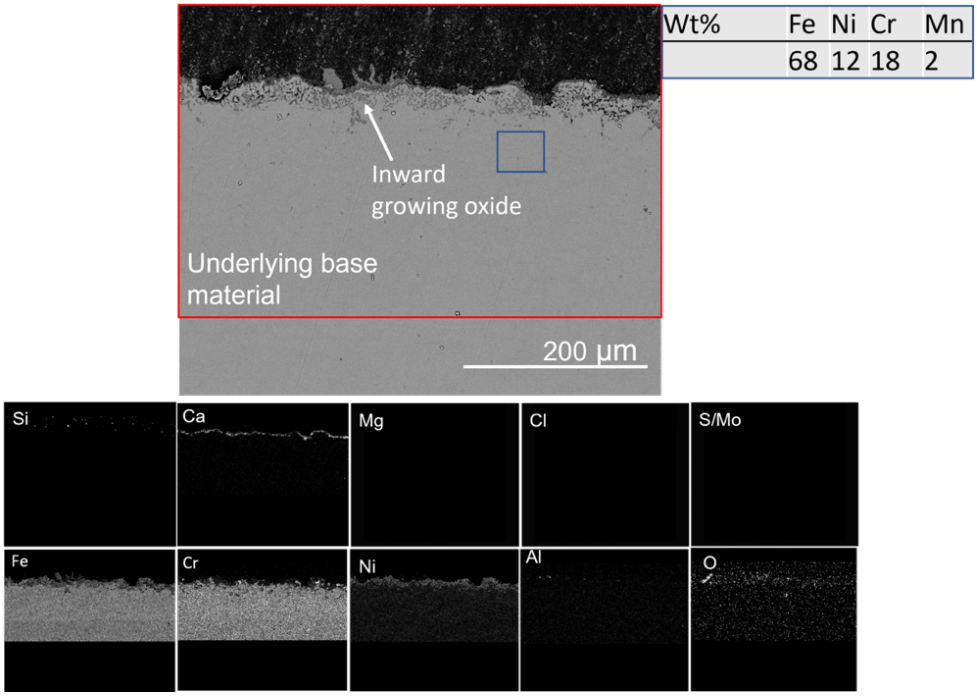

Figure 39. Cross-section and EDX analysis of APMT20c coating after 12 months of exposure positioned in row 8. EDX point analysis of the highlighted blue area (right).

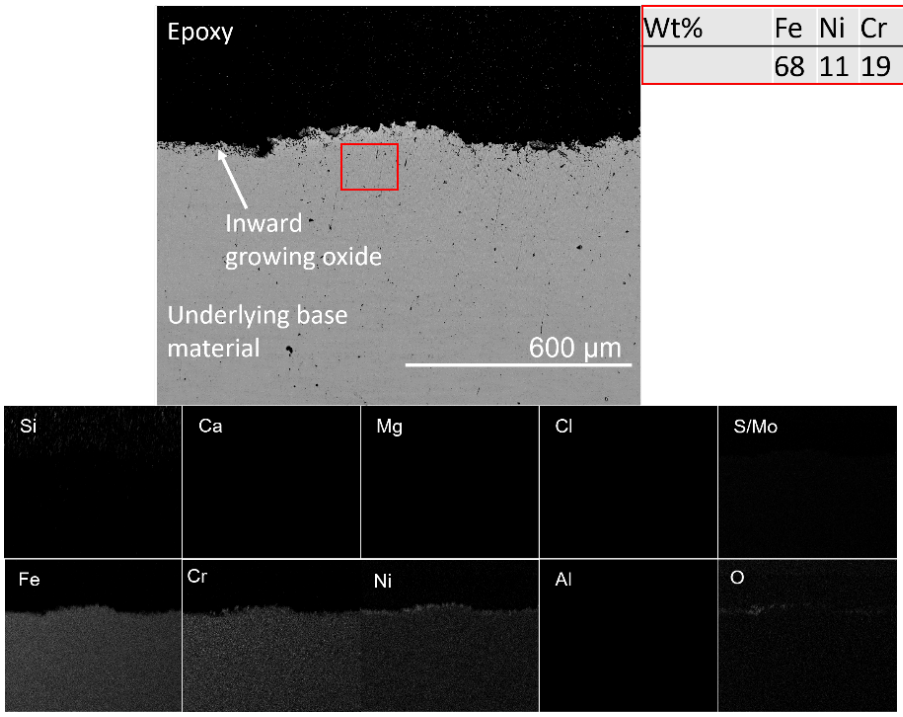

Figure 40. Cross-section and EDX analysis of APMT50c coating after 12 months of exposure positioned in row 8. EDX point analysis of the highlighted red area (right). EDX mapping of highlighted red area (below).

Figure 41 shows the SEM cross-section image of the CorEr-coated material exposed in row 8. No sign of the coated material was detected throughout the cross-section, indicating severe coating failure. Moreover, the underlying base material had similar corrosion features as the APMT-coated samples, indicating that the coating failure might have occurred early in the exposure.

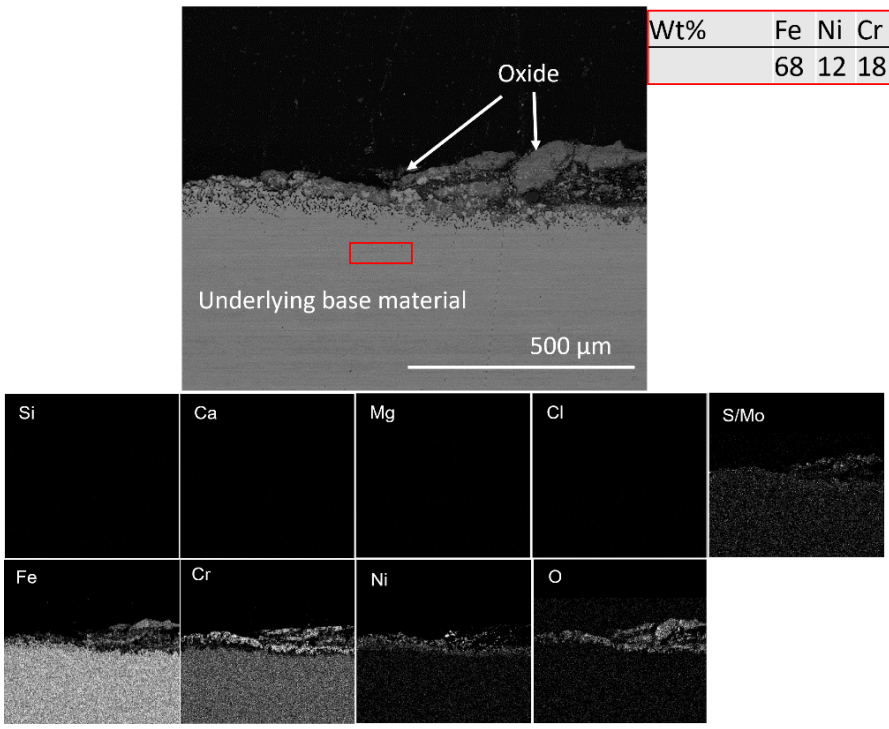

Wt%	Fe	Ni	Cr	Mn
	68	12	18	2

Figure 41. Cross-section of CorEr coating after 12 months positioned in row 8. EDX point analysis of the highlighted red area (right).

4.3.2 Clamp exposures on FBHE - Händelö P15

Clamp exposures were conducted on FBHE in the P15 waste-fired boiler in Händelö in continuous mode lasting for 6 and 12 months. As it was explained in P6 Högdalen exposures presented above, the exposure times include the planned shutdowns of the boiler. The samples were mounted as two half-moon rings on the fluidized bed heat exchanger. In this study, the wind side samples, i.e., the half-moon samples facing down towards the loop seal air nozzle, were analyzed in the superheater 2 position.

Material loss

A summary of the material loss for the different materials and time intervals are shown in Figure 42. The filled circle for each data set represents the arithmetic mean value of the material loss.

The conventional austenitic stainless steels, 316Ti and Esshete 1250, exhibited severe material loss after 6 months of exposure reaching average values of roughly 0.68-0.73 mm respectively. The Esshete 1250 sample had quite a large spread in material loss data ranging from 0.5-1.1 mm indicating that local attacks play an important role in this set of environments. The material loss rate for these samples was reduced with time, which might occur if corrosive attacks are slowed down after the initial attack. The high Si-containing austenitic stainless steel SX outperformed all samples and obtained a maximum material loss of 0.07 mm and 0.3 mm after 6 and 12 months respectively.

All three alumina forming materials outperformed the majority of the other samples after 12 months of exposure, SX being the exception. EF100 performed better compared to the conventional APMT and the EF101 material, reaching a maximum material loss of 0.28 mm/year which was lower than the average material loss of the SX sample. The material loss data show great variation for EF101 and APMT, which again suggests that local degradation mechanism may occur in this set of environments.

The Ni-base alloy Sanicro69 showed large variation in performance over time (from negligible after 6 months to roughly 1mm/year in average loss). Lastly, the CorEr coating obtained an average material loss of 0.32 mm and a maximum material loss of 0.8 mm after 6 months of exposure indicating that severe local attacks had occurred during exposure.

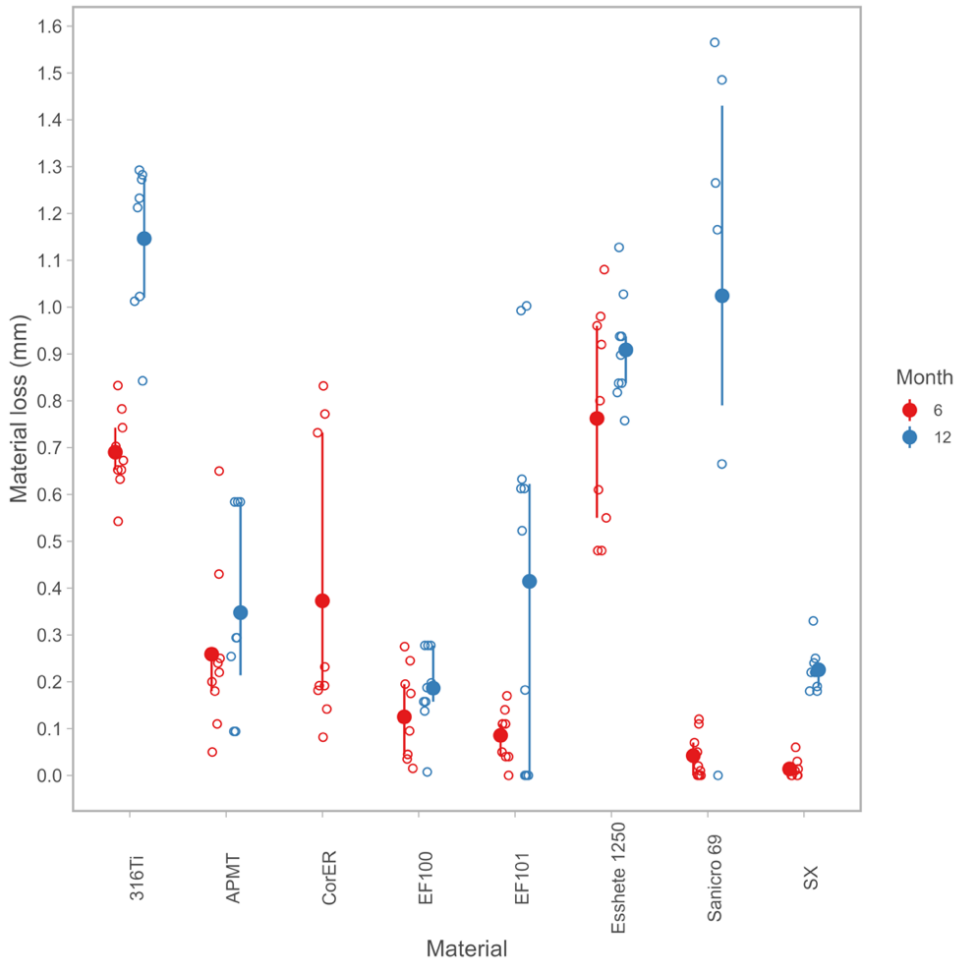

Figure 42. Material loss of the tested clamps exposed for 6 and 12 months in the fluidized bed heat exchanger positioned in superheater 2, P15 boiler, Händelö.

Microstructure analysis

An SEM cross-sectional view of the EF100 sample exposed for 6 months is shown in Figure 43 (a). An approximately 250 µm thick deposit was observed, consisting primarily of S, Ca and O. Beneath the deposit layer, an approximately 100 µm thick iron oxide had formed. The oxide contained small cracks and displayed void formation, whereas it was difficult to distinguish regions of inward and outward oxide layer formation. An Al/Cr-rich thin oxide layer was detected across the metal/oxide interface (see Figure 43(b)). The SEM analysis revealed no indications of internal oxidation. However, a nitridation zone can be seen below the metal/oxide interface. The thickness of the region varied greatly (between 0-200 µm) and was observed in a patch wise fashion throughout the cross section of the sample.

EF100 displayed similar features after 6 and 12 months of exposure (see Figure 43a) and Figure 44a)). However, for the sample exposed for 12 months, most of the deposit layer had spalled off. This may be an effect of sample outtake and subsequent sample preparation for post-analysis. A Fe-rich oxide was observed (about 600 µm in thickness) containing voids and cracks and traces of Cr and Al. The nitridation zone had also grown larger compared to after 6 month of exposure (about 400 µm in thickness for the 12 months sample) and was observed throughout the cross section of the sample in a homogenous fashion. The EDX analysis confirmed that the dark particles shown in the nitridation zone consisted of Alumina Nitride (AlN) precipitates embedded in a Fe-rich alloy matrix. The observed microstructures and corrosion attacks agree well with the measured material losses. The material loss for EF100 after 6 and 12 months was 0.13 and 0.19 mm, respectively. The SEM/EDX analysis after 12 months of exposure also shows that a region (roughly 125 µm thick) depleted in Cr was detected at the nitridation/metal interface (see Figure 44b). This Cr-depletion zone was homogenous and observed throughout the sample. No Cl was detected in the corrosion front nor in the deposit.

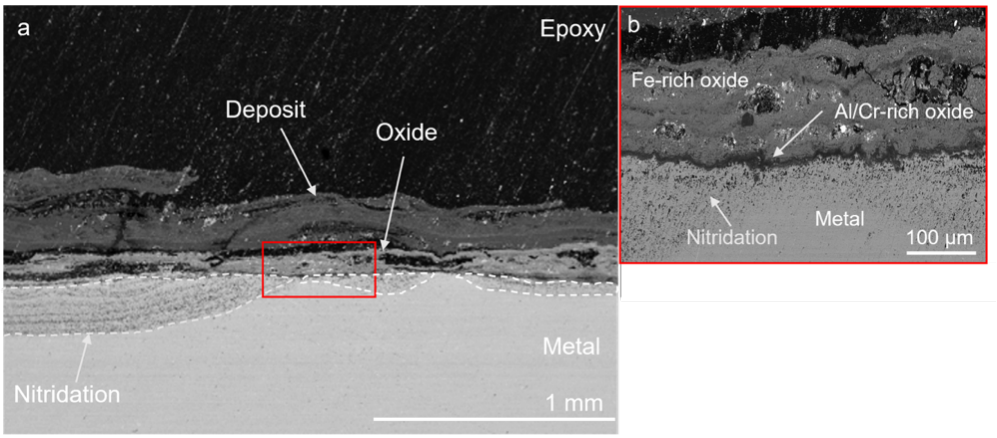

Figure 43. (a) SEM BSE cross-section image of EF100 after 6 months of exposure. (b) Higher magnification of the marked area in (a).

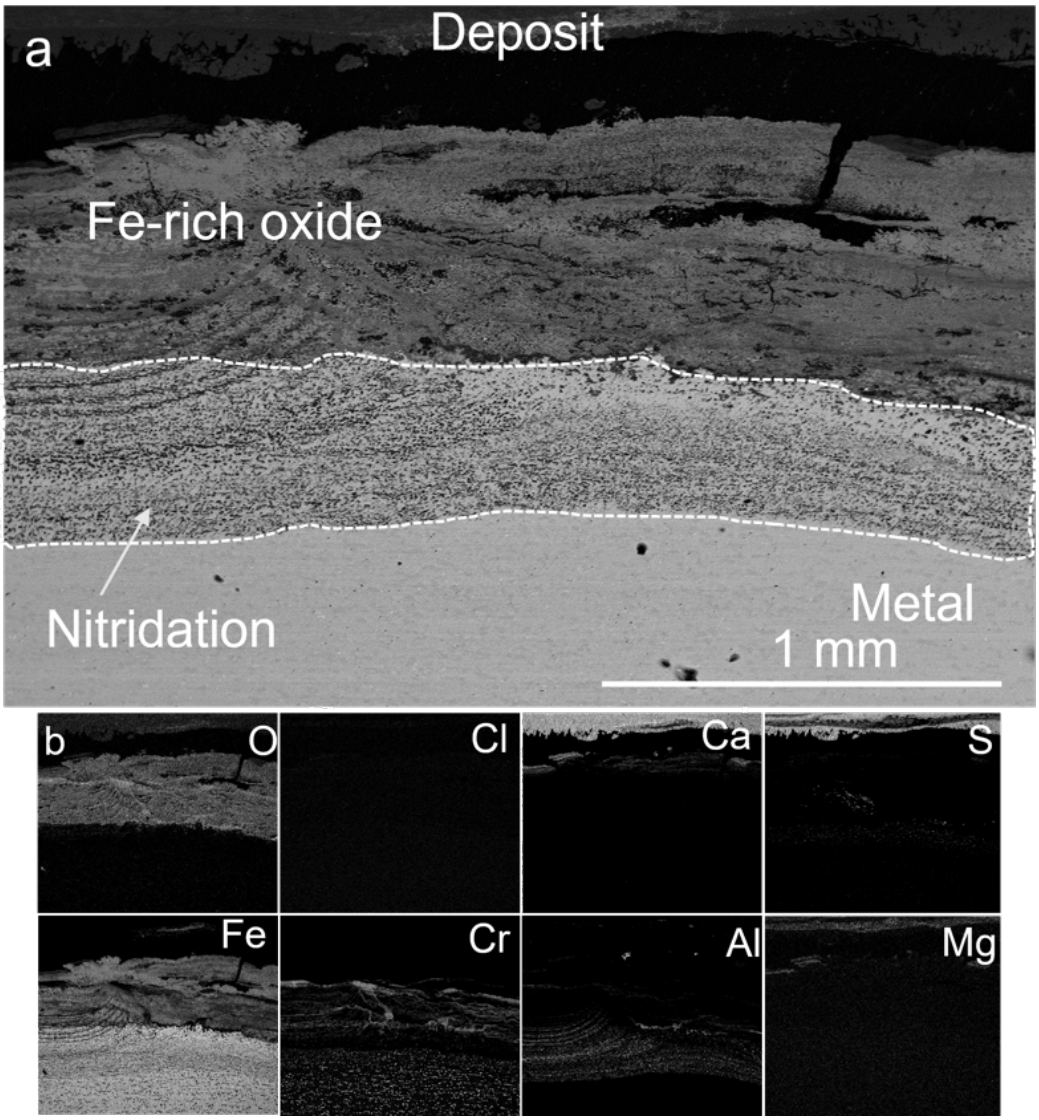

Figure 44. SEM BSE cross-section image of Ef100 (a) after 12 months of exposure. (b) EDX mapping of (a).

EF101 displayed similar features as EF100 after 6 months of exposure (see Figure 45 (a)). The EDX map analysis of EF101 presented in Figure 45(c) shows that a thin deposit layer (about 25 μm in thickness) had formed above the oxide layer containing large amounts of Ca. In addition, no traces of chlorine containing chemical species were observed throughout the cross section. The oxide scale was composed of an Fe-rich oxide containing cracks and voids (see Figure 45(b)) and traces of Cr rich oxide were observed, but to a lower extent. A thin Al-rich oxide layer (about 8 μm) at the metal/oxide interface was observed. In addition, below the metal/oxide interface a Cr-depleted zone of approximately 100 μm was seen. Compared to EF100, the EF101 sample exhibited a more pronounced nitridation zone. The thickness of the nitridation zones were 450 μm and 200 μm for EF101 and EF100, respectively after 6 months.

Figure 46 presents the SEM/EDX analysis of the EF101 after 12 months of exposure. Only traces of deposit have been detected after the exposure. The corrosion mechanism agrees with the behavior observed after the 6-month exposure (Figure 45). An approximately 100 µm thick Fe-rich oxide layer is present homogeneously on the top of the sample and a Cr-rich oxide is formed below, followed by a Cr-depleted zone. The nitridation zone is also present all around the sample after the 12-month exposure, but it does not seem to increase in thickness compared with the 6-month exposure.

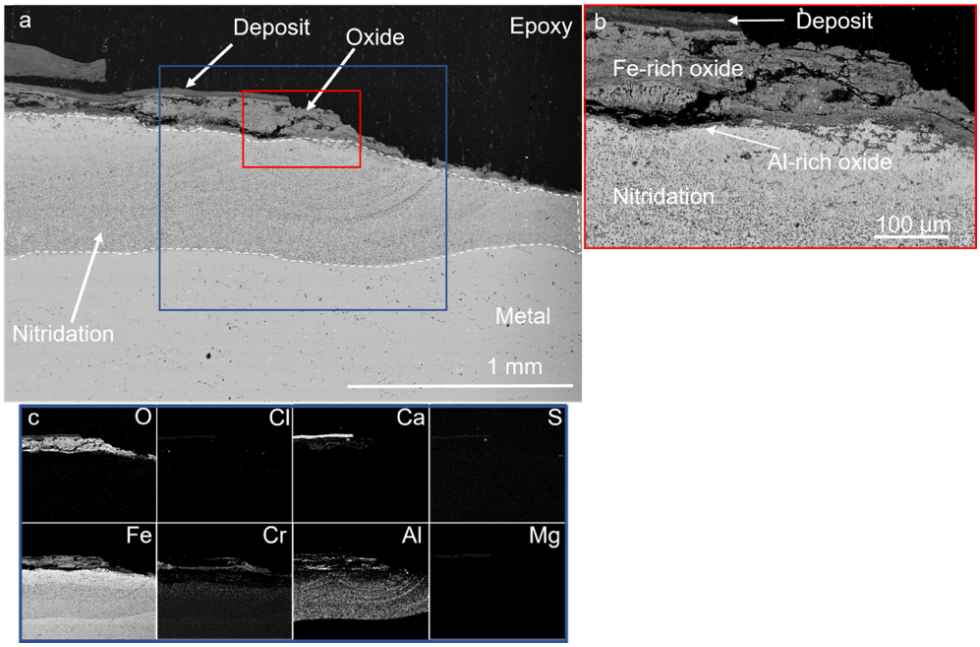

Figure 45. SEM BSE cross-section image of Ef101 (a) after 6 months of exposure. (b) Higher magnification of the marked area in (a). (c) EDX mapping of (a).

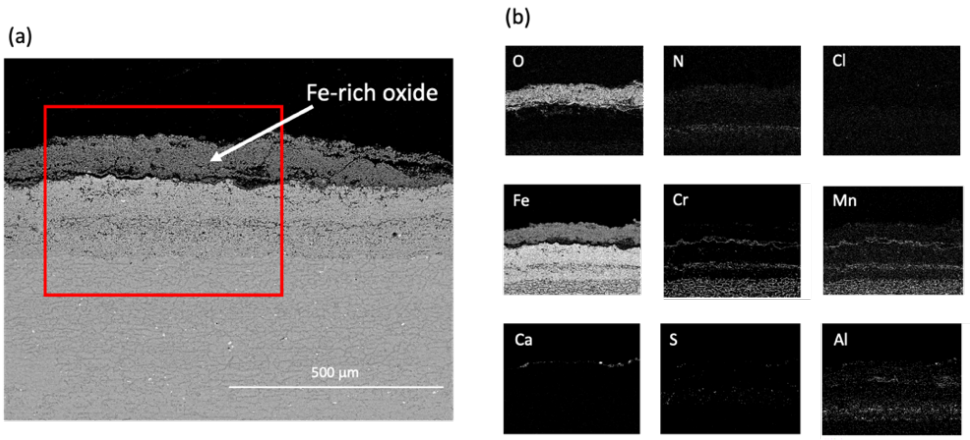

Figure 46. SEM BSE cross-section image of EF101 (a) after 12 months of exposure. (b) EDX mapping of (a).

Figure 47 and Figure 48 shows the SEM cross section of Kanthal APMT sample after 6 months and 12 months of exposure. A discontinuous Fe/Cr-rich oxide was detected at the metal/oxide interface with a thickness between 7-20 µm, followed by a roughly 50 µm outward growing Fe-rich oxide after 6 months of exposure. Thus, similar microstructure features were detected as with the novel FeCrAl alloys (see figure 38-40). However, as is shown in figure 52a, extreme nitridation of this sample was detected, exceeding over 1mm in thickness. The nitridation zone for APMT after 6 months was close to four times greater than the novel FeCrAl alloys EF100 and EF101.

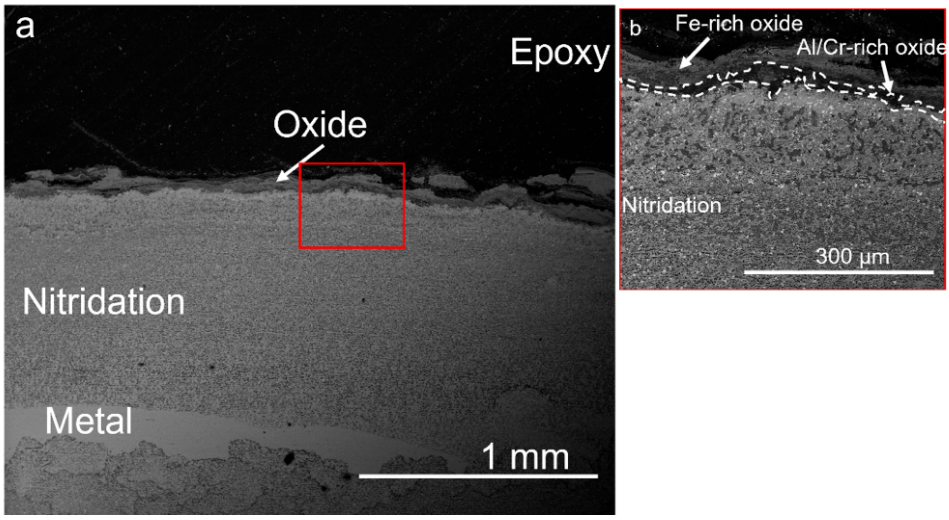

Figure 47. SEM BSE cross-section image of APMT after 6 months of exposure. (b) highlighted red area from (a).

Figure 48 shows the Kanthal APMT sample after 12 months of exposure. According to EDX analysis a discontinuous deposit layer had formed on top of the sample containing large amounts of Ca and traces of P and Cl. Regarding the oxide scale, similar features were observed as for the sample exposed for 6 months, i.e., a roughly 200 µm thick outward growing Fe-rich oxide was detected below the deposit followed by a Cr/Al-rich oxide. The Cr/Al rich oxide close to the metal/oxide interface was not as easily detected as compared to the sample exposed for 6 months. Lastly, severe nitridation was observed for this sample reaching a thickness of roughly 800 µm, albeit not as severe as for the sample exposed for 6 months.

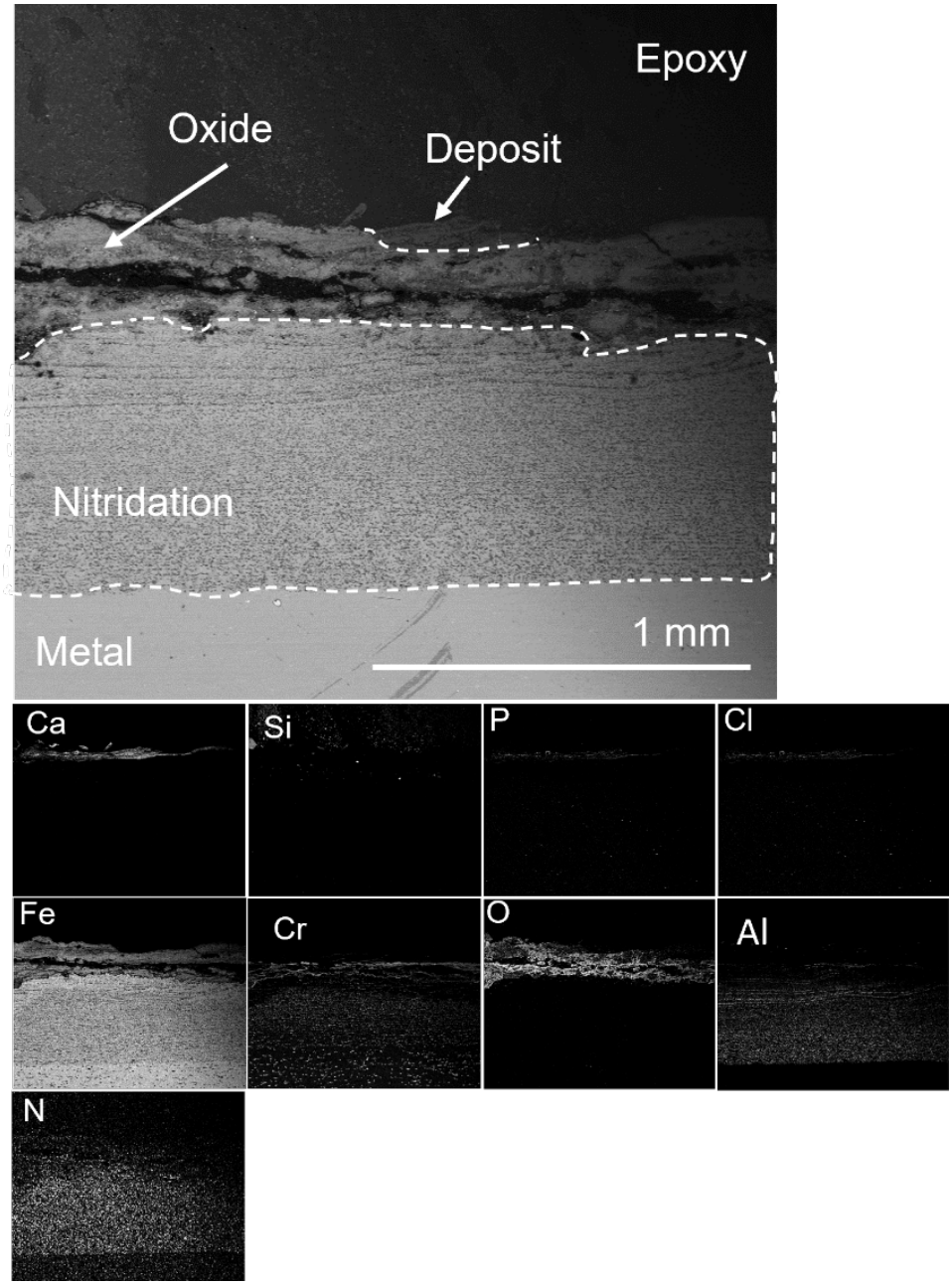

Figure 48.(a) Kanthal APMT sample after 12 months of exposure in SH2 (b) EDX analysis.

Figure 49a and b show the cross-section of the SX samples exposed for 6 and 12 months. Similar features were observed for both samples. Thus, chemical analysis via EDX mapping is only shown for the sample exposed for 12 months. A homogenous deposit layer was observed on both samples and consisted mainly of Ca, S, O, and traces of Na. In addition, traces of Cl were detected in the inner regions of the deposit. The thickness of the deposit was in the order of 60 and 50 μm for 12 and 6 months. The SX material formed an adherent outer corrosion product layer composed mainly of an Fe-rich oxide (see Figure 49c). The outer oxide layer became less adherent with time, which is displayed when comparing Figure 42 a and b, where cracks were observed after 12 months of exposure. As

with 316Ti, grain boundary attacks were noticeable after 6 months of exposure and became more severe with time. The internal oxidation at the metal/oxide interface consisted mainly of a Cr and Si-rich oxide propagating via grain boundaries through the material. After 12 months of exposure, at roughly 60 μm, a Cr-depletion was observed at the grain boundaries together with Fe-enrichments at the border of the grain boundaries.

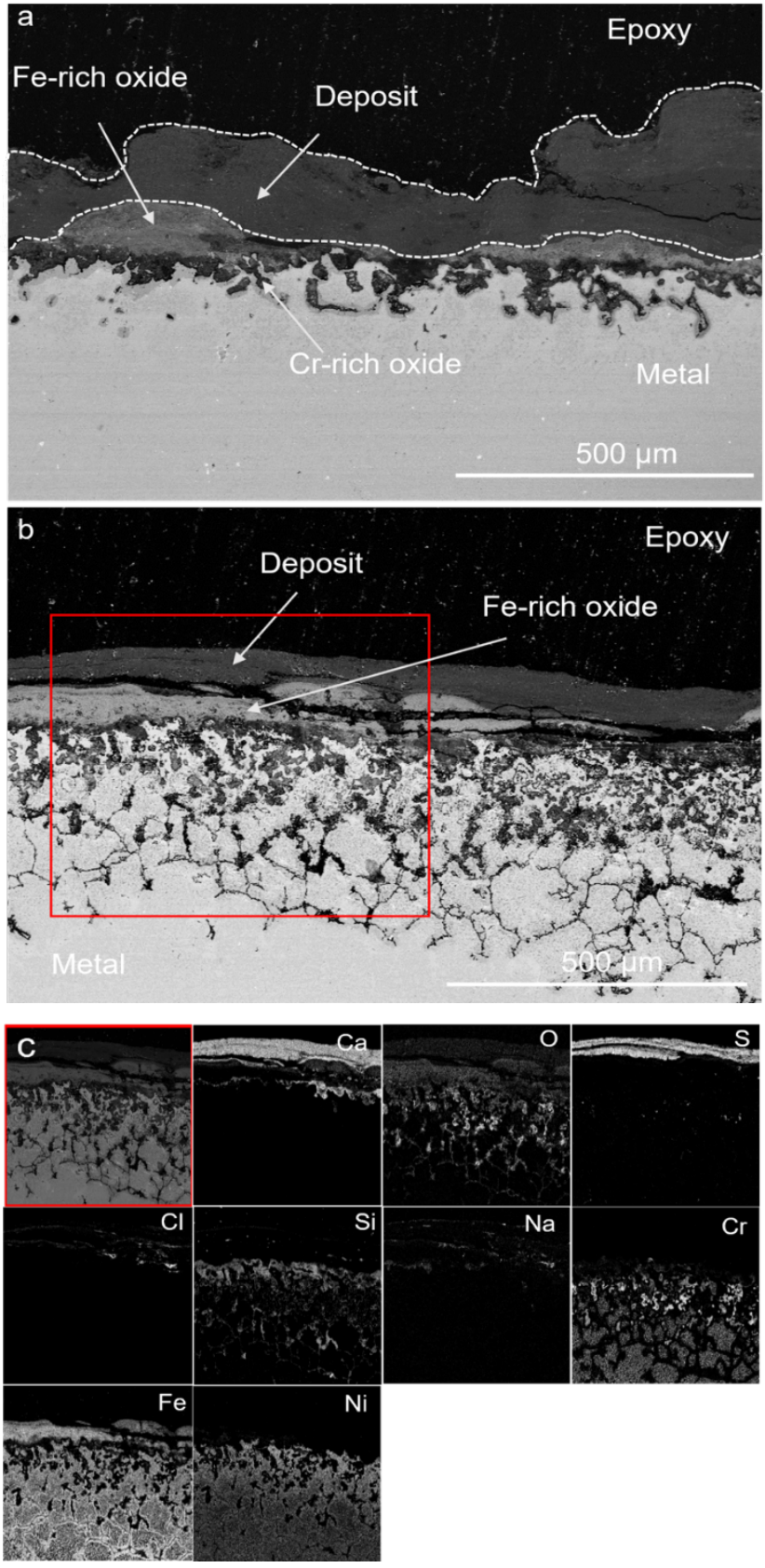

Figure 49. SEM BSE cross-section image of SX after (a) 6 months of exposure (b) 12 months of exposure (c) EDS mapping of SX from highlighted area in (b).

Figure 50 shows a cross-section region of the Sanicro 69 sample after 6 months of exposure. An approximately 50 μm thick deposit layer was observed containing mainly S, Ca, and O with traces of P and Mg. No significant deposit components were identified in the formed oxide scale (see Figure 50b). Furthermore, the EDX mapping showed that a Ni-rich oxide was formed underneath the deposited layer, and at the metal/oxide interface, a Cr-rich oxide was detected. In addition, a Cr-rich oxide was also detected further into the metal as an internal oxidation region approximately 80 μm below the corrosion product layer. This feature is presumably a 3D effect of this 2D cross-section imaging. From the EDX mapping, it can also be observed that the metal is mainly depleted of Cr, while nickel remains the main alloy element in the material matrix close to the corrosion front. The material loss measurement of San69 was negligible after 6 months of exposure. However, based on the SEM/EDX analysis, the internal corrosion attack can be seen up to 0.3 mm into the metal.

Figure 51a shows the cross-section of the Sanicro 69 material after 12 months of exposure. The corrosion mechanism is the same as in the 6-month exposure presenting a Cr-rich oxide on the top of the Ni-rich oxide. Nevertheless, the corrosion attack is much higher this time. The thickness of the oxide after the 12-month exposure is over 500 μm and the material loss is 1.01 mm/year in average. The EDX analysis presented in Figure 51b shows that no deposit was detected after the 12 months exposure. This indicates that the outer part of the oxide might have been lost during exposure or during the handling of the samples. This explains the absence of Fe-oxide at the top of the oxide scale.

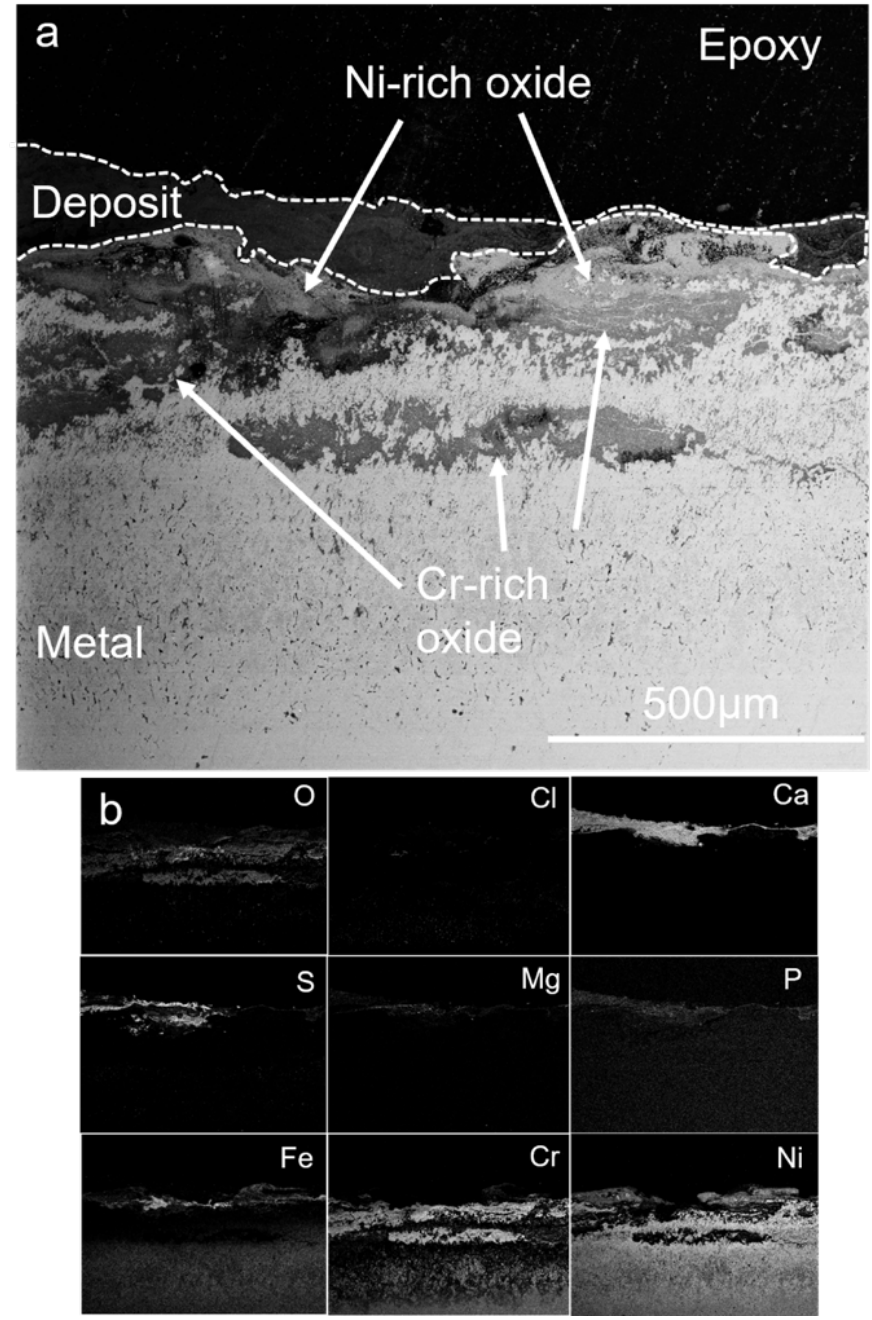

Figure 50. SEM BSE cross section image of San69 (a) after 6 months of exposure. (b) EDX mapping of (a).

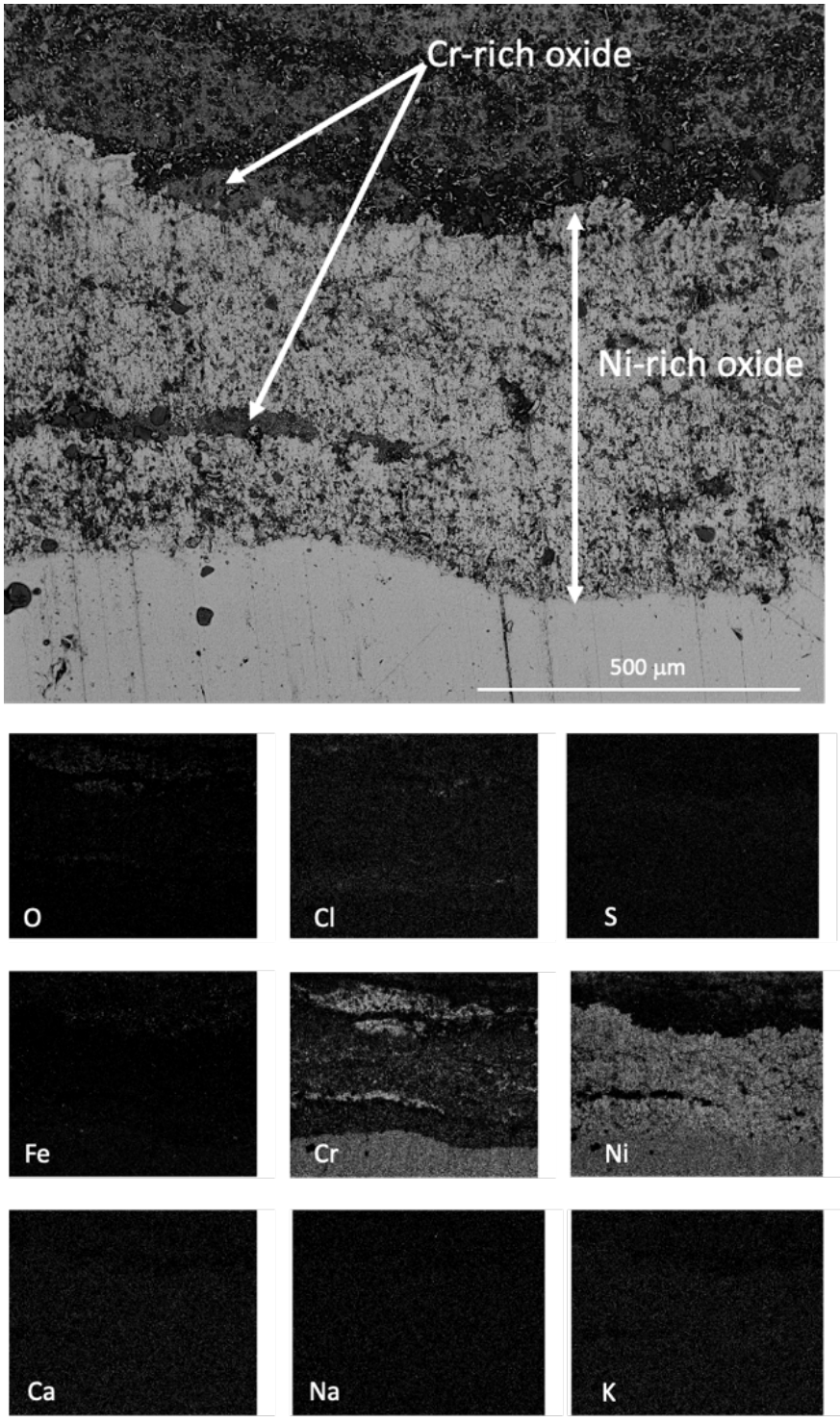

Figure 51. SEM BSE cross section image of Sanicro 69 (a) after 12 months of exposure. (b) EDX mapping of (a).

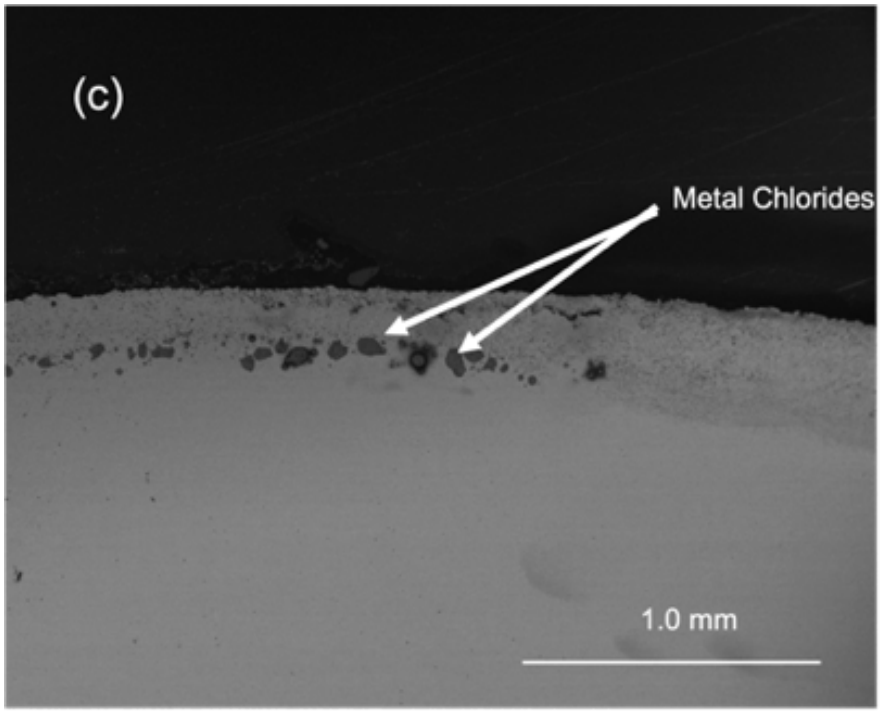

Figure 52 shows the (a) SEM cross-section of a 27Cr33Ni3Mo sample after 12 months of exposure and (b) the EDX analysis. No deposit was detected on the top of this sample meaning that it was lost during the removal/handling of the samples. A very thick and porous oxide was detected all around the sample. The thickness is at least 300 μm and more than 500 μm in some areas.

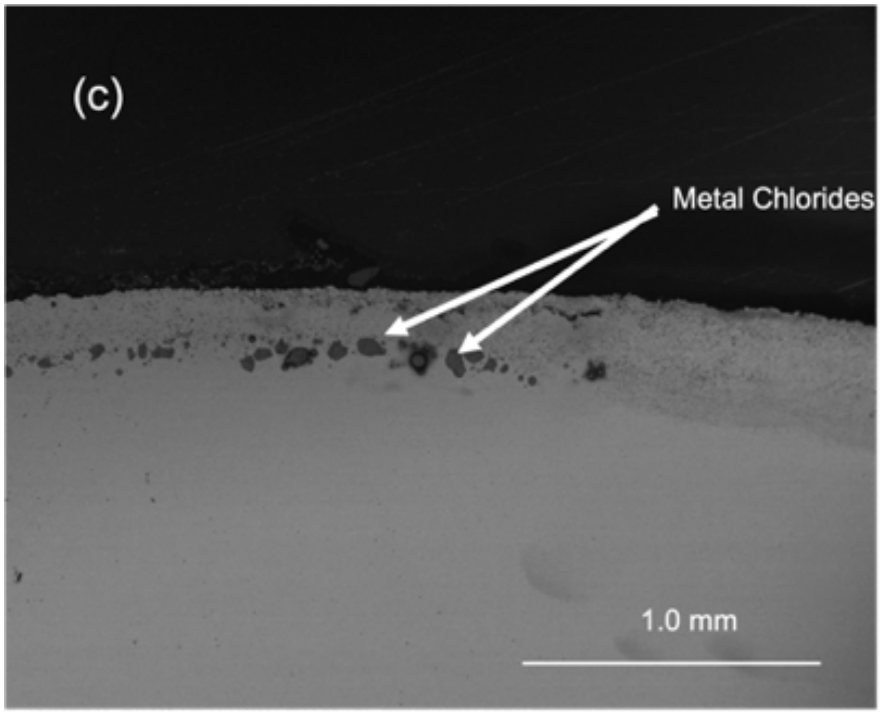

Figure 52 (a) the oxide cracks and detaches in some parts. The composition is mainly Fe and Ni with a Cr-rich layer on the top. Some Cl is detected in the oxide/bulk interface Figure 52(c)

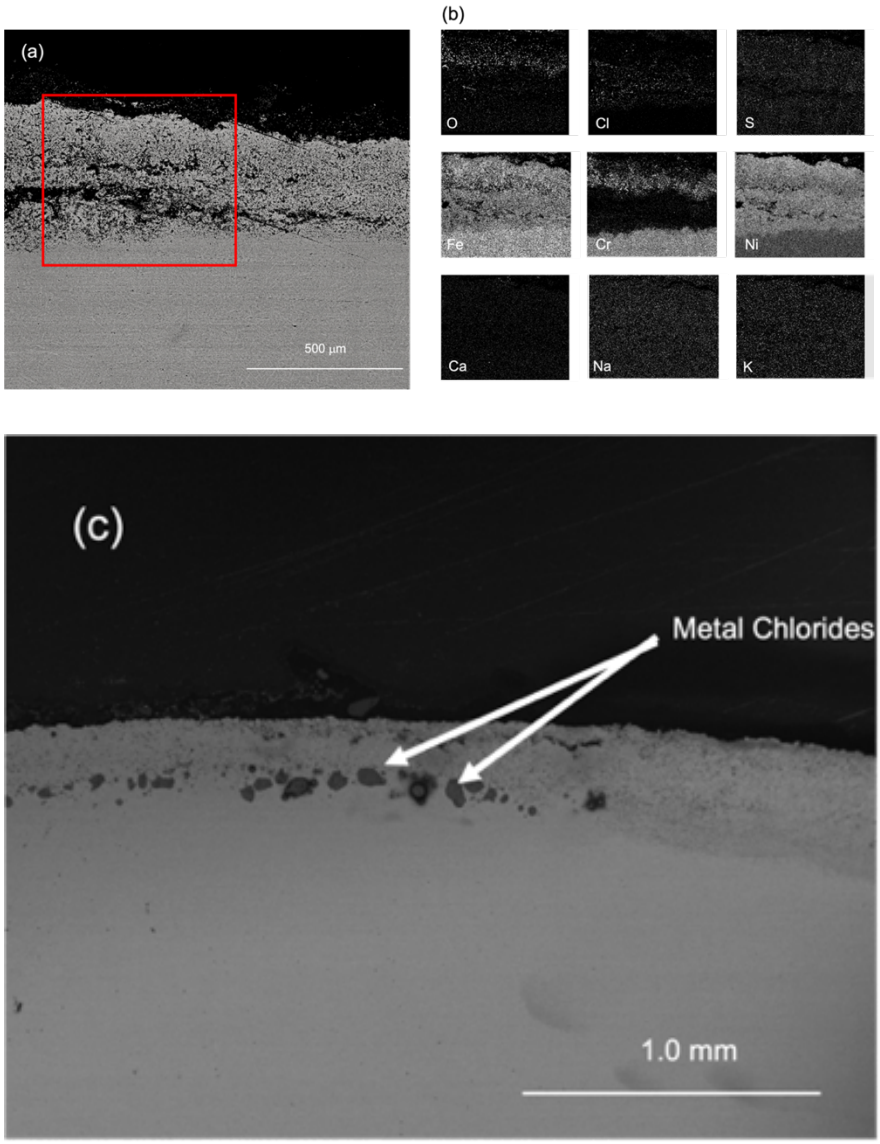

Figure 52. SEM BSE cross section image of 27Cr33Ni3Mo (a) after 12 months of exposure. (b) EDX mapping of (a), (c) detail of metal chlorides on the surface of the sample.

Figure 53 and Figure 54 show the results from Esshete 1250 after 6 and 12 months of exposure, respectively. A similar corrosion attack was observed after 6 and 12 months and thus EDX analysis is only shown for the sample exposed for 12 months. For both samples, an inward growing oxide was observed well adherent to the material. The outer part of the oxide consisted of an Fe-rich oxide, while the inner part is dominated by a Cr-rich oxide, as is shown in the EDX map for the sample exposed for 12 months. The thickness of the Fe-rich oxide was about 150 µm for both samples. Like the previously described austenitic steels shown, the outer part of the steel substrate was depleted in Cr, leaving behind a Ni and Fe-enriched steel substrate.

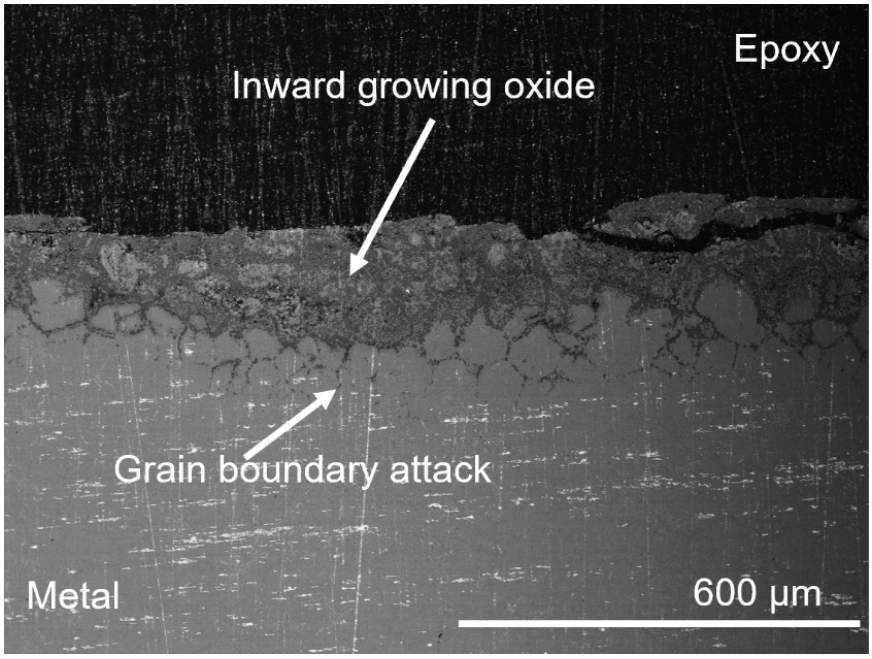

Figure 53. SEM cross-section of Esshete 1250 after 6 months of exposure.

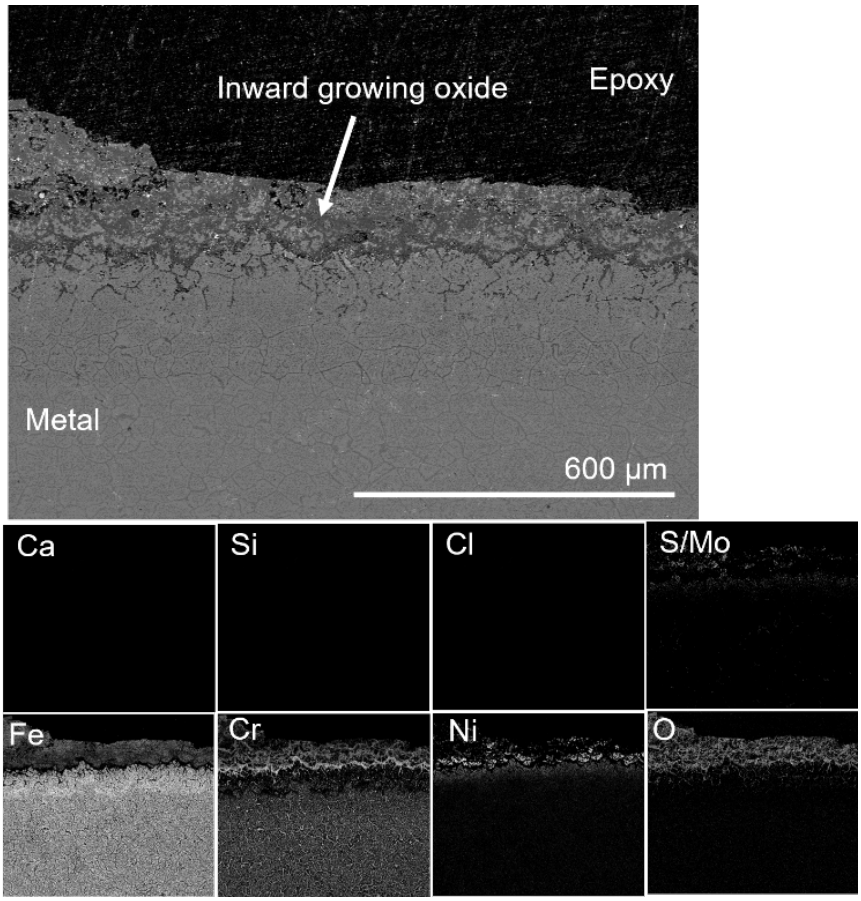

Figure 54. SEM cross-section of Esshete 1250 after 12 months of exposure

The SEM cross-section images after 6 and 12 months of exposure in Händelö P15 for 316Ti are presented in Figure 55. Similar features were observed for both samples and thus, chemical analysis via EDX mapping is only shown for the sample exposed for 12 months. For 316Ti, the cross section showed little or no deposit layer as well as minor indication of formation of an outer corrosion product layer. Instead, the cross sections revealed signs of intergranular corrosion attacks.

Figure 55c shows the EDX mapping of the 316Ti sample exposed for 12 months. A thin outer layer of oxide was observed on top of the sample consisting mainly of Cr and trace amounts of Fe. 316Ti suffered from an intergranular corrosion attack after 6 months of exposure (see highlighted area). This attack progressed with increased severity as a function of exposure time (see highlighted area in Figure 55b). The corrosion products formed in the steel grain boundaries mainly consisted of Cr-rich oxide and no traces of Cl were detected. Below the metal/oxide surface, a roughly 150 µm thick Cr-depleted region had been formed throughout the sample.

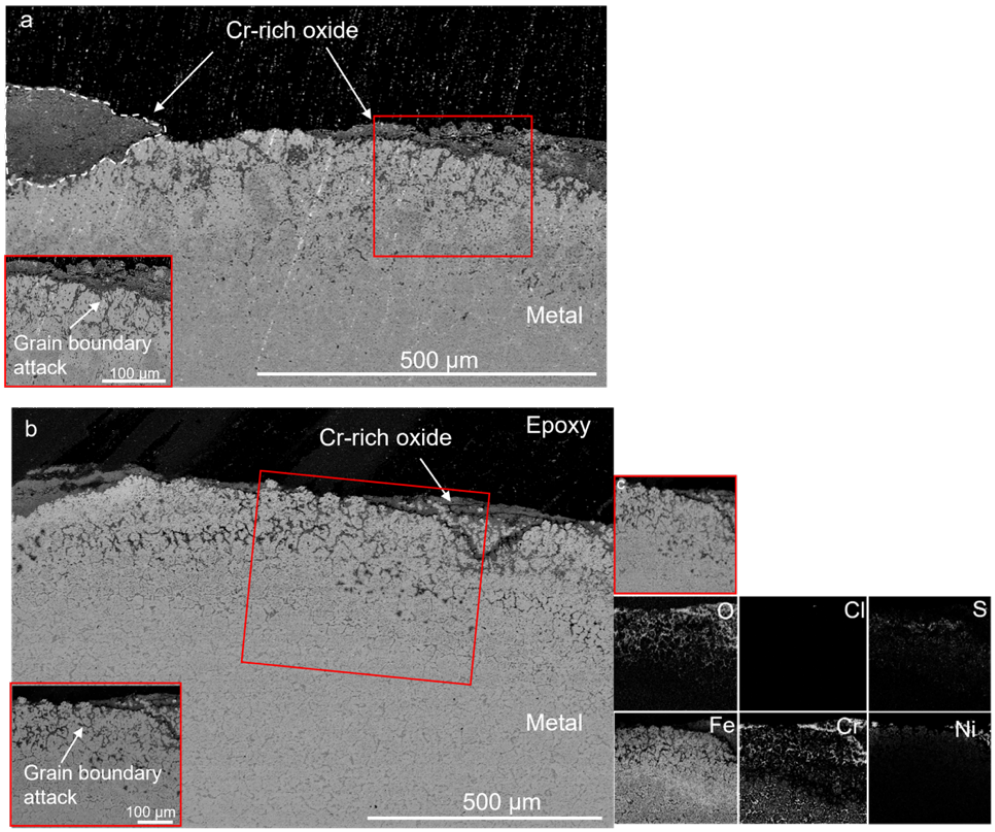

Figure 55. SEM BSE cross-section image of 316Ti (a) 6 months of exposure. (b) 12 months of exposure. (c) EDS mapping of 316Ti from highlighted area in (b).

Figure 56 presents the SEM cross section (a) and EDX analysis (b) from the reference material, Alloy 59 after 12 months of exposure. This material has been overlay welded on the top of a tube to mimic the real operation conditions. Due to the difference in thickness of the welding cords it is not possible to measure

material loss in this sample. Nevertheless, it is possible to observe the corrosion attack in the SEM images. No traces of deposit were detected on the top of the sample. The deposit was probably lost during the removal/handling of the samples. The top part of the corrosion products is usually attached to the inner part of the deposit, so, the most external part of the corrosion products is usually lost with the deposit. The remaining oxide is approximately 500 µm thick all around the sample and it is mainly composed by Ni with some Cr-rich areas, mainly on the top of it. Below this oxide, on the top of the remaining sample a Ni-rich and Cr-depleted zone is detected.

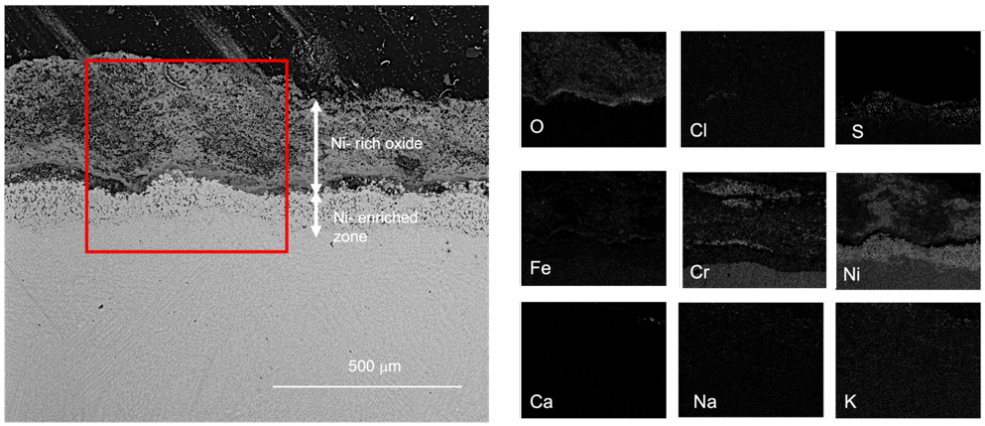

Figure 56. (a) BSE SEM cross-section image of Alloy 59 sample after 12 months of exposure in SH3 (b) EDX analysis.

The results of the overlay welded samples exposed in the P15 boiler in Händelö are described in the section below. The welded structure obtains a characteristic heterogenous surface, which makes accurate material loss measurements challenging. Thus, no material loss measurements were conducted on these samples.

The SEM images and EDX map analysis of EF101 after 6 months of exposure are shown in Figure 57. A roughly 170 µm thick adherent deposit was observed on top of the sample containing mostly Ca, S and O. Below the deposit layer a roughly 40 µm thick oxide layer was observed, containing mostly Al and traces of Cr. Below the oxide, an approximately 100-200 µm thick nitridation zone was observed. The nitridation zone was observed in a homogenous fashion throughout the cross section. The weld overlay EF101 sample exposed for 12 months could not be retrieved.

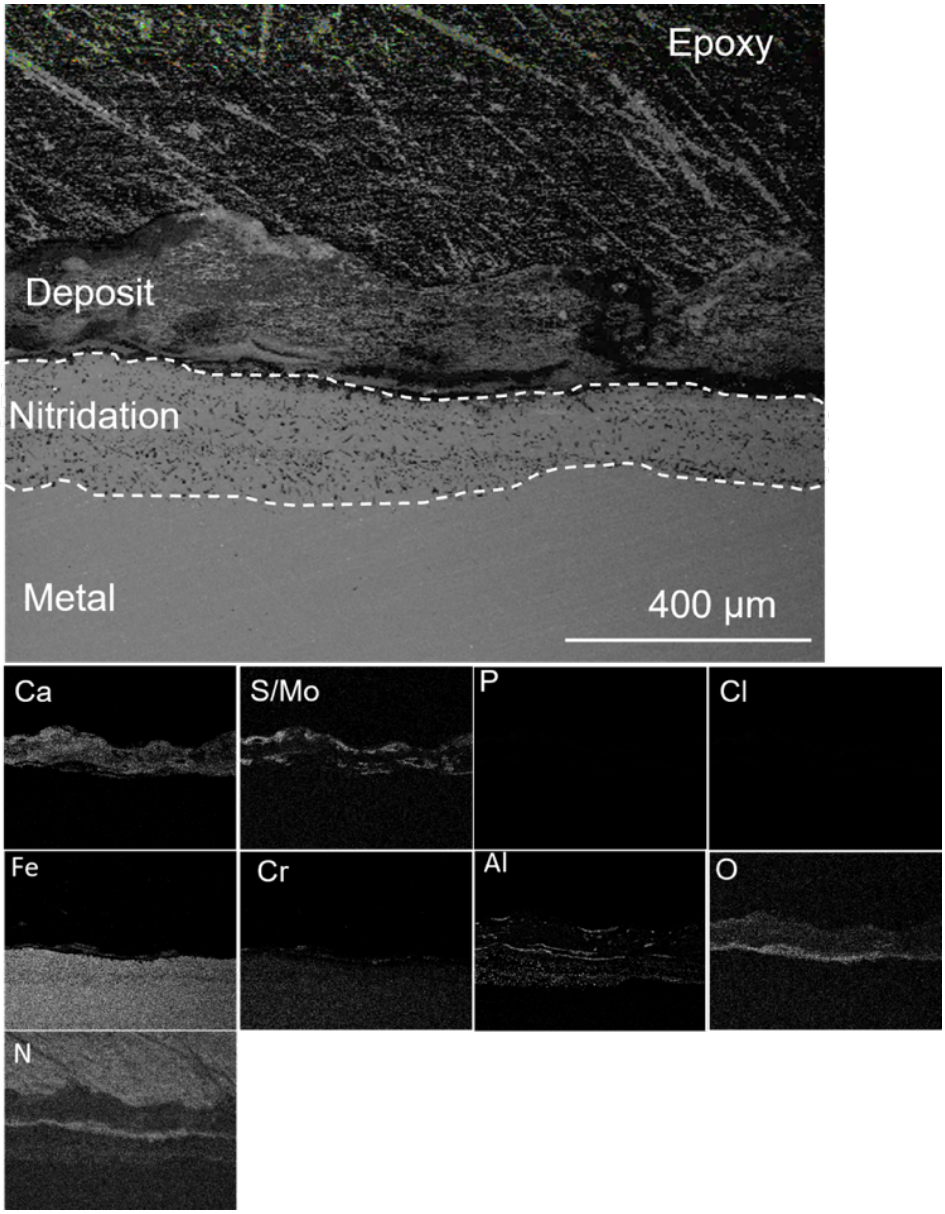

Figure 57. BSE SEM cross-section image of weld overlay EF101 sample after 6 months of exposure in SH3 together with EDX analysis below.

Compared to the weld overlay EF101 sample exposed to 6 months, the EF100 weld overlay sample achieved a significantly thicker oxide with large cracks visible after similar exposure time (see Figure 58). The oxide thickness was estimated to 450 µm. In addition, EDX signal of both Cr and Fe was observed throughout the whole oxide making it challenging to distinguish between Fe-rich and Cr-rich regions. A nitridation zone below the oxide was formed and was displayed in a patch-wise fashion throughout the cross section with a thickness ranging from 20- 260 µm.

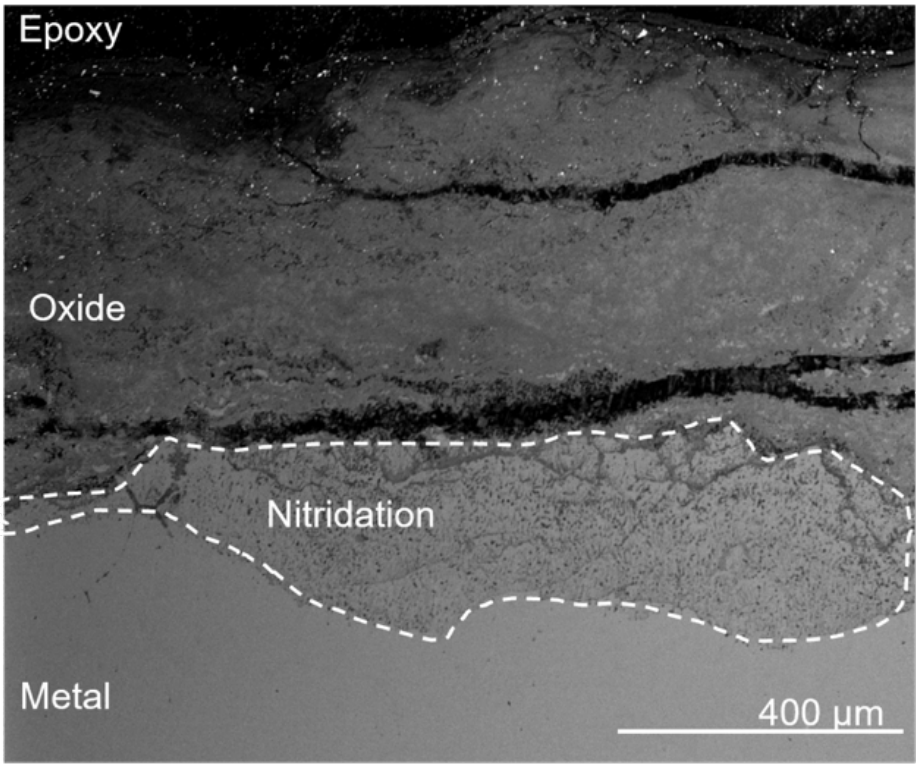

Figure 58. BSE SEM cross-section image of weld overlay EF100 sample after 6 months of exposure in SH3.

Similar features for the overlay welded EF100 sample exposed for 12 months were observed as for the 6 months (Figure 59 and Figure 60). An Fe and Cr rich oxide was formed on top of a Cr-rich oxide. Similar to the sample exposed for 6 months, large cracks and voids were detected on the oxide scale. Below the Cr-rich oxide an approximately 200 micrometers thick nitridation zone had formed. Compared to the previous sample, the nitridation region was more homogenous throughout the cross section reaching similar thickness.

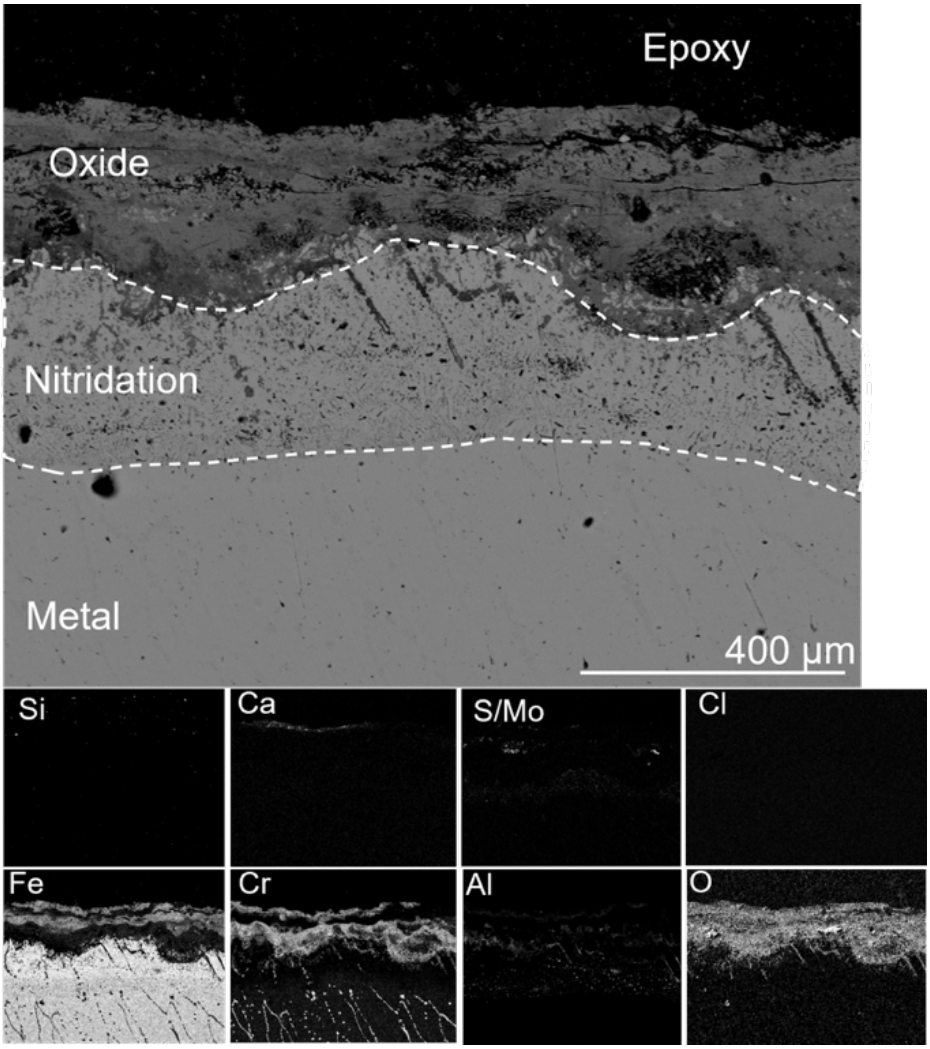

Figure 59. BSE SEM cross-section image of weld overlay EF100 sample after 12 months of exposure in SH3 together with EDX analysis below.

Figure 60 shows the SEM cross section and EDX mapping of the APMT weld overlay sample exposed for 6 months. An approximately 70-100 µm thick and adherent deposit was observed on top of the sample containing mostly Ca, S, Cl, Mg, and O. Below the deposit an Fe-rich oxide with traces of Cr-rich oxide was observed. Again, a nitridation zone was observed below the oxide. Below the oxide a 50 µm thick Cr-depleted zone was observed. The nitridation zone was identified in a patch-wise fashion reaching a thickness ranging from 10-380 µm. Unfortunately, the weld overlay APMT sample exposed for 12 months could not be retrieved.

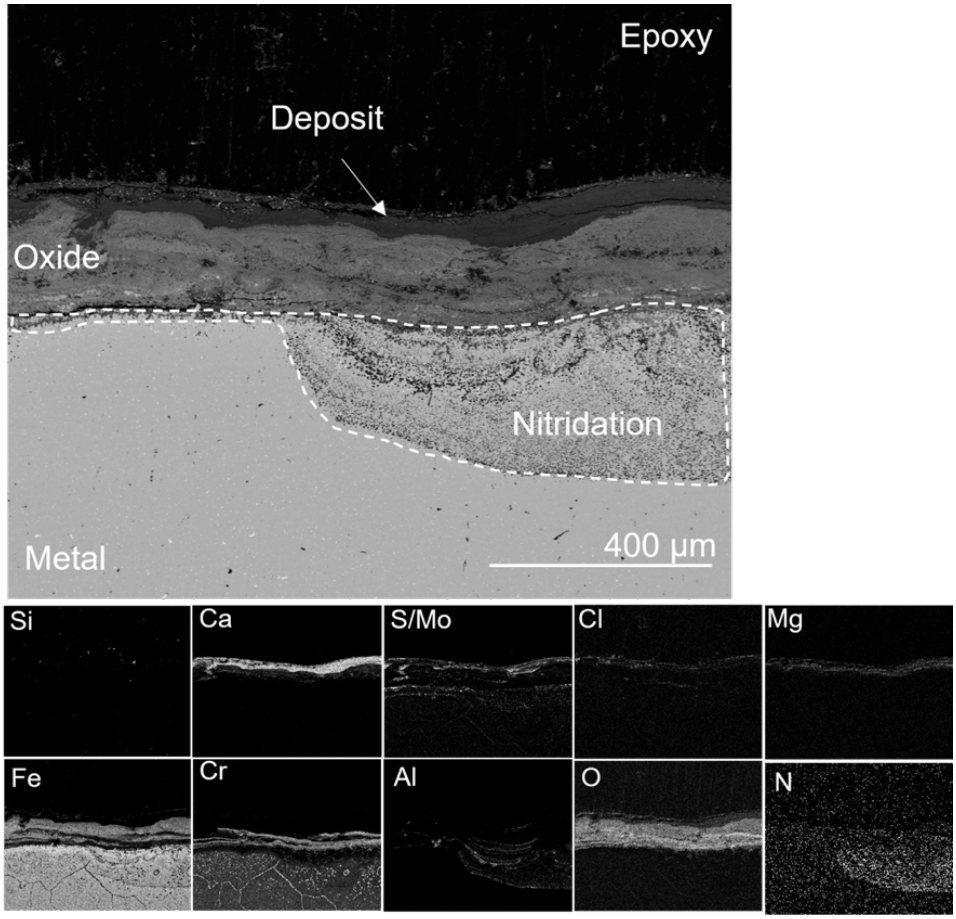

Figure 60. BSE SEM cross-section image of weld overlay APMT sample after 6 months of exposure in SH3 together with EDX analysis below.

Lastly, the weld overlay of Alloy 625 exposed for 6 months is shown in Figure 61. The EDX analysis presented below the cross-section image shows that the presence of Ca, S, and O in the deposit is high. No chlorine species were detected on the sample. Below the deposit a 170 µm thick Ni containing oxide was present and at the metal/oxide interface a Cr-rich oxide was observed. Below this oxide a Cr-depleted zone was observed leading to a Ni-enriched steel substrate. Unfortunately, the weld overlay Alloy 625 sample exposed for 12 months could not be retrieved.

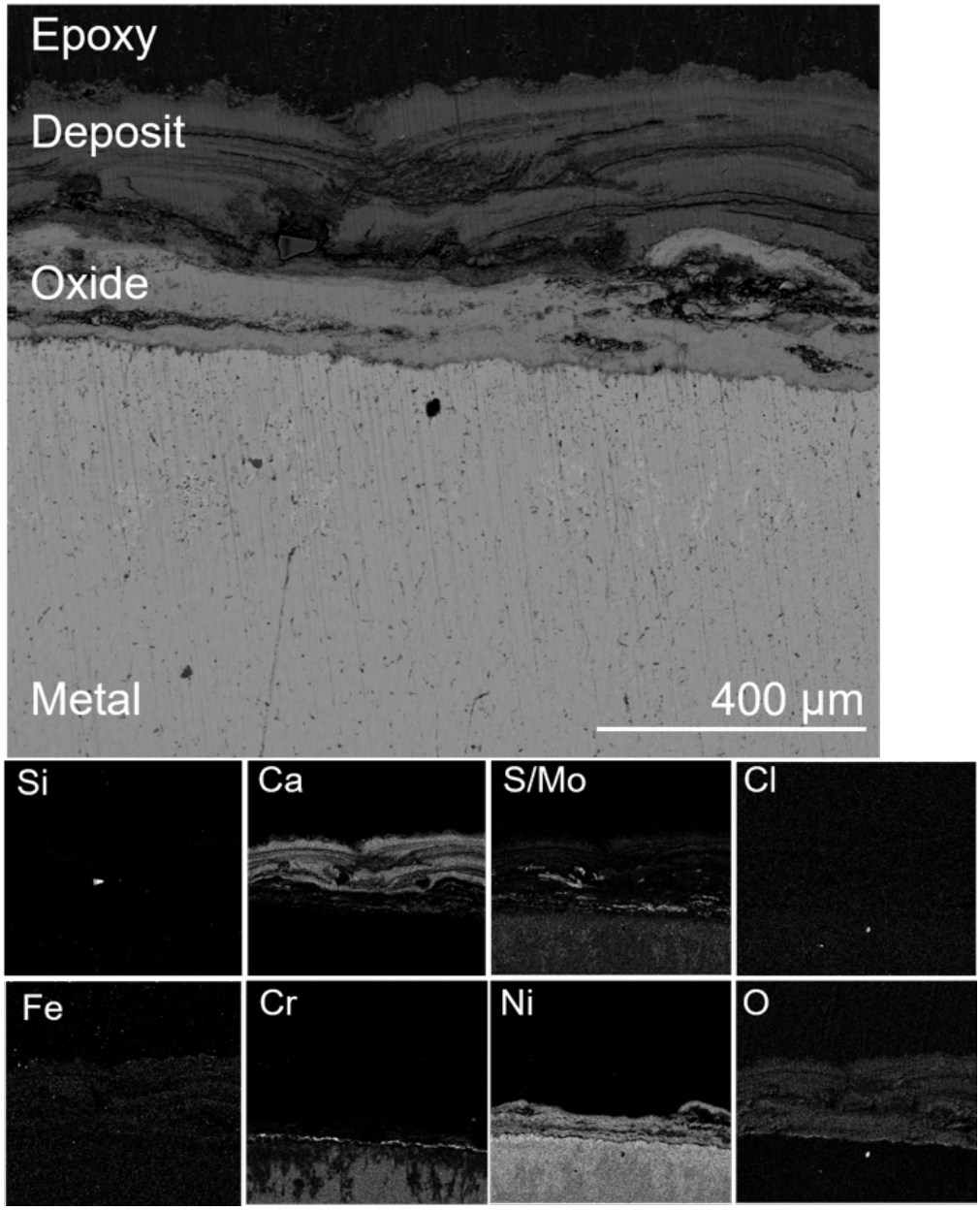

Figure 61. BSE SEM cross-section image of weld overlay Alloy 625 sample after 6 months of exposure in SH3 together with EDX analysis below.

5 Analysis of the results

This project has aimed to address the material degradation challenges facing FBHE and water wall tube panels in bio and waste-fired boilers, which today is a crucial factor that currently limits the fuel flexibility and efficiency in these power plants. In this section a thorough discussion of the results presented in this report is performed. The discussion part will be divided into the two major work packages presented in this report, one directed towards water wall (WP1) corrosion and the other towards FBHE corrosion/erosion (WP2).

- In WP1, short term testing (1 week) in the water tube panels was carried out in the P6 boiler in Högdalen. The exposure was carried out using three small sized air-cooled probes (see section 3.2.2 for set-up design). A comprehensive experimental matrix was designed using various materials including low alloyed steels, novel Al-containing alloys, Ni base alloy and austenitic stainless steels. The task of this work package has been to perform microstructure analysis of the materials after exposure to evaluate and compare the corrosion performance and mechanisms between the different materials in order to improve material selection in this region of the boiler.
- In WP2, the material loss due to erosion and corrosion of fluidized bed heat exchangers were addressed. Long-term exposures of the different materials were carried out in two different boilers; the waste-fired boiler P15 Händelö operated by E.ON (Navirum), Norrköping, and the waste-fired boiler P6 Högdalen operated by Stockholm Exergi. The materials were exposed for a total of 6, 12 and 24 months by mounting two half-moon sample rings for each material on the top- and bottom-most rows of the FBHE tube bundles during boiler shutdown. A complete description of the exposures is given in section 3. A comprehensive experimental matrix was designed using various materials, including low alloyed steels, austenitic stainless steel, novel Al-containing alloys, Ni base alloy, spray coatings, and overlay welded material. The exposures were carried out by clamping the different samples on existing fluidized bed heat exchangers (see section 3.2 for set-up design). Material loss analysis together with microstructure analysis were carried out after exposure with the aim of understanding the interplay between corrosion and erosion mechanisms with regards to material degradation rate in order to improve material selection in this region of the boiler.

In addition, a discussion on the influence of Oxygen Carrier Aided Combustion (OCAC) is described in section 5.3

5.1 WP1- WATER WALL CORROSION TESTING

Accelerated corrosion of water walls in waste-boilers remains a challenge for efficient electricity and heat production. From the results obtained in this study, the only visible oxide formation after 1 week of exposure was seen on the low alloyed steel sample 16Mo3. A Fe-rich oxide had been formed, where a high concentration of Cl was observed close to the metal/oxide interface (see Figure 9). Similar features have been reported in many studies concerning corrosion of low alloyed steel in contact with alkali/heavy metal chlorides [1-3] . Authors have contributed to the accelerating corrosion rate for low alloyed steels in these studies through the presence of chlorine. Previous studies have shown that alkali chlorides may react with water and oxygen to form Cl ions that can diffuse through grain boundaries towards the metal surface and form metal chlorides, such as $FeCl_2$. $FeCl_2$ has been shown to facilitate high diffusion rate of oxygen and iron in the grain boundaries, thus accelerating the corrosion rate [4] .

In addition, the accelerated corrosion rate can also be explained by the formation of eutectic melts facilitating the diffusion rate of chlorines at the deposit layer. Such melt formation has been suggested to form in contact with $PbCl_2$, $ZnCl_2$ and alkali chlorides [5] . The melt formation may lead to an increase of solubility of metal chlorides in the molten phase, which leads to an increased diffusion rate and subsequently a higher oxidation rate of the material. Thus, the solubility of metal chlorides in eutectic melts may influence the corrosion rate. From the SEM/EDX analyses in this study, a clear migration of Cl to the metal/oxide interface was shown, indicating the formation of iron chlorides for the low alloy steel sample. In addition, Zn, Pb, K cations were observed in the deposit, which suggests that the chlorine ions have migrated from respective counter ions. Lastly, from the EDX point analysis it was clear that some of the white bright areas showed a complex chemical composition of Zn, Pb, K and O indicating possible melt formation. It is likely that the oxide formation in this case has occurred due to the previously mentioned mechanisms regarding melt formation and metal chloride formation.

For stainless steels, the corrosion resistance is highly governed by its ability to form a protective Cr-rich oxide scale. The breakdown of this Cr-rich oxide scale cannot be explained by the previous mechanisms introduced for the low alloyed steel. Rather, it has been shown in previous studies that cations from alkali and heavy metal chlorides, such as K, Pb and Na among others, play an important role in the breakdown of the Cr-rich oxide and the formation of a less protective oxide scale as seen in the equations below:

$$4xKCl(s) + (Cr_x, Fe_{1-x})_2O_3(s) + 2xH_2O(g) \rightarrow 2xK_2CrO_4(s) + (1-x)\ Fe_2O_3(s) + 4xHCl(g)$$

$$4NaCl\ (s) + Cr_2O_3 + 5/2\ O_2 \rightarrow Na_2CrO_4\ (s) + 2\ Cl_2(g)$$

$$PbCl_2\ (l) + Cr_2O_3 + 5/2\ O_2 \rightarrow 2PbCrO_4\ (s) + 2Cl_2(g)$$

As mentioned in this report, no oxide scale or significant material degradation were observed on any of the stainless-steel types exposed in the water wall. In addition, no Pb/K/Na-chromate was observed close to the metal interface that would reveal breakdown of the protective Cr-rich oxide. However, the SEM/EDX analysis revealed a high number of corrosive species such as K, Cl, Pb, Zn, which

have been shown in previous studies to have an important impact on corrosion rates in these environments [5] .The temperature is of great importance when studying this corrosion mechanism. Melt formation in the deposit is governed not only by the chemical species, but also by the temperature. It is possible that the low temperature together with the short period of exposure does not facilitate high corrosion rates. In order to properly evaluate the corrosion resistance of these materials, it is suggested for future work to increase the exposure time in this environment. Previous studies have shown that Alloy 625 can reduce the corrosion rate of water walls significantly in these environments. Y. Alipour et al studied the corrosion effect of low alloyed steel and a Ni base alloy in the water wall region of a waste fired boiler [6] . The exposure was carried out for three years at a temperature of 340 °C. They concluded that the Ni base alloy drastically reduced the corrosion rate of the water wall compared to the low alloyed steel. The high corrosion rate observed for the low alloyed steel was attributed by the diffusion of chloride containing species through the deposit and oxide. The corrosion mechanism of the Ni base alloy was discussed, and it was concluded that the observed corrosion attack was attributed to the combination of K and Pb corrosion attack leading to the breakdown of the protective chromia scale and formation of non-protective K, Pb-chromates. Considering that both K and Pb compounds were observed in the deposit in this study it is possible that similar corrosion attacks may be observed in the present environment at longer exposures and should thus be considered regarding material selection.

From the results obtained for the FeCrAl alloys, no indication of severe material degradation was observed. The surfaces were homogenous after 1 week of exposure and there was no observation of thick oxide formation or depletion of alloy elements close to the metal/atmosphere interface. Their performance was on par with stainless steels and Ni-base alloy Alloy 625. The EF101 sample did obtain a thick deposit with a composition similar to that of the deposit on Sanicro 28. However, only a very thin oxide was observed below the deposit and no indication of chlorine migration to the metal surface was observed. Thus, the FeCrAl alloys show promising results and should be considered as possible material candidates for water wall applications.

Few studies have been carried out regarding exposure of FeCrAl alloys in water wall regions of a waste/bio boiler. Alipour et al [6] performed corrosion tests at the furnace wall in a power boiler burning waste wood. The exposures were performed for 934h at a temperature range of 365-390 °C. It was concluded that the APMT material achieved a lower corrosion rate than the traditional stainless steel 310 and on par with Alloy 625. This suggests that FeCrAl could be a potential candidate for water wall application. The corrosion mechanisms are however not yet fully understood, and more research is needed to fully evaluate FeCrAl in water wall regions.

In this study, no significant material degradation was observed on either the FeCrAl alloy or the austenitic stainless steels. To get a greater understanding of the corrosion mechanisms it is suggested to continue similar exposures, but for a longer time and conduct lab-scaled trials with a controlled environment. As mentioned in [6] , the corrosion attacks on APMT are suggested to occur due to a

combination of Cl, K and Zn, where the latter cations are suggested to break the Cr and Al-rich oxide, thus facilitating high diffusion rate of aggressive corrosive species through the oxide. Johan Eklund et al have conducted field exposure tests on FeCrAl model alloys with various amounts of Si, in a waste-fired boiler at the steam boost position reaching a material temperature of 600 °C for 672 h. From the results obtained it was shown that minor addition of Si drastically reduced the corrosion rate of FeCrAl alloys. Compared to the conventional FeCrAl APMT, the novel FeCrAl EF101 has a Si- addition to the alloy composition. Based on these results it is very interesting to further explore the possibility of FeCrAl alloys in the water wall region [7] .

FeCrAl alloys are usually implemented in regions of the boiler that have higher temperatures due to their ability to form protective alumina oxide scale. Kanthal® EF100 and EF101 have been developed to increase the temperature interval where FeCrAl alloys are normally used down to temperatures as low as 300 °C. By lowering the Cr content to about 10 wt%, the risk for α-α' phase separation, caused by a miscibility gap in the Fe-Cr system, is significantly decreased. This α-α' phase separation is also known as 475 °C embrittlement, and when suppressed, the alloys see a significant improvement in the mechanical properties at these lower temperatures. In addition, the two FeCrAl alloys contain additional alloying elements such as manganese (Mn) reactive elements (RE) and silicon (Si), where the latter element is added to improve the ability to form a protective oxide scale at intermediate temperature as previously discussed.

The results presented in this report clearly show an increased corrosion rate for the low alloyed steel compared to the stainless steels and the FeCrAl alloys, implying that the usage of 16Mo3 uncoated in this environment may not be suitable for long term usage.

5.2 WP2- MATERIAL PERFORMANCE IN FLUIDIZED BED HEAT EXCHANGERS

P6 Högdalen

A wide material testing matrix has been performed in Högalen P6 boiler. The material matrix includes conventional steels used today as well as newly developed stainless steels and FeCrAls and two different types of thermally sprayed coatings, HVOF and HVAF sprayed coatings.

A summary of the results is presented below. Figure 62 shows the different corrosion mechanisms that were observed for the different materials. Table 15 shows a summary of the results and observations of the materials exposed at the P6 boiler in Högdalen after 12 and 24 months of exposure.

The first set of materials analyzed is the FeCrAls, marked in green in the Table 15. As seen in the table, all the FeCrAl materials present nitridation in a certain way. As was mentioned in section 4.2, it is important to clarify that the thickness of the nitridation zone is not included in the material loss calculation. More specific

experiments are needed to have more knowledge about if and how nitridation affects the corrosion behavior of the FeCrAl materials. Within the project results it is not possible to see an increase in the corrosion when nitridation appears. For this reason, the material loss is calculated only taking into account the oxide scale thickness. The oxide depth presented in Table 15 represents the thickness of the oxide and the oxide affected zone when grain boundary attack is present.

By analyzing the material loss and its increase with time, the most promising material of the FeCrAls was found to be EF101. This material presents the lowest material loss and oxide depth even after 24 months exposure. The surface of the samples was smooth in all cases and deposit was found on the top of all the samples. The presence of deposit means that the oxide scale at the moment of the removal of the sample was well preserved. The material loss being close to 0 mm/year in all the positions and at all the exposure times and considering the presence of deposit on top, the observed thickness of the oxide scale should be the total oxide thickness. No oxide has spalled off during the exposure time. Nevertheless, the EF101 samples presented medium to high nitridation both in row 1 and row 9 position. The temperature in row 8 was lower than in row 1 during the 12 months exposure. This could be an explanation for the lower nitridation grade in row 8.

The EF100 material is also a promising candidate for fluidized bed superheater position. The material loss is higher than for EF101, but still low even after 24 months exposure. The deposit is still present on the top of all samples, meaning that the oxide scale has not spalled off during the exposure or handling of the samples. The nitridation zone is thinner than for EF101 but, as explained above, it is not certain that this is a factor affecting corrosion. The surface of EF100 is also more uneven than in EF101, which presents a very smooth surface with well adherent oxide over the whole sample.

The APMT material also presents good results, but worse than both EF101 and EF100 in terms of material loss and nitridation. The sample exposed for 24 months was almost completely nitridated. Taking the price into account, both EF101 and EF100 are better candidates than APMT, as the latter is the most expensive of the three FeCrAls.

The next block of materials, presented in yellow in Table 15 is the austenitic stainless steels. Besides the 16Mo3, which also presents the highest material loss and the most non-adherent oxide, all the stainless steels (SX, Sanicro 69, Esshete 1250, Sanicro28 and 316Ti) present intergranular corrosion attack propagating via grain boundaries. The oxide product consisted mainly of Cr-rich oxide on the surface of the bulk material, followed by Fe-rich oxide.

The most promising material of this kind is the SX. The SX samples contain a high amount of Si. They present an internal oxidation at the metal/oxide interface consisting of Si-rich oxide instead of the Cr-rich + Fe-rich scale presented for the rest of the materials. The material loss for the SX material was low in all the cases (max 0.06 μm/year), even after 24 months exposure. The thickness of the oxide and grain boundary attack is low during the first 12 months of exposure (around 70 μm) and reaches 200 μm after 24 months exposure. The presence of Si in high-

temperature materials has been reported in previous works to have a beneficial effect on corrosion protection [8-10] which aligns well with these results. By comparing with Sanicro 69, which is in the same price range, the material loss of the latter is lower than for SX even after 24 months of exposure, but the depth of the corrosion attack is higher in all the cases. Also, an accumulation of metal chlorides was detected on the Sanicro69 samples regardless of position. The formation of these metal chlorides reveals chlorine diffusion through corrosion product layers into the material. Previous studies have shown that this may result in poor scale adhesion after prolonged exposure that may enhance the diffusion rate of corrosive species to the metal/oxide interface and thus further increase the corrosion rate of the material [11] .

The rest of the materials in this block (Esshete 1250, Sanicro28 and 316Ti) present more material loss and oxide thickness than both SX and Sanicro 69. The Sanicro 28 material is in the same price range as SX and Sanicro 69, which makes it a poor competitor. Both Esshete 1250 and 316Ti are cheaper materials. By comparing their corrosion behavior at 12 months exposure, the 316Ti presents a smaller depth in the corrosion attack. Unfortunately, the 316Ti sample was not recovered after 24 months exposure. This can be due to a welding failure, or a sample failure, but the lack of information after 24 months makes it impossible to compare both materials in the long term.

Finally, the coating samples are marked in blue in Table 15. None of the coatings (CorEr, APMT20c, APMT40c) remained attached to the bulk metal surface after 12 months of exposure. As is shown in the results chapter (4.3.1), the underlaying base material had undergone internal corrosion, which indicates that corrosion attack might have already occurred at an early stage of the exposure suggesting an early failure of the coatings.

The microstructure analyses show corrosion products in all the samples. Grain boundary attack is detected in most of the conventional steels and nitridation is observed in all the FeCrAl materials exposed. The EDX mapping reveals traces of chlorine species in some of the deposits and in some of the samples, like Sanicro 69, metal chlorides were formed potentially resulting in poor scale adhesion and an increased corrosion attack. The fluidized bed heat exchanger is surrounded by fluidized bed material, so also erosion is expected to influence the samples. The microstructure analysis shows that deposit and oxide spallation occur, sometimes very locally, indicating a strong erosion in certain parts of the heat exchanger. Thus, it is suggested that local erosion attacks happen in this boiler position, which may lead to increased material loss after prolonged exposures. The results obtained from all the different kinds of materials exposed in this project, in the different positions of the heat exchanger and at different exposure times, suggest that the attack suffered by the material is a combination of erosion and corrosion. In Appendix A of the present report, it is explained how the simultaneous mechanism of erosion and corrosion attack can occur and how it affects the formation and spallation of the oxides [12] .

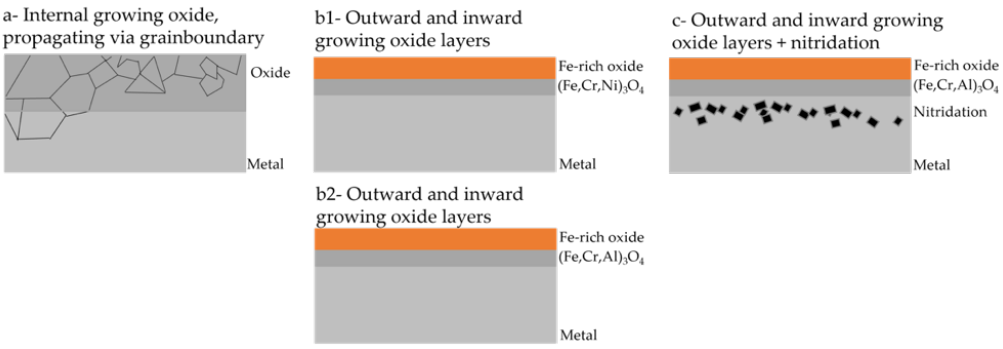

Figure 62. Illustration of the different corrosion mechanisms and microstructure observations.

Table 15. Summary of the most important findings of the material analysis in the waste-fired boiler P6, Högdalen. The corrosion type is related to Figure 60.

Material	Exposure time (months)	Position	Material loss (mm/year), $\bar{x}$	Corrosion type	Oxide depth (mm)	Deposit left	Nitridation	Price
EF101	12	Row 1	0.02 ± 0.01	c	25	Y	Medium	$$$
EF101	12	Row 8	0.00 ± 0.01	c	40	Y	Low	$$$
EF101	24	Row 9	0.00 ± 0.01	c	200	Y	Medium/ High	$$$
EF100	12	Row 1	0.16 ±0.01	c	50	Y	High	$$$
EF100	12	Row 8	0.09 ±0.01	c	140	Y	Medium	$$$
EF100	24	Row 9	0.36 ± 0.01	c	200	Y	Low	$$$
APMT	12	Row1	0.18 ±0.01	c	Cracked	N	Medium	$$$$
APMT	12	Row 8	0.00 ± 0.01	c	80	Y	High	$$$$
APMT	24	Row 9	0,27± 0.01	c	300	N	High	$$$$
SX	12	Row 1	0.02 ±0.01	a+b1	70	N	x	$$$$
SX	12	Row 8	0.06 ± 0.01	a	70	N	x	$$$$
SX	24	Row 9	0.05± 0.01	a+b1	200	Y	x	$$$$
Sanicro 69	12	Row 1	0.00 ± 0.01	a+b1	>150	N	x	$$$$
Sanicro 69	12	Row 8	0.00 ± 0.00	a	>200	N	x	$$$$
Sanicro 69	24	Row 9	0.00 ± 0.00	a+b1	>200	Y		$$$$
Esshete 1250	12	Row 1	0.66 ±	a	250	N	x	$$$
Esshete 1250	12	Row 8	0.33 ±	a	300	N	x	$$$

Esshete 1250	24	Row 9	0.89 ±0.01	a+b1	>300	N	x	$$$
Sanicro 28	12	Row 1	0.34 ±	a+b1	Cracked	Traces	x	$$$ ($)
316Ti	12	Row 1	0.80 ±	a	200	N	x	$$
316Ti	12	Row 8	0.58 ±	a	100	N	x	$$
16Mo3	12	Row 8	1.17 ±	b	200	N	x	$$
Alloy 625	12	Row 1	WOL	b	200	Y		$$$$
Alloy 625	12	Row 8	WOL	a	200	Y		$$$$
Alloy 625	24	Row 9	WOL	a+b1	200	Y	x	$$$$
APMT50c	12	Row 8	Coating failure!	x		N	x	$$$$
APMT20c	12	Row 8	Coating failure!	x		N	x	$$$$
CorEr	12	Row 8	Coating failure!	x		N	x	

P15 Händelö

A wide material testing matrix has been performed in Händelö P15 boiler. The material matrix includes conventional steels used today as well as newly developed stainless steels and FeCrAls, both in bulk form and overlay welded. The reference material is alloy 59 overlay welded as it is the material used in the fluidized bed heat exchangers today.

A summary of the results is presented below. Figure 62 shows the different corrosion mechanisms that were observed for the different materials. The Table 16 shows a summary of the results and observations of the materials exposed at P15 boiler in Händelö after 6 and 12 months of exposure.

Table 16. Summary of the most important findings of the material analysis in the waste-fired boiler P15, Händelö

Material	Exposure time (months)	Material loss (mm/year), $\bar{x}$	Corrosion type	Oxide depth (mm)	Deposit left	Nitridation	Price
EF101	6	0.09 ± 0.06	c	100	Y	High	$$$
EF101	12	0.41 ± 0.43	c	100	Traces	Medium	$$$
EF100	6	0.13 ± 0.09	c	200	Y	Medium	$$$
EF100	12	0.19 ± 0.09	c	100	N	Medium	$$$
APMT	6	0.26 ± 0.18	c	70	N	High	$$$$
APMT	12	0.36 ± 0.21	c	200	N	High	$$$$
SX	6	0.01 ± 0.02	a	100	Y	x	$$$$
SX	12	0.23 ± 0.05	a	400	Y	x	$$$$
Sanicro 69	6	0.04 ± 0.05	a+b1	400	Y	x	$$$$
Sanicro 69	12	1.02 ± 0.59	b1	500	N	x	$$$$
27Cr33Ni3Mo	12	0.33 ± 0.45	a+b1	>300	N	x	R&D
Esshete 1250	6	0.76 ± 0.24	a	300	N	x	$$$
Esshete 1250	12	0.90 ± 0.11	a	300	N	x	$$$
316Ti	6	0.69 ± 0.09	a	250 cracked	N	x	$$
316Ti	12	1.15 ± 0.17	a	300 cracked	N	x	$$
CorER	6	Coating failure!	x	x		x	

Alloy 59	12	WOL	b1	500	N	x	$$$$
EF101 WOL	6	WOL	c	40	Y	Low	$$$
EF101 WOL	12	Lost sample	x	x	x	x	$$$
EF100 WOL	6	WOL	c	450 cracked	N	Low/ medium	$$$
EF100 WOL	12	WOL	c	>300 cracked	N	Medium	$$$
APMT WOL	6	WOL	c	200	Y	Medium	$$$$
APMT WOL	12	Lost sample	x	x	x	x	$$$$
Alloy 625	6	WOL	b1	170	Y	x	$$$$

The first block of materials analyzed is the FeCrAls, marked in green in the

Table 16. As seen in the table, all the FeCrAl materials (bulk and overlay welded) present nitridation in a certain way. As explained above, it is important to clarify that the thickness of the nitridation zone is not included in the material loss calculation.

The behavior of the FeCrAl materials in P15 boiler at Händelö matches the results obtained at P6 in Högdalen presented above. The most promising materials are EF101 and EF100. Both present low material loss and the oxide depth does not exceed 200 μm for any of the exposure times. In the P6 boiler at Högdalen, the EF101 performed slightly better than EF100 after 24 months of exposure, having a very low material loss. At P15 in Händelö, only 6- and 12-months exposures were performed so it is not possible to make an evaluation of the behavior of those materials for longer exposures. Nevertheless, the behavior after 6 months exposure is very similar for both materials. After 12 months, the average material loss is 0.19 mm/year for EF100 vs 0.41 mm/year in EF101, the oxide depth being the same for both the materials after the 12 hours exposure.

The APMT material presents higher material loss both at 6 and 12 months exposure and, just as in P6 Högdalen, the APMT samples are almost totally nitridated. As this material is more expensive than both EF101 and EF100 it is not a good competitor for the fluidized bed heat exchangers in P15 Händelö. The next group of materials, stainless steels. marked in yellow in Table 16, is the austenitic Matching the results in P6 Högdalen boiler, the most promising material is the SX. After 6 months exposure it presents a protective Si-rich oxide both on the top of the sample and in the grain boundaries. The material loss is only 0.01 mm/year after 6 months exposure and 0.23 mm/year after 12 months exposure. Sanicro 69, which is in the same price range, does not perform as good as SX, presenting higher material loss both at 6 and 12 months exposure. The depth of the attack is also higher for both exposure times. Alloy 27Cr33Ni3Mo presents less material loss than Sanicro 69 after 12 months, the average value being 0.33 mm/year. This material loss value is in the same range as the SX material after 12 months (0.23 mm/year), but 27Cr33Ni3Mo presents an accumulation of metal chlorides in the grain boundaries. The same effect, which is observed for Sanicro 69 in the P6 Högdalen boiler. This may result in poor scale adhesion after prolonged exposure, which may enhance the diffusion rate of corrosive species to the metal/oxide interface and thus further increase the corrosion rate of the material [11]

Considering these results and P6 Högdalen results, the SX is the most promising material of this group. Compared to Sanicro 69 and 27Cr33Ni3Mo, the SX alloy contains a higher amount of Si. The presence of Si in high-temperature materials has been reported to have a beneficial effect on corrosion protection [8-10] . Increased corrosion resistance and the formation of a SiO_2 layer was also observed for an Fe-20Cr and an Fe-20Cr-20Ni alloy upon addition of silicon in Ar-20CO_2 and Ar-20CO_2-20H_2O at 650 °C [13]. In more corrosive environments (in the presence of KCl) modification of Fe-15Cr alloys by addition of aluminum/silicon showed positive synergistic effects on the corrosion behavior when exposed to air at 650 °C [13, 14] .

The two conventional austenitic stainless steels, 316Ti and Esshete 1250, were subjected to a large degree of intergranular corrosion and the severity of the

corrosion attack was increased as a function of time exposed to the present environment. None of them has deposit left over the surface and the 316Ti material presents low quality cracked oxides after both 6 and 12 months exposure. In mild environments, austenitic stainless steels are expected to form a chromium-rich and protective oxide [15] . In environments rich in alkali chlorides, these materials are readily attacked by both alkali and chlorine, forming alkali chromates and metal with a corrosion product layer often consisting of an outward-growing hematite (Fe_2O_3) and an inward-growing (mixed) spinel oxide layer (Me_3O_4) [16] . In this study, only the inward-growing spinel oxide (rich in Cr and Ni) remains on the sample, whereas the outward-growing hematite as well as the deposited layer, have been lost. It is expected that the presence of alkali in the environment has destroyed the protective properties of the initial chromium-rich oxide [17, 18] . Furthermore, a grain boundary attack can be seen. In a recent study, the attack is associated with small levels of chlorine in the grain boundaries, where chlorine is suggested to increase the diffusivity at the grain boundaries and thereby causing accelerated corrosion [19] . This type of behavior is expected to be detrimental to the material over time, either by continuing the attack to spread laterally or by losing whole steel grains, as the attack decreases the mechanical stability of the material.

The last group of samples, marked in blue in Table 16, are coated materials. Being overlay welded materials, it is not possible to calculate a reliable material loss to compare with the rest of the exposed materials. The corrosion behavior is evaluated by means of SEM images and the depth of the oxide. The reference material is alloy 59, which presents a smooth surface after 12 months of exposure but a very thick oxide (around 500 µm) which is more than 10 times the thickness of the attack at the FeCrAl EF101 overlay weld for the 6 months exposure time. Due to the high thickness of the alloy 59 welded material, there is still much untouched material after the exposure, even having such a thick oxide layer on top. The attack in the alloy 59 is severe so the material “lost” in favor of the oxide still more than for the EF101 overlay weld material. That makes the EF101 WOL very promising for this application. The nitridation level for the EF101 WOL is very low at 6 months exposure too. Unfortunately, the 12 months exposure EF101 sample was lost during the exposure and was not possible to recover for analysis.

The EF100 overlay weld samples do not perform as well as EF100 bulk material for any of the exposure times. Both at 6 and 12 months exposure the overlay weld material presents cracked oxides, which lead to significant local diffusion of oxygen throughout the sample. At 6-month exposure the thickness of the oxide on EF100 is 10 times higher than on EF101. In addition, the oxide formed on EF101 is very smooth and well adherent, not presenting any cracks or detachment from the surface of the sample. The deposit is still present over the EF101 overlay weld.

The APMT overlay weld sample performs well at 6 months exposure presenting a smooth 200 µm oxide. The nitridation in this case is local, presenting zones with very thick nitridation and zones where it is not nitridation at all. Unfortunately, the 12 months exposure APMT WOL sample was lost during the exposure.

The Alloy 625 overlay weld sample presents a 170 µm thick oxide, which is well adherent to the metal surface, but it presents several deep cracks on its own surface, which can lead to local diffusion of oxygen.

Finally, the CorER sample was lost during exposure so no results can be presented in this report.

5.3 REVIEW OF POTENTIAL CORROSION ISSUES USING OCAC

Fluidized bed (FB) boilers are the preferred type of boiler for fuel flexible green heat and power production. FB boilers can burn a wide range of biomass and waste fuels with high efficiency and low emissions. This boiler type relies on a bed of particles that are being fluidized by a gas, typically air. When combusting biomass or waste, the bed particles conventionally use sand. Sand particles are becoming well mixed with fuel particles, which leads to improved combustion of the fuel particles in the presence of the fluidizing air. Besides enabling a good mixing capability, the sand bed is also the bearer of heat to the combustion process of the fuel particles. The main drawback with using sand high in silica as bed material is its agglomeration tendencies [20, 21] .Specially when combusting fuels containing alkali, the silica sand reacts with alkali to form low melting point alkali silicates and/or alkali alumina silicates. Furthermore, from a material degradation point of view, silica particles may possess erosive properties when fluidized. Despite these drawbacks with sand high in silica, the cost has been fairly low, and it is the most used bed material for FB boilers. However, there has been some research and tests with other types of bed materials, e.g., olivine [22] or dolomite [23] .Besides achieving good heat transfer properties, the bed material can achieve other valuable properties such as e.g., resistance towards agglomeration or the ability to capture SO_2.

During recent years, a new bed material, Ilmenite [24-26] has been presented. Ilmenite is a part of a group of bed materials that possess oxygen carrier properties. This means that the bed material can take up and release oxygen depending on the surroundings. Components of natural sand, e.g., silica (SiO_2) and feldspar (aluminosilicates) do not have this property. During combustion of the fuel particles in FB boilers using a sand bed, additional oxygen is necessary and is supplied via the fluidizing air (or in secondary air inlet). However, by utilizing a bed with bed particles having oxygen carrier abilities there is no necessity for additional oxygen supply at oxygen lean locations as the oxygen carrier particles transport oxygen from oxygen-rich to oxygen-lean locations. Thus, there is an even distribution of heat and oxygen within the reactor. This type of combustion is denoted as OCAC (Oxygen Carrier Aided Combustion) [27] .With OCAC, the surplus of air to the boiler can be decreased without risking poor combustion properties, e.g., high emissions of CO. Bed materials with oxygen carrier abilities are also a key aspect when designing the next generation of FB boilers where CCS (Carbon, Capture & Storage) is integrated (the so-called CLC (Chemical Looping Combustion) plant [28]

One of this project's aims was to investigate how the material degradation (corrosion and/or erosion) may be affected by changing the bed material from sand

to Ilmenite (an oxygen carrier material). The initial plan was to conduct corrosion exposures at the FBHE-tubes in the two boilers included in this project. However, due to delays emerging from the COVID pandemic and thereby renewed commercial considerations there has not been any possibility to perform such planned exposures. Instead, this section has been focusing on literature studies in order to estimate potential material degradation. Furthermore, there has been a dialogue and sharing of results between this project and another Biokraft project "46450-1 Syrebärarstödd förbränning för effektivare bränsleomvandling I FB-pannor med samtidig återvinning av alkaliföreningar" regarding the use of ilmenite as bed material. Some of which are summarized below.

Ilmenite is an ore consisting mainly of titanium-iron oxide with formula $FeTiO_3$. It is a weakly magnetic ore and is today mostly used to produce titanium dioxide, for use in paints, plastics, paper, sunscreen and food. It is the presence of iron (Fe) that gives Ilmenite its oxygen carrier properties as iron can switch between its two oxidation states (Fe^{2+} and Fe^{3+}). Ilmenite is, like SiO_2 in sand, readily reacting with alkali at higher temperatures. However, in contrast to alkali silicates, the alkali titanates that form have a much higher melting point. Thus, the ilmenite has compared to sand rich in silica a much lower risk of forming low melting point compounds that will make the particles stick together. As a consequence, the agglomeration risk is considerably lower for ilmenite compared to many varieties of natural sand.

The use of ilmenite as bed material in FB boilers is a rather new experience, however tests have been conducted in industrial scaled boilers in the size from 12 – 400 MW_{th} [29] .The majority of the work has been connected to its oxygen carrier ability, agglomeration tendencies and alkali uptake. From the corrosion point of view, the ability to take up alkali from the fuel and the ability to decrease local "hot-spots" high temperature zones within the furnace are probably the most important parameters.

For superheaters, either placed in the convective pass or in the fluidized bed, the uptake of alkali in the bed is important. Because the alkali not captured by the bed is potentially ending up as corrosive alkali compounds, e.g., KCl or NaCl, on the superheater tubes, causing an accelerated corrosion attack. The use of ilmenite as bed material in CFB boilers has been investigated earlier in literature, however, the published data on utilizing an Ilmenite bed in connection to corrosion is scarce. Thus, the full scale testing investigating the effect of changing bed material to Ilmenite is not fully elucidated. As mentioned above, knowing the mass balance of alkali in the boiler will be of uttermost importance. Recent studies in lab/pilot scale suggest however that the Ilmenite bed will act perfectly as an alkali getter. According to Lu at al. [30] the ilmenite captured about 40-65% of the alkali (K) during a 5h exposure. The formed alkali titanate was KTi_8O_{16}. The potassium uptake with Ilmenite was similar to olivine.

Based on the laboratory and pilot studies using Ilmenite, it shows good ability to capture alkali (with considerably less risk of agglomeration), comparatively to silica sand. However, the release of alkali to the flue gases will be dependent on several operational parameters where the most important will probably be the rate of bed renewal. For natural sand based beds, the renewal rate is usually in the

order of 1-3 kg/MWh for biomass fuels and 6 kg/MWh for waste fuels. The total bed inventory differs but can be roughly 60 tons for a FB-boiler in the thermal size of 75 MW. The long-term experiences reached so far with using Ilmenite as bed material, the renewal rate have been decreased with a factor of 8 compared to a silica sand bed. Even though the material performance of e.g., superheater tubes have not been studied in detail, successful operation with an Ilmenite bed for 12 000 hours have been demonstrated [31] . Based on the alkali uptake capability of Ilmenite and long term successful operation, it is anticipated that the corrosion of superheater tube will not increase if changing the bed material from silica sand to Ilmenite. However, this needs to be investigated in depth and primarily in full scale exposures, i.e., in operating commercial plants.

6 Goal fulfillment

This project addresses two problem areas related to material wastage that today limits availability and fuel flexibility of biomass and waste fired power plants, corrosion/erosion of heat exchangers and water walls. The project's goal is to improve plant economy of plants using renewable fuels and increase the competitiveness towards fossil fueled plants by targeting these two problem areas in the (fluidized bed) boilers. Below the different goals are specified in detail and if the goal has been reached or not.

- Reduce the total cost of water walls and/or fluidized bed superheaters by enabling new materials and/or by mitigating the corrosive environment by changing bed material or optimized design. The total cost can be reduced by improving the material lifetime or by lowering the cost.

This project aimed at improving the plant economy for plants using renewable fuels and thereby increasing the competitiveness towards fossil fueled plants by targeting areas in the plants where material issues are of concern. A key parameter in increasing the plant economy is to decrease the maintenance cost. The replacement of failing heat exchanger materials inside the plant is a larger contributor to the maintenance costs. By optimizing the materials, in such a way that the most cost-effective materials are used, the overall maintenance can be decreased. We have performed a substantial number of material testing campaigns including a wide palette of materials for two positions in the boiler, which has high degradation rates when burning challenging fuels: the water walls and fluidized bed superheaters. From a material perspective, almost 20 types of material including low alloyed steels, stainless steels, nickel-based alloys and FeCrAl alloys have been investigated. Furthermore, the material selection has included both commercial alloys and newly developed alloys, in the form of bulk material as well as weld overlay coatings and metallic spray coatings.

The main aim of this goal has been to provide reliable data on the material performance of the abovementioned materials and thereby enable more accurate cost calculations to be done by the industry. As such, the material selection of boiler components can be optimized, and the maintenance cost be decreased. The exact cost of the materials is unfortunately not open to the public and furthermore, the material cost is changing constantly due to the price of alloying elements, etc. However, in order to provide an estimate about the cost difference between different materials (which is fairly stable over time), Table 15 and Table 16 was provided in chapter 5 “Analysis of the results”. Hereby, the reader can get a rough idea about the material cost, which can be combined with their performance.

This goal is considered as fulfilled.

- Increase the knowledge of material degradation mechanisms and environmental parameters at play in fluidized bed superheaters.

Overall, the large exposure matrix together with a wide and in-depth microstructural analysis had provided the material community with valuable

information relevant for corrosion performance. This for two positions in the power plants that today are subject to high material wastage rates.

For the FBHE tubes, there was a special interest in deducing if the material wastage was primarily driven by erosion or by corrosion. The collective analysis of all the clamp samples that have been exposed on top of the tubes within the FBHE section indicates that it is a combination of erosive and corrosive forces that causes the degradation. In many cases, the samples were covered by a deposit, which suggests that erosive forces have been mild. In other cases, the deposit layer was minimal or non-existent leading to the conclusion that erosive forces were at play. Furthermore, it is probable that corrosion and erosion influence each other synergistically, leading to higher material wastages. The results showed signs of steel grain boundary attacks (on several occasions in combination with the presence of Cl) and it is expected that a material suffering from steel GB attack is also more susceptible to erosion.

This goal is considered as fulfilled.

- Investigate the properties of newly developed alloys together with commercially available materials for water walls. Both thermal spray coating and overlay welding will be investigated.

As above, the material matrix executed in the exposures has been wide, covering both materials that are used today and newly developed steels, FeCrAls and coatings. The corrosion analysis has primarily been performed by means of material loss determination and cross-sectional SEM/EDX analysis. Special focus has been put towards the newly developed materials (EF100 and EF101) in order to investigate their potential use for both water walls and for tubes to be used as FBHE material. The results show that the newly developed FeCrAl alloys (EF100 and EF101) are potential candidates as boiler materials, taking a corrosion/erosion perspective. However, both these types of materials suffered from nitridation, which needs to be further studied. It is not clear how the nitridation process affects the corrosion performance on a longer perspective than one year. Furthermore, as these materials are not classed as pressure bearing materials, they cannot be used as monotubes. Instead, their initial use would be as corrosion/erosion resistant coatings and/or co-extruded tubes. The new insights in the performance of these alloys were presented in journal article.

This goal is considered as fulfilled.

- Publish 1 scientific article, present the results at two conferences and complete two academic theses within the project.

Within this project the following have been achieved within the sub-goals:

Publish 1 scientific article.

- A material degradation study of novel FeCrAl alloys, stainless steels and nickel base alloy in fluidized bed heat exchangers of a waste fired CFB boiler
  Hampus Lindmark, Julien Phother, Maria Dolores Paz Olausson, Johanna

Nockert, Fredrik Lind, Anna Jonasson, Vesna Barišić, Kyösti Vänskä, Laura Rioja-Monllor and Jesper Liske

Fuel 338, 127299, 2023

Present the results at two conferences.

- **Investigating the performance of novel FeCrAl alloys in a fluidized bed heat exchanger application of a waste fired CFB boiler**
  Hampus Lindmark, Julien Phother, Maria Dolores Paz Olausson, Johanna Nockert, Fredrik Lind, Anna Jonasson, Vesna Barišić, Kyösti Vänskä, Laura Rioja-Monllor and Jesper Liske

Oral presentation at the 24th Fluidized bed conversion conference, FBC-24, May 2022, Gothenburg Sweden

- **HTC/KME conference 2019**
  KME 803: New materials and Oxygen Carrier Aided Combustion for improved competitiveness of FB plants using renewable fuels

Oral presentation by Julien Phother and Jesper Liske, Gothenburg 12-13 March 2019

- **HTC/KME conference 2020**
  KME 803: New materials and Oxygen Carrier Aided Combustion for improved competitiveness of FB plants using renewable fuels

Oral presentation by Julien Phother and Jesper Liske, Digital conference, 4-5 November 2020

- **KME conference/workshop (planned 6th March 2023)**
  KME 803: New materials and Oxygen Carrier Aided Combustion for improved competitiveness of FB plants using renewable fuels

Oral presentation by Hampus Lindmark and Maria Dolores Paz

Complete two academic theses

- **Julien Phother Ph.D. thesis**
  High Temperature Corrosion Behavior in Biomass- and Waste-Fired Boilers - Insights into catastrophic corrosion and corrosion mitigation techniques
  Ph. D. thesis, Chalmers, 2020

- **Hampus Lindmark, Licentiate thesis**
  Title to be decided
  Lic. Thesis planned for fall 2023

This goal is considered as fulfilled. This includes a planned licentiate thesis to be presented in the fall 2023, based on the results and conclusions obtained within this project. The other subgoals (publishing one journal article and two conference presentations) are reached within the project's timeframe.

7 Summary and conclusions

The project has successfully conducted several corrosion tests in two commercially operated boilers; the waste-fired P15 boiler at Händelö and the waste-fired P6 boiler in Högdalen. The corrosion tests were carried out at two different positions in the boiler; the water wall region and the fluidized bed heat exchanger region. The water wall tests were carried out in the P6 boiler in Högdalen and lasted for 1 week while the fluidized bed heat exchanger tests were carried out both in Högdalen and Händelö with an exposure time ranging from 6 to 24 months. A wide range of materials, ranging from low alloyed steels, stainless steels, Ni-base alloys, FeCrAl alloys and different coating techniques including overlay weld materials has been investigated. The following conclusions can be made from the findings:

Water wall exposures:

- Oxide formation was only observed for the low alloyed steel (16Mo3) after 1 week of exposure in the water wall region of the waste fired P6 boiler in Högdalen. High concentration of chlorine was observed close to the metal/oxide interface suggesting that Cl diffusion through the oxide plays an important role in the material degradation rate.
- Neither Ni-base steel nor stainless steel showed any indication of material degradation, and no accumulation of Cl was observed at the metal/deposit interface for these samples.
- Both conventional and newly developed FeCrAl alloy showed promising results as their performance was on par with the Ni-base and stainless-steel samples.

Fluidized bed heat exchangers:

- The newly developed FeCrAl EF101 showed the most promising results after 12 and 24 months of exposure in Händelö and Högdalen, respectively, obtaining a material loss significantly lower than conventional stainless steels and Ni-base alloys.
- Nitridation zones were observed on all FeCrAl alloys regardless of boiler type with the following severity ranked: APMT > EF100 > EF101. It is not known how nitridation affects the corrosion behavior. In the present project the material presented an increase of thickness of the nitridated zone without an increase in the material loss, so it is unclear how nitridation affects corrosion in this particular application or if it affects at all.
- EF101 WOL is the most promising material from the overlay weld samples at Händelö. It performs better than all the other coatings at 6 months. It performs better than the EF101 bulk material for the same exposure time.

No sample could be recovered from the P15 boiler in Händelö after 12 months exposure.

- The most promising material from the austenitic stainless-steel block is the alloy SX. It experienced the lowest material loss regardless of boiler type and time. A Si-rich/Cr-rich oxide was observed in the grain boundaries at the corrosion front of the material. It is suggested that Si oxide may improve the resistance towards both corrosion and erosion mechanisms.
- Both HVAF and CorEr coating failed after 12 months of exposure regardless of boiler type. The oxide formation on the underlaying bulk material indicate that the failure occurred at an early stage of the exposure.

8 References

[1] H. Kinnunen, M. Hedman, M. Engblom, D. Lindberg, M. Uusitalo, S. Enestam and P. Yrjas. The influence of flue gas temperature on lead chloride induced high temperature corrosion. Fuel, 2017; 196:241-251

[2] A. Persdotter, M. Sattari, E. Larsson, M. A. O. Ogaz, J. Liske and T. Jonsson. Oxidation of Fe-2.25Cr-1Mo in presence of KCl(s) at 400 degrees C - Crack formation and its influence on oxidation kinetics. Corrosion Science, 2020; 163:

[3] M. A. Olivas-Ogaz, J. Eklund, A. Persdotter, M. Sattari, J. Liske, J. E. Svensson and T. Jonsson. The Influence of Oxide-Scale Microstructure on KCl(s)-Induced Corrosion of Low-Alloyed Steel at 400 degrees C. Oxidation of Metals, 2019; 91:291-310

[4] N. Folkeson, T. Jonsson, M. Halvarsson, L. G. Johansson and J. E. Svensson. The influence of small amounts of KCl(s) on the high temperature corrosion of a Fe-2.25Cr-1Mo steel at 400 and 500°C. Materials and Corrosion, 2011; 62:606-615

[5] H. Kinnunen, M. Hedman, D. Lindberg, S. Enestam and P. Yrjas. Corrosion in Recycled Wood Combustion-Reasons, Consequences, and Solutions. Energy & Fuels, 2019; 33:5859-5866

[6] Y. Alipour and P. Henderson. Corrosion of furnace wall materials in waste-wood fired power plant. Corrosion Engineering Science and Technology, 2015; 50:355-363

[7] J. Eklund, M. D. Paz, B. Jönsson, J. Liske, J. E. Svensson and T. Jonsson. Field exposure of FeCrAl model alloys in a waste-fired boiler at 600°C: The influence of Cr and Si on the corrosion behaviour. Materials and Corrosion, 2019; 70:1476-1485

[8] V. Asokan, J. Eklund, S. Bigdeli and T. Jonsson. The influence of Si on the primary protection of lean FeCrAl model alloys in O2 and O2+H2O at 600 °C—A microstructural investigation. Corrosion Science, 2021; 179:

[9] J. Eklund, I. Hanif, S. Bigdeli and T. Jonsson. High temperature corrosion behavior of FeCrAlSi model alloys in the presence of water vapor and KCl at 600 °C – The influence of Cr content. Corrosion Science, 2022; 198:

[10] T. Sand, A. Edgren, C. Geers, V. Asokan, J. Eklund, T. Helander, J. E. Svensson and L. G. Johansson. Exploring the Effect of Silicon on the High Temperature Corrosion of Lean FeCrAl Alloys in Humid Air. Oxidation of Metals, 2021; 95:221-238

[11] M. D. Paz. Increased steam temperature with Steamboost superheater in grate-fired boilers- Linking deposit formation and high temperature corrosion. Impacts of Fuel Quality on Power Production, Prague 2016

[12] D. M. Rishel, F. S. Pettit and N. Birks. Some Principal Mechanisms in the Simultaneous Erosion and Corrosion Attack of Metals at High-Temperatures. Materials Science and Engineering a-Structural Materials Properties Microstructure and Processing, 1991; 143:197-211

[13] Y. S. Li, Y. Niu and M. Spiegel. High temperature interaction of Al/Si-modified Fe-Cr alloys with KCl. Corrosion Science, 2007; 49:1799-1815

[14] Y. S. Li, M. Spiegel and S. Shimada. Effect of Al/Si addition on KCl induced corrosion of 9% Cr steel. Materials Letters, 2004; 58:3787-3791

[15] J. Pettersson, J. E. Svensson and L. G. Johansson. KCl-induced corrosion of a 304-type austenitic stainless steel in O 2 and in O 2 + H 2O environment: The influence of temperature. Oxidation of Metals, 2009; 72:159-177

[16] A. Persdotter, J. Eklund, J. Liske and T. Jonsson. Beyond breakaway corrosion – Influence of chromium, nickel and aluminum on corrosion of iron-based alloys at 600 °C. Corrosion Science, 2020; 177:108961

[17] T. Jonsson, J. Froitzheim, J. Pettersson, J. E. Svensson, L. G. Johansson and M. Halvarsson. The influence of KCl on the corrosion of an Austenitic stainless steel (304L) in oxidizing humid conditions at 600°C: A microstructural study. Oxidation of Metals, 2009; 72:213-239

[18] J. Pettersson, H. Asteman, J. E. Svensson and L. G. Johansson. KCl induced corrosion of a 304-type austenitic stainless steel at 600°C; the role of potassium. Oxidation of Metals, 2005; 64:23-41

[19] J. Phother-Simon, I. Hanif, J. Liske and T. Jonsson. The influence of a KCl-rich environment on the corrosion attack of 304 L: 3D FIB/SEM and TEM investigations. Corrosion Science, 2021; 183:109315

[20] M. Zevenhoven-Onderwater, M. Ohman, B. J. Skrifvars, R. Backman, A. Nordin and M. Hupa. Bed agglomeration characteristics of wood-derived fuels in FBC. Energy & Fuels, 2006; 20:818-824

[21] H. B. He, D. Bostrom and M. Ohman. Time Dependence of Bed Particle Layer Formation in Fluidized Quartz Bed Combustion of Wood-Derived Fuels. Energy & Fuels, 2014; 28:3841-3848

[22] R. Faust, K. Fürsatz, P. Aonsamang, M. Sandberg, M. Kuba, N. Skoglund and P. Knutsson. Early layer formation on K-feldspar during fluidized bed combustion with phosphorus-rich fuel. Fuel, 2023; 331:

[23] P. Ninduangdee and V. I. Kuprianov. Combustion of oil palm shells in a fluidized-bed combustor using dolomite as the bed material to prevent bed agglomeration. 2013 International Conference on Alternative Energy in Developing Countries and Emerging Economies (2013 Aedcee), 2014; 52:399-409

[24] H. Leion, A. Lyngfelt, M. Johansson, E. Jerndal and T. Mattisson. The use of ilmenite as an oxygen carrier in chemical-looping combustion. Chemical Engineering Research & Design, 2008; 86:1017-1026

[25] A. Corcoran, P. Knutsson, F. Lind and H. Thunman. Mechanism for Migration and Layer Growth of Biomass Ash on Ilmenite Used for Oxygen Carrier Aided Combustion. Energy & Fuels, 2018; 32:8845-8856

[26] R. Faust, I. Lamarca, A. Schaefer, F. Lind and P. Knutsson. Magnetic properties of ilmenite used for oxygen carrier aided combustion. Fuel, 2023; 340:

[27] F. Lind, A. Corcoran and H. Thunman. Validation of the oxygen buffering ability of bed materials used for OCAC in a large scale CFB boiler. Powder Technology, 2017; 316:462-468

[28] A. Lyngfelt, B. Leckner and T. Mattisson. A fluidized-bed combustion process with inherent CO2 separation; application of chemical-looping combustion. Chemical Engineering Science, 2001; 56:3101-3113

[29] F. Storner, F. Lind and M. Ryden. Oxygen Carrier Aided Combustion in Fluidized Bed Boilers in Sweden-Review and Future Outlook with Respect to Affordable Bed Materials. Applied Sciences-Basel, 2021; 11:

[30] D. Y. Lu, Y. Tan, M. A. Duchesne and D. McCalden. Potassium capture by ilmenite ore as the bed material during fluidized bed conversion. Fuel, 2023; 335:

[31] F. Lind, A. Corcoran, B. Å. Andersson and H. Thunman. 12,000 hours of operation with oxygen-carriers in industrially relevant scale. VGB PowerTech, 2017

[32] P. Kofstad. High Temperature Corrosion. 1988

[33] H. Nielsen, F. Frandsen, K. Dam-Johansen and L. Baxter. The implications of chlorine-associated corrosion on the operation of biomass-fired boilers. Progress in energy and combustion science, 2000; 26:283-298

[34] H. P. Nielsen, F. J. Frandsen and K. Dam-Johansen. Lab-scale investigations of high-temperature corrosion phenomena in straw-fired boilers. Energy & Fuels, 1999; 13:1114-1121

[35] M. Sánchez Pastén and M. Spiegel. High temperature corrosion of metallic materials in simulated waste incineration environments at 300–600° C. Materials and corrosion, 2006; 57:192-195

[36] Y. Shinata. Accelerated oxidation rate of chromium induced by sodium chloride. Oxidation of Metals, 1987; 27:315-332

[37] M. Spiegel. Salt melt induced corrosion of metallic materials in waste incineration plants. Materials and corrosion, 1999; 50:373-393

[38] A. Ruh and M. Spiegel. Thermodynamic and kinetic consideration on the corrosion of Fe, Ni and Cr beneath a molten KCl–ZnCl2 mixture. Corrosion science, 2006; 48:679-695

[39] H. Kinnunen, D. Lindberg, T. Lauren, M. Uusitalo, D. Bankiewicz, S. Enestam and P. Yrjas. High-temperature corrosion due to lead chloride mixtures simulating fireside deposits in boilers firing recycled wood. Fuel processing technology, 2017; 167:306-313

[40] D. Bankiewicz, S. Enestam, P. Yrjas and M. Hupa. Experimental studies of Zn and Pb induced high temperature corrosion of two commercial boiler steels. Fuel processing technology, 2013; 105:89-97

[41] D. Bankiewicz, P. Yrjas, D. Lindberg and M. Hupa. Determination of the corrosivity of Pb-containing salt mixtures. Corrosion science, 2013; 66:225-232

[42] A. Talus, R. Norling, L. Wickstrom and A. Hjornhede. Effect of Lead Content in Used Wood Fuel on Furnace Wall Corrosion of 16Mo3, 304L and Alloy 625. Oxidation of Metals, 2017; 87:813-824

[43] B. J. Skrifvars, R. Backman, M. Hupa, K. Salmenoja and E. Vakkilainen. Corrosion of superheater steel materials under alkali salt deposits - Part 1: The effect of salt deposit composition and temperature. Corrosion science, 2008; 50:1274-1282

[44] Y. Alipour. Furnace Wall Corrosion in a Wood-fired Boiler. KTH Royal Institute of Technology 2015; 2015:52:xx, 73

[45] R. F. A. Pettersson, J. Storesund and M. Nordling. Corrosion of overlay weld cladding in waterwalls of waste fired CFB boiler. Corrosion Engineering, Science and Technology, 2009; 44:218-226

[46] P. Henderson, P. Ljung, P. Kallner and J. Tollin. 2000;

[47] P. Henderson, J. Högberg and M. Mattsson. 2002; II:883-892

[48] C. T. Kang, F. S. Pettit and N. Birks. Mechanisms in the Simultaneous Erosion-Oxidation Attack of Nickel and Cobalt at High-Temperature. Metallurgical Transactions a-Physical Metallurgy and Materials Science, 1987; 18:1785-1803

[49] R. Norling and I. Olefjord. Erosion-corrosion of Fe- and Ni-based alloys at 550 degrees C. Wear, 2003; 254:173-184

[50] A. Nafari. Superheater corrosion in the loop seal of a wood-fired CFB boiler. Chalmers University of Technology 2003; Licenciate of Philosophy:

[51] A. Nafari and A. Nylund. Field study on superheater tubes in the loop seal of a wood fired CFB plant. Materials and Corrosion-Werkstoffe Und Korrosion, 2004; 55:909-920

[52] A. Ekström. Förutsättningar för ökad livslängd av sandlåsöverhettare. Uppsala Universitet 2018; Master:

9 Appendix: LITERATURE Review

In order to reduce the net emission of CO_2, biomass and waste are being used as fuel instead of fossil fuels for power plants and combined heat and power plants (CHPs). This change in fuel is environmentally friendly as biomass and waste, considered as renewable fuels, have a lower net emission of CO_2 compared to fossil fuels.

However, the share of fossil fuels in heat and power production in the world is about 70-75% whereas the share of renewable fuels is minor. In order to increase the share of renewables, on the expense of fossil fuels, the competitiveness of boilers using renewable fuels needs to increase. One of the main reasons why using renewable fuels is more expensive than fossil fuels is the maintenance cost. The combustion of biomass and waste leads to a more corrosive environment for the superheaters and water walls. In particular, superheater tubes placed in the loop seal suffer from extensive material degradation. This results in both, planned and unplanned revision stops and leading to direct costs (replacing tubes, building scaffolding, etc.) as well as loss of revenue.

Thus, in order to increase the share of renewable fuels, it is necessary to enhance the competitiveness of plants using renewable fuels. This can be achieved by three different ways:

- Increase the revenue by enhancing the efficiency of the production.
- Reduce the cost by minimizing the maintenance of the plant.
- Reduce the cost by using cheaper fuels.

Work package 1: Water walls

Introduction

Water walls of boilers using renewable fuels are commonly made from low-alloyed steels with a material temperature reaching up to 400 °C and with a flue gas temperature of 750 - 1000 °C. However, the water walls experience accelerated corrosion due to the presence of corrosive species in the deposit and flue gas. The deposits are often reported to contain molten species, which is expected to accelerate the corrosion attack. The temperatures of the material and the flue gas facilitate the deposit to be fully or partly molten. Furthermore, the melting points of the deposits can also be lowered if there is a specific composition of the deposit so that a eutectic melting point could occur between two (or more) mixed salts. The melting point of some salts resulting in a compound/mixture with a lower melting point than each individual salt is listed in Table 17. The presence of e.g. lead (Pb) and zinc (Zn) compounds are usually pointed out as harmful compounds since their melting points are particular low. The presence of lead and zinc compounds is often detected in recycled waste wood and other waste fuels from industry.

In order to reduce the corrosion attack, overlay weldings or coatings are applied onto the water walls to protect the low alloyed-steels. By using a more corrosion-resistant materials, such as e.g. nickel-based alloys, the overall lifetime of the water wall could be prolonged. However, the use of nickel-based materials leads to high costs since nickel-based materials are expensive and the application of the welding/coating needs to be performed during a revision stop of the boiler. Thus, to increase the overall plant economy of boilers using renewable fuels, it is necessary to explore the possibilities of using cheaper materials (having at least as long lifetime as nickel-based materials) or using materials with longer lifetime (and still manageable costs).

Table 17.Salts and mixture with their respective melting temperature

Salt and mixture	Melting point (°C)
$ZnCl_2$	318
$PbCl_2$	489
KCl	772
NaCl	801
$FeCl_2$	673
KCl-$ZnCl_2$	230
KCl-$PbCl_2$	412
KCl-$FeCl_2$	355
NaCl-$ZnCl_2$	262
NaCl-$PbCl_2$	415
NaCl-$FeCl_2$	375

Corrosion mechanisms

The majority of the corrosion mechanisms regarding water walls in biomass- and waste-fired boilers presented in the literature are connected towards a melted deposit and/or corrosion product [32-39] . Kofstad [32] has suggested several reasons for the corrosiveness of melted/liquid phases. First, the liquid itself provides fast transport of ions. Second, a liquid phase provides an electrolyte that can act as a pathway for ionic charge transfer for an electrochemical attack. Thirdly, the melt can dissolve the protective oxide, which exposes the metal to the environment.

In waste-fired boilers, the presence of zinc and lead compounds has also been suggested to account for severe corrosion by lowering the melting point of the deposits [37] .

Ruh, et al have shown using thermodynamic calculations that $FeCl_2$ is soluble in molten KCl-$ZnCl_2$ near eutectic compositions [38] . In this manner, the outward diffusion of $FeCl_2$ is favored and diffuses easily to the outer part of the salt melt layer. As $FeCl_2$ reaches the outer part of the salt melt, $FeCl_2$ will be oxidized due to the high partial pressure of oxygen. The authors have concluded that the solubility of metal chlorides in molten KCl-$ZnCl_2$ leads to higher diffusion rate and subsequently to higher oxidation rate. Thus, the solubility of metal chlorides in molten salts influences the corrosion. A suggested mechanism for the chloride melt-induced dissolution of the steel can be seen in Figure 63.

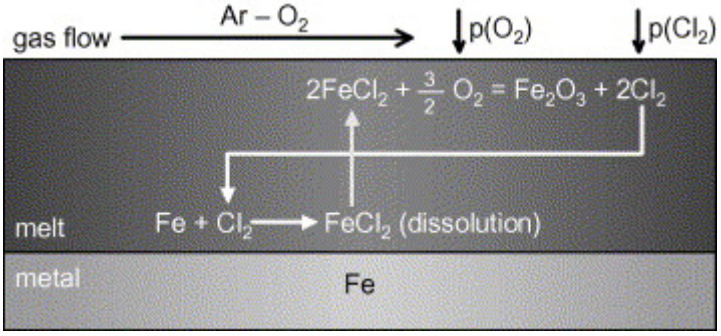

Figure 63. Schematic model of chloride melt induced high temperature corrosion process, showing the transport of gas species and chemical reactions forming iron oxide and iron chloride [38] .

The overall corrosive effect of $ZnCl_2$ and $PbCl_2$ has been studied in several papers [39-42] . The results showed for instance that $PbCl_2$ is more corrosive compared to $ZnCl_2$ [40] . Also, severe corrosion attack could be observed already below the melting point of $PbCl_2$ containing salt mixtures (with KCl or K_2SO_4) on low-alloyed steels such as T22 [39, 41] . Thus, the presence of 100% melted phase is not necessary in order to obtain an accelerated corrosion attack. The terms of sub-T-0 corrosion, indicating corrosion taking place below any melting of the deposit and (2) super-T-0 corrosion, indicating corrosion taking place when the deposit contains melt have been introduced [43] .

In general, the eutectic composition, forming the melt in the deposit, is hard to prove with analytical tools used (primarily SEM/EDX and XRD). The eutectic point

between two salts, of which the phase is 100% in liquid form, is seldom confirmed by the EDX data. This could be due to unavoidable fact that the analysis is always performed post-exposure and at room temperature.

Field exposures

- Furnace Wall Corrosion in a Wood-fired Boiler [44]

The investigation was performed in the Idbäcken power plant of Vattenfall AB in Nyköping, Sweden. The 97.5 MW boiler in which investigations took place is of a BFB type. The steam temperature is 540 °C at 140 bar. The fuel used is 100 % waste wood.

The water walls are made of 16Mo3 which corrodes rapidly when burning waste wood. The cause of the corrosion attack was suggested to be due to chlorides leading to the formation of a continuous but thin layer of iron chloride under a thick iron oxide. Similar corrosion rates were measured from tests lasting 1 000 and 20 000 hours, respectively, indicating a linear corrosion rate. The corrosion mechanism is described as active oxidation by HCl and H_2O where HCl plays a catalytic role in the process rather than Cl_2. The partial pressure of Cl_2 (g) was calculated to be less than 0.1 ppm in this type of boiler environment.

The deposition of KCl and the corrosion rate of 16Mo3 increases with increasing temperature in the furnace walls area of a wood-fired boiler. The corrosion mechanism was found to be similar at low and high temperature. Even at a low metal temperature (285 °C) the corrosion rate of the furnace wall exceeded 0.5 mm per firing season which implied 16Mo3 without a coating is not a suitable material for water walls when burning waste wood. Testing different coating materials showed:

- Nickel-base alloy 625 can reduce the corrosion rate drastically. However, some corrosion attack could still be seen, and the Alloy 625 samples were attacked by a combination of potassium and lead leading to the formation of non-protective potassium lead chromate.
- FeCrAl alloy APMT also showed a very low corrosion rate. APMT samples were mainly attacked by K and Cl. Pb was not found in the corrosion product of APMT.
- Stainless steel 310S showed a moderate corrosion rate and could be a less-expensive alternative to nickel-based alloys. Stainless steel 310S was suggested to be corroded by two mechanisms, a combination of K-Pb and chloride-induced corrosion.

- Corrosion of overlay weld cladding in water walls of waste fired CFB boiler [45]

The investigation was performed in a 75MW CFB boiler in Händelö, Sweden. The steam temperature is 470 °C at 65 bar. During the study the fuel consisted of 50 % household waste and 50 % industrial waste. Test panels were welded on the front wall of the boiler using six different materials:

- Alloy 625
- Alloy 625mod (3 wt-% W)
- Alloy 59
- Alloy 650
- Alloy 22
- Alloy 310

The panels were inspected after 3 827 hours and again after a total of 7 727 hours.

The following statements were made:

- The exposure of overlay welded test water wall panels in a CFB waste fired boiler showed that conditions were extremely corrosive, with metal losses of 0.3 – 1.1 mm measured with an *in-situ* thickness gauge during the 7 727 hours exposure period.
- Extensive pitting occurred on all five of the nickel-based alloys tested. The maximum pit depth measured on specimens removed from the panels was roughly 1 mm. The pit depth was often significantly larger than the metal loss estimated from thickness gauge measurements. This means that there is a danger that the latter underestimates local metal wastage which can lead to premature tube failure
- There was no clear differentiation between the alloying strategies for nickel-based alloys of adding niobium (in alloy 625), tungsten (in alloy 22 and a modified alloy 625 type) or increasing the molybdenum content (in alloy 59). However, alloy 650, which is a cheaper alternative by virtue of its higher iron content of 14% showed a higher corrosion rate and developed the deepest pits.
- The austenitic stainless steel 310 appears to be an attractive alternative to the more expensive nickel-based alloys. This steel exhibited uniform corrosion but no pitting, with the result that metal wastage is predictable and easy to monitor. The uniform metal loss was on a par with the pit depth seen for the nickel-based alloy 650.
- Analysis of the deposits and corrosion products indicated predominant presence of alkali chlorides, also significant amounts of copper, zinc, lead and mercury. The corrosion mechanism was considered to be fluxing or dissolution of the otherwise protective oxide by a complex molten salt.

Work package 2: Fluidized bed heat exchangers

Introduction

In a Circulating Fluidized Bed (CFB) boiler the fuel is combusted in a fluidized sand bed. The sand particles are separated from the produced flue gases in a cyclone and the hot flue gases are subsequently passing superheaters, that are located in the convective pass. However, this position is often rather corrosive and in order to avoid too high corrosion rates the steam temperatures, and thereby also the material temperatures, are kept low. In newer CFB boilers, superheaters have also been mounted in the loop seal, the position of the boiler where the sand is recirculated back into the combustion chamber after been separated from the flue gases in the cyclone. In this position, the heat is transferred to the superheaters from the hot sand, instead of the hot flue gases. By installing a superheater in the loop seal the electrical efficiency of the boiler can be increased. This since higher steam temperatures can be utilized in this, in comparison, mild environment. Also, the heat transfer coefficient between the sand and the superheater tubes is very large resulting in a higher heat transfer per unit area of tube surface compared to the superheaters situated in the convective pass [46, 47] .

The loop seal superheaters are however suffering from material wastages. The supposed mild environment is probably harsher than anticipated due to a combination of corrosive species brought in by contaminated sand particles and erosion. However, little of this problem has been studied in literature.

Corrosion/material degradation mechanisms

The few published works about corrosion in the loop seal points out the erosion corrosion as the main degradation mechanism. This mechanism is especially pronounced at higher temperatures and it is due to the synergism between erosion and corrosion. High temperature erosion-corrosion has been described according to four categories [12, 48]

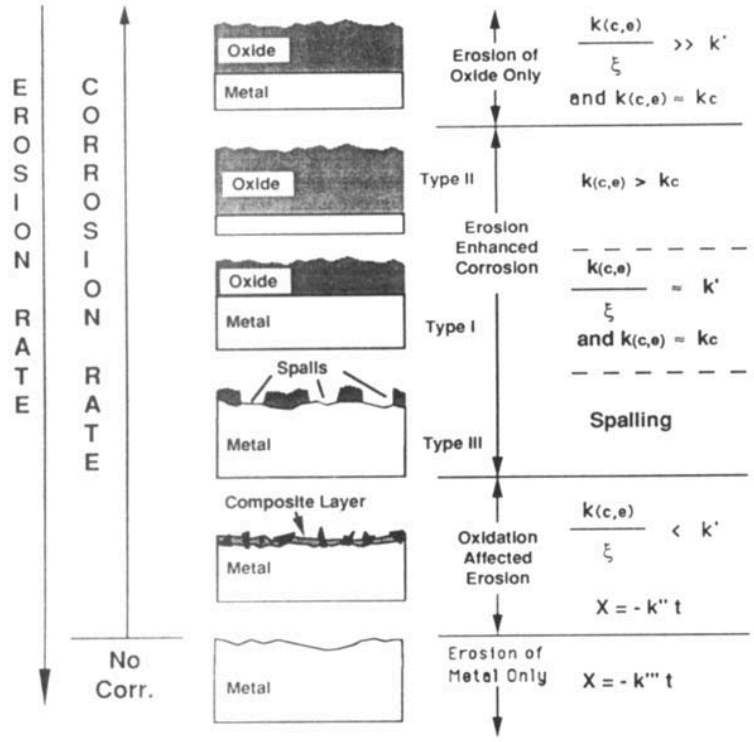

Figure 64. Erosion-corrosion interaction regimes, incorporating three types of erosion enhanced-corrosion behavior [12]

1. *Pure corrosion*. In this regime the effect of erosion is confined to erosion of the oxide layer and is negligible compared with corrosion. The rate of scale thickening can be described by a parabolic relationship (assuming a diffusion-controlled process).
2. *Erosion enhanced-corrosion*. The erosion process does not alter the scale growth mechanism but simply modifies the way in which the scale thickness varies with time and, therefore, influences the variation of the oxidation rate with time. As occurring when erosion thinned the oxide scale such that the oxidation rate increased to balance the erosion rate and a constant steady state scale thickness resulted. Owing to erosive thinning of the scale, the rate of corrosion is increased or enhanced--hence the term erosion-enhanced oxidation. This kind of erosion-corrosion is divided in three types (Figure 64):
    a. Type I occurs if the oxide is eroded to the degree that it is thinner than in the case of pure oxidation. Compare to pure oxidation the material wastage is larger
    b. Type II. The oxide is thicker than in the case of pure oxidation. Formation of cracks in the oxide layer creates short circuit diffusion paths for the reacting species, thereby increasing the corrosion rate [49] . The mechanism is illustrated in Figure 65.
    c. Type III. In the case when the oxide layer has partially spalled due to the thermal and mechanical stresses is no longer protective

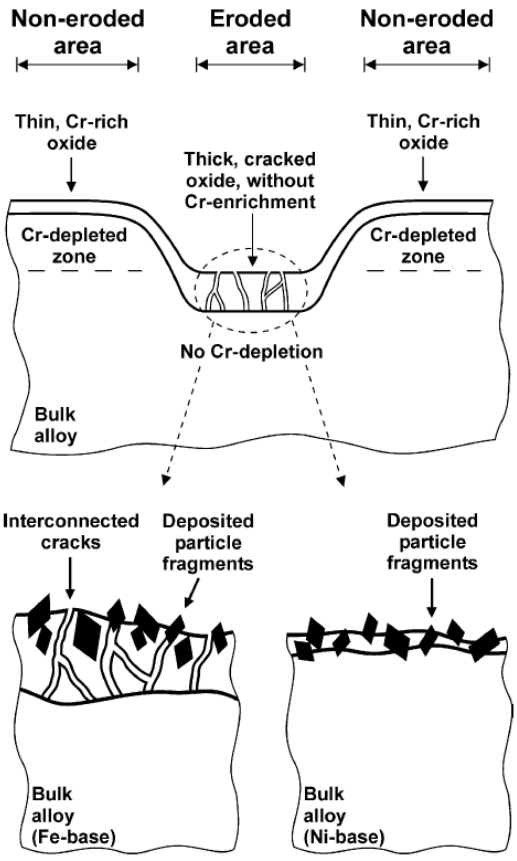

Figure 65. Model illustrating the oxide formation during oxidation and erosion-corrosion at 550°C

3. *Oxidation affected erosion*. It is considered the most serious with a high wastage rate. For this regime, it is no longer meaningful to describe degradation in terms of a corrosion product layer; instead it is necessary to consider the metal or alloy to be covered with a composite layer composed of deformed metal, corrosion products and embedded erodent particles.
4. *Erosion of pure metal*. No oxidation takes place at all. This requires conditions of very high erosion rates or a non-oxidizing surface/atmosphere which are usually not of importance in real applications [50] .

Materials and plants

Very few field tests in the loop seal area have been published. The tests have been performed in two boilers:

1. CFB plant in Nässjö, Sweden. The boiler produces heat and electricity with an efficiency of
   26 MW and 9 MW, respectively. The working temperature in the

combustion chamber is about 850 °C. The plant is fired with wood chips by full or half load depending on the demand and outside temperature. The incoming water vapour at full load is 300 °C and 8 bar in the combustion chamber and 480 °C and 8 bar after the superheaters. The fluidizing sand has a mean particle diameter of 0.25 mm and consists of 91% quartz with no additives. The sintering temperature is about 1225 °C.

The superheater tubes in the tube bundle were welded together from smaller 50 cm long tubes. The tube bundle consists of 4 loops with an incoming steam temperature of 475 °C and an outlet temperature of 538 °C. The corresponding material were measured to be about 510 °C and 550 °C, respectively.
The materials tested were commercially available high temperature austenitic and ferritic steels as well as coatings.
The tested materials were:

- 347H
- AC66
- Esshete 1250
- X10

The results show:

- The corrosion products usually consist in two layers: An outer Fe oxide and an inner mix oxide of Fe and Cr
- The degree of internal corrosion is largest on the alloy with the highest Cr content, AC66
- The corrosion rate is higher on the tubes subjected to a higher temperature
- The oxide growth kinetics in the loop seal environment is non-linear, after initial attack it stabilizes at an approximate constant thickness. [50]

In addition to the solid monotubes presented above, also coatings (primarily thermal sprayed) were tested:

- Alloy 625
- Kanthal 2 (Fe25Cr6Al)
- Stellit 21
- Hastelloy 276
- Metco 8222
- Alloy800
- SS 928L
- Metco12782
- Metco12782+80Ni20Al
- Metco 8443
- 80Ni20Al
- Metcoloy 2
- Metcoloy 2 + 80Ni20Al
- Metco 3006
- Metco 3007

The results show:

- The material degradation on most of the materials tested is very low due to the non-aggressive environmental conditions in the loop seal.
- The oxide growth kinetics is non-linear suggesting pure corrosion and only a minor degree of erosion-corrosion.
- The material wastage increases with increasing steam temperature.
- The corrosion layers on the uncoated steel tubes are composed of one outer iron rich oxide and one internal iron/ chromium oxide.
- Generally, the austenitic steels are subjected to a larger degree of internal and grain boundary corrosion, which is most pronounced in the tube area with the thinnest deposit layers.
- Eight out of 17 tested coating qualities are unaffected by the exposure. These are above all the nickel and high alloyed iron-based coatings.
- Thicker corrosion layers are only developed on the Metcoloy 2, Metcoloy 2 fl 80Ni20Al and Hastelloy 276 coatings.
- Carbide containing coatings are subjected to oxidation and a large degree of delamination. [51]

2. P15 CBF boiler in Händelöverket, Norrköping, Sweden. The thermal capacity is 85 MW supplied by former Sumitomo SHI FW. The boiler produces steam, primarily used for production of electricity, industrial process steam and district heating. The loop seal, which is a feature of the CFB process, offers a location of the final superheater (SH) for two reasons:
   - The heat transfer coefficient in the bubbling bed is 5 to 10 times higher than in the back pass. Hence, the SH area required is reduced by 80 to 90%.
   - The gaseous atmosphere in the loop seal contains less of chlorine and water vapor since the chlorine and water released during the combustion of the RDF is in a gaseous form in the cyclone and therefore follows the flue gas to the back pass. Only the particles separated by the cyclone reach the loop seal.

   The materials used in this boiler were:
   - TP310H (2010-2012)
   - 347H (2012-2014)
   - Base material 316L(N) + overlay welded alloy 59 (2016 -)

A test of the installed material, tube shield and deposit, was performed in 2017-2018 [52] . The results show that the dominant mechanism for material loss in the loop seal superheater is erosion. Overall, all analyses showed low levels of corrosive substances, however, there was a certain corrosion tendency, which indicates that the material loss at the loop seal can also be caused by corrosion-assisted erosion. Erosion is also considerably greater in the cooler loop seal superheater and at its highest on the top rows, which is probably due to a lower sand level around the loop seal superheater two compared to superheater three. In addition, it was seen that at a lower material temperature of the loop seal superheater a higher degree of condensation of the corrosive alkali chlorides NaCl and KCl occurs. This has probably accelerated erosion in the superheater two.

However, the tube shield on the top row is something that proved to be good to minimize the material loss and the erosive load on the tubes.

References

[1] H. Kinnunen, M. Hedman, M. Engblom, D. Lindberg, M. Uusitalo, S. Enestam and P. Yrjas. The influence of flue gas temperature on lead chloride induced high temperature corrosion. Fuel, 2017; 196:241-251
[2] A. Persdotter, M. Sattari, E. Larsson, M. A. O. Ogaz, J. Liske and T. Jonsson. Oxidation of Fe-2.25Cr-1Mo in presence of KCl(s) at 400 degrees C - Crack formation and its influence on oxidation kinetics. Corrosion Science, 2020; 163:
[3] M. A. Olivas-Ogaz, J. Eklund, A. Persdotter, M. Sattari, J. Liske, J. E. Svensson and T. Jonsson. The Influence of Oxide-Scale Microstructure on KCl(s)-Induced Corrosion of Low-Alloyed Steel at 400 degrees C. Oxidation of Metals, 2019; 91:291-310
[4] N. Folkeson, T. Jonsson, M. Halvarsson, L. G. Johansson and J. E. Svensson. The influence of small amounts of KCl(s) on the high temperature corrosion of a Fe-2.25Cr-1Mo steel at 400 and 500°C. Materials and Corrosion, 2011; 62:606-615
[5] H. Kinnunen, M. Hedman, D. Lindberg, S. Enestam and P. Yrjas. Corrosion in Recycled Wood Combustion-Reasons, Consequences, and Solutions. Energy & Fuels, 2019; 33:5859-5866
[6] Y. Alipour and P. Henderson. Corrosion of furnace wall materials in waste-wood fired power plant. Corrosion Engineering Science and Technology, 2015; 50:355-363
[7] J. Eklund, M. D. Paz, B. Jönsson, J. Liske, J. E. Svensson and T. Jonsson. Field exposure of FeCrAl model alloys in a waste-fired boiler at 600°C: The influence of Cr and Si on the corrosion behaviour. Materials and Corrosion, 2019; 70:1476-1485
[8] V. Asokan, J. Eklund, S. Bigdeli and T. Jonsson. The influence of Si on the primary protection of lean FeCrAl model alloys in O2 and O2+H2O at 600 °C—A microstructural investigation. Corrosion Science, 2021; 179:
[9] J. Eklund, I. Hanif, S. Bigdeli and T. Jonsson. High temperature corrosion behavior of FeCrAlSi model alloys in the presence of water vapor and KCl at 600 °C – The influence of Cr content. Corrosion Science, 2022; 198:
[10] T. Sand, A. Edgren, C. Geers, V. Asokan, J. Eklund, T. Helander, J. E. Svensson and L. G. Johansson. Exploring the Effect of Silicon on the High Temperature Corrosion of Lean FeCrAl Alloys in Humid Air. Oxidation of Metals, 2021; 95:221-238
[11] M. D. Paz. Increased steam temperature with Steamboost superheater in grate-fired boilers- Linking deposit formation and high temperature corrosion. Impacts of Fuel Quality on Power Production, Prague 2016
[12] D. M. Rishel, F. S. Pettit and N. Birks. Some Principal Mechanisms in the Simultaneous Erosion and Corrosion Attack of Metals at High-Temperatures. Materials Science and Engineering a-Structural Materials Properties Microstructure and Processing, 1991; 143:197-211
[13] Y. S. Li, Y. Niu and M. Spiegel. High temperature interaction of Al/Si-modified Fe-Cr alloys with KCl. Corrosion Science, 2007; 49:1799-1815
[14] Y. S. Li, M. Spiegel and S. Shimada. Effect of Al/Si addition on KCl induced corrosion of 9% Cr steel. Materials Letters, 2004; 58:3787-3791
[15] J. Pettersson, J. E. Svensson and L. G. Johansson. KCl-induced corrosion of a 304-type austenitic stainless steel in O 2 and in O 2 + H 2O environment: The influence of temperature. Oxidation of Metals, 2009; 72:159-177
[16] A. Persdotter, J. Eklund, J. Liske and T. Jonsson. Beyond breakaway corrosion – Influence of chromium, nickel and aluminum on corrosion of iron-based alloys at 600 °C. Corrosion Science, 2020; 177:108961

[17] T. Jonsson, J. Froitzheim, J. Pettersson, J. E. Svensson, L. G. Johansson and M. Halvarsson. The influence of KCl on the corrosion of an Austenitic stainless steel (304L) in oxidizing humid conditions at 600°C: A microstructural study. Oxidation of Metals, 2009; 72:213-239
[18] J. Pettersson, H. Asteman, J. E. Svensson and L. G. Johansson. KCl induced corrosion of a 304-type austenitic stainless steel at 600°C; the role of potassium. Oxidation of Metals, 2005; 64:23-41
[19] J. Phother-Simon, I. Hanif, J. Liske and T. Jonsson. The influence of a KCl-rich environment on the corrosion attack of 304 L: 3D FIB/SEM and TEM investigations. Corrosion Science, 2021; 183:109315
[20] M. Zevenhoven-Onderwater, M. Ohman, B. J. Skrifvars, R. Backman, A. Nordin and M. Hupa. Bed agglomeration characteristics of wood-derived fuels in FBC. Energy & Fuels, 2006; 20:818-824
[21] H. B. He, D. Bostrom and M. Ohman. Time Dependence of Bed Particle Layer Formation in Fluidized Quartz Bed Combustion of Wood-Derived Fuels. Energy & Fuels, 2014; 28:3841-3848
[22] R. Faust, K. Fürsatz, P. Aonsamang, M. Sandberg, M. Kuba, N. Skoglund and P. Knutsson. Early layer formation on K-feldspar during fluidized bed combustion with phosphorus-rich fuel. Fuel, 2023; 331:
[23] P. Ninduangdee and V. I. Kuprianov. Combustion of oil palm shells in a fluidized-bed combustor using dolomite as the bed material to prevent bed agglomeration. 2013 International Conference on Alternative Energy in Developing Countries and Emerging Economies (2013 Aedcee), 2014; 52:399-409
[24] H. Leion, A. Lyngfelt, M. Johansson, E. Jerndal and T. Mattisson. The use of ilmenite as an oxygen carrier in chemical-looping combustion. Chemical Engineering Research & Design, 2008; 86:1017-1026
[25] A. Corcoran, P. Knutsson, F. Lind and H. Thunman. Mechanism for Migration and Layer Growth of Biomass Ash on Ilmenite Used for Oxygen Carrier Aided Combustion. Energy & Fuels, 2018; 32:8845-8856
[26] R. Faust, I. Lamarca, A. Schaefer, F. Lind and P. Knutsson. Magnetic properties of ilmenite used for oxygen carrier aided combustion. Fuel, 2023; 340:
[27] F. Lind, A. Corcoran and H. Thunman. Validation of the oxygen buffering ability of bed materials used for OCAC in a large scale CFB boiler. Powder Technology, 2017; 316:462-468
[28] A. Lyngfelt, B. Leckner and T. Mattisson. A fluidized-bed combustion process with inherent CO2 separation; application of chemical-looping combustion. Chemical Engineering Science, 2001; 56:3101-3113
[29] F. Storner, F. Lind and M. Ryden. Oxygen Carrier Aided Combustion in Fluidized Bed Boilers in Sweden-Review and Future Outlook with Respect to Affordable Bed Materials. Applied Sciences-Basel, 2021; 11:
[30] D. Y. Lu, Y. Tan, M. A. Duchesne and D. McCalden. Potassium capture by ilmenite ore as the bed material during fluidized bed conversion. Fuel, 2023; 335:
[31] F. Lind, A. Corcoran, B. Å. Andersson and H. Thunman. 12,000 hours of operation with oxygen-carriers in industrially relevant scale. VGB PowerTech, 2017
[32] P. Kofstad. High Temperature Corrosion. 1988
[33] H. Nielsen, F. Frandsen, K. Dam-Johansen and L. Baxter. The implications of chlorine-associated corrosion on the operation of biomass-fired boilers. Progress in energy and combustion science, 2000; 26:283-298
[34] H. P. Nielsen, F. J. Frandsen and K. Dam-Johansen. Lab-scale investigations of high-temperature corrosion phenomena in straw-fired boilers. Energy & Fuels, 1999; 13:1114-1121
[35] M. Sánchez Pastén and M. Spiegel. High temperature corrosion of metallic materials in simulated waste incineration environments at 300–600° C. Materials and corrosion, 2006; 57:192-195
[36] Y. Shinata. Accelerated oxidation rate of chromium induced by sodium chloride. Oxidation of Metals, 1987; 27:315-332

[37] M. Spiegel. Salt melt induced corrosion of metallic materials in waste incineration plants. Materials and corrosion, 1999; 50:373-393
[38] A. Ruh and M. Spiegel. Thermodynamic and kinetic consideration on the corrosion of Fe, Ni and Cr beneath a molten KCl–ZnCl2 mixture. Corrosion science, 2006; 48:679-695
[39] H. Kinnunen, D. Lindberg, T. Lauren, M. Uusitalo, D. Bankiewicz, S. Enestam and P. Yrjas. High-temperature corrosion due to lead chloride mixtures simulating fireside deposits in boilers firing recycled wood. Fuel processing technology, 2017; 167:306-313
[40] D. Bankiewicz, S. Enestam, P. Yrjas and M. Hupa. Experimental studies of Zn and Pb induced high temperature corrosion of two commercial boiler steels. Fuel processing technology, 2013; 105:89-97
[41] D. Bankiewicz, P. Yrjas, D. Lindberg and M. Hupa. Determination of the corrosivity of Pb-containing salt mixtures. Corrosion science, 2013; 66:225-232
[42] A. Talus, R. Norling, L. Wickstrom and A. Hjornhede. Effect of Lead Content in Used Wood Fuel on Furnace Wall Corrosion of 16Mo3, 304L and Alloy 625. Oxidation of Metals, 2017; 87:813-824
[43] B. J. Skrifvars, R. Backman, M. Hupa, K. Salmenoja and E. Vakkilainen. Corrosion of superheater steel materials under alkali salt deposits - Part 1: The effect of salt deposit composition and temperature. Corrosion science, 2008; 50:1274-1282
[44] Y. Alipour. Furnace Wall Corrosion in a Wood-fired Boiler. KTH Royal Institute of Technology 2015; 2015:52:xx, 73
[45] R. F. A. Pettersson, J. Storesund and M. Nordling. Corrosion of overlay weld cladding in waterwalls of waste fired CFB boiler. Corrosion Engineering, Science and Technology, 2009; 44:218-226
[46] P. Henderson, P. Ljung, P. Kallner and J. Tollin. 2000;
[47] P. Henderson, J. Högberg and M. Mattsson. 2002; II:883-892
[48] C. T. Kang, F. S. Pettit and N. Birks. Mechanisms in the Simultaneous Erosion-Oxidation Attack of Nickel and Cobalt at High-Temperature. Metallurgical Transactions a-Physical Metallurgy and Materials Science, 1987; 18:1785-1803
[49] R. Norling and I. Olefjord. Erosion-corrosion of Fe- and Ni-based alloys at 550 degrees C. Wear, 2003; 254:173-184
[50] A. Nafari. Superheater corrosion in the loop seal of a wood-fired CFB boiler. Chalmers University of Technology 2003; Licenciate of Philosophy:
[51] A. Nafari and A. Nylund. Field study on superheater tubes in the loop seal of a wood fired CFB plant. Materials and Corrosion-Werkstoffe Und Korrosion, 2004; 55:909-920
[52] A. Ekström. Förutsättningar för ökad livslängd av sandlåsöverhettare. Uppsala Universitet 2018; Master:

New materials for improved competitiveness of FB plants using renewable fules New materials and Oxygen Carrier Aided Combustion for improved competitiveness of FB plants using renewable fuels

This project addresses two problem areas related to material wastage that today limits availability and fuel flexibility of biomass and waste fired power plants, corrosion/erosion of heat exchangers and water walls. The overall goal of the project is to improve the economy of CHP plants using renewable fuels and thereby increase the competitiveness towards fossil fueled plants by targeting these two problem areas in the (fluidized bed) boilers. The project has successfully conducted several corrosion tests in two commercially operated boilers.

Energiforsk is the Swedish Energy Research Centre – an industrially owned body dedicated to meeting the common energy challenges faced by industries, authorities and society. Our vision is to be hub of Swedish energy research and our mission is to make the world of energy smarter.
www.energiforsk.se

Energiforsk

New materials and Oxygen Carrier Aided Combustion for improved competitiveness of FB plants using renewable fuels

HAMPUS LINDMARK, FREDRIK LIND, JESPER LISKE,
MARIA DOLORES PAZ, LAURA RIOJA-MONLLOR, BERTIL WAHLUND,
ANNA JONASSON, JOHANNA NOCKERT, MATTI HAUTAKANGAS,
HANS LARSSON, KYÖSTI VÄNSKÄ & VESNA BARISIC

ISBN 978-91-7673-931-0 | © Energiforsk March 2023
Energiforsk AB | Phone: 08-677 25 30 | E-mail: kontakt@energiforsk.se | www.energiforsk.se

Foreword

The project has been performed within the framework of the materials technology research programme KME, Consortium materials technology for thermal energy processes, period 2018-2023. The consortium is at the forefront of developing material technology to create maximum efficiency for energy conversion of renewable fuels and waste.

KME was established 1997 and is a multi-cliental group of companies over the entire value chain, including stakeholders from the material producers, manufacturers of systems and components for energy conversion and energy industry (utilities), that are interested in materials technology research. The consortium is managed by Energiforsk.

The program activities are characterized by long term industry and demand driven research and contribute to the development of thermal energy processes for efficient utilization of renewable fuels and waste in power and heat production. The KME goals are to bring about cost-effective materials solutions for increased availability and power production, improved fuel flexibility and improved operating flexibility, with low environmental impact.

The specific project has focused on corrosion and erosion of heat exchangers and water walls in biomass and waste fired boilers; two problems that today limits boilers availability and fuel flexibility. The project aims to decrease the corrosion attack of the water walls and the fluidized bed heat exchangers in waste fired CFB boilers through improved corrosion resistance of the materials and mitigation of the corrosive/erosive environment by changing the bed material or by optimized boiler design. Maria Dolores Paz, Chalmers, has been the project leader. Hampus Lindmark, Fredrik Lind, Jesper Liske & Maria Dolores Paz, Chalmers, Laura Rioja-Monllor, Alleima, Bertil Wahlund, Energiforsk, Anna Jonasson, E.ON, Johanna Nockert, Kanthal, Matti Huhtakangas, MH Engineering, Hans Larsson, Stockholm Exergi, and Kyösti Vänskä & Vesna Barisic, Sumitomo SHI FW Energia have been project members and co-authors of the report. The industry has participated in the project through own investment (60 %) and the Swedish Energy Agency has financed the academic partners (40 %).

Energiforsk would like to thank all the participants for a well performed project.

Bertil Wahlund, Energiforsk

These are the results and conclusions of a project, which is part of a research programme run by Energiforsk. The authors are responsible for the content.

Summary

The use of biomass and waste as fuel for power plants as well as combined heat and power plants (so called CHPs) has steadily been increasing in the last decades. The reason for this increase is primarily environmental, the net emission of CO_2 is considerably less for renewable fuels, such as biomass and waste, compared to fossil fuels, such as e.g., coal. In Sweden, the increase in the use of renewable fuels was achieved by the introduction of a CO_2-tax targeting the combustion of fossil fuels. As consequence, the share of renewable fuels in heat and power production is much higher in Sweden compared to the rest of the world. In fact, the share of renewable fuels in heat and power production is about 65-70% in Sweden. However, despite the positive effects on decreasing CO_2 emissions by renewable fuels, the use of fossil fuels in these plants is still indisputably the primary fuel choice worldwide.

Thus, to increase the share of renewable fuels, at the expense of fossil fuels, the competitiveness needs to increase for power plants and CHPs using renewable fuels. Without using (governmental, EU, etc.) substitutes, there is in practice only three different routes towards obtaining this goal:

- Increase the revenue by increasing the efficiency of heat and power production (e.g., increased electrical efficiency).
- Decrease the costs by using cheaper (but usually more corrosive) fuels.
- Decrease the costs by minimizing maintenance of the plant.

Furthermore, these three routes are usually interlinked and will affect each other. Today renewable fuels may compete in the second route (i.e., fuel costs), depending of course on the quality of the fuel. However, if comparing the other two routes affecting the overall plant economy, using renewable fuels instead of fossil fuels, the more climate neutral fuels come out short. The state of the art of coal fired boilers has today an electrical efficiency up to 45 % whereas the best biomass fired boiler is up to 40 % (using virgin and clean biomass).

In CHPs, the total efficiency is high, around 90 %, this is since the heat produced is used and should also be taken into account. However, in countries where the need for heat is low, electrical efficiency is of greater importance. In addition to a decrease in electrical efficiency, the plants using renewable fuels also exhibit higher maintenance costs compared to fossil fueled plants. One of the reasons for this is the much higher corrosion rate of e.g., superheater tubes and water walls in plants using renewable fuels. This leads to both planned and unplanned revision stops where these tubes need to be replaced. These stops are very costly as it leads not only to an increase in direct costs (e.g., replacing tubes, building scaffolding, etc.) but also to the loss of revenue. This is particularly devastating if the plant owner is forced to stop the boiler during cold periods, when the demand for heat and power is normally at its highest.

This project addresses two problem areas related to material wastage that today limits availability and fuel flexibility of biomass and waste fired power plants, corrosion/erosion of heat exchangers and water walls. The overall goal of the project is to improve the economy of CHP plants using renewable fuels and thereby increase the competitiveness towards fossil fueled plants by targeting these two problem areas in the (fluidized bed) boilers. The project will utilize a two-pronged approach towards decreasing the extent of the corrosion attack of the water walls and the fluidized bed heat exchangers (FBHE) in waste fired CFB boilers:

1. Improving the corrosion resistance of the materials
2. Mitigating the corrosive/erosive environment by changing the bed material or by optimized boiler design.

The project has successfully conducted several corrosion tests in two commercially operated boilers; the waste-fired P15 boiler at Händelö and the waste-fired P6 boiler in Högdalen. The corrosion tests were carried out at two different positions in the boiler; the water wall region and the fluidized bed heat exchanger region. The water wall tests were carried out in the P6 boiler in Högdalen and lasted for 1 week while the fluidized bed heat exchanger tests were carried out both in Högdalen and Händelö with an exposure time ranging from 6 to 24 months. A wide range of materials, ranging from low alloyed steels, austenitic stainless steels, Ni-base alloys, FeCrAl alloys and different coating techniques including overlay weld materials has been investigated. The following conclusions can be made from the findings:

Water wall exposures:

- Oxide formation was only observed for the low alloyed steel (16Mo3) after 1 week of exposure in the water wall region of the waste fired P6 boiler in Högdalen. High concentration of chlorine was observed close to the metal/oxide interface suggesting the formation of metal chlorides which is attributed to the rapid oxidation of the material.
- Neither Ni-base steel nor stainless steel showed any indication of material degradation, and no accumulation of Cl was observed at the metal/deposit interface for these samples.
- Both conventional and newly developed FeCrAl alloy showed promising results as their performance was on par with the Ni-base and stainless-steel samples.

Fluidized bed heat exchangers:

- The newly developed FeCrAl EF101 showed the most promising results after 12 and 24 months of exposure in Händelö and Högdalen, respectively, obtaining a material loss significantly lower than conventional stainless steels and Ni-base alloys.
- Nitridation zones were observed on all FeCrAl alloys regardless of boiler type with the following severity ranked: APMT > EF100 > EF101. It is not known how nitridation affects corrosion behavior. In the present project the material presented an increase of thickness of the nitridated zone without an increase in the material loss, so it is unclear how nitridation affects corrosion in this particular application or if it affects at all.
- EF101 WOL is the most promising material from the overlay weld samples at Händelö. It performs better than all the other coatings exposed for 6 months. It performs better than the EF101 bulk material for the same exposure time. No sample could be recovered from the P15 boiler in Händelö after 12-month exposure.
- The most promising material from the austenitic stainless-steel block is the alloy SX. It experienced the lowest material loss regardless of boiler type and time. A Si-rich/Cr-rich oxide was observed in the grain boundaries at the corrosion front of the material. It is suggested that Si oxide may improve the resistance towards both corrosion and erosion mechanisms.
- Both HVAF and CorEr coating failed after 12 months of exposure regardless of boiler type. The oxide formation on the underlaying bulk material indicates that the failure occurred at an early stage of the exposure.

Goal fulfillment

This project addresses two problem areas related to material wastage that today limits availability and fuel flexibility of biomass and waste fired power plants, namely corrosion/erosion of heat exchangers and water walls. Below the different goals are specified in detail and if the goal has been reached or not.

- **Reduce the total cost of water walls and/or fluidized bed superheaters by enabling new materials and/or by mitigating the corrosive environment by changing bed material or optimized design. The total cost can be reduced by improving the material lifetime or by lowering the cost.**

This project aimed at improving the plant economy for plants using renewable fuels and thereby increasing the competitiveness towards fossil fueled plants by targeting areas in the plants where material issues are of concern. A key parameter in increasing the plant economy is to decrease the maintenance cost. The replacement of failing heat exchanger materials inside the plant is a larger contributor to the maintenance costs. By optimizing the materials, in such a way that the most cost-effective materials are used, the overall maintenance can be decreased. We have performed a substantial number of material testing campaigns

including a wide palette of materials for two positions in the boiler, which has high degradation rates when burning challenging fuels, namely water walls and fluidized bed superheaters. From a material perspective, almost 20 types of material including low alloyed steels, stainless steels, nickel-based alloys and FeCrAl alloys have been investigated. Furthermore, the material selection has included both commercial alloys and newly developed alloys, in the form of bulk material as well as weld overlay coatings and metallic spray coatings.

The main aim of this goal has been to provide reliable data on the material performance of the abovementioned materials and thereby enable more accurate cost calculations to be done by the industry. As such, the material selection of boiler components can be optimized, and the maintenance cost be decreased. The exact cost of the materials is unfortunately not open to the public and furthermore, the material cost is changing constantly due to the price of alloying elements, etc. However, in order to provide an estimate about the cost difference between different materials (which is fairly stable over time), Table 15 and Table 16 was provided in chapter 5 "Analysis of the results". Hereby, the reader can get a rough idea about the material cost, which can be combined with their performance.

This goal is considered as fulfilled.

- **Increase the knowledge of material degradation mechanisms and environmental parameters at play in fluidized bed superheaters.**

Overall, the large exposure matrix together with a wide and in-depth microstructural analysis had provided the material community with valuable information relevant for corrosion performance. This for two positions in the power plants that today are subject to high material wastage rates.

For the FBHE tubes, there was a special interest in deducing if the material wastage was primarily driven by erosion or by corrosion. The collective analysis of all the clamp samples that have been exposed on top of the tubes within the FBHE section indicates that it is a combination of erosive and corrosive forces that causes the degradation. In many cases, the samples were covered by a deposit, which suggests that erosive forces have been mild. In other cases, the deposit layer was minimal or non-existent leading to the conclusion that erosive forces were at play. Furthermore, it is probable that corrosion and erosion influence each other synergistically, leading to higher material wastages. The results showed signs of steel grain boundary attacks (on several occasions in combination with the presence of Cl) and it is expected that a material suffering from steel GB attack is also more susceptible to erosion.

This goal is considered as fulfilled.

- **Investigate the properties of newly developed alloys together with commercially available materials for water walls. Both thermal spray coating and overlay welding will be investigated.**

As above, the material matrix executed in the exposures has been wide, covering both materials that are used today and newly developed steels, FeCrAls and coatings. The corrosion analysis has primarily been performed by means of

material loss determination and cross-sectional SEM/EDX analysis. Special focus has been put towards the newly developed materials (EF100 and EF101) in order to investigate their potential use for both water walls and for tubes to be used as FBHE material. The results show that the newly developed FeCrAl alloys (EF100 and EF101) are potential candidates as boiler materials, taking a corrosion/erosion perspective. However, both these types of materials suffered from nitridation, which needs to be further studied. It is not clear how the nitridation process affects the corrosion performance on a longer perspective than one year. Furthermore, as these materials are not classed as pressure bearing materials, they cannot be used as monotubes. Instead, their initial use would be as corrosion/erosion resistant coatings and/or co-extruded tubes. The new insights in the performance of these alloys were presented in a journal article.

This goal is considered as fulfilled.

- **Publish 1 scientific article, present the results at two conferences and complete two academic theses within the project.**

Within this project the following have been achieved within the sub-goals:

Publish 1 scientific article

- **A material degradation study of novel FeCrAl alloys, stainless steels and nickel base alloy in fluidized bed heat exchangers of a waste fired CFB boiler**
  Hampus Lindmark, Julien Phother, Maria Dolores Paz Olausson, Johanna Nockert, Fredrik Lind, Anna Jonasson, Vesna Barišić, Kyösti Vänskä, Laura Rioja-Monllor and Jesper Liske

  Fuel 338, 127299, 2023

Present the results at two conferences

- **Investigating the performance of novel FeCrAl alloys in a fluidized bed heat exchanger application of a waste fired CFB boiler**
  Hampus Lindmark, Julien Phother, Maria Dolores Paz Olausson, Johanna Nockert, Fredrik Lind, Anna Jonasson, Vesna Barišić, Kyösti Vänskä, Laura Rioja-Monllor and Jesper Liske

  Oral presentation at the 24th Fluidized bed conversion conference, FBC-24, May 2022, Gothenburg Sweden

- **HTC/KME conference 2019**
  KME 803: New materials and Oxygen Carrier Aided Combustion for improved competitiveness of FB plants using renewable fuels

  Oral presentation by Julien Phother and Jesper Liske, Gothenburg 12-13 March 2019

- **HTC/KME conference 2020**
  KME 803: New materials and Oxygen Carrier Aided Combustion for improved competitiveness of FB plants using renewable fuels

Oral presentation by Julien Phother and Jesper Liske, Digital conference, 4-5 November 2020

- **KME conference/workshop (planned 6th March 2023)**
  KME 803: New materials and Oxygen Carrier Aided Combustion for improved competitiveness of FB plants using renewable fuels

  Oral presentation by Hampus Lindmark and Maria Dolores Paz

Complete two academic theses

- **Julien Phother Ph.D. thesis**
  High Temperature Corrosion Behavior in Biomass- and Waste-Fired Boilers - Insights into catastrophic corrosion and corrosion mitigation techniques
  Ph. D. thesis, Chalmers, 2020

- **Hampus Lindmark, Licentiate thesis**
  Title to be decided
  Lic. Thesis planned for fall 2023

This goal is considered as fulfilled. This includes a planned licentiate thesis to be presented in the fall 2023, based on the results and conclusions obtained within this project. The other subgoals (publishing one journal article and two conference presentations) are reached within the project's timeframe.

Keywords

New materials, EF100, EF101, Biomass and Waste combustion, High Temperature corrosion, Water wall corrosion and FBHE corrosion.

Sammanfattning

Användningen av biomassa och avfall som bränsle, framför fossil olja och kol, för kraftverk och kraftvärmeverk (så kallade CHP) har stadigt ökat de senaste decennierna. Anledningen till denna ökning är främst miljömässig, nettoutsläppet av CO_2 är betydligt lägre för förnybara bränslen, som biomassa och avfall, jämfört med fossila bränslen, såsom kol. Trots de positiva effekterna på minskande CO_2-utsläpp från förnybara bränslen är användningen av fossila bränslen i dessa anläggningar fortfarande det primära bränslevalet, sett globalt.

För att öka andelen förnybara bränslen, på bekostnad av fossila bränslen, måste konkurrenskraften öka för kraftverk och kraftvärmeverk som använder förnybara bränslen. I praktiken, kan detta nås genom någon av följande tre spår:

- Öka intäkterna genom att öka effektiviteten i värme- och kraftproduktionen (t.ex. ökad elproduktion).
- Minska kostnaderna genom att använda billigare (men vanligtvis mer korrosiva) bränslen.
- Minska kostnaderna genom att minimera underhållskostnaden av anläggningen.

Detta projekt adresserar två problemområden relaterade till materialslitage som idag begränsar tillgängligheten och bränsleflexibiliteten för biomassabaserade och avfallsvärmeverk: korrosion/erosion av värmeväxlare och vattenväggar. Det övergripande målet med projektet är att förbättra ekonomin i kraftvärmeverk som använder förnybara bränslen och därigenom öka konkurrenskraften gentemot anläggningar som använder fossila bränslen genom att ta itu med dessa två problemområden i (fluidiserade) pannor. Projektet kommer att använda en tvådelad strategi för att minska omfattningen av korrosionsattacken på vattenväggarna och sandlåsvärmeväxlarna i avfallseldade FB-pannor:

1. Förbättra korrosionsbeständigheten hos materialen.
2. Minska den korrosiva/erosiva miljön genom att ändra bäddmaterialet eller genom optimerad pannkonstruktion.

Projektet har framgångsrikt genomfört flera korrosionstester i två kommersiella pannor; den avfallseldade P15-pannan i Händelö och den avfallseldade P6-pannan i Högdalen. Korrosionstesterna utfördes på två olika positioner i pannan; vattenväggar och sandlåsöverhettare. Ett brett spektrum av material, från låglegerade stål, austenitiska rostfria stål, Ni-baslegeringar, FeCrAl-legeringar och olika beläggningstekniker inklusive påläggssvetsade material har undersökts. Följande slutsatser kan dras från resultaten:

Vattenväggsexponeringar:

- Oxidbildning observerades endast för det låglegerade stålet (16Mo3) efter 1 veckas exponering i vattenmantelområdet i den avfallseldade P6-pannan i Högdalen. Höga halter av klor observerades nära metall/oxidgränssnittet vilket antyder bildning av metallklorider som tillskrivs den snabba oxidationen av materialet.
- Varken Ni-bas legeringar eller rostfritt stål visade någon indikation på materialavvverkning, och ingen ansamling av Cl observerades vid metall/beläggningsgränssnittet för dessa prover.
- Både konventionella samt nyutvecklade FeCrAl-legeringar visade lovande resultat eftersom deras prestanda var i paritet med Ni-bas och rostfria stålprover.

Exponeringar i sandlåsöverhettare:

- Det nyutvecklade FeCrAl EF101 visade de mest lovande resultaten efter 12 och 24 månaders exponering i Händelö respektive Högdalen, och erhöll en materilavverkning som var betydligt lägre än konventionella rostfria stål och Ni-baserade legeringar.
- Nitrideringszoner observerades på alla FeCrAl-legeringar oavsett pannans typ, med följande allvarlighetsgrad: APMT > EF100 > EF101. Det är okänt hur nitrideringen påverkar korrosionsbeteendet. I detta projekt ökade tjockleken på nitrideringszonen utan att det uppstod någon ökning av materialförlusten, så det är oklart hur nitrideringen påverkar korrosionen i denna specifika tillämpning eller om den alls påverkar.
- EF101 WOL är det mest lovande materialet av de påläggssvetsade proverna i Händelö. Det presterade bättre än alla andra beläggningar som exponerades i 6 månader och bättre än EF101 som bulkmaterial vid samma exponeringstid.
- Det mest lovande materialet från den austenitiska rostfria stålklassen är legeringen SX. Den hade den lägsta materialförlusten oavsett panntyp och exponeringstid. En Si-rik/Cr-rik oxid observerades i korngränserna vid materialets korrosionsfront. Det föreslås att Si-oxid kan förbättra motståndet mot både korrosions- och erosionsmekanismer.
- Både HVAF- och CorEr-beläggningarna försvann efter 12 månaders exponering oavsett pannans typ. Oxidbildning på det underliggande bulkmaterialet indikerar att beläggningarna försvann i en tidig fas av exponeringen.

List of content

1 Introduction 14
1.1 Motivation 14
1.2 Background 14
1.3 Aim of the project 16
1.4 Project plan 17
1.5 Project organisation 19
2 Description of the plants 20
2.1 P6 Högdalen 20
2.1.1 Design 20
2.1.2 Fuel 21
2.1.3 Steam system 23
2.2 P15 Händelöverket 24
2.2.1 Design 24
2.2.2 Fuel 26
2.2.3 Water/steam system 27
3 Materials 28
3.1 Description of materials 28
3.2 Description of the exposures 31
3.2.1 Clamp samples on FBHE in Händelö P15 and Högdalen P6 31
3.2.2 Furnace water wall probe samples in Högdalen P6 37
3.2.3 Thermal sprayed coatings on the water walls in Händelö P15 38
3.3 Analytical techniques 39
3.3.1 Material loss 39
3.3.2 Scanning Electron Microscopy/Energy Dispersive X-Rays (SEM/EDX) 39
4 Results 40
4.1 Water wall exposures Högdalen P6 waste-fired boiler 40
4.2 Metal sprayed coatings on water walls in Händelö P15 44
4.3 Material loss and microstructural analysis on FBHE 45
4.3.1 Clamp exposures on FBHE - Högdalen P6 45
4.3.2 Clamp exposures on FBHE - Händelö P15 71
5 Analysis of the results 93
5.1 WP1- Water wall corrosion testing 94
5.2 WP2- Material performance in fluidized bed heat exchangers 96
5.3 Review of potential corrosion issues using OCAC 105
6 Goal fulfillment 108
7 Summary and conclusions 112
8 References 114
9 Appendix: LITERATURE Review 118

1 Introduction

1.1 MOTIVATION

This project addresses the corrosion and erosion of fluidized bed heat exchangers (FBHE) and water-wall tube panels that currently limit the availability and fuel flexibility of biomass and waste fired power plants. As the fuel quality shifts from clean, virgin biomass towards cheaper and "dirtier" biomass fractions and waste-derived fuels, the material wastage of boiler tubes becomes increasingly severe, requiring more expensive design and operational solutions.

Even though the fluidized bed heat exchangers are constructed of highly alloyed steels, the corrosion rate with waste-derived fuels causes frequent tube replacements. Simultaneously, mitigating material wastage of evaporative surfaces requires several boiler tube protection options, such as coatings, weld overlays and the use of extended lining of critical components by refractories. By addressing these material issues, we help increase the fuel flexibility, availability, and reliability of these plants, thereby making plants firing green fuels and waste more competitive, compared to e.g., boilers using fossil fuel.

This approach may also be used to increase the steam data and thereby also the electrical efficiency of these types of plants. The two-pronged approach is consisting of both, seeking solutions towards mitigating the material degradation by development of more corrosion resistant materials and decreasing the corrosiveness of the loop seal environment through e.g., new boiler designs and/or operating solutions, e.g., changing the bed material. Regardless of method, both will be based on a knowledge driven approach. The work needed within the project in order to reach the project goals will be divided into several work packages (WPs).

1.2 BACKGROUND

The use of biomass and waste as fuel for power plants as well as combined heat and power plants (so called CHPs) has steadily been increasing in the last decades. The reason for this increase is primarily environmental, the net emission of CO2 is considerably less for renewable fuels, such as biomass and waste, compared to fossil fuels, such as e.g., coal. In Sweden, the increase in the use of renewable fuels was achieved by the introduction of a CO2-tax targeting the combustion of fossil fuels. As consequence, the share of renewable fuels in heat and power production is much higher in Sweden compared to the rest of the world. In fact, the share of renewable fuels in heat and power production is about 65-70% in Sweden. However, despite the positive effects on decreasing CO2 emissions by renewable fuels, the use of fossil fuels in these plants is still indisputably the primary fuel choice worldwide. The share of fossil fuels in heat and power production in the world is about 70-75%. The reason for this is primarily economical, it is today cheaper to produce power and heat using fossil fuels rather than with renewable fuels.

Thus, to increase the share of renewable fuels, at the expense of fossil fuels, the competitiveness needs to increase for power plants and CHPs using renewable fuels. Without using (governmental, EU, etc.) substitutes, there is in practice only three different routes towards obtaining this goal:

- Increase the revenue by increasing the efficiency of heat and power production (e.g., increased electrical efficiency).
- Decrease the costs by using cheaper (but usually more corrosive) fuels.
- Decrease the costs by minimizing maintenance of the plant.

Furthermore, these three routes are usually interlinked and will affect each other. For instance, by decreasing the fuel costs the maintenance costs are usually increased due to increased corrosion rates and other fuel related problems. Hence, if the use of renewable fuels in heat and power production should increase globally the sum of all three routes needs to become a more competitive option compared to the sum of these three routes using fossil fuels.

Today renewable fuels may compete in the second route (i.e., fuel costs), depending of course on the quality of the fuel. For example, virgin (clean) biomass is rather expensive compared to waste (which even could have a negative cost) and ditto for different qualities of coal. However, if comparing the other two routes affecting the overall plant economy, using renewable fuels instead of fossil fuels, the more climate neutral fuels come out short. The state of the art of coal fired boilers has today an electrical efficiency up to 45 % whereas the best biomass fired boiler is up to 40 % (using virgin and clean biomass).

However, if using cheaper biomass sources (e.g., agricultural residues) or waste as fuel the electrical efficiency is only around 30-35 %. In CHPs the total efficiency is high, around 90 %, this since the heat produced is used and should also be taken into account. However, in countries where the need for heat is low, electrical efficiency is of greater importance. In addition to a decrease in electrical efficiency, the plants using renewable fuels also exhibit higher maintenance costs compared to fossil fueled plants. One of the reasons for this is the much higher corrosion rate of e.g., superheater tubes and water walls in plants using renewable fuels. This leads to both planned and unplanned revision stops where these tubes need to be replaced. These stops are very costly as it leads not only to an increase in direct costs (e.g., replacing tubes, building scaffolding, etc.) but also to the loss of revenue. This is particularly devastating if the plant owner is forced to stop the boiler during cold periods, when the demand for heat and power is normally at its highest.

In order to decrease the corrosion rate of the SH tubes in the boilers using renewable fuels, the steam temperature, and thereby also the superheater material temperature, has been decreased. The consequence of this decrease is that the electrical efficiency is lower for boilers using renewable fuels compared to fossil fueled plants. An attempt to increase the electrical efficiency and/or to reduce maintenance costs in fluidized bed boilers using renewable fuels has been to move the final superheating of the steam from the corrosive flue gas to the loop seal of the return leg of the cyclones. By installing a FBHE the aim is to increase the steam

temperature without having the correlated corrosion attack associated with the corrosive flue gas environment. Modern waste/biomass fired CFB boilers are equipped with fluidized bed heat exchangers. However, for some fractions of waste fuels, the corrosion rate is much higher than anticipated. The use of more highly alloyed steels has not seemed to decrease the extent of the problem, the material wastage rate is still unacceptably high. The fluidized bed heat exchangers are in some cases replaced every second year.

The combinatory effect of both corrosion and erosion is particularly detrimental and today's material is not suited to withstand that type of attack. Hence, there is a need for the development of new materials that exhibit improved resilience towards this type of environment. This becomes especially true with the current trend of an increased diversity in the fuel mix, towards more corrosive (cheaper) fuels. The improvement of the materials may be in the form of coatings, weld overlays as well as newly developed alloys, which can be in the form of mono- or compound tubes.

Another area of interest, having potential positive economical outcome, is the water walls of boilers using renewable fuels. Today, a common practice to maintain the availability of the boilers is to coat or overlay weld large water wall areas with nickel base alloys. This type of material has become standard in industry today and it is not unusual that several hundred square meters of water walls with weld overlay are installed in a boiler. However, nickel base materials are usually associated with a high cost, leading to high capital and maintenance costs. If less expensive materials or materials with a higher corrosion resistance can be deployed instead of these nickel-based alloys, the overall plant economy of boilers burning renewable fuels can be improved.

1.3 AIM OF THE PROJECT

The overall goal of the project is to improve the plant economy of power plants and CHPs using renewable fuels and thereby increase the competitiveness towards fossil fueled power plants and CHPs. This is done by targeting two problem areas in the (fluidized bed) boilers: water wall corrosion and fluidized bed heat exchanger corrosion/erosion. The project aimed at utilizing a two-pronged approach towards decreasing the extent of the corrosion attack of the water walls and the fluidized bed heat exchangers in waste fired CFB boilers:

- Improving the corrosion resistance of the materials used.
- Mitigating the corrosive/erosive environment by changing the bed material or optimized design.

The main focus in the project has been topic (1) by deploying a wide range of investigated materials together with newly developed alloys. Due to commercial considerations outside the scope of this project, (2) has mainly been focused on theoretical considerations rather than experimental testing. This, as the planned change of bed material (from sand to Ilmenite) in these boilers was postponed.

Project goals:

The overall project goal, to improve plant economy of power plants and CHPs using renewable fuels, was divided into several individual topics aiming at generating new knowledge and industrial experience:

- Decrease the overall cost of water walls and/or fluidized bed heat exchangers by enabling new materials and/or by mitigating the corrosive environment by changing the bed material or optimized design. The overall cost can be decreased either by improving the material lifetime or by decreasing the material cost.
- Increase the knowledge of what type of material degradation mechanisms as well as environmental parameters are at play in fluidized bed heat exchangers.
- Investigate the performance of newly developed steels and alloys together with commercially available materials for water walls.
- This project will collaborate with other biokraft project(s) in order to facilitate synergistic effects between the projects.
- Academic goals: 2 academic theses; 1 journal article and 2 conference proceedings

1.4 PROJECT PLAN

The project consisted of two major work packages, one directed towards water wall corrosion and the other directed towards FBHE corrosion/erosion. In both work packages (WP1 and WP2), exposures have been performed in two boilers. In addition, a separate work package (WP0) was initiated towards the methodology development and planning of the full-scale tests. Within this WP, the development of procedures and experimental techniques has been discussed and investigated for both FBHE exposures as well as water wall probe exposures. Below, these three work packages are presented in a more detailed manner.

WP0 – Methodology development work package

This WP is aimed at methodology development and planning of full-scale tests. In the two work packages directed towards water walls (WP1) and fluidized bed heat exchangers (WP2), respectively, some methodology development was needed in order for the exposures to proceed in a safe manner. The fluidized bed heat exchanger is, as compared to more "traditional" superheaters situated in the flue gas stream, much less investigated. The environment for the FBHE in the loop seal area is also fundamentally different compared to the environment in the flue gas stream. Within this WP, different exposures techniques (e.g., probes, tube exchange and clamps) have been assessed by the project group and discussed with safety and risk in mind. Furthermore, this WP have also spent time and resources in order to investigate the possibility to change the bed material from silica sand to a bed material with oxygen carrier capabilities (e.g., ilmenite). Since these types of

tests are very costly and, as with everything new, deemed risky, the planned test with OCAC needed to be performed on commercial grounds. Discussions and planning have also been performed in collaboration with other Biokraft-projects. Unfortunately, the planned OCAC exposures were not performed, due to delays from the covid pandemic which resulted in a change in commercial plans. Instead, the focus of the OCAC related work within this project (and this WP) shifted towards a performing a literature study focusing on OCAC in general and its potential effect on material performance of construction materials in the plant.

WP1 – Water wall corrosion work package

This WP has been directed towards investigations of material performance of water walls in waste fired boilers. Within WP0, the planning has been performed whereas within WP1, the actual exposures, analysis and evaluations have been executed. The water wall corrosion tests have been performed in two different boilers. In the P6 boiler at Högdalen, newly developed water wall corrosion probes have been exposed in short term corrosion tests. The current material installed is overlay welding of Inconel625. The aim is to test commercially available materials as well as newly developed alloys and coatings. For the P15 boiler at Händelö, a test section of the water wall in the empty pass was installed with thermal spray coatings.

WP2 – Fluidized bed heat exchanger corrosion work package

In this work package the corrosion/erosion of the fluidized bed heat exchangers have been investigated. This WP was also deployed in the two boilers mentioned above. Both these boilers are constructed by Sumitomo SHI FW and the FBHE's are similar. The material wastage of the tubes has been especially high at the top tubes of the superheater bundle. Within this WP, a wide range of materials have been exposed as clamp samples sitting on top of the FBHE tubes for up to 2 years. The material performance has been investigated both quantitatively in the form of material loss (mm/year) and qualitatively in the form of cross-sectional SEM/EDX analysis (primarily). The exposure matrix includes a great number of samples and the tested materials included low alloyed steels, stainless steels, nickel-based alloys and FeCrAl alloys. Furthermore, the material selection has included both commercial alloys and newly developed alloys, as well as in the form of bulk material, weld overlay coatings and metallic spray coatings. The main aim with the long-term tests was to map out the extent and reasons behind current material degradation, e.g., if the attack primarily was driven by corrosion or erosion.

1.5 PROJECT ORGANISATION

The project is jointly performed by Energiforsk AB, E.ON Värme Sverige AB/E.ON Energiinfrastruktur AB, Kanthal AB, MH Engineering AB, Alleima , Stockholm Exergi AB, Sumitomo SHI FW Energia Oy and HTC at Chalmers University of Technology. The distribution of work was:

Table 1. Participating partners in the project.

Part	Participants role in the project
Energiforsk AB	Responsible for results dissemination, collaboration and continuous knowledge exchange between the academia and the industry stakeholders.
E.ON Energiinfrastruktur AB	Responsible for boiler operation, fuel & gas analysis and collecting other operational data
Kanthal AB	Providing materials, including newly developed model alloys
MH Engineering AB	Providing coating materials
Alleima	Providing materials, including newly developed model alloys
Stockholm Exergi AB	Responsible for boiler operation, fuel & gas analysis and collecting other operational data
Sumitomo SHI FW Energia Oy	Responsible for sample installations, corrosion probe exposures and will also perform some corrosion evaluation and analysis
Chalmers University Technology AB HTC	Project leader. Responsible for corrosion evaluation and analysis. Responsible for communication/collaboration with other projects.
Chalmers University Technology AB Energy Technology	Responsible for evaluation environmental parameters, especially for OCAC.

The project was financed by the Swedish Energy Agency together with cash and in-kind contributions from the company members of the project. The total project budget was 13 704 kSEK and the project time was 2018-2022.

2 Description of the plants

2.1 P6 HÖGDALEN

2.1.1 Design

Högdalen P6 CFB boiler has been in operation since 2000. It features a compact design with FBHE superheaters. The boiler was designed for the following main steam parameters: 32 kg/s of steam at 60 bar(g) and 480 °C. This gives the plant a capacity of 30 MWe, 90 MWth with steam flow of 115 t/h. The design fuels include RDF, woody biomass, and demolition wood. In addition to the boiler, the plant consists of fuel preparation, steam turbine and a flue gas cleaning. The boiler produces steam, primarily used for production of electricity, industrial process steam and district heating.

The boiler is made up of a water-cooled furnace with two integrated water-cooled separators and two loop seals, followed by FBHE chambers containing the final superheaters. On the gas side the separators are followed by a single pass radiation cavity (middle pass) and a vertical back pass with superheater banks and boiler banks. Finally, before entering the flue gas treatment system the flue gas meets the economizer banks.

The two separators are hot gas separators, which are used for separation of the bed material entrained by the flue gas as it is leaving the furnace at the furnace top. The separated material is returned to the lower part of the furnace via the loop seal and FBHE chamber. Loop seal is designed to prevent flue gas from the furnace entering the separators through the bed material return leg. The FBHE chamber contains a bubbling fluidized bed and is equipped with several air nozzles to ensure material transport. The final superheater is in the FBHE chamber.

The separators are followed by the overall layout of the boiler.

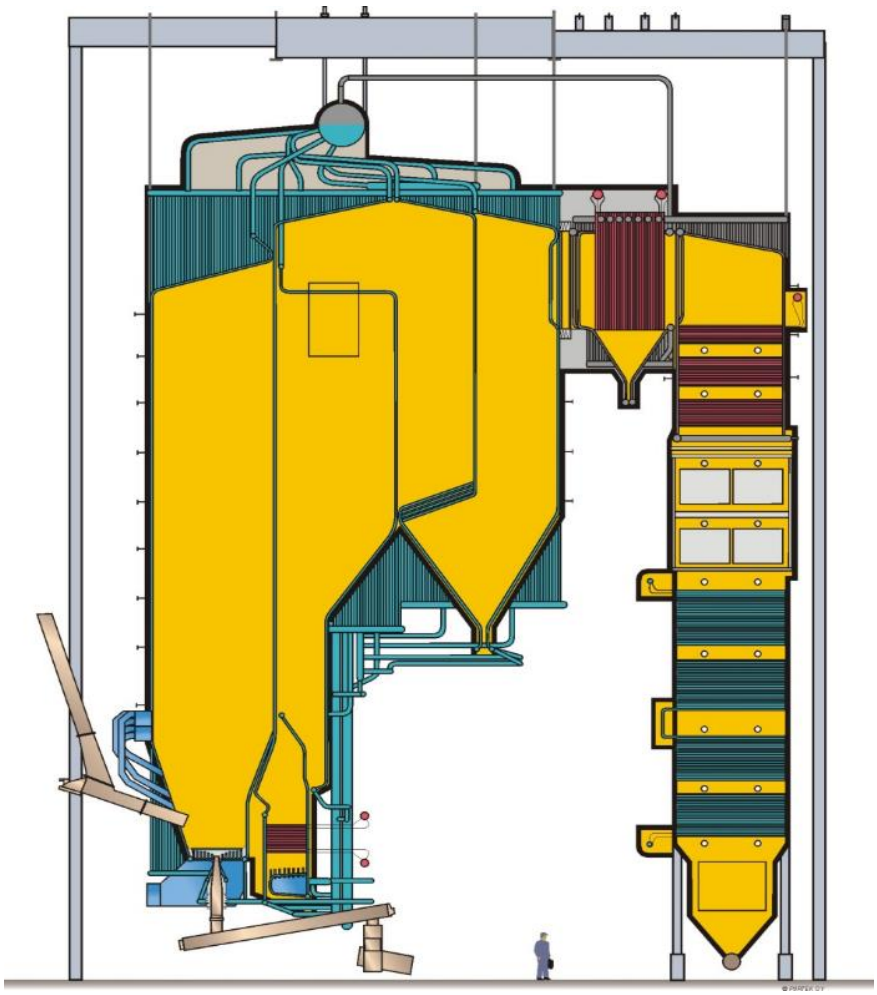

Figure 1. General lay-out of Högdalen P6 boiler.

2.1.2 Fuel

The boiler was originally designed to burn RDF (returbränsle), wood chips, saw dust, bark, wood shavings, wood pellets and briquettes, willow, and rubber chips. The fuel can be fired as a mix of fuels with the maximum fraction of the fuels as shown in Table 2. Fuel specifications are given in Table 3.

Table 2. Design fuel mix for Högdalen P6 boiler

Fuel	RDF	Wood chips	Sawdust	Plywood	Bark	Wood shavings	Pellets	Willow	Rubber chips
Maximum fraction	100 %	100%	40 %	10%	40 %	40%	40%	5%	10%

Table 3. Design fuel properties for Högdalen P6 boiler

Fuel		RDF	Wood chips	Saw dust	Bark	Wood shavings	Pellets
LHV	MJ/kg	13	8.9	8.1	8.6	15.9	17.3
Density	kg/m3	200	250	300	300	110	600
Particle size		100% < 100mm 80% < 80mm 80% > 5 mm	90% < 22 mm	90% < 7 mm	90% < 45 mm	*)	φ6x10-12x30 mm
			50% < 7 mm	50% < 3 mm	50% < 22 mm		
Moisture	%	22	45	50	50	15	8
Ash content	%	10	5	0.5	1	0.5	0.5
C	%	38.8	25	24.8	26.3	42.2	46
H	%	3.9	3	2.9	3.1	5.1	5.4
O	%	24	22	21.7	19.4	37.1	40
N	%	0.5	0.01	0.01	0.1	0.02	0.02
S	%	0.3	0.05	0.05	0.04	0.1	0.1
Cl		0.5**)	-	-	-	-	-

*) Composition can vary based on source; **) Max 0.8%

RDF is further defined in Table 4 and it contains max 0.35% PVC.

Table 4. Description of RDF for Högdalen P6 boiler

Composition	mass-%
Paper *)	< 90
Wood	< 90
Plastic	< 20
Rubber	< 5
Textile	< 5
Other combustible	< 5
Metals	< 5
Other non-combustible	< 10**)
Aluminum, metallic	< 0.25

*) up to 90% of the paper fraction can be made up of paper laminate (plastic coated paper)

**) normally the total non-combustible fraction is below 10% in the fuel

2.1.3 Steam system

The steam system comprises the following equipment:

Superheaters:

Superheater 1, in the flue gas duct before the economizer

Superheater 2, in the flue gas duct before SH1.

Superheater 3A, under the separator

Superheater 3B, next to SH 3A

Steam coolers:

between SH1 and SH2, Steam cooler 1

between SH2 and SH 3A, Steam cooler 2

between SH3A and SH 3B, Steam cooler 3

Superheaters 1 and 2 are in the back-pass while superheaters 3A and 3B are FBHE superheaters.

2.2 P15 HÄNDELÖVERKET

2.2.1 Design

The Händelö P15 CFB boiler is a Waste-to-Energy boiler designed to burn a wide range of fuels, in commercial operation since 2011. It is of a compact design with FBHE super heaters. The boiler was designed for the following main steam parameters: 31 kg/s of steam at 66 bar(g) and 450 °C. This gives the plant a capacity of 30 MWe, 85 MW_{th} with steam flow of 112 t/h. The design fuels include sorted household and industrial waste with biomass, and recycled wood as secondary fuels. In addition to the boiler, the plant consists of fuel preparation, steam turbine and a flue gas cleaning. The boiler produces steam, primarily used for production of electricity, industrial process steam and district heating.

The boiler is made of a water-cooled, refractory lined, furnace with two integrated water-cooled separators and two FBHE superheaters. On the gas side the separators are followed by a single pass radiation cavity (empty pass) and a horizontal convection pass with evaporator and superheater banks. Finally, before entering the flue gas treatment system the flue gas meets the economizer banks.

The two separators are used for separation of the bed material from the flue gas at the furnace top. The separated material is discharged via loop seals into FBHE superheater units and thereafter returned to the lower part of the furnace via FBHE lift legs. Loop seal prevents that flue gas from the furnace enters the separators. The loop seal is a bubbling fluidized bed and is equipped with several air nozzles to ensure material transport.

On the flue gas side, the separators are followed by an empty pass for lowering the flue gas temperature to a temperature, which makes the ash ”dry” and non-sticky to the back pass tube banks. This is to minimize deposit formation and corrosion attacks. The bottom of the empty pass and the horizontal pass are equipped with an ash extraction conveyor system.

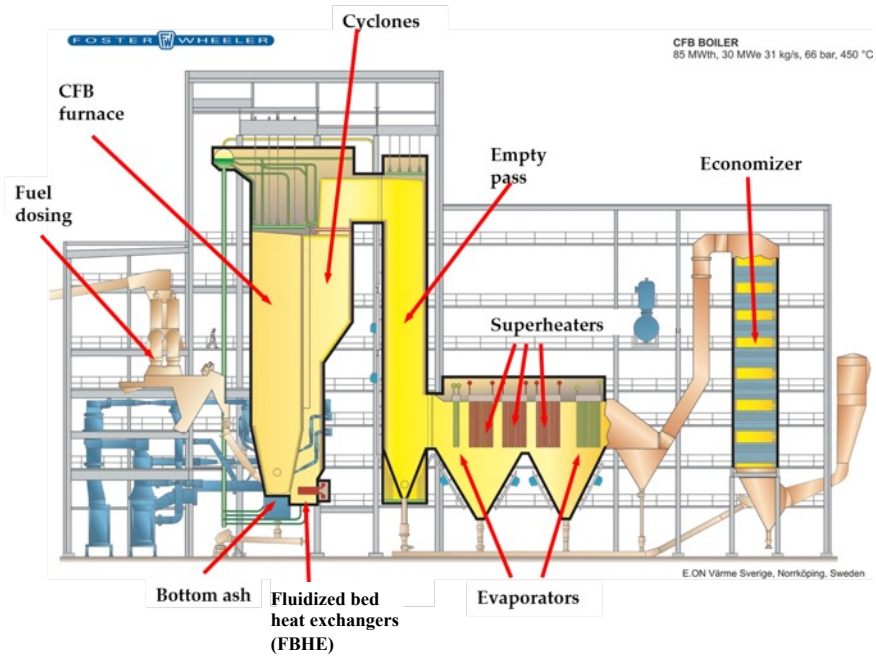

Figure 2. General layout of Händelö P15 boiler.

2.2.2 Fuel

The boiler is designed to burn fuels with specifications given in Table 5, according to ratios given in

Table 6. Table 5

Table 5. Design fuel properties for Händelö P15 (a.r.=as received)

Fuel		Guarantee fuel mixture	Range for guarantee and design fuel mixtures
LHV	MJ/kg	12.9	10.5-16.4
Density	kg/m3	226	150-300
Particle size	90%	-	<100 mm
Moisture	%, a.r.	27	12-37.5
Ash content	%, a.r.	14.3	6.4-16.8
C	%, a.r.	45	35-55
H	%, a.r.	6.1	4-9
0	%, a.r.	28.2	25-45
N	%, a.r.	0.8	0.3-1.2
S	%, a.r.	0.3	0.5
Cl	%, ds	< 0.9	1.0
$Alkali_{total}$	%, ds		<2.0
$Alkali_{weak\ acid\ soluble}$	%, ds		<0.6
Zn	mg/kg, ds	<500	1000
Pb	mg/kg, ds	<90	500

Table 6. Design fuel mix for Händelö P15

Fuel	Sorted and pretreated industrial waste	Sorted and pretreated household waste	Recycled wood
Guarantee Fuel Mixture	60 wt-%	40 wt-%	0 wt-%
Design Fuel Mixture Range	30-100 wt-%	0-70 wt-%	0-20 wt-%

2.2.3 Water/steam system

The water/steam system comprises the following equipment:

1. Water walls
2. Evaporative tube bundle
3. Super heaters:
    a. Superheater 1 (SH1), in the horizontal pass
    b. Superheater 2 (SH2), left FBHE.
    c. Superheater 3 (SH3), right FBHE

3 Materials

3.1 DESCRIPTION OF MATERIALS

A wide material testing matrix has been performed in two boilers designed with a horizontal pass superheater region. The material matrix has included conventional steels used today as well as newly developed stainless steels and FeCrAls and two different types of thermally sprayed coatings, HVOF and HVAF sprayed coatings. Below a short description of the use and benefits of each material type is presented. The complete material matrix of the clamp, tube and probe exposures is presented in 3.2.

The chosen materials are typical for superheaters, carbon steels, low alloyed ferritic steel, austenitic steels and nickel-based alloys. The choice of materials for the superheater depends on the quality of the fuel, placement of the superheater (dependent on the flue gas temperature), material temperature (dependent on the steam temperature), material cost etc. Chromium is often used to increase the corrosion resistance of the steel. Steels with more than 13 % chromium are often referred to as stainless steels. Nickel alloys are also commonly used in order to improve the corrosion resistance of the superheater. The price of low alloy steels may be up to 8 times cheaper than high nickel-based alloys. In Table 15, a rough estimation between the materials and their costs (as well as other information) is shown. The aim is to provide the reader with an estimation of the material costs, although the exact cost of a certain material will vary over time.

The alloys used within this project can be described as:

- **16Mo3, EN10028**

16Mo3 is a pressure vessel grade low alloyed steel for use at elevated working temperatures. The material is used as a weldable steel in boilers as well as steel pressurized vessels found in the oil, gas and chemical industry.

- **316Ti, EN1.4571**

316 is the second most common austenitic stainless steel used in the world with nominal composition 16-chromium, 10-nickel and 2-molybdenum. 316Ti variant is a titanium stabilized version of the high carbon variant 316H, both commonly used in superheaters and reheaters in steam powerplants.

- **347H and 347HFG, EN1.4912 (Alleima® 6R44)**

This is a niobium stabilized austenitic stainless steel, 18-chromium and 10-nickel, used in superheaters in steam powerplants up to 600 °C - 620 °C. The grade also exists in a fine-grained mode, i.e., 347HFG. The fine-grained microstructure is facilitating an increased transport of Cr to the oxide and thereby improves the corrosion properties of the steel.

- **Alleima® Esshete1250, EN1.4982**

This is an austenitic stainless chromium-nickel-manganese 15-9.5-6 steel used in superheaters and reheaters in coal and biomass powerplants. It's allowed for use at metal temperatures up to 650 °C. This alloy is verified in large installations in the UK coal fired power fleet operating at 568 °C superheat and reheat temperatures since the early 70's. Successfully used also in biomass fired boilers delivering superheat and reheat steam at 568 °C. The alloy can be bent to a tight radius as allowed by BS1113 without need for post bend heat treatment. This feature saves significant fabricator costs.

- **310HCbN, EN1.4952**

This is a niobium stabilized nitrogen alloyed austenitic stainless 25 % chromium 20 % nickel type steel. By niobium and nitrogen alloying to high carbon variant 310H, elevated temperature strength and creep resistance is achieved. It is designed for superheater and reheater boiler tubes and suitable in coal fired power stations at 620°C steam temperatures but also suitable to be used in corrosive conditions at metal temperatures up to 525 °C - 540 °C.

- **Alleima® SX**

The SX grade is a high silicon containing austenitic stainless steel, originally developed for use in concentrated sulfuric acid. The grade is characterized by an excellent corrosion resistance in concentrated sulfuric acid, excellent corrosion resistance in high concentrated nitric acid, good mechanical properties and ductility, and good weldability. It is not approved as pressure vessel at the operating temperature of the boiler.

- **Alleima® Sanicro® 28, EN1.4563**

This is an austenitic high alloyed Cr/Ni/Mo (27/31/3.5) very corrosion resistant steel. It was initially developed for wet corrosion applications. It's limited for use at metal temperatures up to 550 °C (VdTUV 483) and 450 °C (ASME Code Case1325-18). To facilitate fabrication/welding, reduce thermal elongation, and increase thermal transfer, it can be co-extruded with a load carrier boiler tube, type 10Cr/T22, X10Cr/T91, to so called composite tubes. Such tubes are used both in superheaters and waterwalls when more corrosive fuels are used.

- **Alleima® Sanicro® 35**

Sanicro® 35 is an alloy combining the best features of a super austenitic stainless steel and a nickel alloy for wet corrosion applications. The grade has excellent corrosion resistance, for service in sea-water applications and other highly corrosive environments. It's limited for use at metal temperatures up to 450 °C, Pre-approval for Particular Material Appraisal (PMA) TÜV file 1326W043219, and ASME Code Case 2982. Boiler and Pressure Vessel Code, Section VIII, Division I and II.

- **Alloy 27Cr33Ni3Mo**

This is a new austenitic heat resistant stainless steel development. It exhibits both high creep strength and high corrosion resistance. This allows the material to be used in environments with high temperature and high pressure at metal temperatures up to 650 °C. The material is not yet approved by any international standard. The grade is targeted for use in superheaters/reheaters in boilers in which more corrosive fuels are used.

- **Kanthal® APMT**

FeCrAl-alloys forms, depending on environment and temperature, a protective layer containing Al_2O_3. The FeCrAl-alloy Kanthal® APMT is an advanced powder metallurgical, dispersion strengthened, ferritic iron-chromium-aluminum alloy. Typical applications for Kanthal® APMT are as radiant tubes in electrically or gas fired furnaces. Kanthal® APMT has also been tested in environments related to biomass and waste fired boilers with good results, which makes FeCrAl alloys interesting for superheater applications, though they are not pressure vessel grades.

- **Kanthal® EF100**

Kanthal® EF is a newly developed group of FeCrAl alloys with a leaner composition than traditional FeCrAls, the baseline being Cr (10%), Al (4%). The aim for this leaner composition is to optimise the alloys for use at lower temperatures by avoiding the 475 °C embrittlement, while retaining their excellent corrosion properties.

- **Kanthal® EF101**

This alloy is an adjustment of EF100 by adding Si (2%) and RE, to improve the corrosion resistance in aggressive environments such as those relevant in boiler applications. As for all the FeCrAl alloys, the material would be used as corrosion protection in the form of overlay welding or tubes co-extruded with a load bearing alloy.

- **Alloy 625**

This is a nickel base alloy containing both chromium and molybdenum for corrosion protection. The alloy exhibits generally good corrosion resistance in chloride containing environments and is today used to a large extent in boilers, primarily as overlay welded and thermal spray coated load carrying tubes.

- **Alleima® Sanicro® 69 (Alloy690)**

This is an austenitic nickel-chromium-iron alloy with high resistance to oxidation, carburization and nitridation, and cracking resistance. This alloy is widely used in black liquor recovery boilers as composite tubes. The corrosion properties and resistance to stress corrosion cracking have been verified in both extensive laboratory testing and in boilers.

- **CorEr thermally sprayed coating**

MH Engineering has developed a nickel-based alloy, with a similar composition to the Inconel625 alloy. However, micro-additives have been added in order to promote precipitation hardening. This hardening process starts when the boiler is started up and after about 3 weeks at 300 °C material temperature the coating is fully hardened. This process increases the hardness to about 800 (HV300) as compared to traditional Inconel625, which has a corresponding hardness of about 300. This increase in hardness is especially useful in CFB boilers burning difficult fuels and where corrosion and erosion is problematic. This coating has both been sprayed on to samples with the HVOF technique (High Velocity Oxy-Fuel) and the newer HVAF technique (High Velocity Air Fuel). The later coating technique is expected to produce more dense coatings and thereby higher corrosion resistance.

3.2 DESCRIPTION OF THE EXPOSURES

3.2.1 Clamp samples on FBHE in Händelö P15 and Högdalen P6

During boiler shutdowns clamp samples were installed on, and removed from, the top and bottom most tube rows of the FBHE tube bundles. Two halfmoon shaped clamp sample halves were mounted around the superheater tubes. Clamping tools were used to hold the clamp halves tightly around the heat exchanger tubes while they were TIG-welded together by using Alloy-625 wire. Three sample batches were installed in Händelö P15 (Apr. 2019, Apr. 2020 and Sep. 2021) and one batch in Högdalen P6 (Aug. 2019). In 2019, all the samples were installed by using method-1 (schematic image in the top of Figure 3. In 2020 and 2021, sample installation was made by using method-2 (schematic image in the bottom of Figure 3. This change was made to reduce the risk of harming the heat exchanger tubes while removing the samples. In Table 7 -

Table 13 the installation locations, together with estimated metal surface temperatures, sample identification names (upward (U) facing on the left and downward (D) facing in the right column) and exposure period / failure by color coding are shown. In the tables, 197 and 198 were the EF101 and EF100 sample respectively. In addition, the "In 625" sample was "alloy 625" sample and "San33" was "27Cr33Ni3Mo alloy".

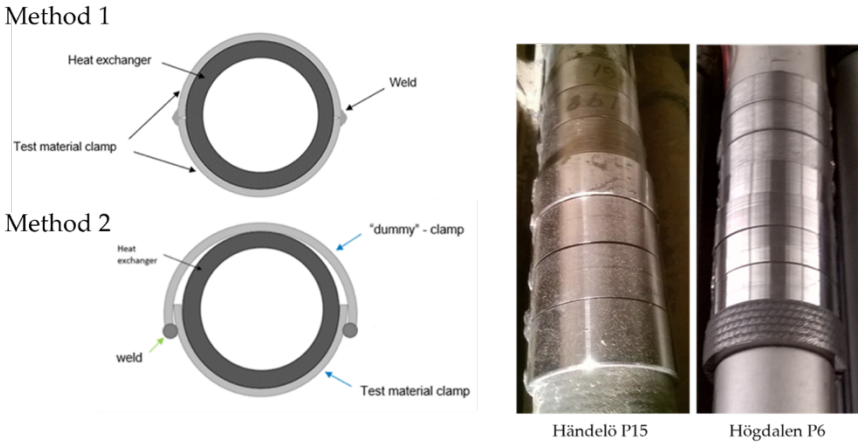

Figure 3. Description of clamp installation. The top left image shows a schematic of the clamp installation according to method 1. The bottom left image shows a schematic of the clamp installation according to method 2.

Table 7. Color describing the dates of exposure in boiler P6, Högdalen positioned in FBHE SH3b row 1 and 8.

	Installed	Removed
	Aug. 2019	Sep. 2020
	Aug. 2019	Sep. 2021
		Not recovered

Table 8. Boiler P6, Högdalen positioned in FBHE SH3b clamp samples installed in Aug. 2019 (shield between the heat exchanger tube and clamp sample on row 1).

SH4, Row 1, Coil 4 (T~600-625 °C)

197'-1U	197'-1D
198'-1U	198'-1D
APMT'-1U	APMT'-1D
316'-1U	316'-1D
K92'-1U	K92'-1D
12RM80'-1U	12RM80'-1D
San69'-1U	San69'-1D
IN625'-1U	IN625'-1D

SH4, Row 1, Coil 6 (T~600-625 °C)

16Mo3'-1U	16Mo3'-1D
San28'-1U	San28'-1D

SH4, Row 1, Coil 8 (T~600-625 °C)

197'-2U	197'-2D
198'-2U	198'-2D
APMT'-2U	APMT'-2D
316'-2U	316'-2D
K92'-2U	K92'-2D
12RM80'-2U	12RM80'-2D
San69'-2U	San69'-2D
IN625'-2U	IN625'-2D

SH4, Row 1, Coil 10 (T~600-625 °C)

16Mo3'-2U	16Mo3'-2D
San28'-2U	San28'-2D

SH4, Row 8, Coil 5 (T~525-550 °C)

197-1U	197-1D
198-1U	198-1D
APMT-1U	APMT-1D
316-1U	316-1D
K92-1U	K92-1D
12RM80-1U	12RM80-1D
San69-1U	San69-1D
IN625-1U	IN625-1D

SH4, Row 8, Coil 7 (T~525-550 °C)

16Mo3-1U	16Mo3-1D
CE-1	CE-2
APMT20C-1	APMT-20C-2
APMT-50C-1	APMT50C-2

SH4, Row 8, Coil 9 (T~525-550 °C)

197-2U	197-2D
198-2U	198-2D
APMT-2U	APMT-2D
316-2U	316-2D
K92-2U	K92-2D
12RM80-2U	12RM80-2D
San69-2U	San69-2D
IN625-2U	IN625-2D

SH4, Row 8, Coil 11 (T~525-550 °C)

16Mo3-2U	16Mo3-2U
CE-3	CE-4
CE-5	APMT-20C-3
CE-6	APMT50C-3

Table 9. Color describing the dates of exposure in boiler P15, Händelö positioned in FBHE SH2 and SH3 region.

	Installed	Removed
	Apr. 2019	Jun. 2019
	Apr. 2019	Sep. 2019
	Apr. 2019	Mar. 2020
	Apr. 2020	Mar. 2021
	Sep. 2021	Mar. 2022
		Not recovered

Table 10. Händelö P15 FBHE SH2 clamp samples installed in Apr. 2019.

SH2, Row 1, Coil 4 (T~500-525 °C)

197-1U	197-1D
198-1U	198-1D
APMT-1U	APMT-1D
316-1U	316-1D
K92-1U	K92-1D
12RM80-1U	12RM80-1D
San69-1U	San69-1D

SH2, Row 1, Coil 6 (T~500-525 °C)

IN625 (WOL)-1U	IN625 (WOL)-1D
"dummy"	APMT (WOL)-1D
"dummy"	197 (WOL) -1D
"dummy"	198 (WOL) -1D
"dummy"	CE-1D
"dummy"	APMT C50-1D

SH2, Row 1, Coil 8 (T~500-525 °C)

197-2U	197-2D
198-2U	198-2D
APMT-2U	APMT-2D
316-2U	316-2D
K92-2U	K92-2D
12RM80-2U	12RM80-2D
San69-2U	San69-2D

SH2, Row 1, Coil 10 (T~500-525 °C)

IN625 (WOL)-2U	IN625 (WOL)-2D
"dummy"	APMT (WOL)-2D
"dummy"	197 (WOL) -2D
"dummy"	198 (WOL) -2D
"dummy"	CE-2D
"dummy"	APMT C20-2D

SH2, Row 1, Coil 12 (T~500-525 °C)

197-3U	197-3D
198-3U	198-3D
APMT-3U	APMT-3D
316-3U	316-3D

SH2, Row 1, Coil 14 (T~500-525 °C)

IN625 (WOL)-3U	IN625 (WOL)-3D
"dummy"	APMT (WOL)-3D
"dummy"	197 (WOL) -3D
"dummy"	198 (WOL) -3D
"dummy"	CE-3D
"dummy"	APMT C50-3D

SH2, Row 6, Coil 3 (T~525-550 °C)

16Mo3-1U	16Mo3-1D

Table 11. Händelö P15 FBHE SH3 clamp samples installed in Apr. 2019.

SH3, Row 1, Coil 4 (T~525-550 °C)

197-4U	197-4D
198-4U	198-4D
APMT-4U	APMT-4D
316-4U	316-4D
K92-3U	K92-3D
12RM80-3U	12RM80-3D
San69-3U	San69-3D

SH3, Row 1, Coil 6 (T~525-550 °C)

IN625 (WOL)-4U	IN625 (WOL)-4D
"dummy"	APMT (WOL)-4D
"dummy"	197 (WOL) -4D
"dummy"	198 (WOL) -4D
"dummy"	CE-4D
"dummy"	APMT C50-4D

SH3, Row 1, Coil 8 (T~525-550 °C)

197-5U	197-5D
198-5U	198-5D
APMT-5U	APMT-5D
316-5U	316-5D
K92-4U	K92-4D
12RM80-4U	12RM80-4D
San69-4U	San69-4D

SH3, Row 1, Coil 10 (T~525-550 °C)

IN625 (WOL)-5U	IN625 (WOL)-5D
"dummy"	APMT (WOL)-5D
"dummy"	197 (WOL) -5D
"dummy"	198 (WOL) -5D
"dummy"	CE-5D
"dummy"	APMT C20-5D

SH3, Row 6, Coil 3 (T~550-575 °C)

197-6U	197-6D
198-6U	198-6D
APMT-6U	APMT-6D
316-6U	316-6D
K92-5U	K92-5D
12RM80-5U	12RM80-5D
San69-5U	San69-5D
16Mo3-2U	16Mo3-2D

SH3, Row 6, Coil 5 (T~550-575 °C)

IN625 (WOL)-6U	IN625 (WOL)-6D
"dummy"	APMT (WOL)-6D
"dummy"	197 (WOL) -6D
"dummy"	198 (WOL) -6D
"dummy"	CE-6D
"dummy"	APMT C20-6D

Table 12. Händelö P15 FBHE SH3 clamp samples installed in Apr. 2020.

SH3, Row 1, Coil 4 (T~525-550 °C)		SH3, Row 1, Coil 18 (T~525-550 °C)	
197-8U	197-8D	197-7U	197-7D
APMT-8U	APMT-8D	APMT-7U	APMT-7D
San69-7U	San69-7D	San69-6U	San69-6D
San33-2U	San33-2D	San33-1U	San33-1D
"dummy"	San59-1D	"dummy"	San59-1U

Table 13. Händelö P15 FBHE SH3 clamp samples installed in Sep. 2021.

SH3, Row 1, Coil 4 (T~525-550 °C)			SH3, Row 1, Coil 18 (T~525-550 °C)	
197-10U	197-10D		197-9U	197-9D
APMT-10U	APMT-10D		AMPT-9U	APMT-9D
San69-9U	San69-9D		San69-8U	San69-8D
San33-4U	San33-4D		San33-3U	San33-3D
"dummy"	San59-3D		"dummy"	San59-3U
197-12U	197-12D		197-11U	197-11D
APMT-12U	APMT-12D		APMT-11U	APMT-11D
San33-6U	San33-6D		San33-5U	San33-5D
"dummy"	San59-4D		"dummy"	San59-4U

3.2.2 Furnace water wall probe samples in Högdalen P6

Högdalen P6 furnace water wall material tests were conducted by using three small sized air-cooled probes. Each probe comprised one sample which was inserted into the furnace via openings made to the membrane panel wall fin (front wall, elevation +17m). The openings were equipped with a double valve system, including pressurized air feeding, allowing safe probe installation and removal. A thermocouple was connected to each sample to verify the exposure temperature. The control unit and mass flow controllers were used to control the air feeding rate required to hold the samples at set temperatures. To reach higher exposure temperatures, insulation material was used between the sample and panel wall fin. The exposure time was one week, and target metal temperatures were 300 and 350 °C. The test matrix is given in

Table 14. The tests were started in Nov. 2022.

Furnace wall probe equipment:

- Probe openings
- Air cooled probes
- Samples
- Thermocouples with K-type compensation cables
- Air hoses for cooling air
- Mass flow controllers
- Control unit box

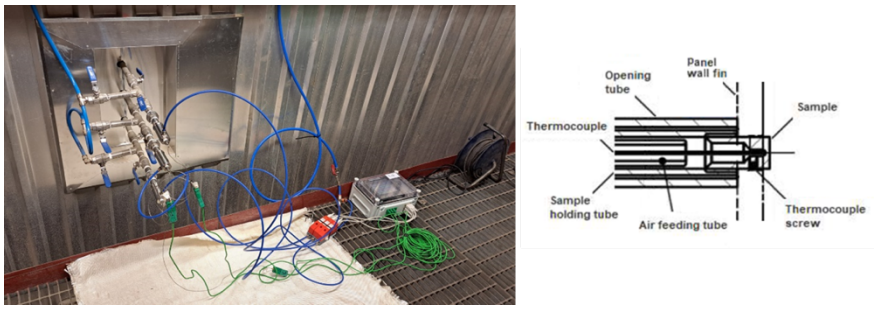

Figure 4. Furnace wall probe set-up (left). Schematic drawing of the probe instrument (left).

Table 14. Högdalen P6 furnace water wall test matrix.

Set	T, °C	Probe-1	Probe-2	Probe-3
1	300	16Mo3	310HCbN	Alloy 625
2	300	EF101	EF100	APMT
3	300	San28	27Cr33Ni3Mo	San35
4	350	16Mo3	310HCbN	Alloy 625
5	350	EF101	EF100	APMT
6	350	San28	27Cr33Ni3Mo	San35

3.2.3 Thermal sprayed coatings on the water walls in Händelö P15

In Händelö P15 a section of the water wall in the empty pass was coated using HVOF, a metallic spray process. This was performed in 2019. In total, four water wall tubes were sprayed. Two of them were coated with APMT and two of them were coated by CorEr. The thickness of the metal spray coatings was measured twice, in 2020 and 2021, in order to elucidate the material wastage.

3.3 ANALYTICAL TECHNIQUES

The exposed samples were investigated by means of quantitative as well as qualitative analytical techniques. The quantitative measures have involved material loss determination and the qualitative analysis has primarily involved cross-sectional SEM/EDX analysis. All the analyses were performed by HTC/Chalmers.

3.3.1 Material loss

The samples were evaluated by means of metal loss determination, performed with an Olympus 38DL Plus ultrasonic thickness gage with a 0.01 mm resolution. Complementary material loss determinations were performed by OM and SEM measurements. Internal oxidation and nitridation zones were not defined as material loss in this report and were thus not included as material loss when conducting thickness measurements after exposure.

3.3.2 Scanning Electron Microscopy/Energy Dispersive X-Rays (SEM/EDX)

After exposure, some selected samples were prepared for cross-sectional SEM/EDX analysis. These samples were cast in epoxy, cut, and polished prior to the SEM/EDX investigation. The samples were cast in the epoxy resin by putting them into a mold which were subjected to a 10-bar pressure to avoid the formation of bubbles during the hardening of the resin. The hardening time was fixed at 24 hours. After the hardening of the epoxy resin was complete, the samples were cut using a silicon carbide disc and a lubricant without any water due to the delicate corrosion products. The samples were then polished dry with Silicon Carbide P4000. The cross-section was coated with gold to avoid charging in the SEM. The polished cross-sections of the samples were subsequently investigated by scanning electron microscopy, SEM. In addition, an Energy Dispersive X-rays (EDX) system was used to analyze the sample's elemental composition in the SEM image. The resolution and depth of focus in an SEM are much higher than in an optical microscope, revealing more details of the corrosion attack. The samples were examined with an FEI Quanta 200 FEG ESEM. The SEM has a field emission electron gun (FEG) and is equipped with an Oxford Inca energy dispersive X-ray (EDX) system. SEM/EDX was used for elemental mapping and quantification. For imaging and EDX analysis, an accelerating voltage of 20 kV was used.

4 Results

4.1 WATER WALL EXPOSURES HÖGDALEN P6 WASTE-FIRED BOILER

The temperature profile of the three different sets of materials evaluated in the water wall in Högdalen P6 waste-fired boiler is shown in Figure 5-7. A couple of noticeable trends should be addressed. For instance, in Set#1 the 16Mo3 sample achieved an approximately 20 °C higher temperature than 310HCbN and Alloy 625 throughout the exposure (see Figure 5) In set 2, the temperature profile shows that EF101 obtained a temperature between 290-300 °C, while EF100 and APMT had an average temperature around 275 and 270 °C, respectively (see Figure 6). The sudden temperature drop observed in set #3 was due to a sudden boiler shut down, hence the exposure was only carried out for approximately six days. In addition, the 27Cr33Ni3Mo sample was not retrieved.

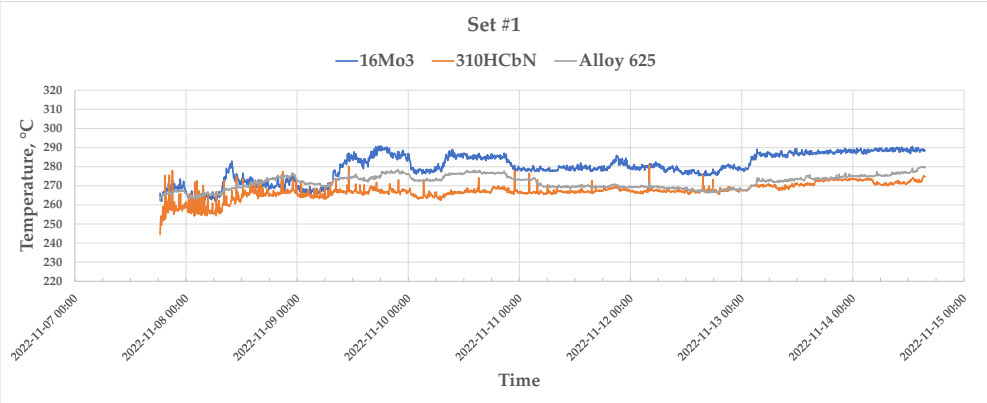

Figure 5. Temperature profile for Set #1.

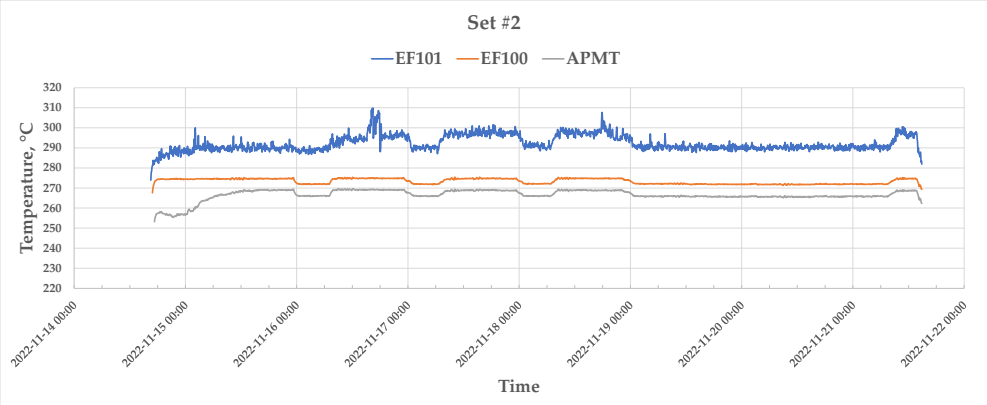

Figure 6. Temperature profile for Set #2.

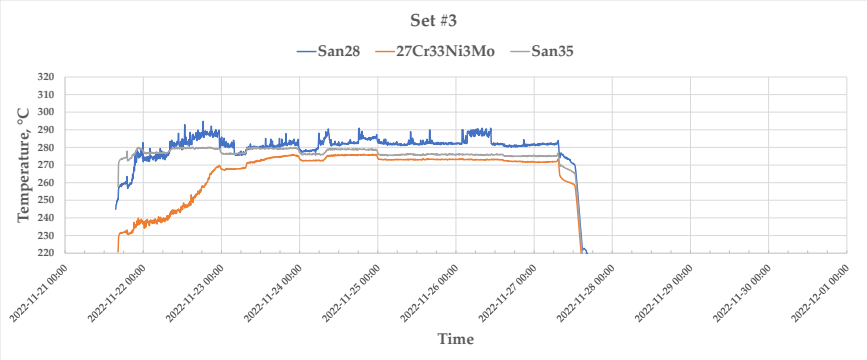

Figure 7. Temperature profile for Set #3.

A SEM cross section overview of all samples tested in the water wall region is shown in Figure 8. As is shown the only sample displaying high oxidation rate was the low alloyed steel 16Mo3. The 310HCbN and Alloy 625 sample from Set #1 showed no indication of significant material loss or oxidation, e.g., a homogenous surface and no alloy element depletion close to the metal/atmosphere interface was observed with SEM/EDX analysis.

A more detailed microstructure investigation of 16Mo3 is shown in Figure 9. A roughly 20 micrometer thick Fe-rich oxide was observed, adherent to the metal substrate. On top of the oxide an adherent deposit with various thickness was covering the oxide surface. The deposit contained mainly Cu, S, O, Na, K, Ca and traces of heavy metals such as Zn and Pb. The bright areas displayed in the deposit and, in some cases the Fe-oxide, were confirmed via EDX point analysis to consist of a mixture of both high concentrations of Cu/O and a mixture of Pb/K/Na/O (see Figure 9). The oxide formed was divided into two regions, where the darker area closest to the metal/oxide interface was confirmed via EDX point analysis to consist of a high concentration of Cl. From the EDX mapping it is evident the Cl ions have migrated from the deposit layer and separated from potential initial cations such as Na, K, Pb and Ca. The overlap between the L series peak of Pb and the Kα peak of S makes it very challenging to distinguish these two elements in EDX mapping and point analysis, which is observed in the EDX mapping. Thus, the quantity of these elements should be considered with caution.

For the FeCrAl alloys exposed in Set #2 the APMT and EF100 sample remained intact with no indication of heavy oxidation nor material losses. Furthermore, none of the FeCrAl samples showed any indication of nitridation close to the metal/deposit interface. For the EF101 sample, a 40 µm thick deposit was observed on the sample after 1 week of exposure. A SEM cross section and EDX analysis were conducted on this sample and is shown in Figure 10. Similar deposit composition was observed as with the 16Mo3 sample. However, as is shown in the EDX mapping and point analysis, it is evident that the Cl ions have not migrated from the deposit layer towards the metal/deposit interface and are thus still in the vicinity of their initial counter ions. Below the deposit a thin Fe,Cr,Al oxide was observed in patch wise fashion with a thickness of roughly 2 µm (see point analysis “b” in Figure 10).

Lastly the Sanicro 28 and 35 sample in Set #3 displayed no indication of heavy oxidation nor material losses. EDX analysis confirmed that the deposit observed on the Sanicro 28 sample had similar composition as the previous mentioned samples. As with the EF101 sample, the Cl remained well distributed over the deposit layer and had not migrated to the metal/deposit interface. In addition, from EDX analysis no indication of internal or outward growing oxide was seen.

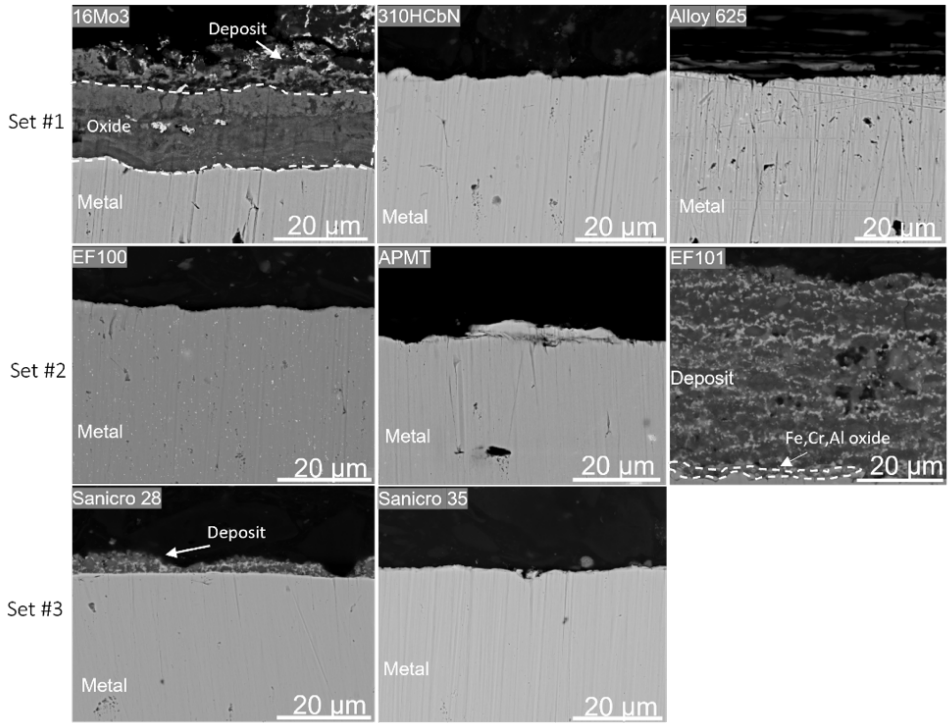

Figure 8. SEM cross section overview of material tested in the water wall region for 1 week at approximately 300 °C in Boiler P6, Högdalen.

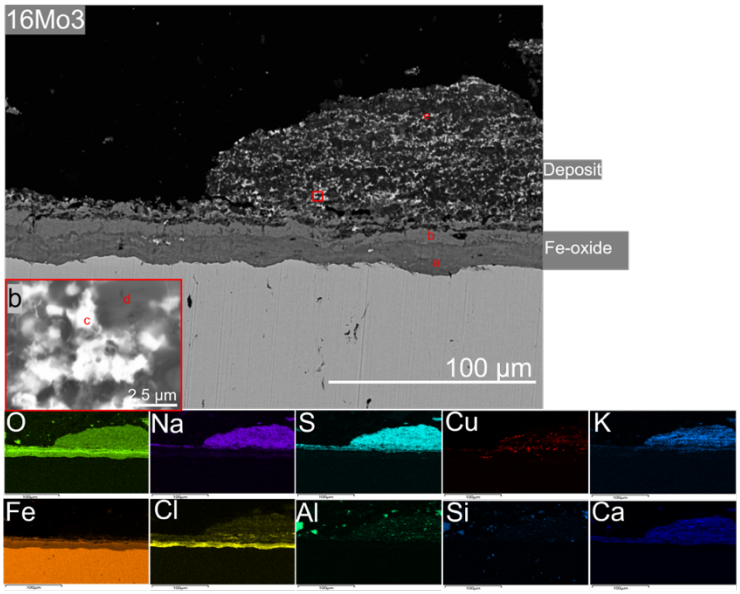

at%	Fe	O	Si	S	Zn	Ca	K	Na	Cl	Cu	Pb
Spectrum a	35.5	47.9	0.2	0.5	1.4	0	0.5	0.6	13.4	0	0
Spectrum b	39.2	55.7	0.5	0.4	0.2	0.1	0.3	1.4	2	0	0
Spectrum c	3	26.1	1.5	4.6	0.2	1.5	0.6	6	0.6	55.7	0.7
Spectrum d	1	54.4	1.6	14.4	0.6	5.4	7.5	11.2	1.3	2.5	0.8
Spectrum e	0	57.6	0	13.8	0.6	2.2	7.7	8.18	3	0	6.8

Figure 9. SEM cross section and EDX analysis of 16Mo3 exposed for 1 week at approximately 300°C in Boiler 6, Högdalen.

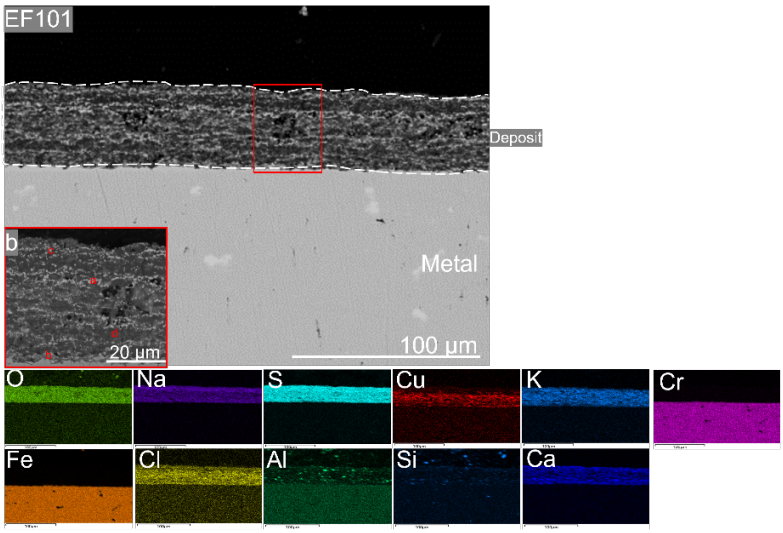

at%	Fe	O	Al	Si	S	Zn	Ca	K	Na	Cl	Cu	Pb
Spectrum a	1	50	1	1	15.8	2	4.5	4.9	7	2	11	1
Spectrum b	46	25	5.6	2	2	2	1	1	1	3	0	0
Spectrum c	0	50.6	1	1	13.8	0.6	2	7.5	8	8	0	8
Spectrum d	0.5	58.1	2	3.3	13.5	1.5	7.1	3	6.4	2	0.9	1

Figure 10. SEM cross section and EDX analysis of EF101 exposed in the water wall region for 1 week at approximately 300 °C in boiler P6, Högdalen.

4.2 METAL SPRAYED COATINGS ON WATER WALLS IN HÄNDELÖ P15

Two test areas, about 1.2 meter in height and about two tubes wide, were HVOF sprayed with APMT and CorEr, respectively. The number 3 and 4 tubes were metallized APMT and the number 7 and 8 tubes were metallized with material CorEr™, see Figure 13. Both materials had been coated in the spring 2019.

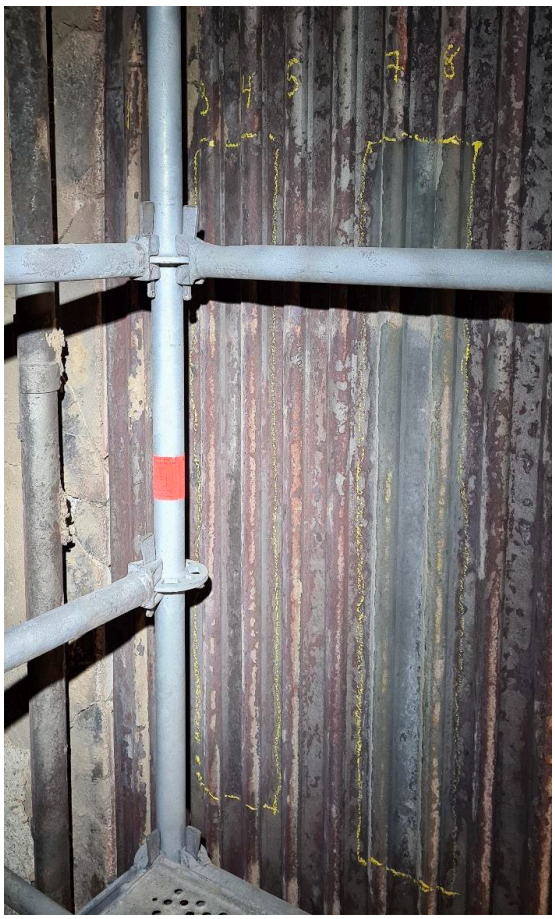

Figure 11. The two areas HVOF sprayed. Tubes 3-4 are metallized with AMPT and tubes 7-8 are metallized with CorEr. The image is taken during the first revision, about 1 year of exposure.

Already at the time of the first inspection, on 2020-03-25, it was noted that only tubes number 7 and 8 (with CorEr) had any metallization left on the tubes. For tubes 3 and 4 (with APMT), only small remnants of metal left in the junction between the tube and the fin could be seen.

At the second inspection (2021-03-25), after about two years of exposure, there was no APMT coating left on the tubes number 3 and 4. For the CorEr coating on tubes number 7 and 8, the metallization was still visibile. The nominal layer thickness of material CorEr™ was approx. 400 ± 50 µm, see Figure 12. The variation depends primarily on manual application. Thus, there has been no appreciable stripping of the metallization on tubes number 7 and 8, after two operating seasons.

Figure 12. Thickness measurement of the HVOF sprayed CorEr coating at the 2021 revision in the P15 boiler in Händelö.

4.3 MATERIAL LOSS AND MICROSTRUCTURAL ANALYSIS ON FBHE

4.3.1 Clamp exposures on FBHE - Högdalen P6

Clamp exposures were conducted on fluidized bed heat exchangers in the P6 waste-fired boiler in Högdalen in continuous mode during two periods: 12 and 24 months. In this exposure times the planned shutdowns of the boiler are counted. The material loss calculations are presented in mm/year to be able to compare with P15 Händelö exposures as well as previous or future research studies. The samples were mounted as two half-moon rings on the top and bottom-most rows of the fluidized bed heat exchanger bundle. The first batch samples, exposed 12 months, were placed in rows 1 and 8, respectively. The second batch samples, exposed 24 months, were placed in row 9.

Material loss

Figure 13 shows the material loss rate for each sample expressed as mm/y. The filled circle for each data set represents the arithmetic mean value of the material loss.

An increase in material loss rate in row 1 compared to row 8 was observed for all materials exposed for 12 months, except for the SX and Sanicro 69 samples.

All three FeCrAl alloys sustained low material loss throughout the exposure ranging from approximately 0-0.35 mm/year, expressed as maximum material loss rate. The Novel FeCrAl alloy EF101 achieved the lowest material loss rate of the FeCrAl alloys, obtaining a material loss close to zero regardless of position and with a maximum material loss rate of 0.09 mm/year observed in row 1. In addition, the spread of the material loss values for EF101 were very low throughout the cross section, indicating that a homogenous surface remained on the sample. This behavior is consistent with the material loss results after the 24 months exposure. The EF101 FeCrAl material presents negligible material loss, while a larger spread in material loss values was observed for the EF100 alloy. After 24 months exposure this alloy obtained an average material loss of 0.36 mm/year, the maximum material loss being 0.55 mm/year. The surface of the EF101 alloy is smoother and it presents less nitridation than the EF100 alloy. This aspect is discussed in the section below.

The APMT bulk sample presents an average material loss of 0.27 mm/year after 24 months exposure with a high grade of nitridation.

The nitridated material has not been considered in the material loss calculation as it is unclear if it affects the corrosion behavior or increases the material loss. This behavior has been observed in several samples and more corrosion experiments are needed to determine if it is a factor affecting corrosion.

The austenitic conventional stainless steel, 316Ti, and Esshete 1250 exhibited high material loss after 12 months exposure, compared to the previously mentioned FeCrAl alloys. An increase in material loss was observed for 316Ti compared to Esshete 1250 in row 1 and row 8. These samples obtained an average material loss rate ranging from 0.33-0.92 mm/year at the two different positions. After 24 months exposure the 316Ti was not recovered. The Esshete 1250 presents higher material loss than after 12 months exposure, with an average value of 0.87 mm/year and a maximum of 1.07 mm/year.

The high Si-containing austenitic steel SX performed significantly better than the previously mentioned austenitic steels both after 12- and 24-months exposure. The average material loss rate for this sample was between 0.02-0.06 mm/year after 12 months exposure for row 1 and 9. The material loss value did not increase after 24 months exposure, with an average of 0.05 mm/year. In addition, the maximum material loss was close to the calculated average value, suggesting that a homogenous surface remained on this sample in both exposures.

The highest material loss was observed for the low alloyed steel, 16Mo3, which obtained an average material loss rate of 1.18 mm/year and a maximum rate of 1.4 mm/year after 12 months.

The high alloyed steel material of the Sanicro series displayed quite different performances, where Sanicro 28 achieved approximately a maximum material loss of 0.55 mm/year and an average value of 0.34 mm/y in row 1 after 12 months exposure. Meanwhile, no noticeable material loss was detected on the Sanicro 69 sample after 12 months, regardless of position. After 24 months exposure, Sanicro 69 still presents negligible material loss.

Finally, as is shown in Figure 13, the coated material of APMT50C, APMT20C and CorEr achieved high material losses, with an average value of 0.55-0.85 mm/year. However, it was later observed during microstructure analysis that these coatings had failed as no coating material remained on the bulk material after exposure (see "microstructure analysis" sector).

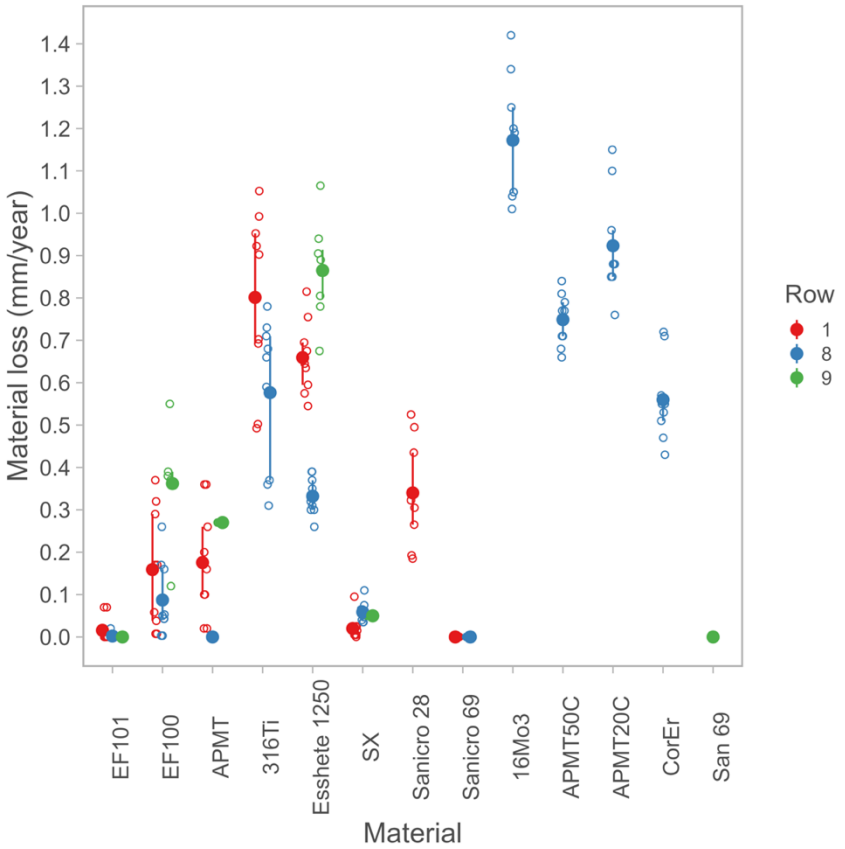

Figure 13. Material loss of the tested clamps exposed in row 1 and 8 for 12 months and row 9 for 24 months in the fluidized bed heat exchanger in P6 boiler, Högdalen.

Microstructure analysis

SEM/EDX analysis were carried out on each exposed sample for microstructure analysis. The results are described below. In many samples, the microstructure contained similar features and chemical composition after 6 and 12 months of exposure, and thus only EDX mapping for 12 month is presented.

Figure 14 presents the SEM cross-section of EF101 positioned in row 1 after 12 months of exposure. A deposited layer of approximately 25 µm of thickness was observed and located on top of a roughly 30 µm Fe-rich oxide. The deposit consisted mainly of Ca, S, Mg, O, and Al (see EDX map analysis below cross-section image). Below the Fe-rich oxide, a Cr/Al-rich oxide was detected at the metal/oxide interface. Compared to the stainless-steel samples of Esshete 1250, 316Ti and SX, there were no indications that the material had been subjected to internal oxidation. However, the EDX analysis confirmed the formation of Al nitrides precipitates below the oxide layer, embedded in a Fe-rich alloy matrix (see EDX point analysis in Figure 14). The thickness of the nitridation region varied

greatly throughout the cross section (between 0-280 µm) and was observed in a patch wise fashion.

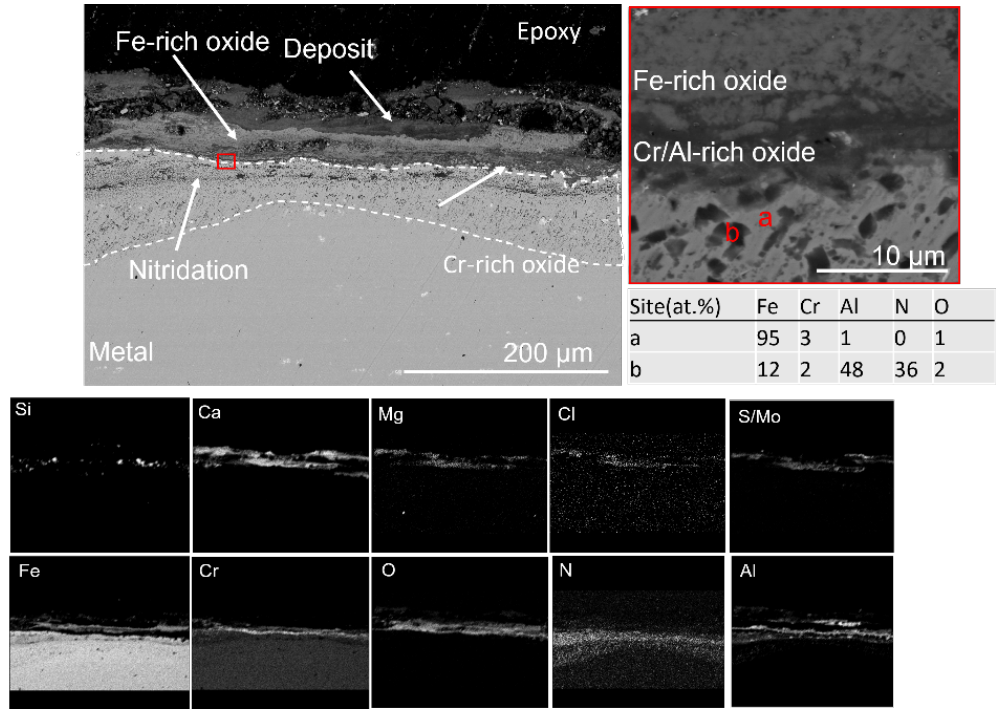

Site(at.%)	Fe	Cr	Al	N	O
a	95	3	1	0	1
b	12	2	48	36	2

Figure 14. Cross-section and EDX analysis of EF101 after 12 months of exposure positioned in row 1. EDX point analysis of highlighted red area (right).

The EF101 sample in row 8 displayed similar features as the previously mentioned sample. An adherent Fe-rich oxide of roughly 40 µm was detected below a 40 µm Ca, S, and Al-rich deposit layer. At the metal/oxide interface, a thin Al/Cr-rich oxide was also observed. Compared to the sample positioned at row 1, a less pronounced nitridation zone was observed. The nitridation was identified throughout the cross section in a patch-wise fashion, with a thickness ranging from 0-150 µm. However, as shown in the figure below, most of the nitridation zones were within the range of 0-10 µm.

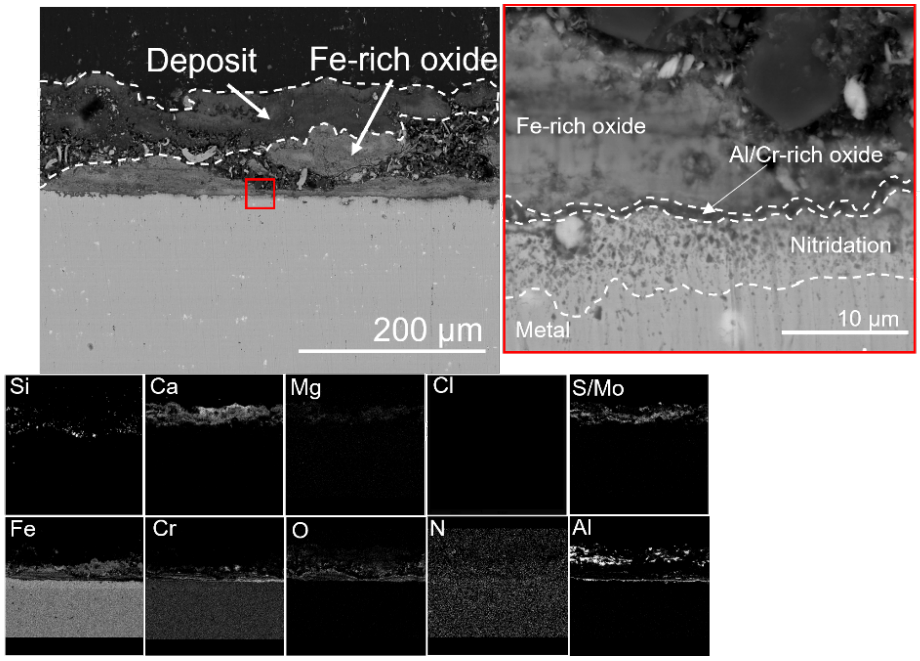

Figure 15. Cross-section and EDX analysis of EF101 after 12 months of exposure positioned in row 8. EDX point analysis of highlighted red area (right).

Figure 16 presents the SEM cross-section and EDX analysis of the EF101 sample after 24 months exposure. The oxide scale is the same as for the 12-month exposed samples presented above. A Cr-rich oxide is formed in contact with the bulk material followed by a thicker Fe-rich oxide. The nitridation zone is over 500 µm thick and it is present all over the sample. However, this value does not seem to affect the material loss, which was still negligible after 24 months exposure (). Some traces of Ca deposit were detected on the top of the oxide scale.

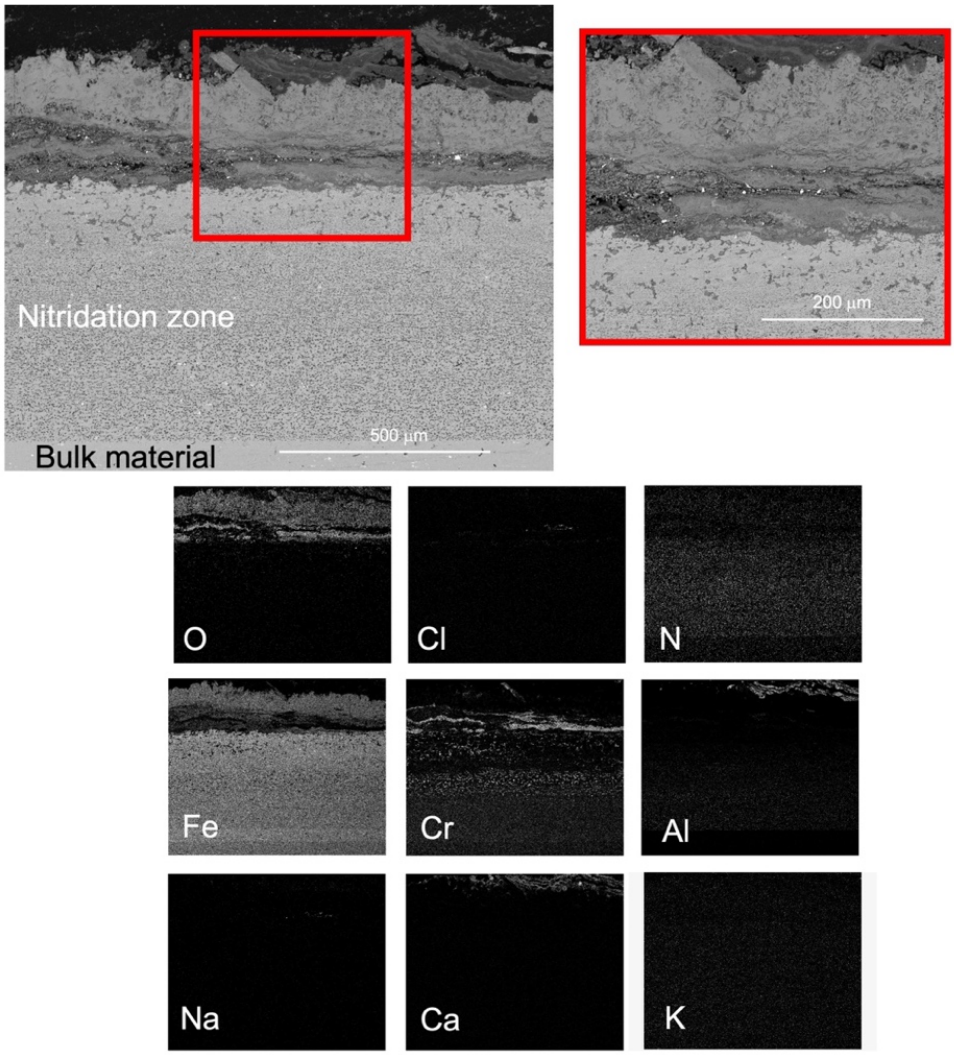

Figure 16. Cross-section and EDX analysis of EF101 after 24 months exposure situated in row 9.

The SEM/EDX cross-section of the EF100 sample situated in row 1 and exposed for 12 months is seen in Figure 17. A thick and adherent deposit layer was observed on the sample containing Ca, S, and Al. In addition, Cl was detected in the deposit. Below, a 140 µm thick, adherent Fe-rich oxide had been formed with elements of void formation, and at the metal/oxide interface, a thin continuous Cr/Al-rich oxide was detected.

Like the EF101 samples, EF100 also developed a nitridation zone below the metal/oxide interface. However, for this sample, a more severe nitration zone was observed, ranging from 75-350 µm thickness, and was seen throughout the cross section in a homogenous fashion.

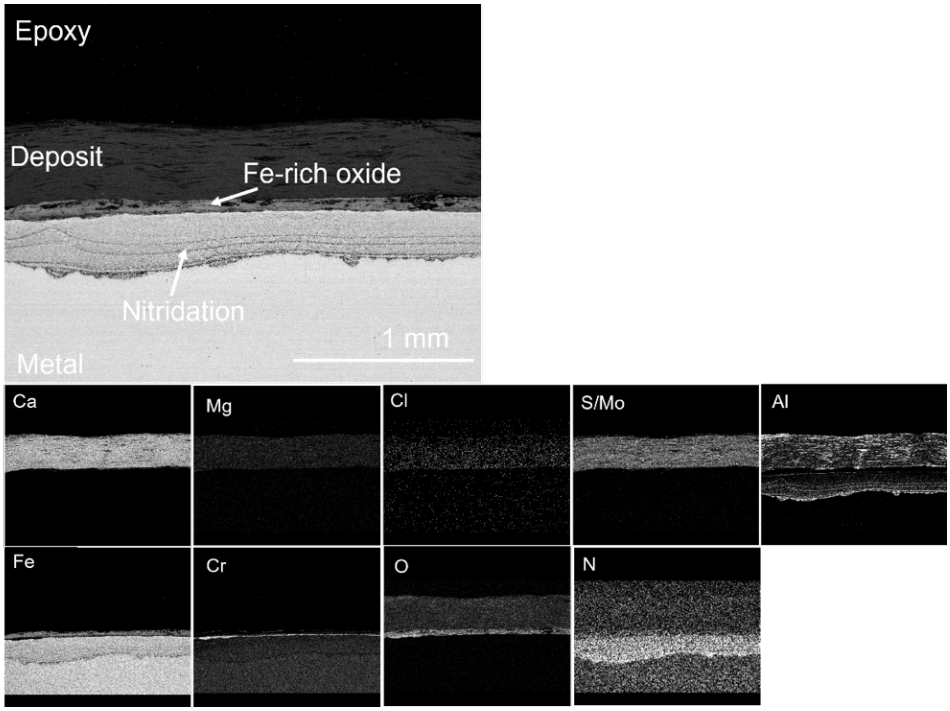

Figure 17. Cross-section and EDX analysis of EF100 after 12 months of exposure positioned in row 1.

The EF100 sample in row 8 displayed similar features as the one in row 1 (see Figure 17). However, no Cl was detected in the deposit. The nitridation zone was less prominent for this sample ranging from 20-200 μm throughout the cross-section. As shown in the material loss figure (Figure 13) described in the previous section, the material loss values varied significantly unlike for the EF101 material. In Figure 18, the image to the right shows a highlighted area of the sample where a more rough and uneven surface was observed, with maximum material losses detected around the middle of the image.

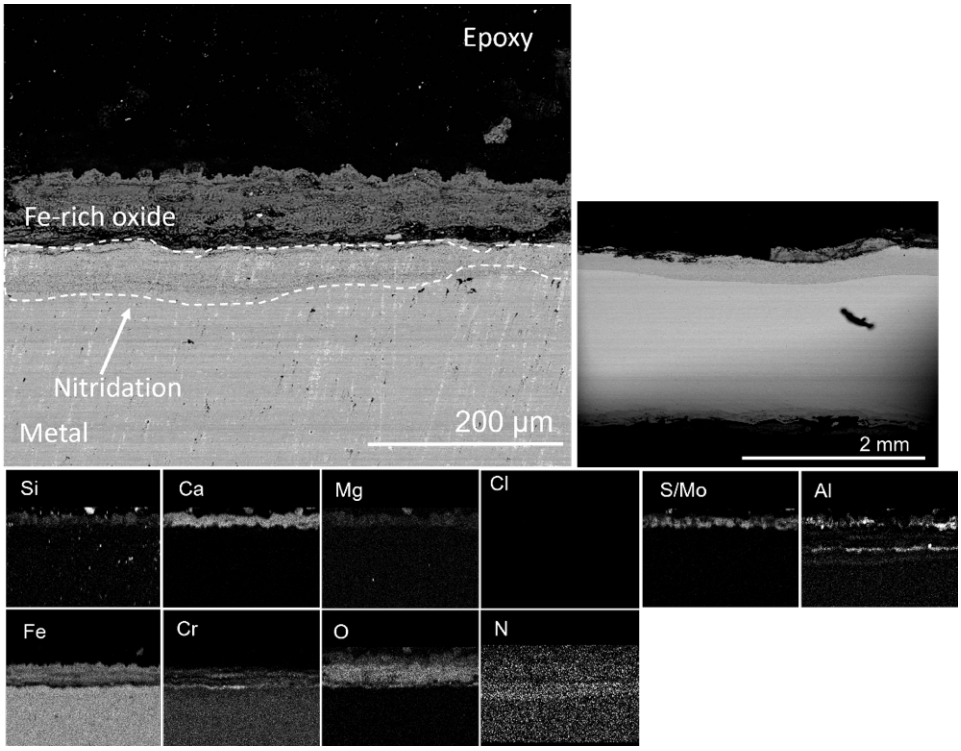

Figure 18. Cross-section and EDX analysis of EF100 after 12 months of exposure positioned in row 8. Cross-section of EF100 positioned in row 8 at lower magnification (right).

Figure 19 presents the SEM cross-section and EDX analysis of the EF100 sample after 24 months exposure. The Fe-rich oxide is thicker than in the 12 months exposure sample (200 µm vs 140 µm thick) and it presents the same void formation. The nitridation zone is also thicker (around 300 µm) and it is present over the whole sample. Regarding the material loss presented in Figure 13, it is still quite low after 24 months, the average value being 0.36 mm/year, but higher than after 12 months (less than 0.2 mm/year).

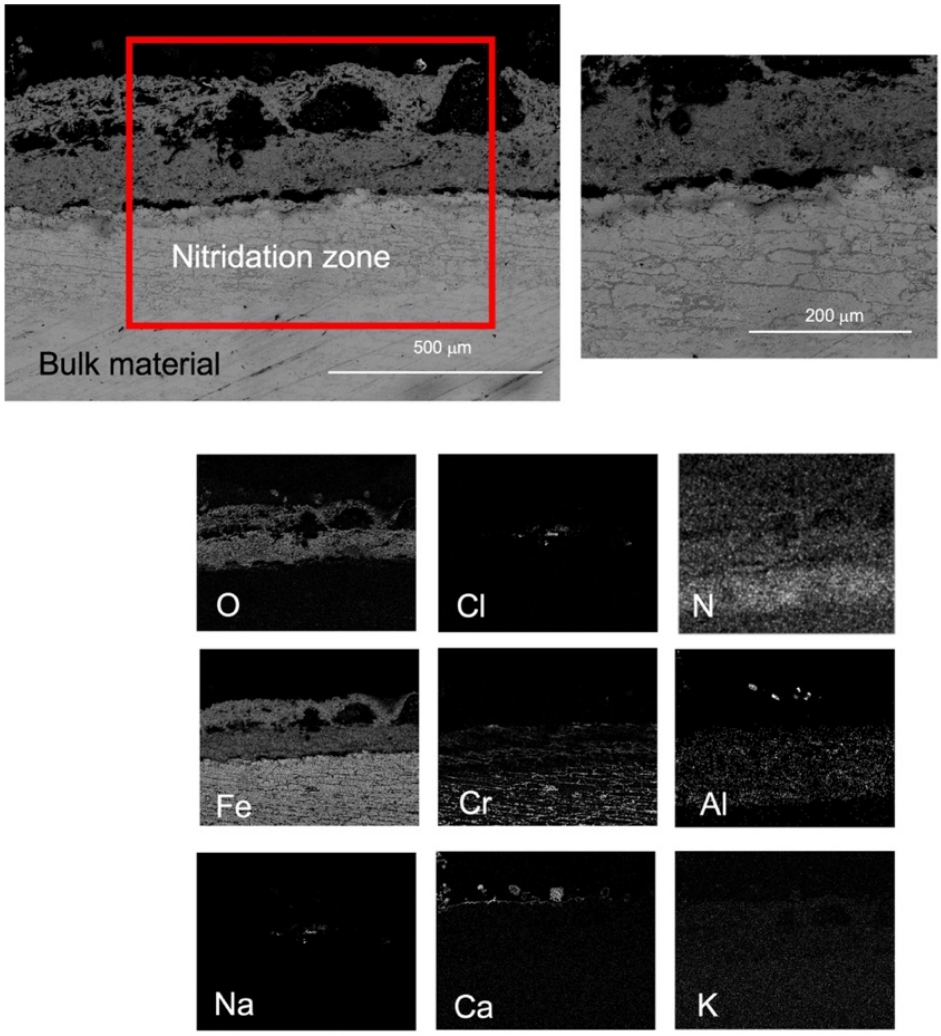

Figure 19. Cross-section and EDX analysis of EF100 after 24 months of exposure positioned in row 9.

To achieve a deeper understanding of the severity of the degradation rate of the newly developed FeCrAl alloys discussed above, a cross-section SEM/EDX analysis was carried out on the corresponding commercial FeCrAl alloy Kanthal APMT in row 1 and row 8 (Figure 20 and Figure 21, respectively).

For the APMT sample positioned in row 1, the deposit layer and oxide had mostly spalled off, which is shown in the EDX mapping. The remaining oxide displayed to the right in the SEM image consisted mainly of a mixture of Cr and Fe, and minor detection of Ca, Si, Mg, and Cl was observed on top of the oxide. The APMT sample suffered from severe nitridation. The thickness of the nitridation zone was measured to roughly 500 µm in row 1 throughout the cross-section with a homogenous structure.

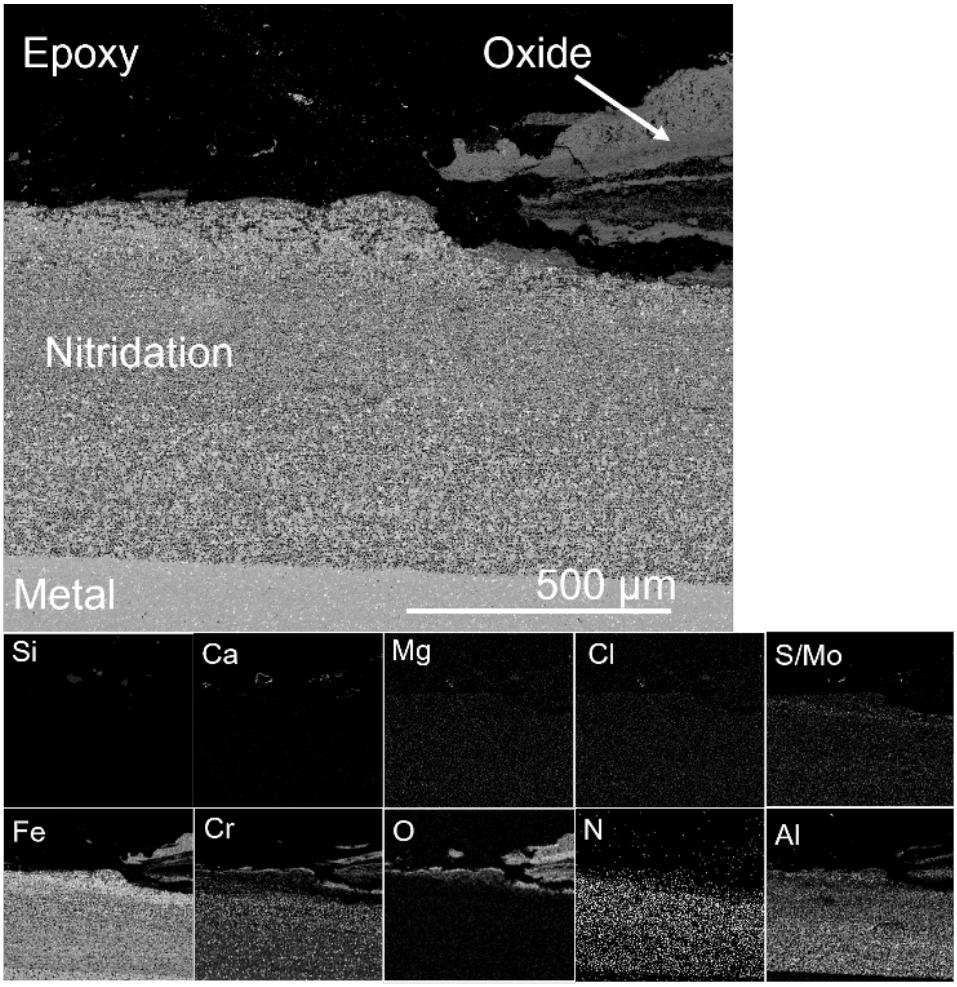

Figure 20. Cross-section and EDX analysis of APMT after 12 months of exposure positioned in row 1.

The APMT sample situated in row 8 displayed less material loss compared to row 1 (see Figure 21). The SEM/EDX image reveals the formation of a Ca, S, Al and O rich deposit with the formation of a Fe-rich oxide below. As for previous FeCrAl alloys, at the metal/oxide interface a Cr/Al-rich oxide was formed. The nitridation zone was significantly thinner for this sample compared to the sample mounted on row 1.

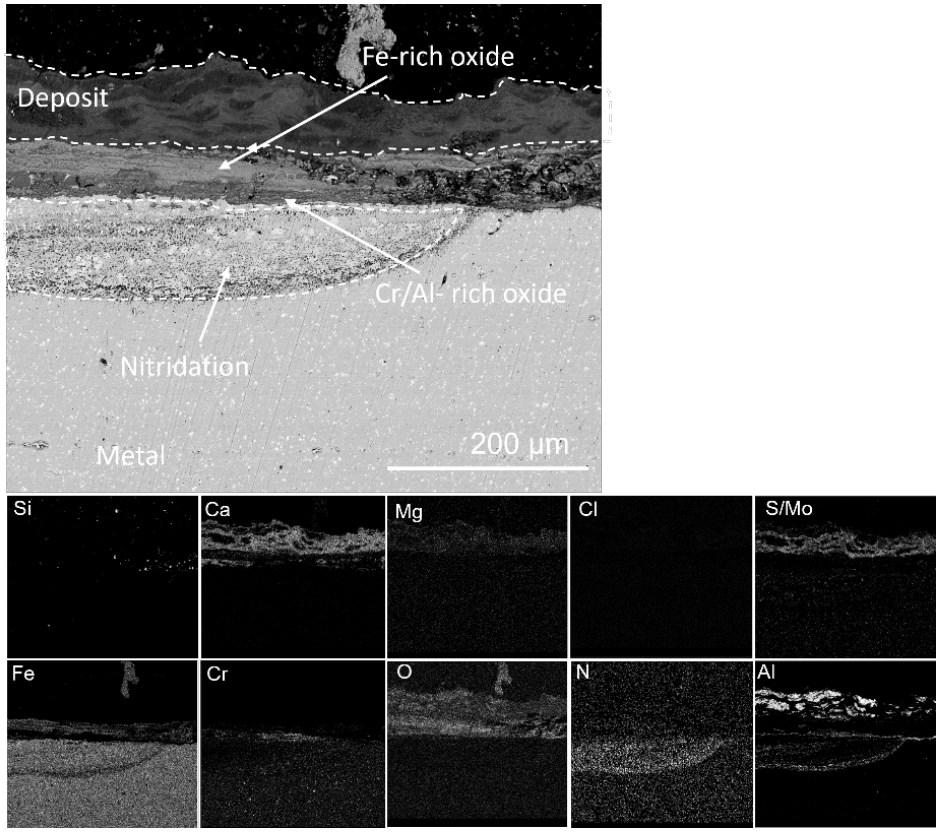

Figure 21. Cross-section and EDX analysis of APMT after 12 months of exposure positioned in row 8.

Figure 22 shows the SEM cross-section and EDX analysis of the APMT sample after 24 months exposure. No traces of deposits were detected. The Fe-rich oxide on the top of the sample reaches a thickness of 300 µm. The sample presents almost a total nitridation of the bulk material but, regardless of that, the material loss after 24 months exposure is still low, with an average value of 0.27 mm/year. As it was explained above, the nitridation zone has not been considered in the material loss calculation.

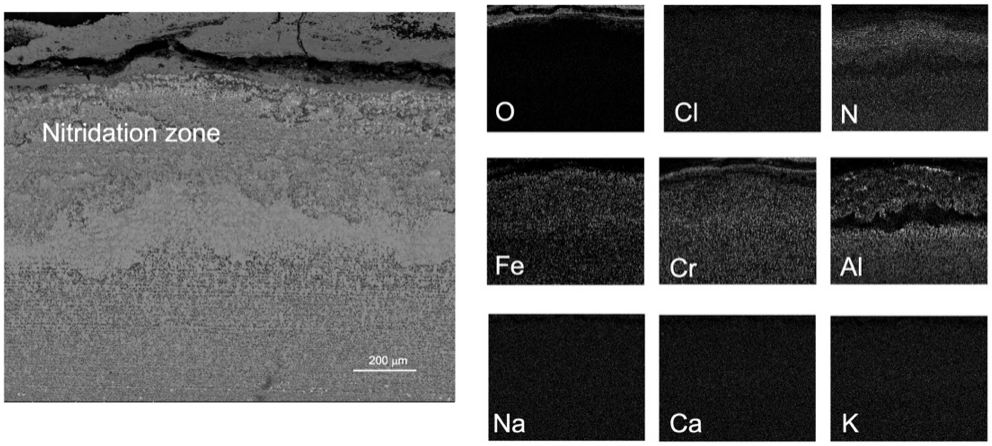

Figure 22. Cross-section and EDX analysis of APMT after 24 months of exposure positioned in row 9.

Figure 23 and Figure 24 show the SEM cross-section image of SX positioned in rows 1 and 8, respectively after 12 months exposure. The material loss analysis concluded that SX showed good resistance toward degradation in the described environment regardless of position (see Figure 11). The highlighted red area in Figure 23 represents the area of interest for the chemical EDX mapping of the sample positioned in row 1. SEM/EDX analysis showed that Ca and Si, together with small traces of S were present on top of the sample, most likely originating from the deposit layer. The corrosion product observed in the cross-section indicates that an internal oxide had been formed that propagated through the sample via grain boundaries to a maximum depth of roughly 70 µm for the sample situated in row 1. Upon detailed EDX point analysis of the internal growing oxide, it was concluded that the oxide mainly consisted of Cr and Si (see Figure 18 to the right). Close to the metal/oxide interface, it was shown that this area was primarily depleted in Cr. At the same time, Ni and Fe remained the main alloy elements in the material matrix. Below the oxide/metal interface, at a depth of roughly 70 µm, small dark precipitates could be observed that were confirmed via EDX point analysis to be Fe-depleted regions.

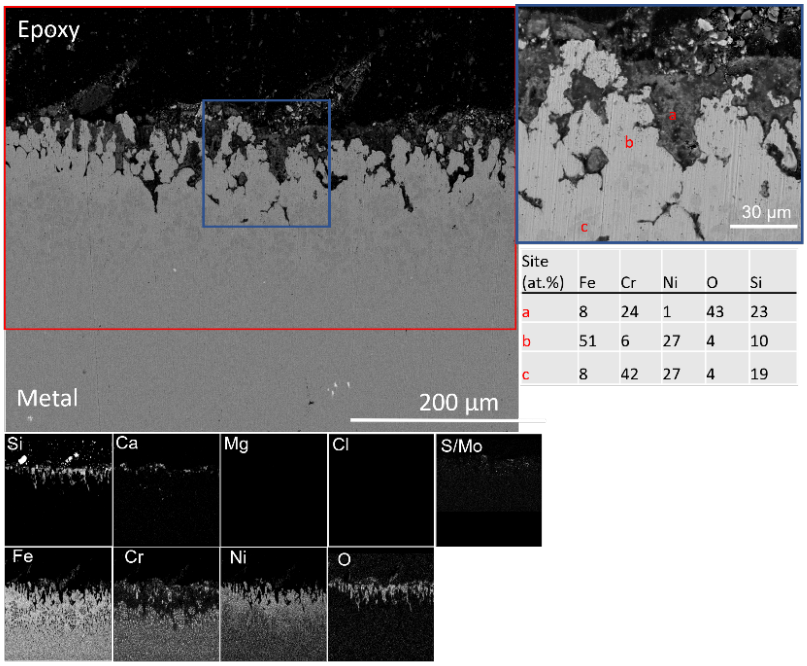

Figure 23. Cross-section and EDX analysis of SX after 12 months of exposure positioned in row 1.

EDX point analysis in highlighted blue area (right) and EDX mapping in highlighted red area. Similar features were observed for the sample in row 8, which aligns well with the material loss results (see Figure 24). A Ca-rich deposit was detected on top of the sample containing traces of Al, S, and Mg.

A Si and Ca-rich oxide was observed at the corrosion front propagating inwards into the bulk material via grain boundaries. A Cr-depletion and Ni enrichment were observed at the metal surface close to the metal/oxide interface.

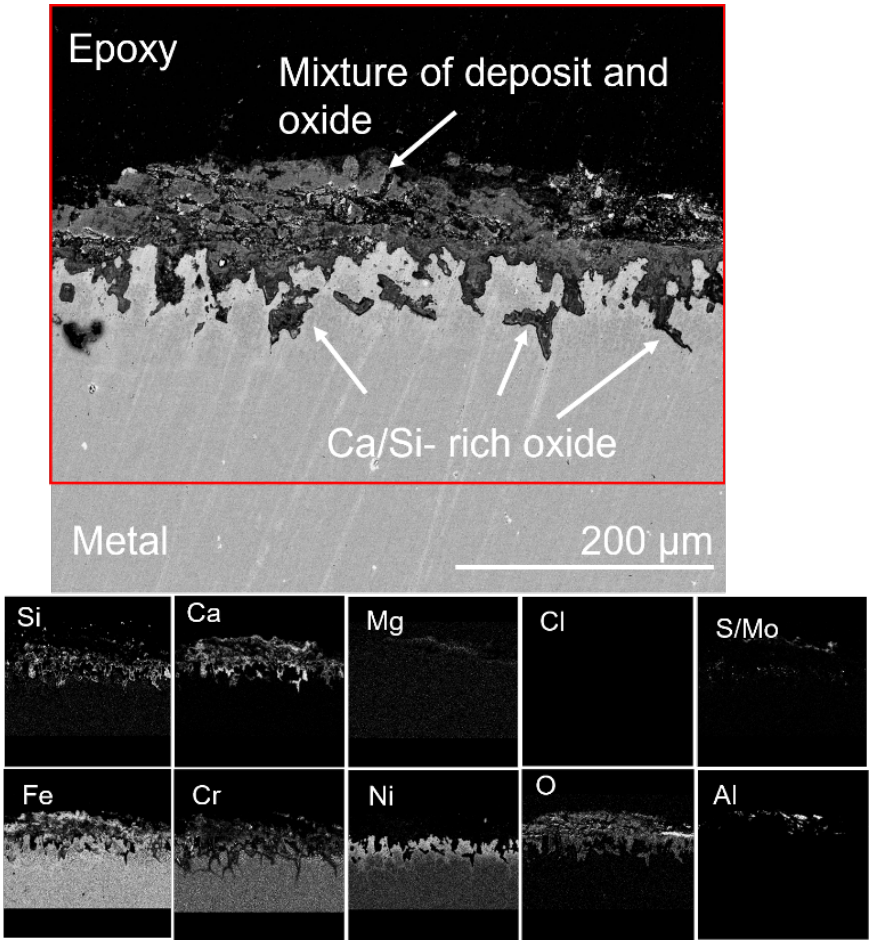

Figure 24. Cross-section and EDX analysis of SX after 12 months of exposure positioned in row 8.

Figure 25 shows the SEM cross-section image and the EDX analysis of the SX positioned in row 9 after 24 months exposure. The Si-rich oxide is still present on the top of the sample after 24 months and the grain boundary attack is around 200 µm thick, in comparison with the 70 µm after the 12 months exposure. This difference in thickness of the grain boundary attack does not seem to affect the material loss, which still was very low (0.05 mm/year) after 24 months and not presenting significant difference compared with this value at 12 months (Figure 13). Some traces of Ca deposit were detected on the top of the oxide scale.

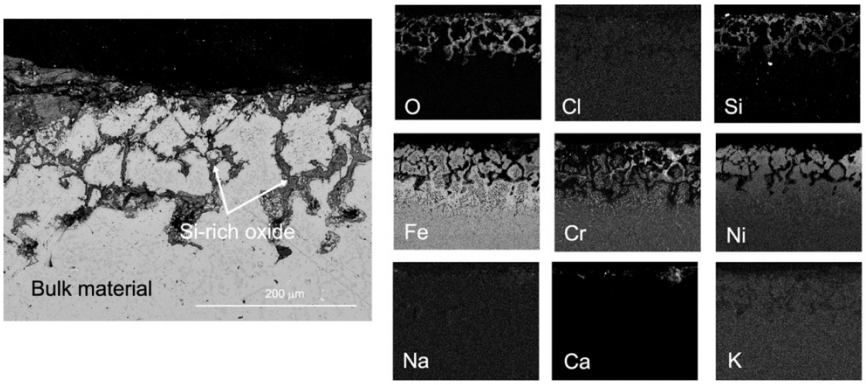

Figure 25. Cross-section and EDX analysis of SX after 24 months of exposure positioned in row 9.

Figure 26 shows the results from the Sanicro 69 sample positioned in row 1. No oxide or deposit was detected on the sample, and only minor material losses were observed. Below the metal/gas interface, a Cr-depleted zone enriched in Ni and Fe was observed, reaching a depth of approximately 150 µm. Further into the material, the alloy composition changed. Cr enrichment was observed at the grain boundaries, while Fe and Ni remained in the bulk matrix. Lastly, as shown in Figure 26 (right), traces of metal chlorides were detected below the Cr-depleted zone. According to EDX analysis, the metal chlorides are suggested to consist of chromium chlorides.

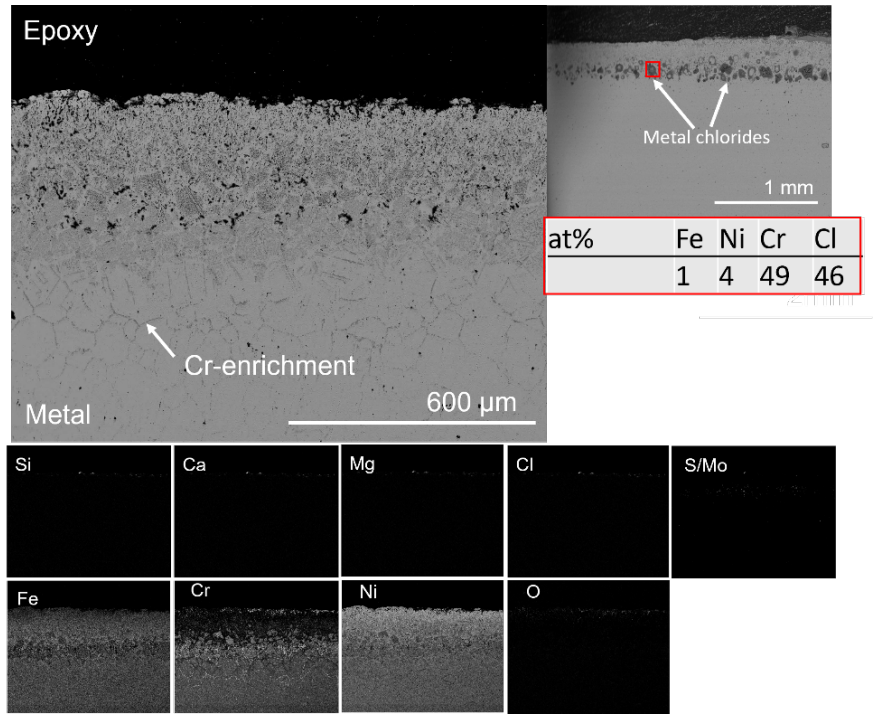

Figure 26. Cross-section of Sanicro 69 after 12 months of exposure positioned in row 1. EDX point analysis of the highlighted red area (right).

The Sanicro 69 sample in row 8 exhibited a roughly 20 µm thin adherent Cr-rich oxide at the material surface (see Figure 27). Similar Cr-depleted zones below the

metal/oxide interface were present as with the sample positioned in row 1. However, compared to the previous sample, a significant increase in metal chlorides was observed below the Cr-depleted zone throughout the cross-section. EDX analysis suggests that the metal chlorides consisted of chromium chlorides.

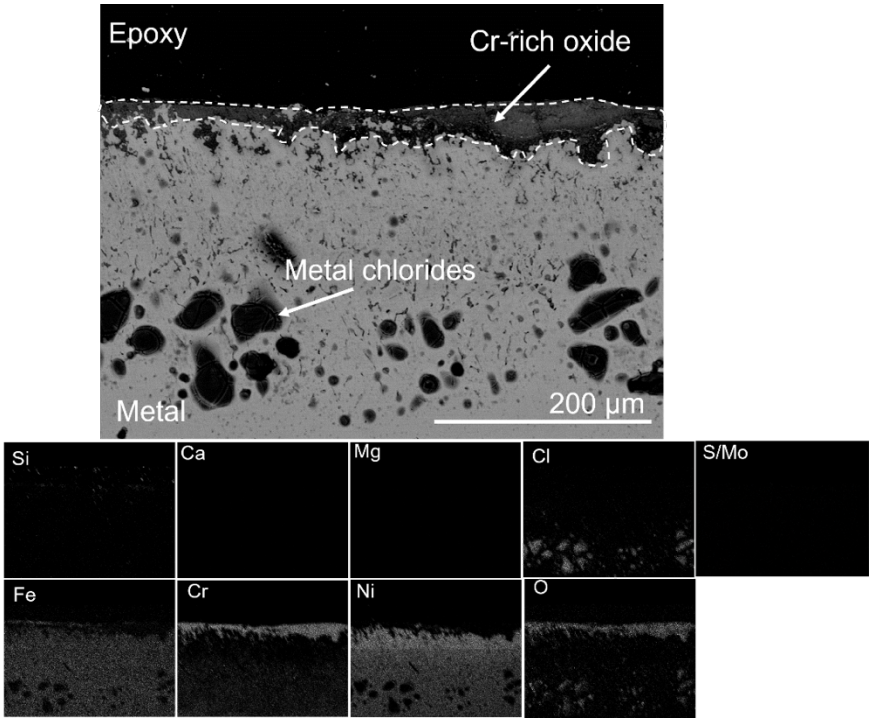

Figure 27. Cross-section and EDX analysis of Sanicro 69 after 12 months of exposure positioned in row 8.

Figure 28 presents the SEM cross-section and EDX analysis of the Sanicro 69 sample after 24 months exposure. The Cr-rich oxide scale is as deep as after 12 months exposure, but no metal chlorides were detected after 24 months. The material loss is still negligible (Figure 13) and some deposit is still detectable on the top of the sample indicating that no oxide scale has been lost during the handling of the samples.

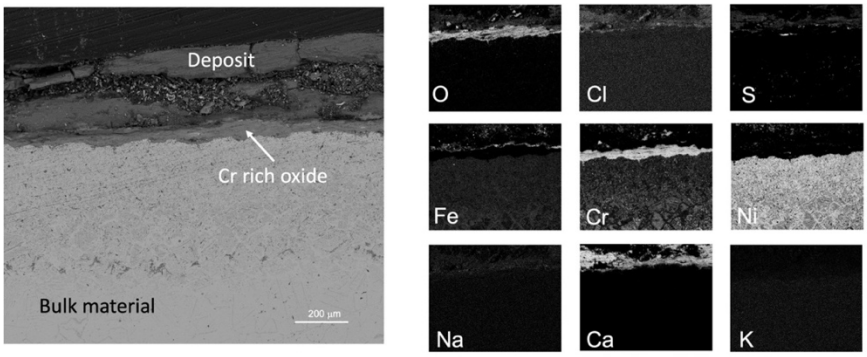

Figure 28. Cross-section and EDX analysis of Sanicro69 after 24 months of exposure positioned in row9.

Figure 29 shows the cross-section SEM image and EDX map analysis for the Esshete 1250 sample situated in row 1 after 12 months exposure. An internal oxide, containing both Cr and Fe, propagating in the grain boundaries of the material, approximately 100 µm deep was observed. No deposit or chlorine compound was detected on the sample as is clearly shown in the EDX map analysis. The remaining alloy elements, such as Ni, tend to stay in the bulk material forming a Ni-rich composition at the corrosion front. Furthermore, below the internal oxide region, a Cr-depleted zone in the grain boundaries was detected propagating in the material.

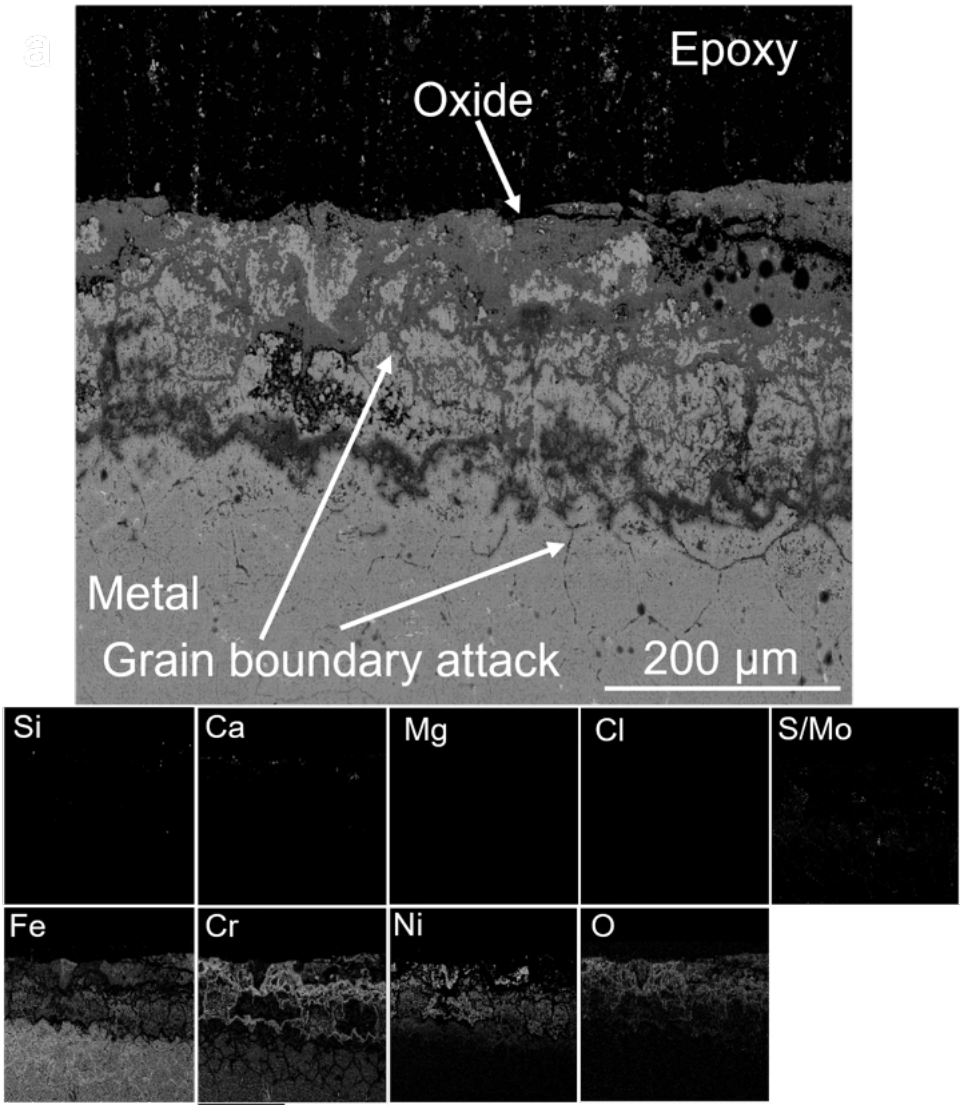

Figure 29. Cross-section and EDX analysis of Esshete 1250 after 12 months of exposure positioned in row 1.

Figure 30 shows the SEM image and EDX mapping of Esshete 1250 positioned in row 8. The degradation mechanism is the same as for the 6 months exposed sample, i.e., internal oxidation propagating within grain boundaries. No deposit was detected on this sample and only minor traces of outward growing oxide remained on the sample. According to EDX analysis the outward growing oxide contained both Fe and Cr. Considering that no adherent outward growing oxide or deposit was detected on the Esshete 1250 sample regardless of position, it is possible that this material is more sensitive to erosion.

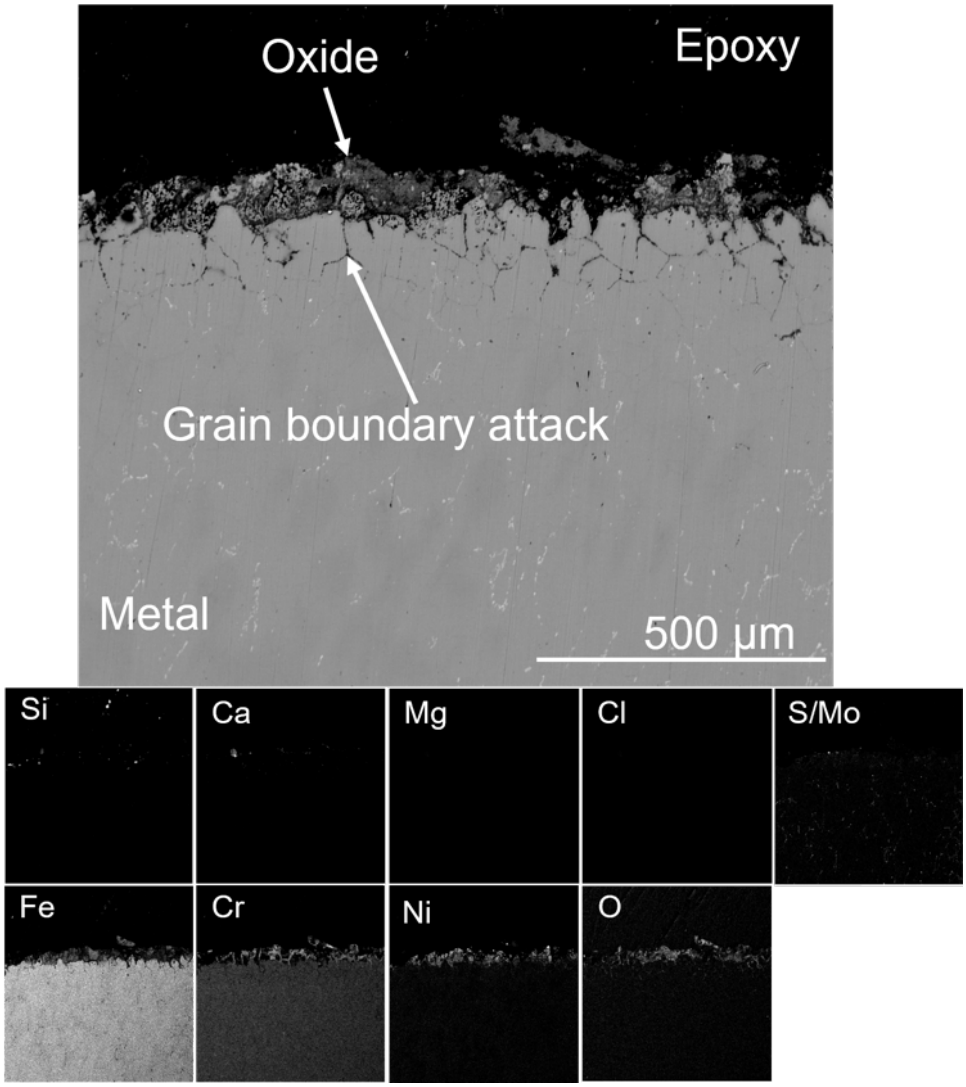

Figure 30. Cross-section and EDX analysis of Esshete 1250 after 12 months of exposure positioned in row 8.

Figure 31 shows the SEM cross-section BSE image of Esshete 1250 after 24 months exposure. The corrosion mechanism is the same as for the previous samples, presenting a clear grain boundary attack on the top of the sample. The depth of the attack is higher this time, around 300 µm. The same occurs with the Cr depleted zone that in this case is around 100 µm thick. No traces of deposit were detected meaning that it was lost during the handling of the samples.

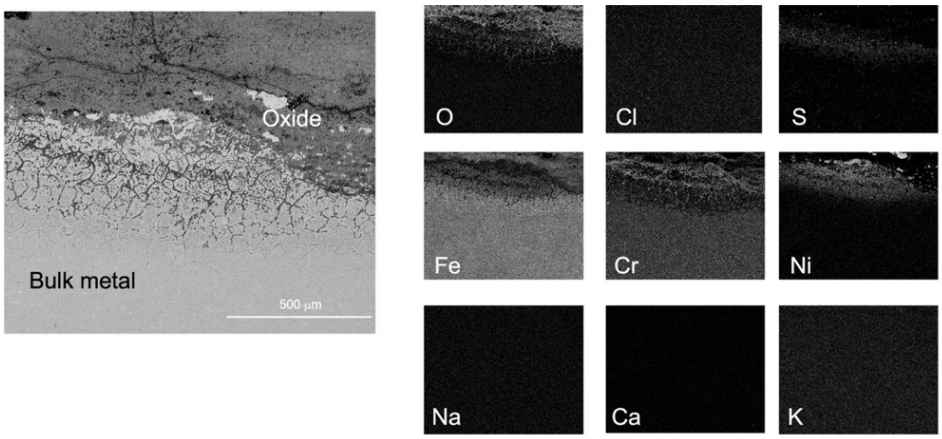

Figure 31. Cross-section and EDX analysis of Esshete 1250 after 24 months of exposure positioned in row 9.

The SEM/EDX cross section of the Sanicro 28 sample is seen in Figure 32. A non-adhesive oxide containing Fe, Cr and Ni was observed on top of the material. No sign of internal oxidation was observed. However, below the metal/oxide interface a roughly 100 µm thick Cr-depleted region was detected in the grain boundaries, leaving a Ni-rich material matrix. At approximately 300 µm in depth the chemical composition changed, and a Cr-enrichment was observed in the grain boundaries.

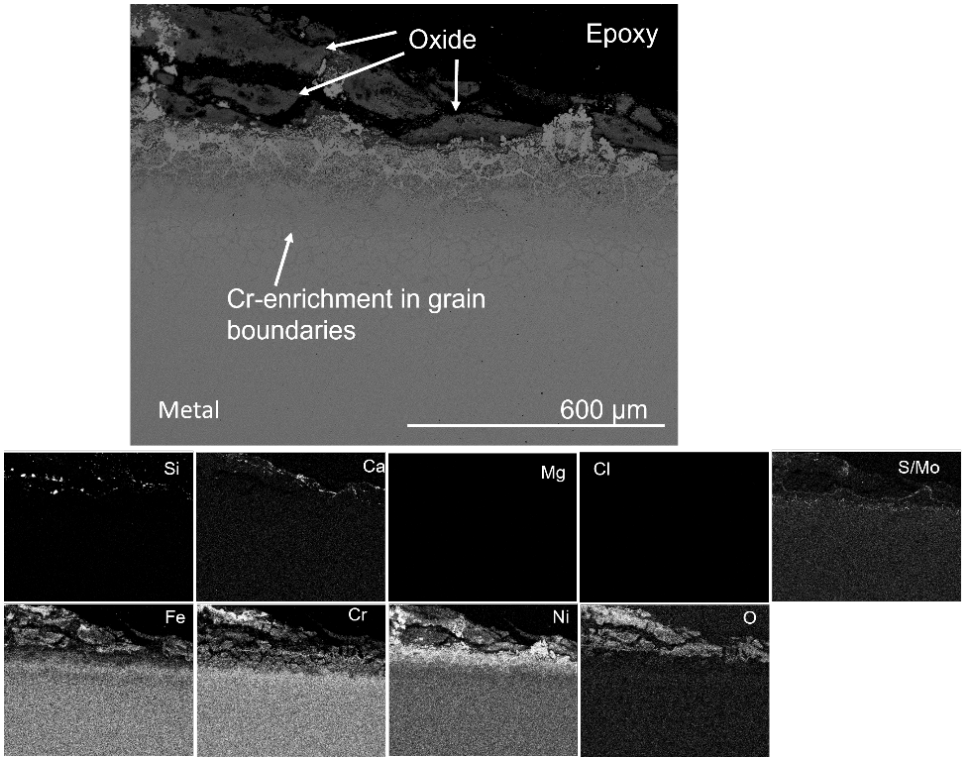

Figure 32. Cross-section and EDX analysis of Sanicro 28 after 12months of exposure positioned in row 8.

Figure 33 and Figure 34 show the SEM cross-section image of 316Ti positioned in row 1 and 8, respectively, after 12 months of exposure. Similar features were observed for both samples. A small amount of remaining outward growing Cr-rich oxide was observed on the sample exposed in row 1. Traces of both Ca and S were observed on top of the material as deposit. The overlap between the L series peak of Mo and the Kα peak of S makes it very challenging to distinguish these elements in EDX mapping. Thus, the signal observed on top of the material should be considered as S and the signal observed in the metal should be regarded as Mo. Both samples suffered from internal oxidation propagating via grain boundaries through the material to a maximum depth of roughly 200 µm and 100 µm, respectively. The remaining material close to the corrosion product consisted of a Ni-enriched region, as is shown in the EDX map for each sample. The chemical composition of the grain boundaries changed drastically after a certain depth through the metal (roughly 50 µm in depth at row 1 and 20 µm in depth at row 8), where initially a Cr-rich oxide was observed close to the metal/oxide interface and at increased depth, a Cr-depletion zone was observed in the grain boundaries leading to an increased concentration of Fe. None of the samples showed traces of deposits on top of the material suggesting that the material is prone to erode in this environment.

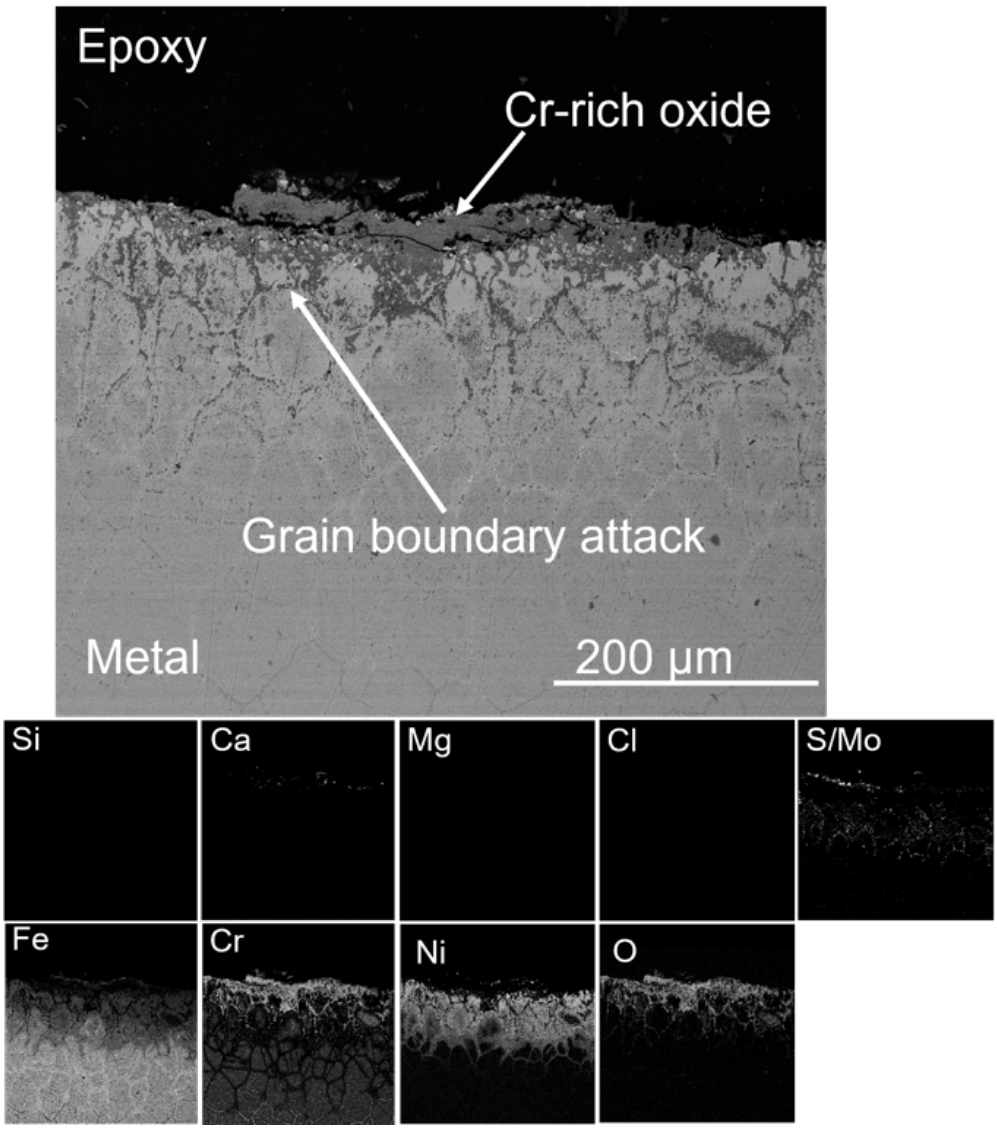

Figure 33. Cross-section and EDX analysis of 316Ti after 12 months of exposure positioned in row 1.

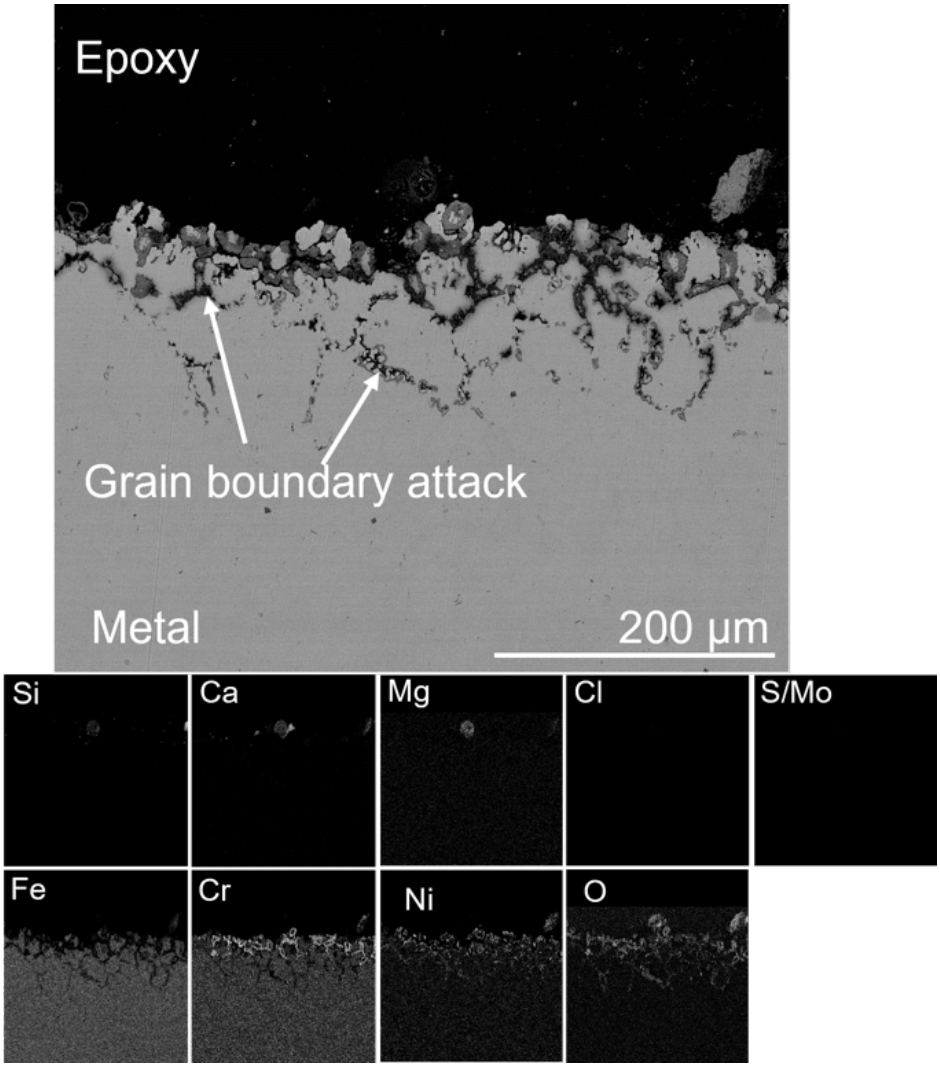

Figure 34. Cross-section and EDX analysis of 316Ti after 12 months of exposure positioned in row 8.

Figure 35 shows the SEM image and EDX mapping of the low alloyed steel 16Mo3 after 12 months of exposure positioned in row 8. The 16Mo3 sample exposed for 24 months was lost during the exposure. As mentioned in the section above, this material suffered from severe material loss. As is shown in Figure 35 and the EDX map below, a slightly undulating surface with minor corrosion products remained adhered to the metal surface. The corrosion product consisted of a Fe-rich oxide poorly adhesive to the material with visible cracks and voids. No signs of deposits nor chloride compounds were observed throughout the cross-section of the sample. However, it is possible that part of the corrosion product and deposit had spalled off during the outtake from the boiler.

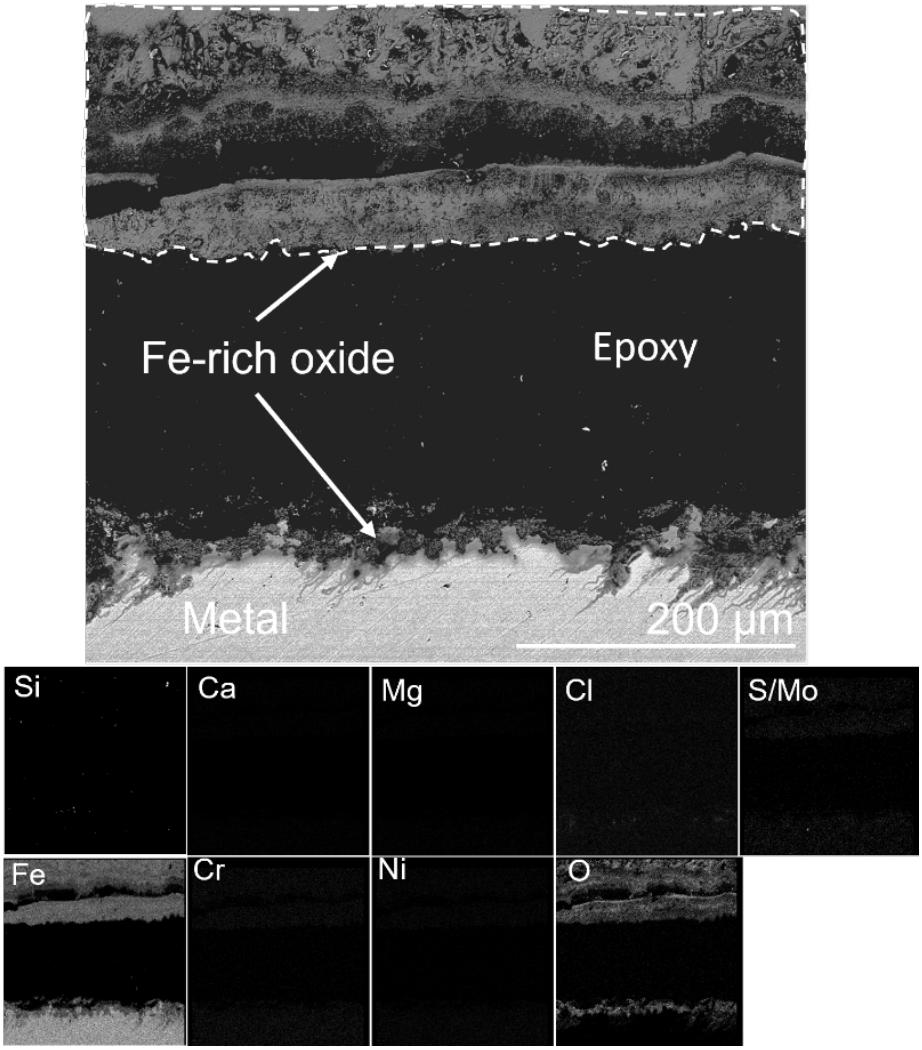

Figure 35. Cross-section and EDX analysis of 16Mo3 after 12 months of exposure positioned in row8.

Figure 36 and Figure 37 show the cross sections of the overlay welded sample Alloy 625 in row 1 and 8, respectively. The welded structure has a characteristic heterogenous surface, which makes accurate material loss measurements challenging. Thus, no material loss measurements were conducted for these samples.

In the case of the overlay welded Alloy 625 sample positioned in row 1, the EDX mapping suggests that a deposit layer containing Ca, Mg, S, O and traces of Cl and Si had been formed on top of a Cr-rich oxide. Traces of internal oxidation were observed below the metal/oxide interface. The internal oxide consisted mainly of Cr-rich oxide and from the EDX mapping analysis it is shown that the remaining material is mostly depleted of Cr, while nickel remains as the main alloy element close to the corrosion front.

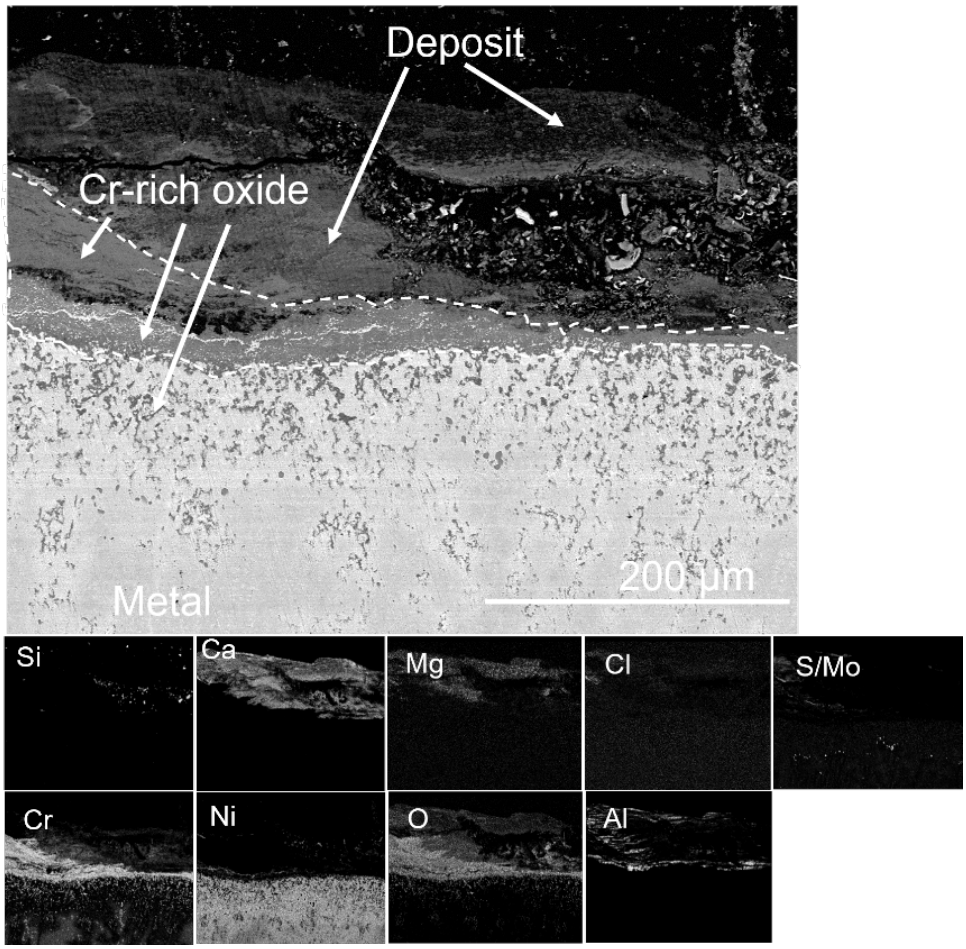

Figure 36. Cross-section and EDX analysis of Alloy 625 overlay weld after 12 months of exposure positioned in row 1.

The SEM/EDX analysis of the weld overlay Alloy 625 positioned in row 8 is shown in Figure 37. A Ca and S rich deposit was observed on the sample and an outward growing oxide containing Ni and Cr rich oxide was detected. Below the metal/oxide interface a roughly 70 µm large Cr-depleted zone was observed.

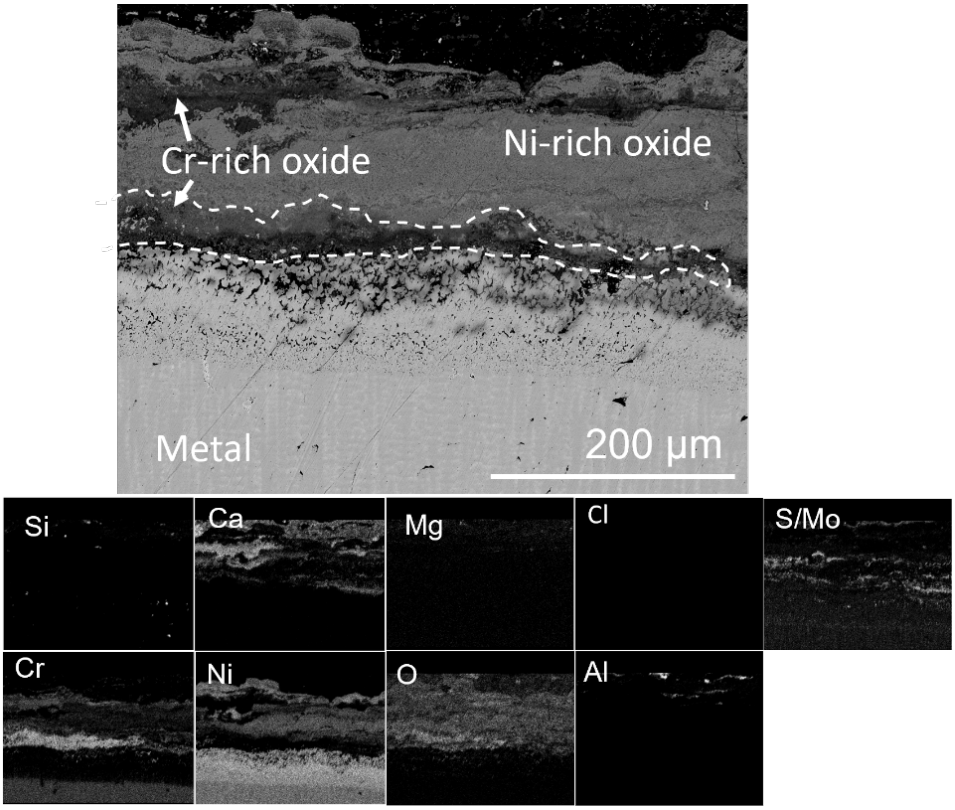

Figure 37. Cross-section and EDX analysis of Alloy 625 weld overlay after 12months of exposure positioned in row 8.

Figure 38 presents the SEM cross-section and EDX analysis of the Alloy 625 overlay weld sample after 24 months exposure. A layer of deposits containing Cl is still present on the top of the sample. The Cr-rich oxide scale is around 100 µm thick. This value is not higher than after the 12-month exposure, indicating a good corrosion behavior.

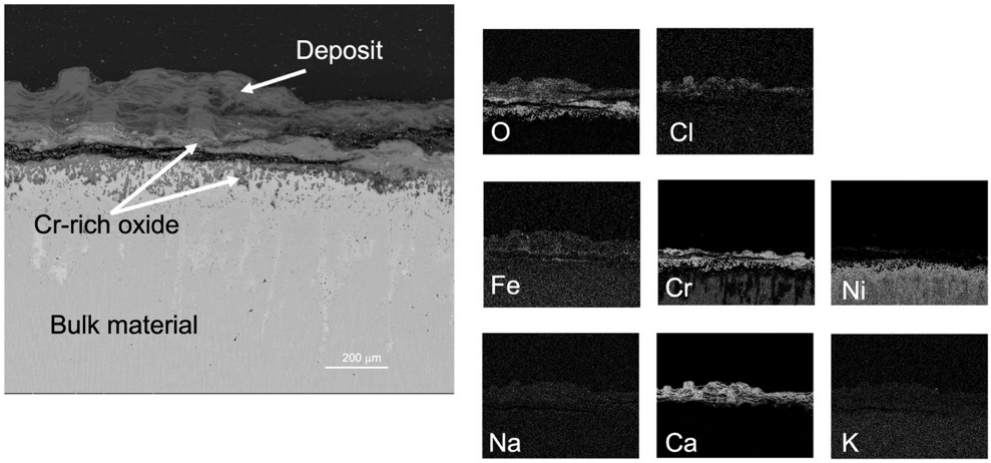

Figure 38. Cross-section and EDX analysis of Alloy 625 weld overlay after 24 months of exposure positioned in row 9.

Exposures were conducted on three different coated materials in row 8. The SEM/EDX analyses of the two APMT-coated materials, APMT20c and APMT50c, are shown in Figure 39 and Figure 40. The results reveal inferior performance for both coatings, as none of the coated material remained attached to the base material after exposure (see EDX map and point analysis in each Figure). In addition, both samples observed corrosion features such as internal growing oxide, indicating that the coating failure might have occurred at an early stage of exposure.

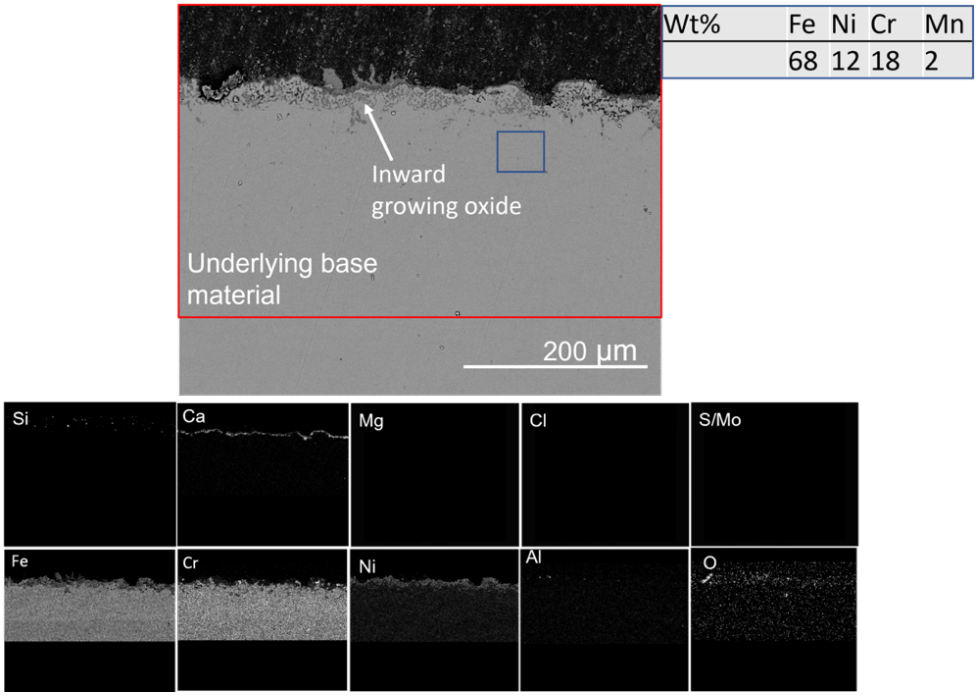

Figure 39. Cross-section and EDX analysis of APMT20c coating after 12 months of exposure positioned in row 8. EDX point analysis of the highlighted blue area (right).

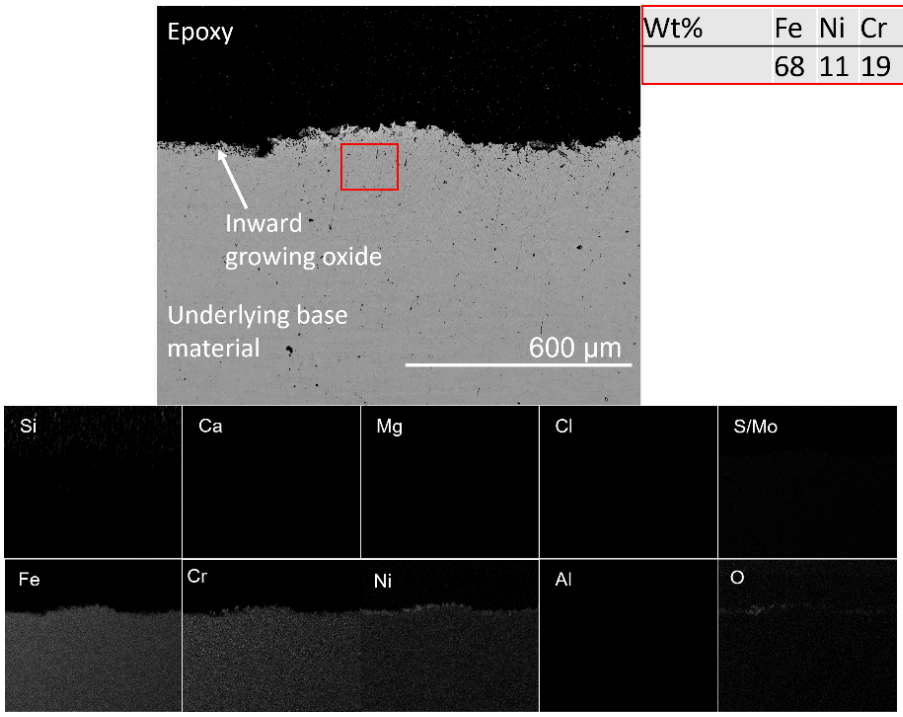

Figure 40. Cross-section and EDX analysis of APMT50c coating after 12 months of exposure positioned in row 8. EDX point analysis of the highlighted red area (right). EDX mapping of highlighted red area (below).

Figure 41 shows the SEM cross-section image of the CorEr-coated material exposed in row 8. No sign of the coated material was detected throughout the cross-section, indicating severe coating failure. Moreover, the underlying base material had similar corrosion features as the APMT-coated samples, indicating that the coating failure might have occurred early in the exposure.

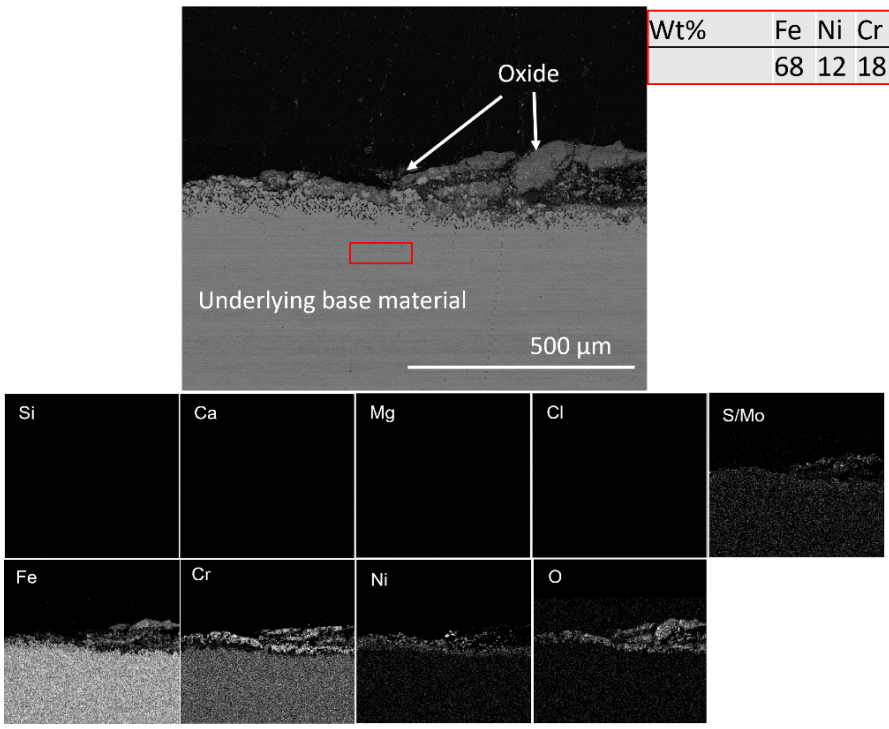

Wt%	Fe	Ni	Cr	Mn
	68	12	18	2

Figure 41. Cross-section of CorEr coating after 12 months positioned in row 8. EDX point analysis of the highlighted red area (right).

4.3.2 Clamp exposures on FBHE - Händelö P15

Clamp exposures were conducted on FBHE in the P15 waste-fired boiler in Händelö in continuous mode lasting for 6 and 12 months. As it was explained in P6 Högdalen exposures presented above, the exposure times include the planned shutdowns of the boiler. The samples were mounted as two half-moon rings on the fluidized bed heat exchanger. In this study, the wind side samples, i.e., the half-moon samples facing down towards the loop seal air nozzle, were analyzed in the superheater 2 position.

Material loss

A summary of the material loss for the different materials and time intervals are shown in Figure 42. The filled circle for each data set represents the arithmetic mean value of the material loss.

The conventional austenitic stainless steels, 316Ti and Esshete 1250, exhibited severe material loss after 6 months of exposure reaching average values of roughly 0.68-0.73 mm respectively. The Esshete 1250 sample had quite a large spread in material loss data ranging from 0.5-1.1 mm indicating that local attacks play an important role in this set of environments. The material loss rate for these samples was reduced with time, which might occur if corrosive attacks are slowed down after the initial attack. The high Si-containing austenitic stainless steel SX outperformed all samples and obtained a maximum material loss of 0.07 mm and 0.3 mm after 6 and 12 months respectively.

All three alumina forming materials outperformed the majority of the other samples after 12 months of exposure, SX being the exception. EF100 performed better compared to the conventional APMT and the EF101 material, reaching a maximum material loss of 0.28 mm/year which was lower than the average material loss of the SX sample. The material loss data show great variation for EF101 and APMT, which again suggests that local degradation mechanism may occur in this set of environments.

The Ni-base alloy Sanicro69 showed large variation in performance over time (from negligible after 6 months to roughly 1mm/year in average loss). Lastly, the CorEr coating obtained an average material loss of 0.32 mm and a maximum material loss of 0.8 mm after 6 months of exposure indicating that severe local attacks had occurred during exposure.

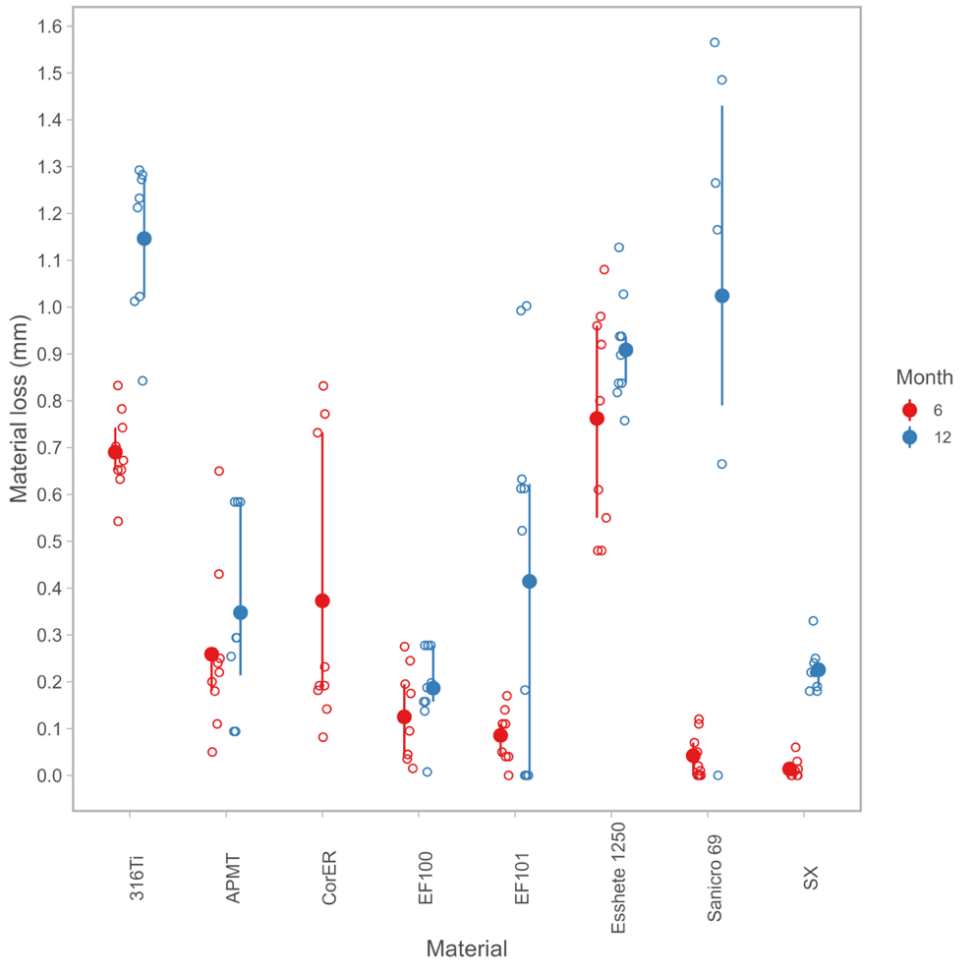

Figure 42. Material loss of the tested clamps exposed for 6 and 12 months in the fluidized bed heat exchanger positioned in superheater 2, P15 boiler, Händelö.

Microstructure analysis

An SEM cross-sectional view of the EF100 sample exposed for 6 months is shown in Figure 43 (a). An approximately 250 µm thick deposit was observed, consisting primarily of S, Ca and O. Beneath the deposit layer, an approximately 100 µm thick iron oxide had formed. The oxide contained small cracks and displayed void formation, whereas it was difficult to distinguish regions of inward and outward oxide layer formation. An Al/Cr-rich thin oxide layer was detected across the metal/oxide interface (see Figure 43(b)). The SEM analysis revealed no indications of internal oxidation. However, a nitridation zone can be seen below the metal/oxide interface. The thickness of the region varied greatly (between 0-200 µm) and was observed in a patch wise fashion throughout the cross section of the sample.

EF100 displayed similar features after 6 and 12 months of exposure (see Figure 43a) and Figure 44a)). However, for the sample exposed for 12 months, most of the deposit layer had spalled off. This may be an effect of sample outtake and subsequent sample preparation for post-analysis. A Fe-rich oxide was observed (about 600 µm in thickness) containing voids and cracks and traces of Cr and Al. The nitridation zone had also grown larger compared to after 6 month of exposure (about 400 µm in thickness for the 12 months sample) and was observed throughout the cross section of the sample in a homogenous fashion. The EDX analysis confirmed that the dark particles shown in the nitridation zone consisted of Alumina Nitride (AlN) precipitates embedded in a Fe-rich alloy matrix. The observed microstructures and corrosion attacks agree well with the measured material losses. The material loss for EF100 after 6 and 12 months was 0.13 and 0.19 mm, respectively. The SEM/EDX analysis after 12 months of exposure also shows that a region (roughly 125 µm thick) depleted in Cr was detected at the nitridation/metal interface (see Figure 44b). This Cr-depletion zone was homogenous and observed throughout the sample. No Cl was detected in the corrosion front nor in the deposit.

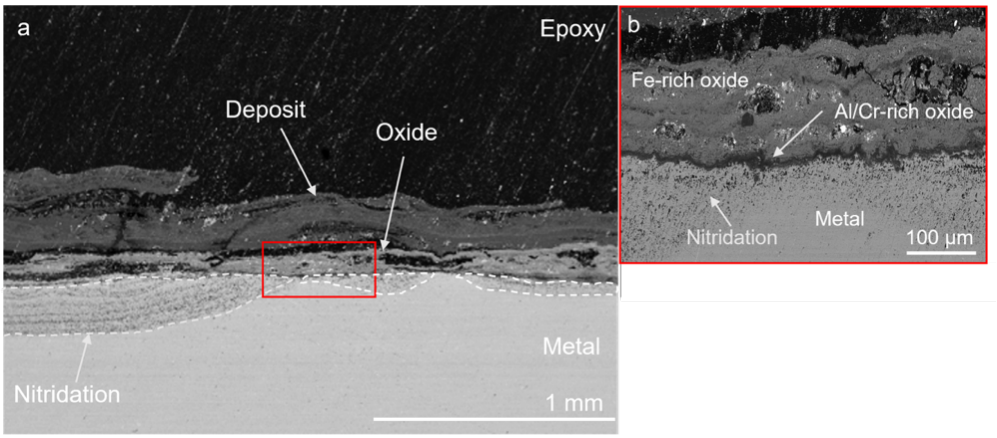

Figure 43. (a) SEM BSE cross-section image of EF100 after 6 months of exposure. (b) Higher magnification of the marked area in (a).

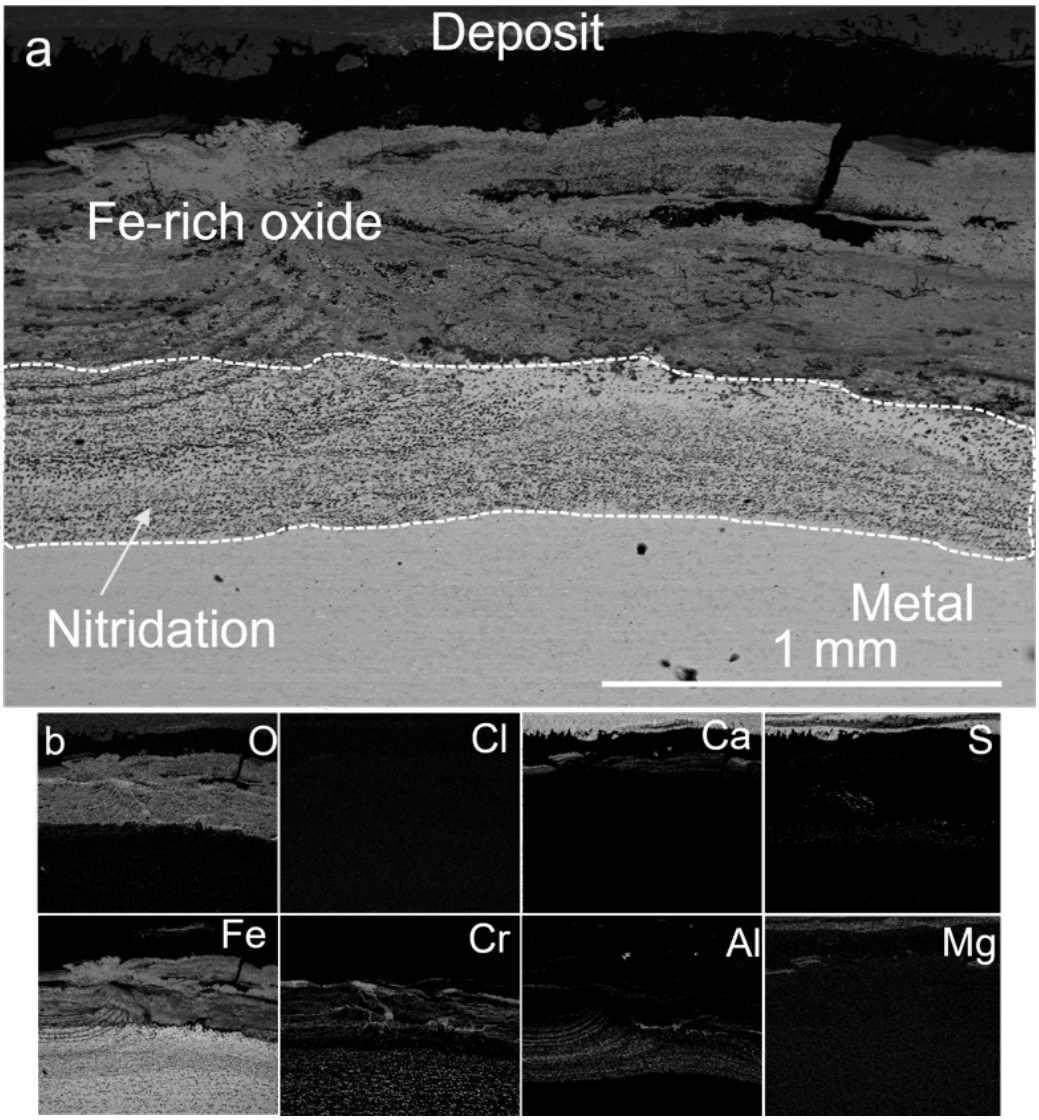

Figure 44. SEM BSE cross-section image of Ef100 (a) after 12 months of exposure. (b) EDX mapping of (a).

EF101 displayed similar features as EF100 after 6 months of exposure (see Figure 45 (a)). The EDX map analysis of EF101 presented in Figure 45(c) shows that a thin deposit layer (about 25 μm in thickness) had formed above the oxide layer containing large amounts of Ca. In addition, no traces of chlorine containing chemical species were observed throughout the cross section. The oxide scale was composed of an Fe-rich oxide containing cracks and voids (see Figure 45(b)) and traces of Cr rich oxide were observed, but to a lower extent. A thin Al-rich oxide layer (about 8 μm) at the metal/oxide interface was observed. In addition, below the metal/oxide interface a Cr-depleted zone of approximately 100 μm was seen. Compared to EF100, the EF101 sample exhibited a more pronounced nitridation zone. The thickness of the nitridation zones were 450 μm and 200 μm for EF101 and EF100, respectively after 6 months.

Figure 46 presents the SEM/EDX analysis of the EF101 after 12 months of exposure. Only traces of deposit have been detected after the exposure. The corrosion mechanism agrees with the behavior observed after the 6-month exposure (Figure 45). An approximately 100 µm thick Fe-rich oxide layer is present homogeneously on the top of the sample and a Cr-rich oxide is formed below, followed by a Cr-depleted zone. The nitridation zone is also present all around the sample after the 12-month exposure, but it does not seem to increase in thickness compared with the 6-month exposure.

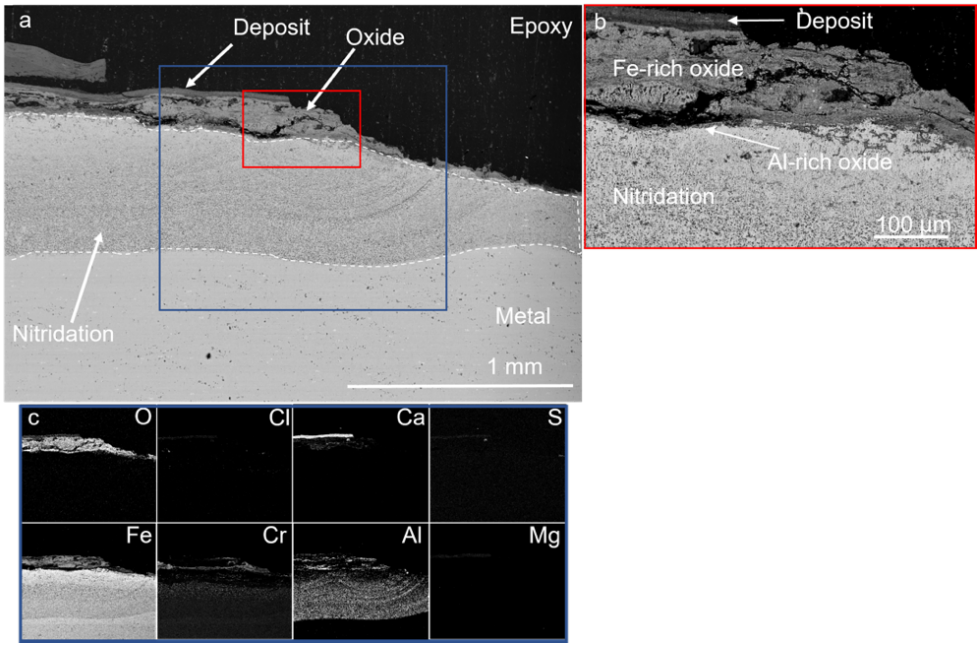

Figure 45. SEM BSE cross-section image of Ef101 (a) after 6 months of exposure. (b) Higher magnification of the marked area in (a). (c) EDX mapping of (a).

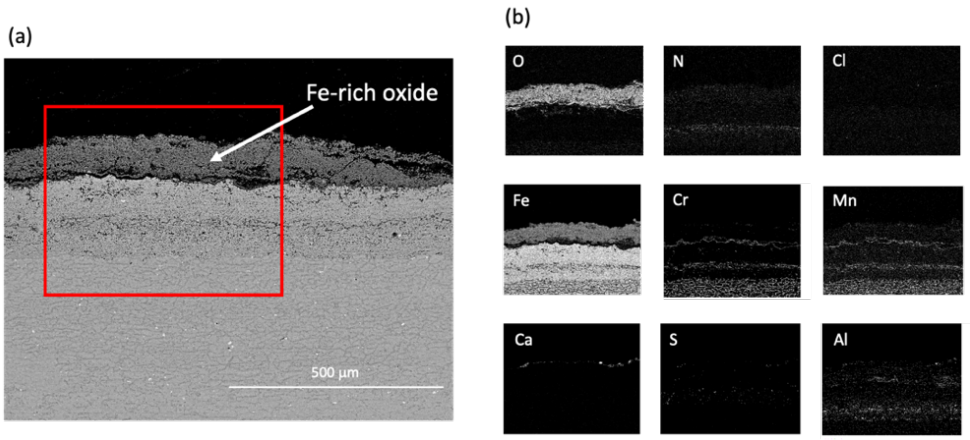

Figure 46. SEM BSE cross-section image of EF101 (a) after 12 months of exposure. (b) EDX mapping of (a).

Figure 47 and Figure 48 shows the SEM cross section of Kanthal APMT sample after 6 months and 12 months of exposure. A discontinuous Fe/Cr-rich oxide was detected at the metal/oxide interface with a thickness between 7-20 µm, followed by a roughly 50 µm outward growing Fe-rich oxide after 6 months of exposure. Thus, similar microstructure features were detected as with the novel FeCrAl alloys (see figure 38-40). However, as is shown in figure 52a, extreme nitridation of this sample was detected, exceeding over 1mm in thickness. The nitridation zone for APMT after 6 months was close to four times greater than the novel FeCrAl alloys EF100 and EF101.

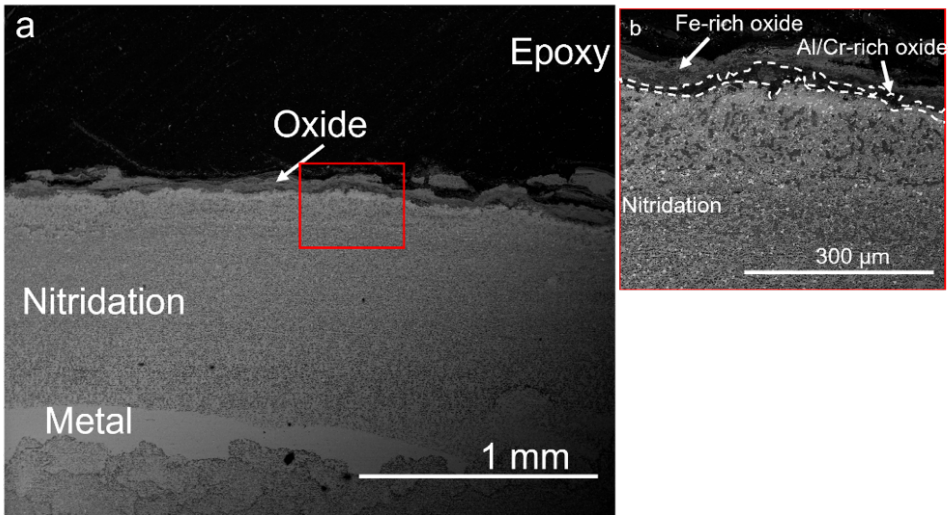

Figure 47. SEM BSE cross-section image of APMT after 6 months of exposure. (b) highlighted red area from (a).

Figure 48 shows the Kanthal APMT sample after 12 months of exposure. According to EDX analysis a discontinuous deposit layer had formed on top of the sample containing large amounts of Ca and traces of P and Cl. Regarding the oxide scale, similar features were observed as for the sample exposed for 6 months, i.e., a roughly 200 µm thick outward growing Fe-rich oxide was detected below the deposit followed by a Cr/Al-rich oxide. The Cr/Al rich oxide close to the metal/oxide interface was not as easily detected as compared to the sample exposed for 6 months. Lastly, severe nitridation was observed for this sample reaching a thickness of roughly 800 µm, albeit not as severe as for the sample exposed for 6 months.

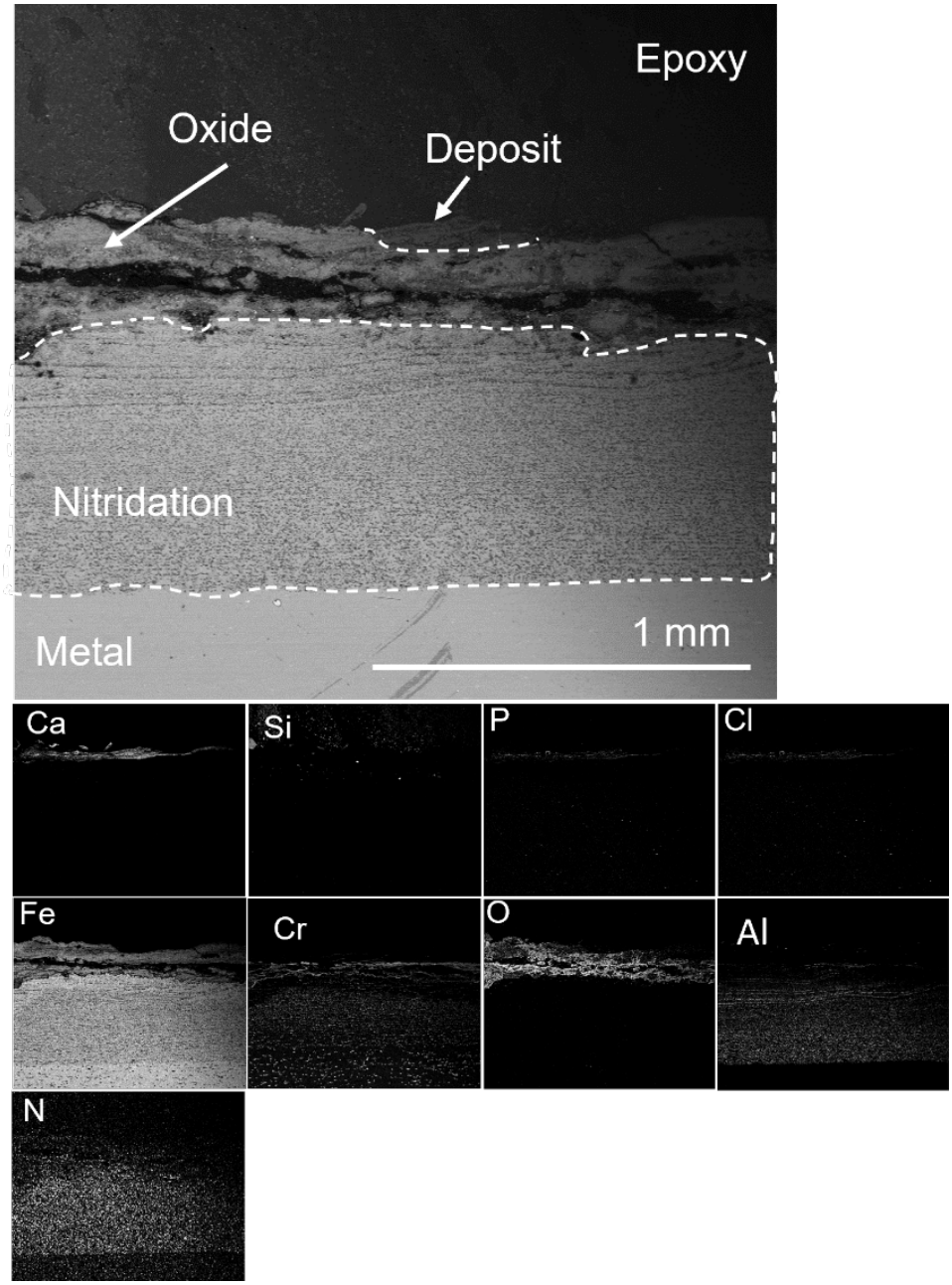

Figure 48.(a) Kanthal APMT sample after 12 months of exposure in SH2 (b) EDX analysis.

Figure 49a and b show the cross-section of the SX samples exposed for 6 and 12 months. Similar features were observed for both samples. Thus, chemical analysis via EDX mapping is only shown for the sample exposed for 12 months. A homogenous deposit layer was observed on both samples and consisted mainly of Ca, S, O, and traces of Na. In addition, traces of Cl were detected in the inner regions of the deposit. The thickness of the deposit was in the order of 60 and 50 μm for 12 and 6 months. The SX material formed an adherent outer corrosion product layer composed mainly of an Fe-rich oxide (see Figure 49c). The outer oxide layer became less adherent with time, which is displayed when comparing Figure 42 a and b, where cracks were observed after 12 months of exposure. As

with 316Ti, grain boundary attacks were noticeable after 6 months of exposure and became more severe with time. The internal oxidation at the metal/oxide interface consisted mainly of a Cr and Si-rich oxide propagating via grain boundaries through the material. After 12 months of exposure, at roughly 60 μm, a Cr-depletion was observed at the grain boundaries together with Fe-enrichments at the border of the grain boundaries.

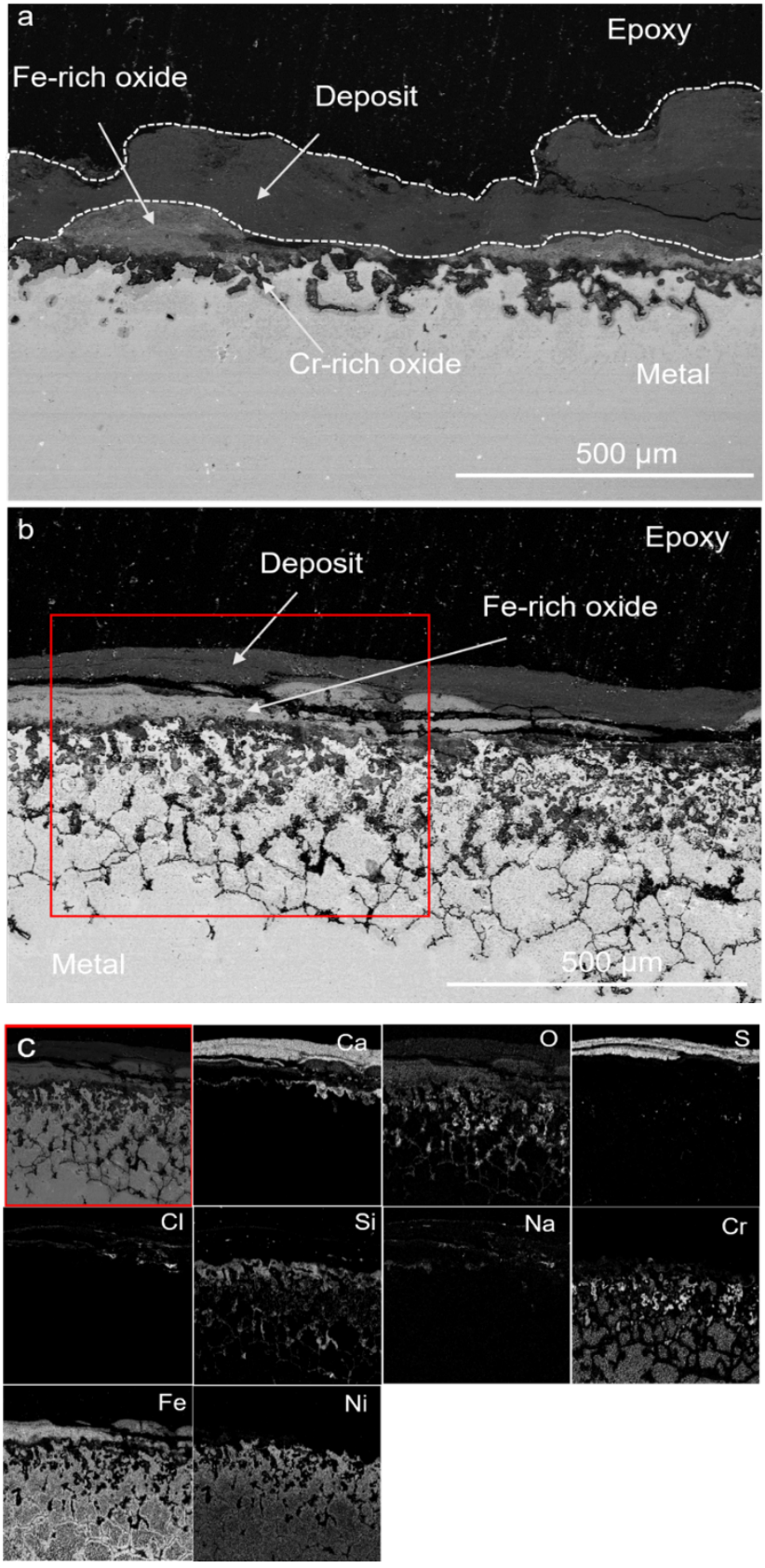

Figure 49. SEM BSE cross-section image of SX after (a) 6 months of exposure (b) 12 months of exposure (c) EDS mapping of SX from highlighted area in (b).

Figure 50 shows a cross-section region of the Sanicro 69 sample after 6 months of exposure. An approximately 50 μm thick deposit layer was observed containing mainly S, Ca, and O with traces of P and Mg. No significant deposit components were identified in the formed oxide scale (see Figure 50b). Furthermore, the EDX mapping showed that a Ni-rich oxide was formed underneath the deposited layer, and at the metal/oxide interface, a Cr-rich oxide was detected. In addition, a Cr-rich oxide was also detected further into the metal as an internal oxidation region approximately 80 μm below the corrosion product layer. This feature is presumably a 3D effect of this 2D cross-section imaging. From the EDX mapping, it can also be observed that the metal is mainly depleted of Cr, while nickel remains the main alloy element in the material matrix close to the corrosion front. The material loss measurement of San69 was negligible after 6 months of exposure. However, based on the SEM/EDX analysis, the internal corrosion attack can be seen up to 0.3 mm into the metal.

Figure 51a shows the cross-section of the Sanicro 69 material after 12 months of exposure. The corrosion mechanism is the same as in the 6-month exposure presenting a Cr-rich oxide on the top of the Ni-rich oxide. Nevertheless, the corrosion attack is much higher this time. The thickness of the oxide after the 12-month exposure is over 500 μm and the material loss is 1.01 mm/year in average. The EDX analysis presented in Figure 51b shows that no deposit was detected after the 12 months exposure. This indicates that the outer part of the oxide might have been lost during exposure or during the handling of the samples. This explains the absence of Fe-oxide at the top of the oxide scale.

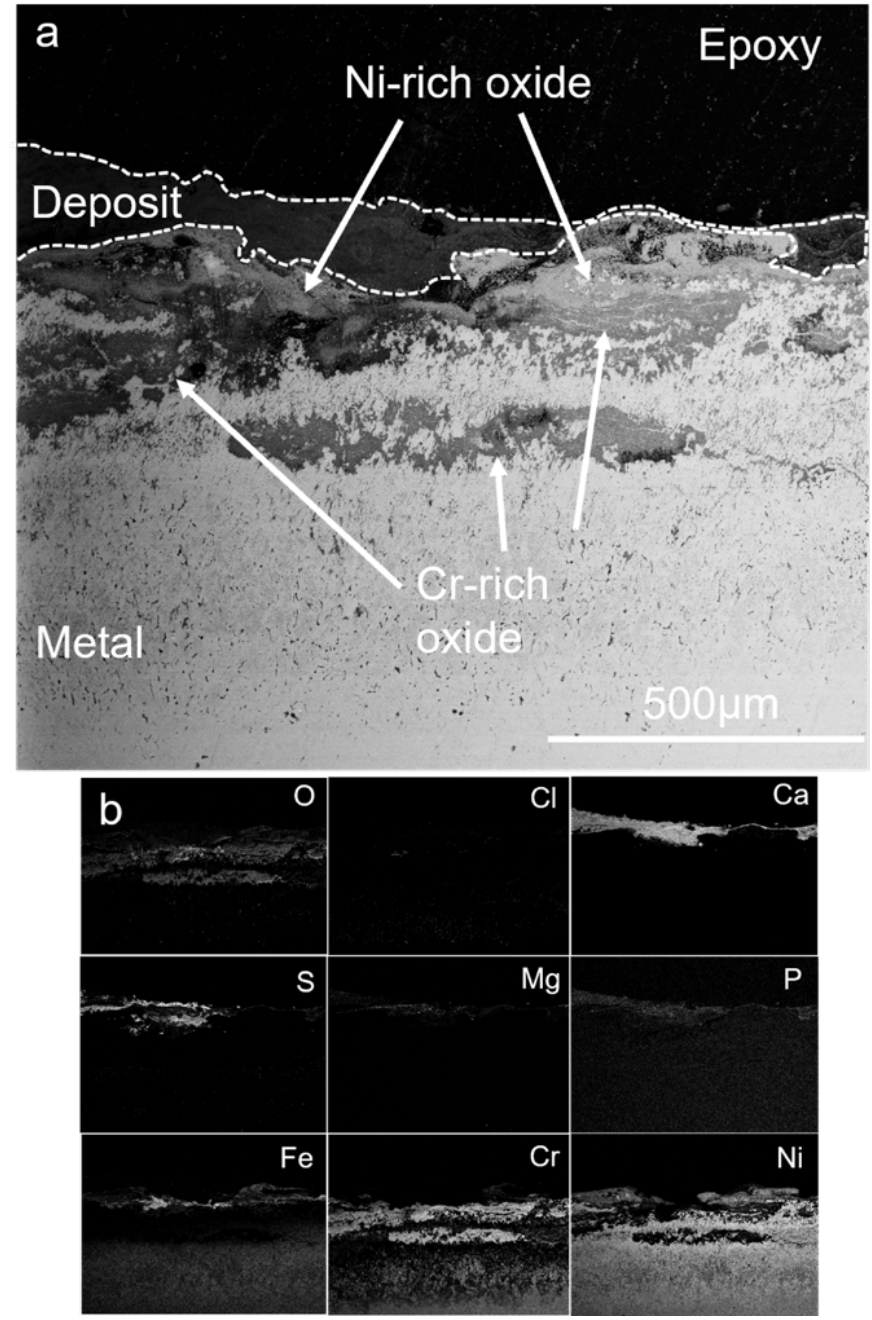

Figure 50. SEM BSE cross section image of San69 (a) after 6 months of exposure. (b) EDX mapping of (a).

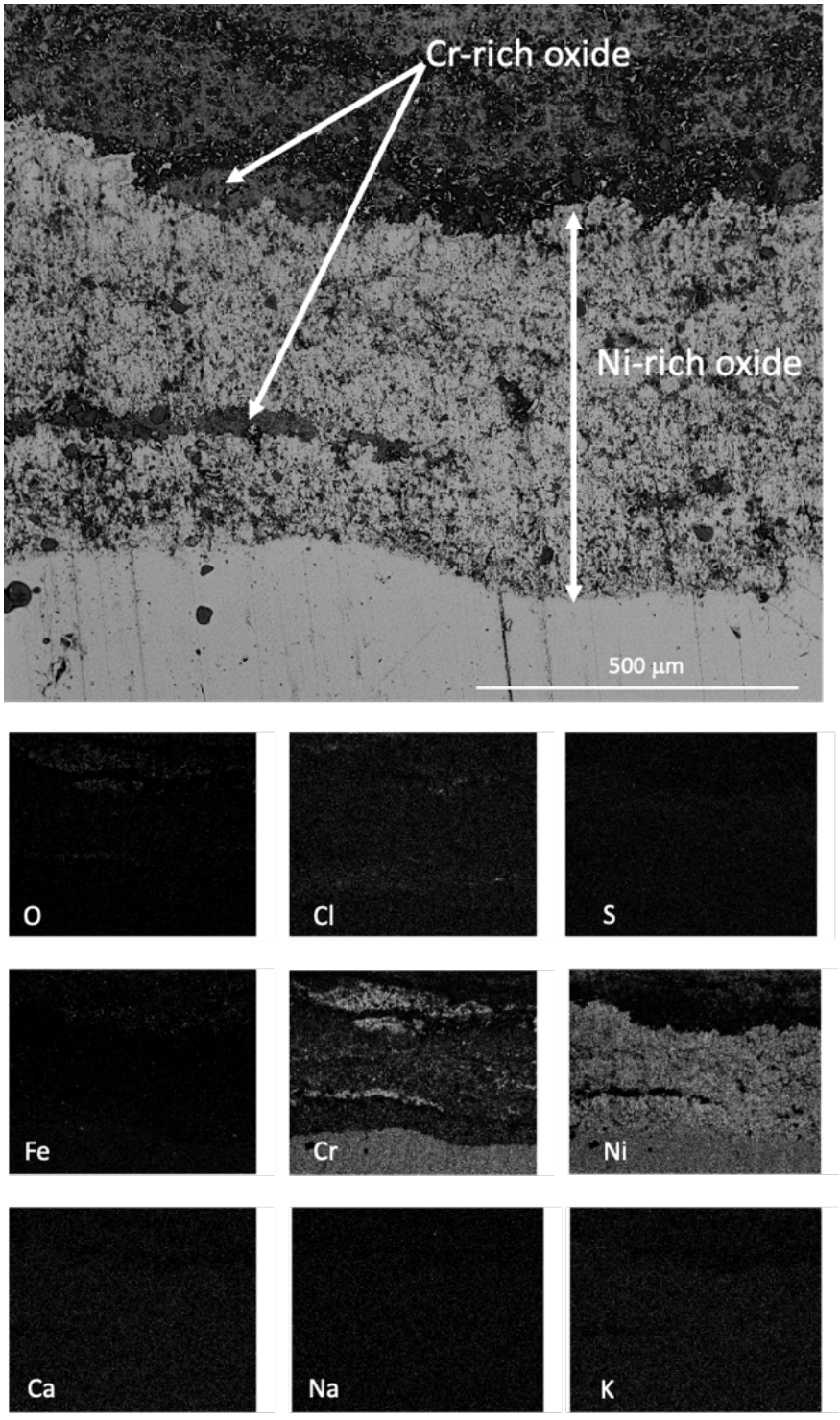

Figure 51. SEM BSE cross section image of Sanicro 69 (a) after 12 months of exposure. (b) EDX mapping of (a).

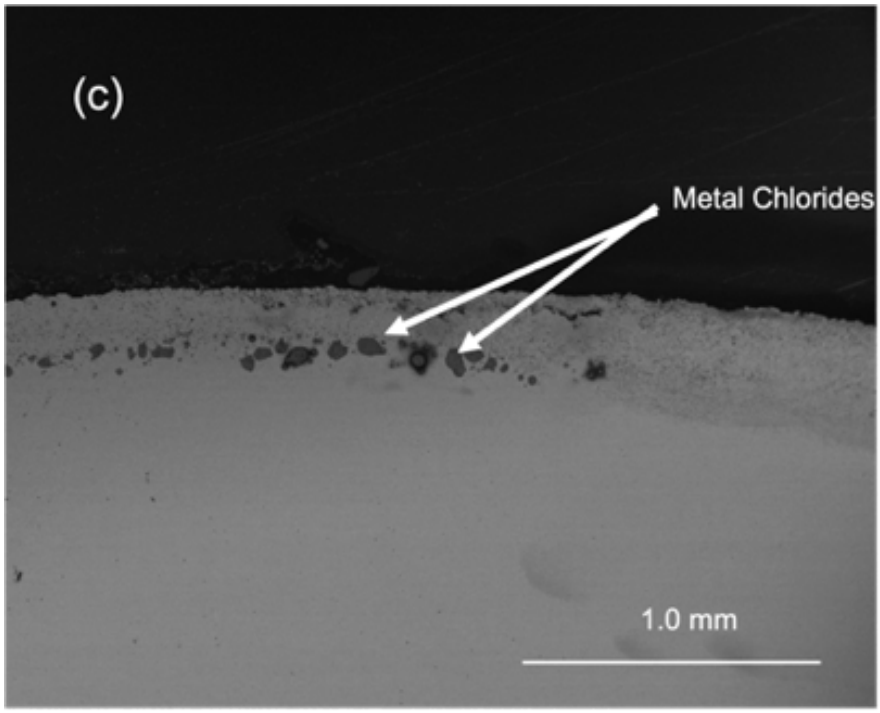

Figure 52 shows the (a) SEM cross-section of a 27Cr33Ni3Mo sample after 12 months of exposure and (b) the EDX analysis. No deposit was detected on the top of this sample meaning that it was lost during the removal/handling of the samples. A very thick and porous oxide was detected all around the sample. The thickness is at least 300 μm and more than 500 μm in some areas.

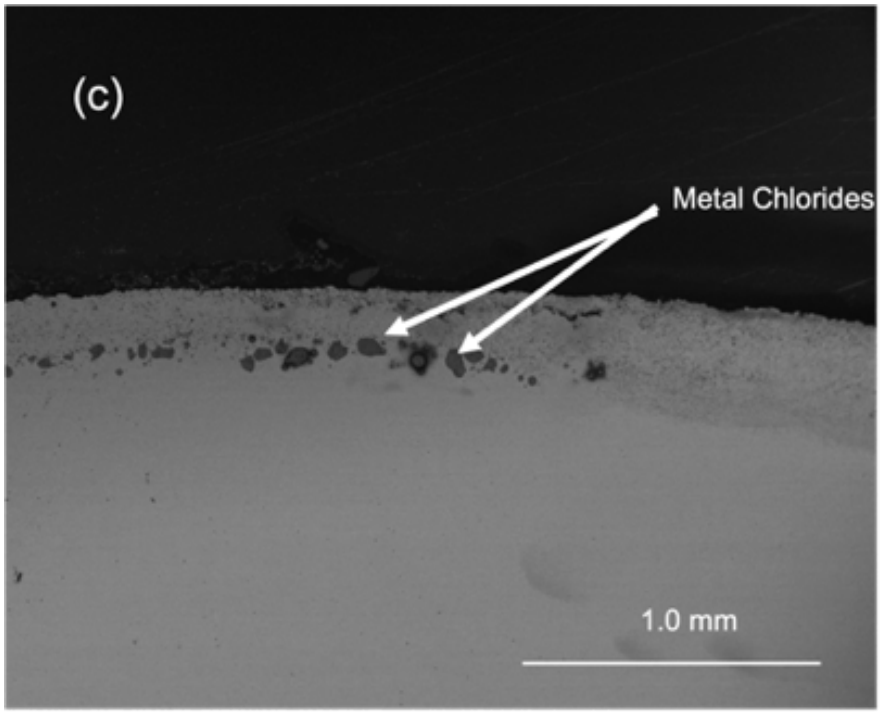

Figure 52 (a) the oxide cracks and detaches in some parts. The composition is mainly Fe and Ni with a Cr-rich layer on the top. Some Cl is detected in the oxide/bulk interface Figure 52(c)

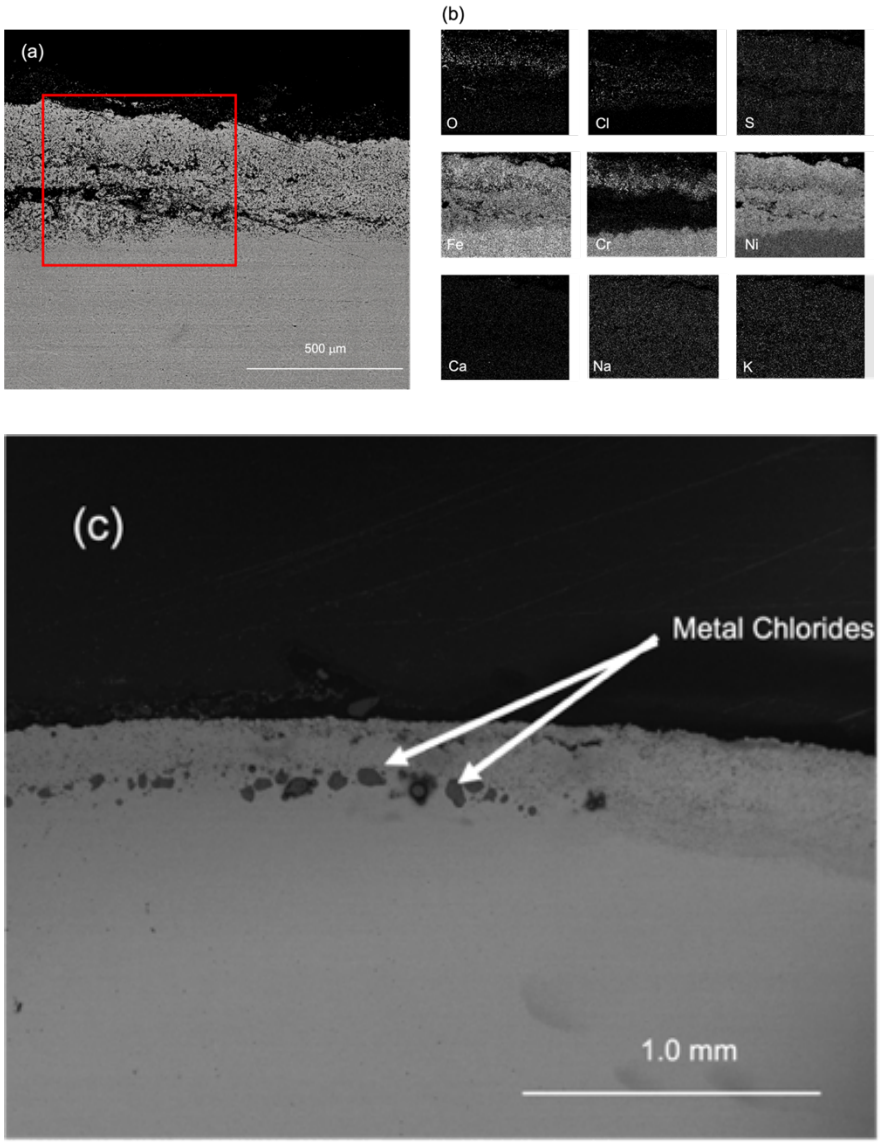

Figure 52. SEM BSE cross section image of 27Cr33Ni3Mo (a) after 12 months of exposure. (b) EDX mapping of (a), (c) detail of metal chlorides on the surface of the sample.

Figure 53 and Figure 54 show the results from Esshete 1250 after 6 and 12 months of exposure, respectively. A similar corrosion attack was observed after 6 and 12 months and thus EDX analysis is only shown for the sample exposed for 12 months. For both samples, an inward growing oxide was observed well adherent to the material. The outer part of the oxide consisted of an Fe-rich oxide, while the inner part is dominated by a Cr-rich oxide, as is shown in the EDX map for the sample exposed for 12 months. The thickness of the Fe-rich oxide was about 150 µm for both samples. Like the previously described austenitic steels shown, the outer part of the steel substrate was depleted in Cr, leaving behind a Ni and Fe-enriched steel substrate.

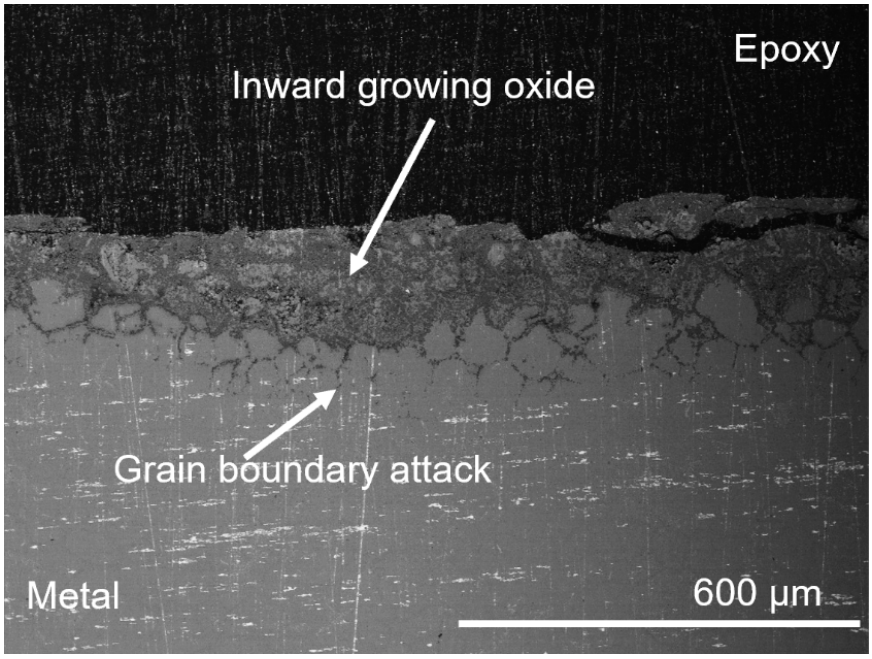

Figure 53. SEM cross-section of Esshete 1250 after 6 months of exposure.

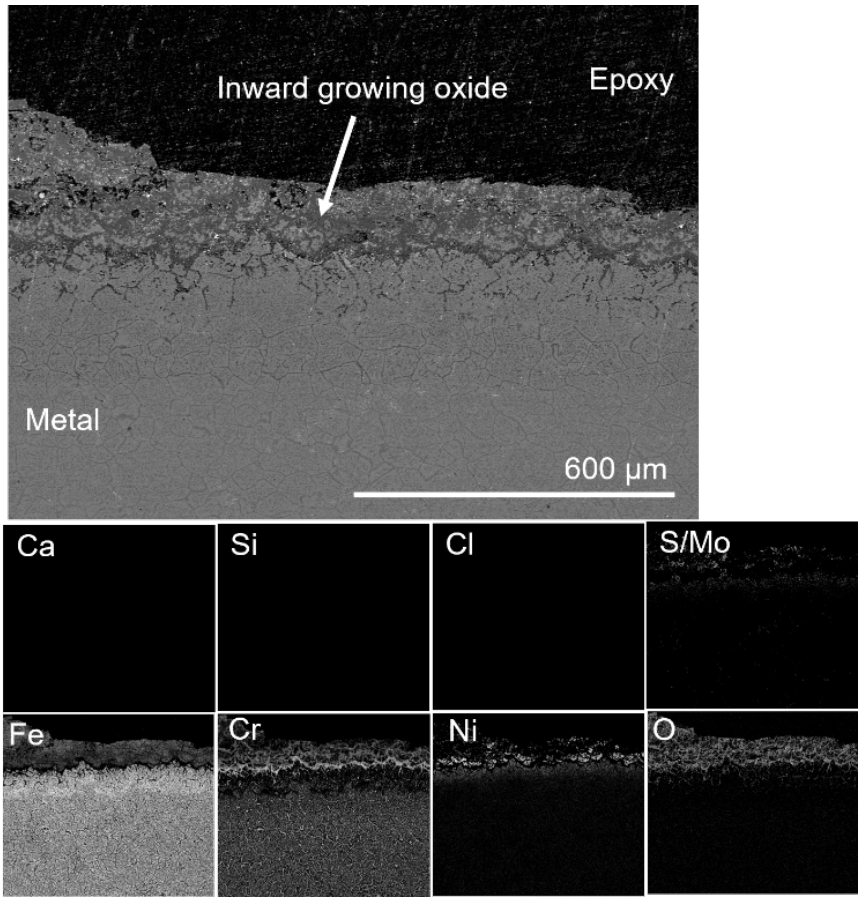

Figure 54. SEM cross-section of Esshete 1250 after 12 months of exposure

The SEM cross-section images after 6 and 12 months of exposure in Händelö P15 for 316Ti are presented in Figure 55. Similar features were observed for both samples and thus, chemical analysis via EDX mapping is only shown for the sample exposed for 12 months. For 316Ti, the cross section showed little or no deposit layer as well as minor indication of formation of an outer corrosion product layer. Instead, the cross sections revealed signs of intergranular corrosion attacks.

Figure 55c shows the EDX mapping of the 316Ti sample exposed for 12 months. A thin outer layer of oxide was observed on top of the sample consisting mainly of Cr and trace amounts of Fe. 316Ti suffered from an intergranular corrosion attack after 6 months of exposure (see highlighted area). This attack progressed with increased severity as a function of exposure time (see highlighted area in Figure 55b). The corrosion products formed in the steel grain boundaries mainly consisted of Cr-rich oxide and no traces of Cl were detected. Below the metal/oxide surface, a roughly 150 µm thick Cr-depleted region had been formed throughout the sample.

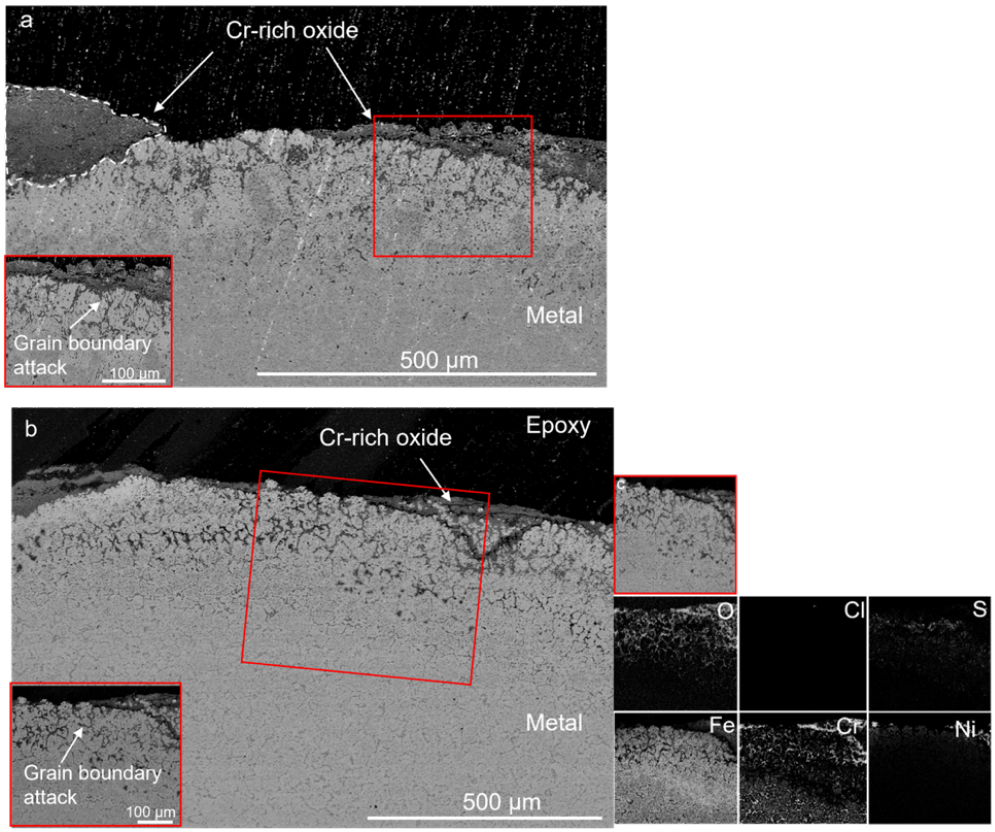

Figure 55. SEM BSE cross-section image of 316Ti (a) 6 months of exposure. (b) 12 months of exposure. (c) EDS mapping of 316Ti from highlighted area in (b).

Figure 56 presents the SEM cross section (a) and EDX analysis (b) from the reference material, Alloy 59 after 12 months of exposure. This material has been overlay welded on the top of a tube to mimic the real operation conditions. Due to the difference in thickness of the welding cords it is not possible to measure

material loss in this sample. Nevertheless, it is possible to observe the corrosion attack in the SEM images. No traces of deposit were detected on the top of the sample. The deposit was probably lost during the removal/handling of the samples. The top part of the corrosion products is usually attached to the inner part of the deposit, so, the most external part of the corrosion products is usually lost with the deposit. The remaining oxide is approximately 500 µm thick all around the sample and it is mainly composed by Ni with some Cr-rich areas, mainly on the top of it. Below this oxide, on the top of the remaining sample a Ni-rich and Cr-depleted zone is detected.

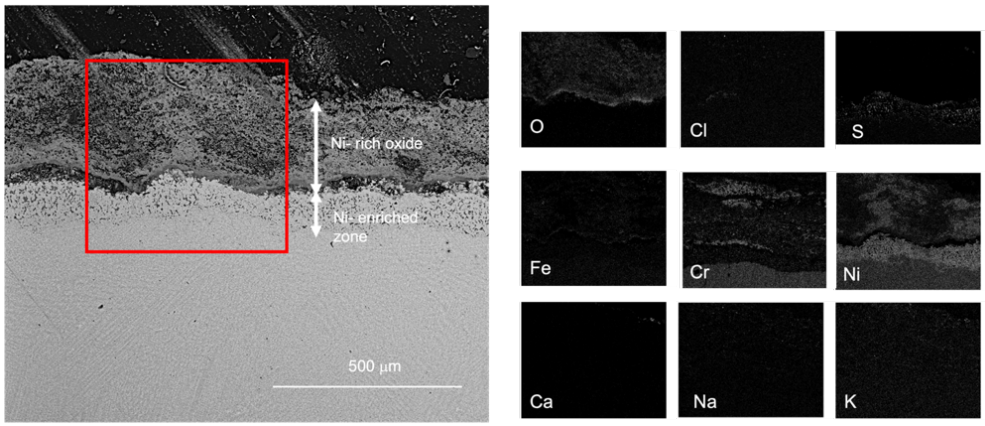

Figure 56. (a) BSE SEM cross-section image of Alloy 59 sample after 12 months of exposure in SH3 (b) EDX analysis.

The results of the overlay welded samples exposed in the P15 boiler in Händelö are described in the section below. The welded structure obtains a characteristic heterogenous surface, which makes accurate material loss measurements challenging. Thus, no material loss measurements were conducted on these samples.

The SEM images and EDX map analysis of EF101 after 6 months of exposure are shown in Figure 57. A roughly 170 µm thick adherent deposit was observed on top of the sample containing mostly Ca, S and O. Below the deposit layer a roughly 40 µm thick oxide layer was observed, containing mostly Al and traces of Cr. Below the oxide, an approximately 100-200 µm thick nitridation zone was observed. The nitridation zone was observed in a homogenous fashion throughout the cross section. The weld overlay EF101 sample exposed for 12 months could not be retrieved.

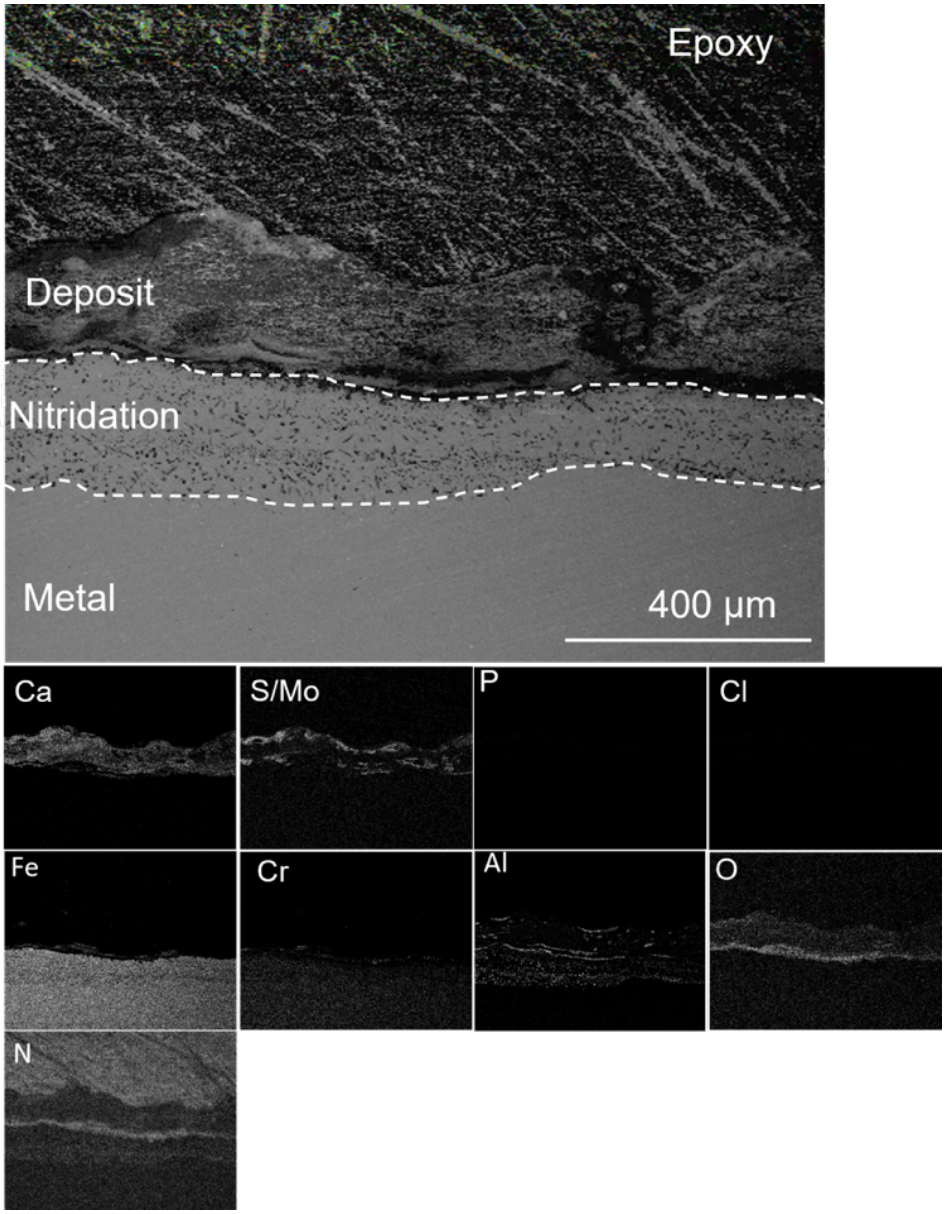

Figure 57. BSE SEM cross-section image of weld overlay EF101 sample after 6 months of exposure in SH3 together with EDX analysis below.

Compared to the weld overlay EF101 sample exposed to 6 months, the EF100 weld overlay sample achieved a significantly thicker oxide with large cracks visible after similar exposure time (see Figure 58). The oxide thickness was estimated to 450 µm. In addition, EDX signal of both Cr and Fe was observed throughout the whole oxide making it challenging to distinguish between Fe-rich and Cr-rich regions. A nitridation zone below the oxide was formed and was displayed in a patch-wise fashion throughout the cross section with a thickness ranging from 20- 260 µm.

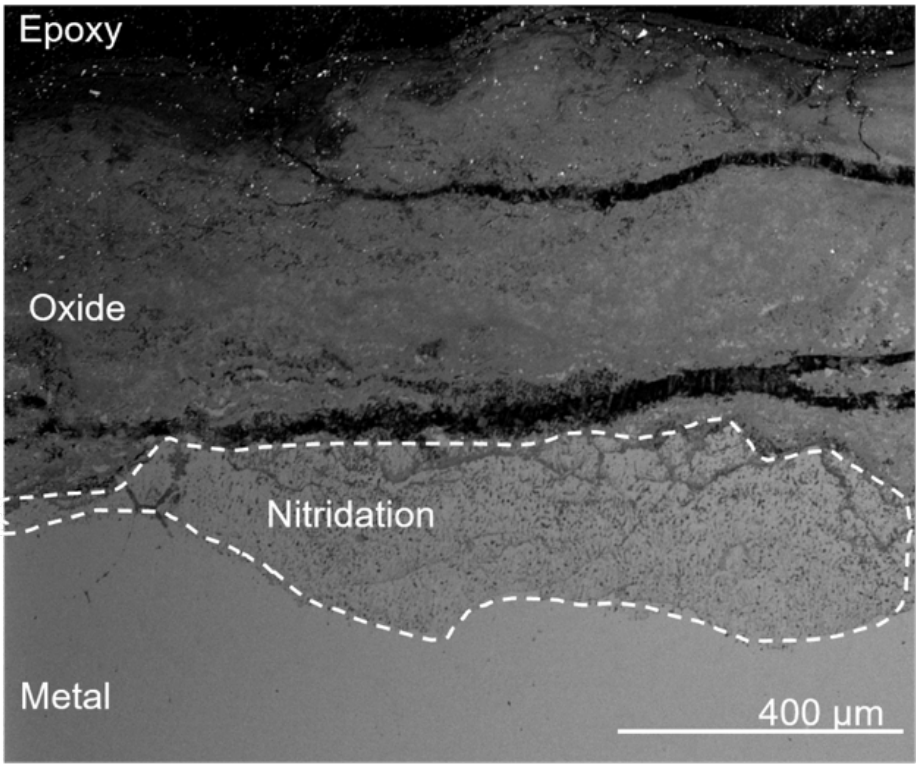

Figure 58. BSE SEM cross-section image of weld overlay EF100 sample after 6 months of exposure in SH3.

Similar features for the overlay welded EF100 sample exposed for 12 months were observed as for the 6 months (Figure 59 and Figure 60). An Fe and Cr rich oxide was formed on top of a Cr-rich oxide. Similar to the sample exposed for 6 months, large cracks and voids were detected on the oxide scale. Below the Cr-rich oxide an approximately 200 micrometers thick nitridation zone had formed. Compared to the previous sample, the nitridation region was more homogenous throughout the cross section reaching similar thickness.

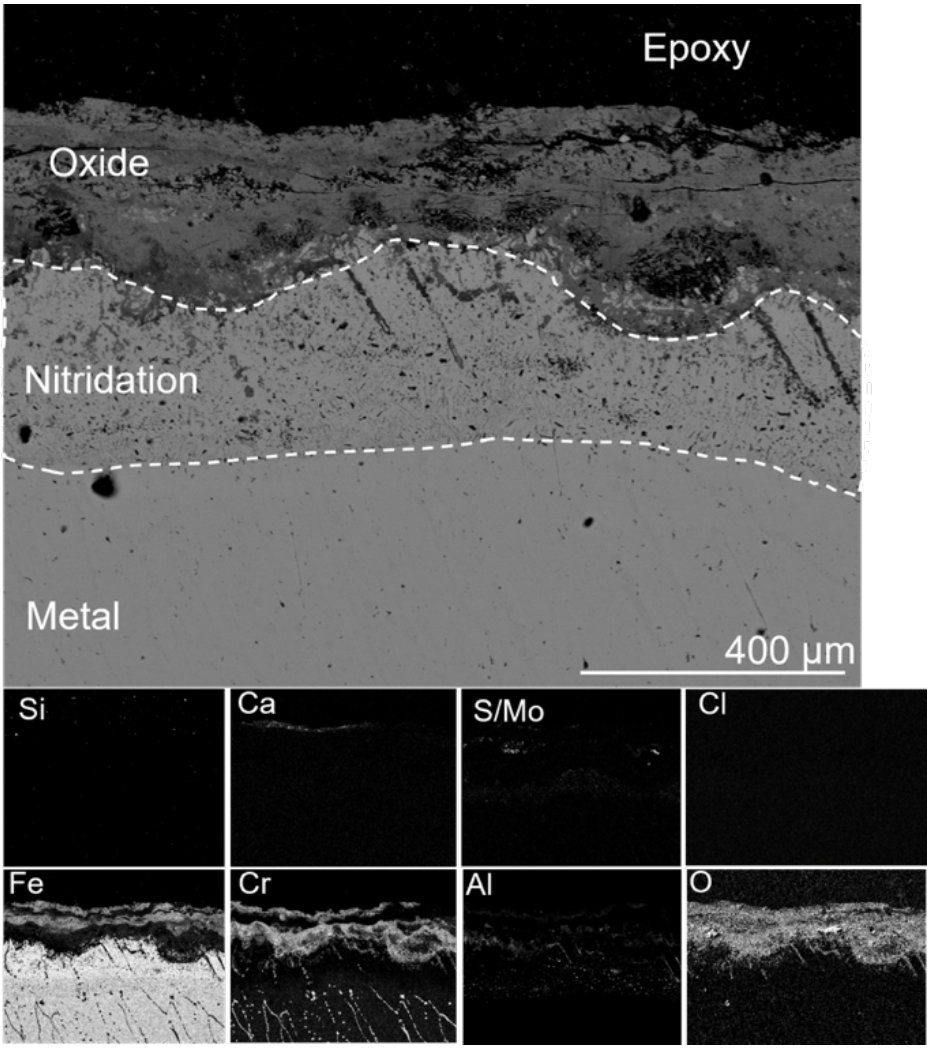

Figure 59. BSE SEM cross-section image of weld overlay EF100 sample after 12 months of exposure in SH3 together with EDX analysis below.

Figure 60 shows the SEM cross section and EDX mapping of the APMT weld overlay sample exposed for 6 months. An approximately 70-100 µm thick and adherent deposit was observed on top of the sample containing mostly Ca, S, Cl, Mg, and O. Below the deposit an Fe-rich oxide with traces of Cr-rich oxide was observed. Again, a nitridation zone was observed below the oxide. Below the oxide a 50 µm thick Cr-depleted zone was observed. The nitridation zone was identified in a patch-wise fashion reaching a thickness ranging from 10-380 µm. Unfortunately, the weld overlay APMT sample exposed for 12 months could not be retrieved.

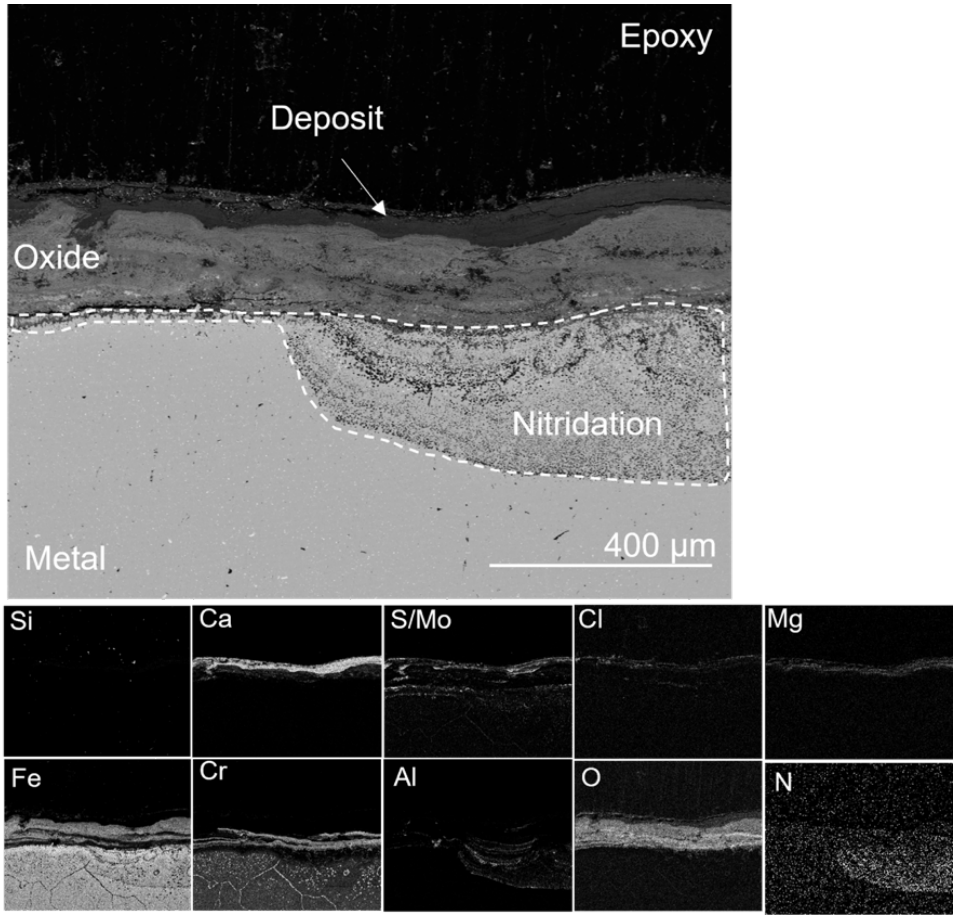

Figure 60. BSE SEM cross-section image of weld overlay APMT sample after 6 months of exposure in SH3 together with EDX analysis below.

Lastly, the weld overlay of Alloy 625 exposed for 6 months is shown in Figure 61. The EDX analysis presented below the cross-section image shows that the presence of Ca, S, and O in the deposit is high. No chlorine species were detected on the sample. Below the deposit a 170 µm thick Ni containing oxide was present and at the metal/oxide interface a Cr-rich oxide was observed. Below this oxide a Cr-depleted zone was observed leading to a Ni-enriched steel substrate. Unfortunately, the weld overlay Alloy 625 sample exposed for 12 months could not be retrieved.

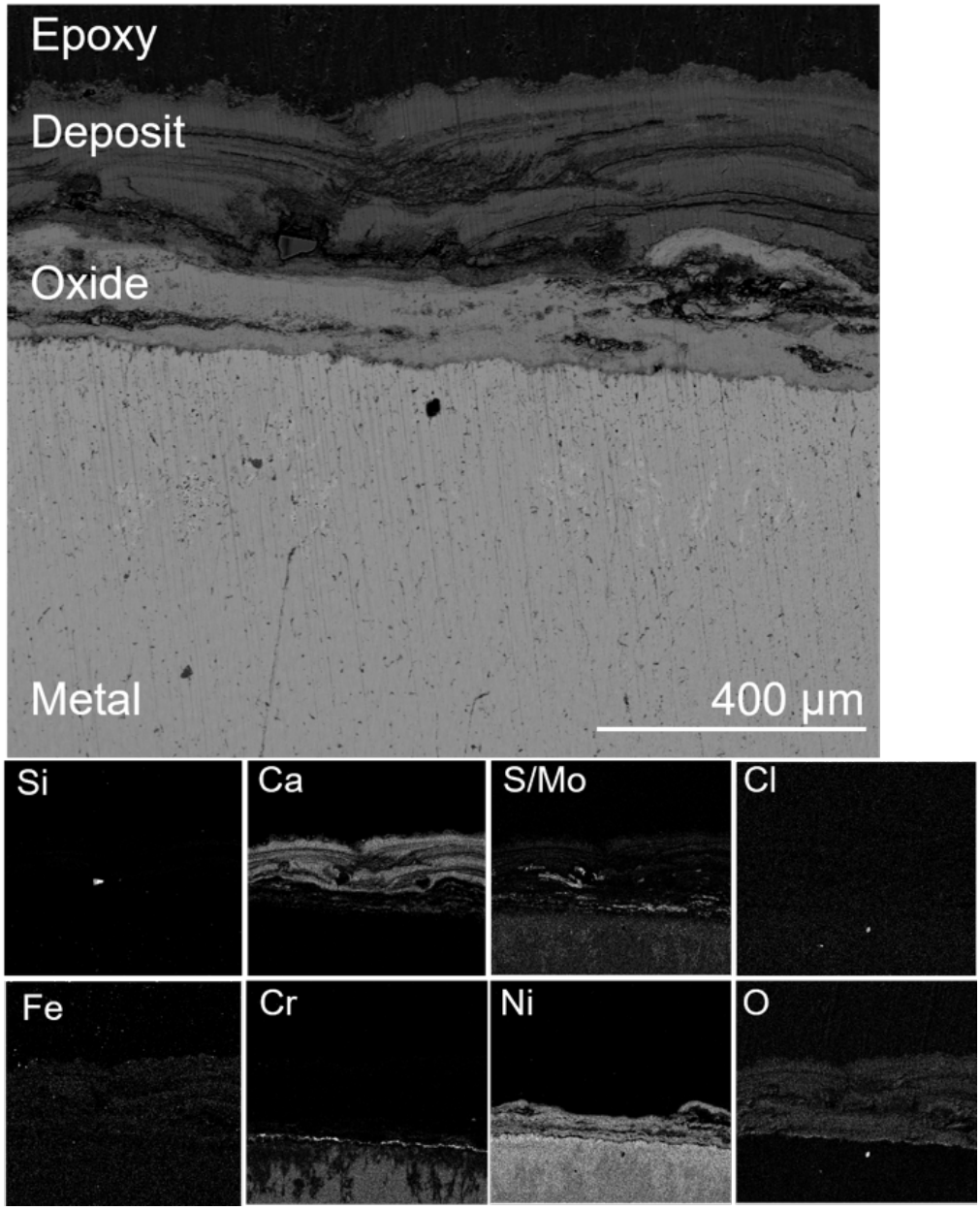

Figure 61. BSE SEM cross-section image of weld overlay Alloy 625 sample after 6 months of exposure in SH3 together with EDX analysis below.

5 Analysis of the results

This project has aimed to address the material degradation challenges facing FBHE and water wall tube panels in bio and waste-fired boilers, which today is a crucial factor that currently limits the fuel flexibility and efficiency in these power plants. In this section a thorough discussion of the results presented in this report is performed. The discussion part will be divided into the two major work packages presented in this report, one directed towards water wall (WP1) corrosion and the other towards FBHE corrosion/erosion (WP2).

- In WP1, short term testing (1 week) in the water tube panels was carried out in the P6 boiler in Högdalen. The exposure was carried out using three small sized air-cooled probes (see section 3.2.2 for set-up design). A comprehensive experimental matrix was designed using various materials including low alloyed steels, novel Al-containing alloys, Ni base alloy and austenitic stainless steels. The task of this work package has been to perform microstructure analysis of the materials after exposure to evaluate and compare the corrosion performance and mechanisms between the different materials in order to improve material selection in this region of the boiler.
- In WP2, the material loss due to erosion and corrosion of fluidized bed heat exchangers were addressed. Long-term exposures of the different materials were carried out in two different boilers; the waste-fired boiler P15 Händelö operated by E.ON (Navirum), Norrköping, and the waste-fired boiler P6 Högdalen operated by Stockholm Exergi. The materials were exposed for a total of 6, 12 and 24 months by mounting two half-moon sample rings for each material on the top- and bottom-most rows of the FBHE tube bundles during boiler shutdown. A complete description of the exposures is given in section 3. A comprehensive experimental matrix was designed using various materials, including low alloyed steels, austenitic stainless steel, novel Al-containing alloys, Ni base alloy, spray coatings, and overlay welded material. The exposures were carried out by clamping the different samples on existing fluidized bed heat exchangers (see section 3.2 for set-up design). Material loss analysis together with microstructure analysis were carried out after exposure with the aim of understanding the interplay between corrosion and erosion mechanisms with regards to material degradation rate in order to improve material selection in this region of the boiler.

In addition, a discussion on the influence of Oxygen Carrier Aided Combustion (OCAC) is described in section 5.3

5.1 WP1- WATER WALL CORROSION TESTING

Accelerated corrosion of water walls in waste-boilers remains a challenge for efficient electricity and heat production. From the results obtained in this study, the only visible oxide formation after 1 week of exposure was seen on the low alloyed steel sample 16Mo3. A Fe-rich oxide had been formed, where a high concentration of Cl was observed close to the metal/oxide interface (see Figure 9). Similar features have been reported in many studies concerning corrosion of low alloyed steel in contact with alkali/heavy metal chlorides [1-3] . Authors have contributed to the accelerating corrosion rate for low alloyed steels in these studies through the presence of chlorine. Previous studies have shown that alkali chlorides may react with water and oxygen to form Cl ions that can diffuse through grain boundaries towards the metal surface and form metal chlorides, such as $FeCl_2$. $FeCl_2$ has been shown to facilitate high diffusion rate of oxygen and iron in the grain boundaries, thus accelerating the corrosion rate [4] .

In addition, the accelerated corrosion rate can also be explained by the formation of eutectic melts facilitating the diffusion rate of chlorines at the deposit layer. Such melt formation has been suggested to form in contact with $PbCl_2$, $ZnCl_2$ and alkali chlorides [5] . The melt formation may lead to an increase of solubility of metal chlorides in the molten phase, which leads to an increased diffusion rate and subsequently a higher oxidation rate of the material. Thus, the solubility of metal chlorides in eutectic melts may influence the corrosion rate. From the SEM/EDX analyses in this study, a clear migration of Cl to the metal/oxide interface was shown, indicating the formation of iron chlorides for the low alloy steel sample. In addition, Zn, Pb, K cations were observed in the deposit, which suggests that the chlorine ions have migrated from respective counter ions. Lastly, from the EDX point analysis it was clear that some of the white bright areas showed a complex chemical composition of Zn, Pb, K and O indicating possible melt formation. It is likely that the oxide formation in this case has occurred due to the previously mentioned mechanisms regarding melt formation and metal chloride formation.

For stainless steels, the corrosion resistance is highly governed by its ability to form a protective Cr-rich oxide scale. The breakdown of this Cr-rich oxide scale cannot be explained by the previous mechanisms introduced for the low alloyed steel. Rather, it has been shown in previous studies that cations from alkali and heavy metal chlorides, such as K, Pb and Na among others, play an important role in the breakdown of the Cr-rich oxide and the formation of a less protective oxide scale as seen in the equations below:

$$4xKCl(s) + (Cr_x, Fe_{1-x})_2O_3(s) + 2xH_2O(g) \rightarrow 2xK_2CrO_4(s) + (1-x)\ Fe_2O_3(s) + 4xHCl(g)$$

$$4NaCl\ (s) + Cr_2O_3 + 5/2\ O_2 \rightarrow Na_2CrO_4\ (s) + 2\ Cl_2(g)$$

$$PbCl_2\ (l) + Cr_2O_3 + 5/2\ O_2 \rightarrow 2PbCrO_4\ (s) + 2Cl_2(g)$$

As mentioned in this report, no oxide scale or significant material degradation were observed on any of the stainless-steel types exposed in the water wall. In addition, no Pb/K/Na-chromate was observed close to the metal interface that would reveal breakdown of the protective Cr-rich oxide. However, the SEM/EDX analysis revealed a high number of corrosive species such as K, Cl, Pb, Zn, which

have been shown in previous studies to have an important impact on corrosion rates in these environments [5] .The temperature is of great importance when studying this corrosion mechanism. Melt formation in the deposit is governed not only by the chemical species, but also by the temperature. It is possible that the low temperature together with the short period of exposure does not facilitate high corrosion rates. In order to properly evaluate the corrosion resistance of these materials, it is suggested for future work to increase the exposure time in this environment. Previous studies have shown that Alloy 625 can reduce the corrosion rate of water walls significantly in these environments. Y. Alipour et al studied the corrosion effect of low alloyed steel and a Ni base alloy in the water wall region of a waste fired boiler [6] . The exposure was carried out for three years at a temperature of 340 °C. They concluded that the Ni base alloy drastically reduced the corrosion rate of the water wall compared to the low alloyed steel. The high corrosion rate observed for the low alloyed steel was attributed by the diffusion of chloride containing species through the deposit and oxide. The corrosion mechanism of the Ni base alloy was discussed, and it was concluded that the observed corrosion attack was attributed to the combination of K and Pb corrosion attack leading to the breakdown of the protective chromia scale and formation of non-protective K, Pb-chromates. Considering that both K and Pb compounds were observed in the deposit in this study it is possible that similar corrosion attacks may be observed in the present environment at longer exposures and should thus be considered regarding material selection.

From the results obtained for the FeCrAl alloys, no indication of severe material degradation was observed. The surfaces were homogenous after 1 week of exposure and there was no observation of thick oxide formation or depletion of alloy elements close to the metal/atmosphere interface. Their performance was on par with stainless steels and Ni-base alloy Alloy 625. The EF101 sample did obtain a thick deposit with a composition similar to that of the deposit on Sanicro 28. However, only a very thin oxide was observed below the deposit and no indication of chlorine migration to the metal surface was observed. Thus, the FeCrAl alloys show promising results and should be considered as possible material candidates for water wall applications.

Few studies have been carried out regarding exposure of FeCrAl alloys in water wall regions of a waste/bio boiler. Alipour et al [6] performed corrosion tests at the furnace wall in a power boiler burning waste wood. The exposures were performed for 934h at a temperature range of 365-390 °C. It was concluded that the APMT material achieved a lower corrosion rate than the traditional stainless steel 310 and on par with Alloy 625. This suggests that FeCrAl could be a potential candidate for water wall application. The corrosion mechanisms are however not yet fully understood, and more research is needed to fully evaluate FeCrAl in water wall regions.

In this study, no significant material degradation was observed on either the FeCrAl alloy or the austenitic stainless steels. To get a greater understanding of the corrosion mechanisms it is suggested to continue similar exposures, but for a longer time and conduct lab-scaled trials with a controlled environment. As mentioned in [6] , the corrosion attacks on APMT are suggested to occur due to a

combination of Cl, K and Zn, where the latter cations are suggested to break the Cr and Al-rich oxide, thus facilitating high diffusion rate of aggressive corrosive species through the oxide. Johan Eklund et al have conducted field exposure tests on FeCrAl model alloys with various amounts of Si, in a waste-fired boiler at the steam boost position reaching a material temperature of 600 °C for 672 h. From the results obtained it was shown that minor addition of Si drastically reduced the corrosion rate of FeCrAl alloys. Compared to the conventional FeCrAl APMT, the novel FeCrAl EF101 has a Si- addition to the alloy composition. Based on these results it is very interesting to further explore the possibility of FeCrAl alloys in the water wall region [7] .

FeCrAl alloys are usually implemented in regions of the boiler that have higher temperatures due to their ability to form protective alumina oxide scale. Kanthal® EF100 and EF101 have been developed to increase the temperature interval where FeCrAl alloys are normally used down to temperatures as low as 300 °C. By lowering the Cr content to about 10 wt%, the risk for α-α' phase separation, caused by a miscibility gap in the Fe-Cr system, is significantly decreased. This α-α' phase separation is also known as 475 °C embrittlement, and when suppressed, the alloys see a significant improvement in the mechanical properties at these lower temperatures. In addition, the two FeCrAl alloys contain additional alloying elements such as manganese (Mn) reactive elements (RE) and silicon (Si), where the latter element is added to improve the ability to form a protective oxide scale at intermediate temperature as previously discussed.

The results presented in this report clearly show an increased corrosion rate for the low alloyed steel compared to the stainless steels and the FeCrAl alloys, implying that the usage of 16Mo3 uncoated in this environment may not be suitable for long term usage.

5.2 WP2- MATERIAL PERFORMANCE IN FLUIDIZED BED HEAT EXCHANGERS

P6 Högdalen

A wide material testing matrix has been performed in Högalen P6 boiler. The material matrix includes conventional steels used today as well as newly developed stainless steels and FeCrAls and two different types of thermally sprayed coatings, HVOF and HVAF sprayed coatings.

A summary of the results is presented below. Figure 62 shows the different corrosion mechanisms that were observed for the different materials. Table 15 shows a summary of the results and observations of the materials exposed at the P6 boiler in Högdalen after 12 and 24 months of exposure.

The first set of materials analyzed is the FeCrAls, marked in green in the Table 15. As seen in the table, all the FeCrAl materials present nitridation in a certain way. As was mentioned in section 4.2, it is important to clarify that the thickness of the nitridation zone is not included in the material loss calculation. More specific

experiments are needed to have more knowledge about if and how nitridation affects the corrosion behavior of the FeCrAl materials. Within the project results it is not possible to see an increase in the corrosion when nitridation appears. For this reason, the material loss is calculated only taking into account the oxide scale thickness. The oxide depth presented in Table 15 represents the thickness of the oxide and the oxide affected zone when grain boundary attack is present.

By analyzing the material loss and its increase with time, the most promising material of the FeCrAls was found to be EF101. This material presents the lowest material loss and oxide depth even after 24 months exposure. The surface of the samples was smooth in all cases and deposit was found on the top of all the samples. The presence of deposit means that the oxide scale at the moment of the removal of the sample was well preserved. The material loss being close to 0 mm/year in all the positions and at all the exposure times and considering the presence of deposit on top, the observed thickness of the oxide scale should be the total oxide thickness. No oxide has spalled off during the exposure time. Nevertheless, the EF101 samples presented medium to high nitridation both in row 1 and row 9 position. The temperature in row 8 was lower than in row 1 during the 12 months exposure. This could be an explanation for the lower nitridation grade in row 8.

The EF100 material is also a promising candidate for fluidized bed superheater position. The material loss is higher than for EF101, but still low even after 24 months exposure. The deposit is still present on the top of all samples, meaning that the oxide scale has not spalled off during the exposure or handling of the samples. The nitridation zone is thinner than for EF101 but, as explained above, it is not certain that this is a factor affecting corrosion. The surface of EF100 is also more uneven than in EF101, which presents a very smooth surface with well adherent oxide over the whole sample.

The APMT material also presents good results, but worse than both EF101 and EF100 in terms of material loss and nitridation. The sample exposed for 24 months was almost completely nitridated. Taking the price into account, both EF101 and EF100 are better candidates than APMT, as the latter is the most expensive of the three FeCrAls.

The next block of materials, presented in yellow in Table 15 is the austenitic stainless steels. Besides the 16Mo3, which also presents the highest material loss and the most non-adherent oxide, all the stainless steels (SX, Sanicro 69, Esshete 1250, Sanicro28 and 316Ti) present intergranular corrosion attack propagating via grain boundaries. The oxide product consisted mainly of Cr-rich oxide on the surface of the bulk material, followed by Fe-rich oxide.

The most promising material of this kind is the SX. The SX samples contain a high amount of Si. They present an internal oxidation at the metal/oxide interface consisting of Si-rich oxide instead of the Cr-rich + Fe-rich scale presented for the rest of the materials. The material loss for the SX material was low in all the cases (max 0.06 μm/year), even after 24 months exposure. The thickness of the oxide and grain boundary attack is low during the first 12 months of exposure (around 70 μm) and reaches 200 μm after 24 months exposure. The presence of Si in high-

temperature materials has been reported in previous works to have a beneficial effect on corrosion protection [8-10] which aligns well with these results. By comparing with Sanicro 69, which is in the same price range, the material loss of the latter is lower than for SX even after 24 months of exposure, but the depth of the corrosion attack is higher in all the cases. Also, an accumulation of metal chlorides was detected on the Sanicro69 samples regardless of position. The formation of these metal chlorides reveals chlorine diffusion through corrosion product layers into the material. Previous studies have shown that this may result in poor scale adhesion after prolonged exposure that may enhance the diffusion rate of corrosive species to the metal/oxide interface and thus further increase the corrosion rate of the material [11] .

The rest of the materials in this block (Esshete 1250, Sanicro28 and 316Ti) present more material loss and oxide thickness than both SX and Sanicro 69. The Sanicro 28 material is in the same price range as SX and Sanicro 69, which makes it a poor competitor. Both Esshete 1250 and 316Ti are cheaper materials. By comparing their corrosion behavior at 12 months exposure, the 316Ti presents a smaller depth in the corrosion attack. Unfortunately, the 316Ti sample was not recovered after 24 months exposure. This can be due to a welding failure, or a sample failure, but the lack of information after 24 months makes it impossible to compare both materials in the long term.

Finally, the coating samples are marked in blue in Table 15. None of the coatings (CorEr, APMT20c, APMT40c) remained attached to the bulk metal surface after 12 months of exposure. As is shown in the results chapter (4.3.1), the underlaying base material had undergone internal corrosion, which indicates that corrosion attack might have already occurred at an early stage of the exposure suggesting an early failure of the coatings.

The microstructure analyses show corrosion products in all the samples. Grain boundary attack is detected in most of the conventional steels and nitridation is observed in all the FeCrAl materials exposed. The EDX mapping reveals traces of chlorine species in some of the deposits and in some of the samples, like Sanicro 69, metal chlorides were formed potentially resulting in poor scale adhesion and an increased corrosion attack. The fluidized bed heat exchanger is surrounded by fluidized bed material, so also erosion is expected to influence the samples. The microstructure analysis shows that deposit and oxide spallation occur, sometimes very locally, indicating a strong erosion in certain parts of the heat exchanger. Thus, it is suggested that local erosion attacks happen in this boiler position, which may lead to increased material loss after prolonged exposures. The results obtained from all the different kinds of materials exposed in this project, in the different positions of the heat exchanger and at different exposure times, suggest that the attack suffered by the material is a combination of erosion and corrosion. In Appendix A of the present report, it is explained how the simultaneous mechanism of erosion and corrosion attack can occur and how it affects the formation and spallation of the oxides [12] .

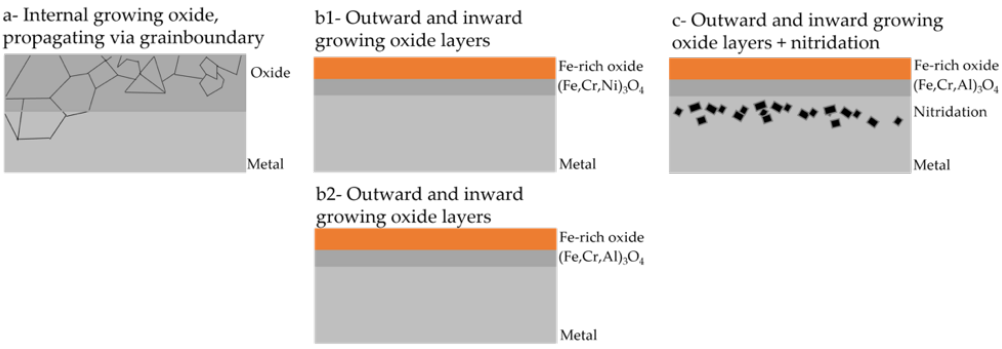

Figure 62. Illustration of the different corrosion mechanisms and microstructure observations.

Table 15. Summary of the most important findings of the material analysis in the waste-fired boiler P6, Högdalen. The corrosion type is related to Figure 60.

Material	Exposure time (months)	Position	Material loss (mm/year), $\bar{x}$	Corrosion type	Oxide depth (mm)	Deposit left	Nitridation	Price
EF101	12	Row 1	0.02 ± 0.01	c	25	Y	Medium	$$$
EF101	12	Row 8	0.00 ± 0.01	c	40	Y	Low	$$$
EF101	24	Row 9	0.00 ± 0.01	c	200	Y	Medium/ High	$$$
EF100	12	Row 1	0.16 ±0.01	c	50	Y	High	$$$
EF100	12	Row 8	0.09 ±0.01	c	140	Y	Medium	$$$
EF100	24	Row 9	0.36 ± 0.01	c	200	Y	Low	$$$
APMT	12	Row1	0.18 ±0.01	c	Cracked	N	Medium	$$$$
APMT	12	Row 8	0.00 ± 0.01	c	80	Y	High	$$$$
APMT	24	Row 9	0,27± 0.01	c	300	N	High	$$$$
SX	12	Row 1	0.02 ±0.01	a+b1	70	N	x	$$$$
SX	12	Row 8	0.06 ± 0.01	a	70	N	x	$$$$
SX	24	Row 9	0.05± 0.01	a+b1	200	Y	x	$$$$
Sanicro 69	12	Row 1	0.00 ± 0.01	a+b1	>150	N	x	$$$$
Sanicro 69	12	Row 8	0.00 ± 0.00	a	>200	N	x	$$$$
Sanicro 69	24	Row 9	0.00 ± 0.00	a+b1	>200	Y		$$$$
Esshete 1250	12	Row 1	0.66 ±	a	250	N	x	$$$
Esshete 1250	12	Row 8	0.33 ±	a	300	N	x	$$$

Esshete 1250	24	Row 9	0.89 ±0.01	a+b1	>300	N	x	$$$
Sanicro 28	12	Row 1	0.34 ±	a+b1	Cracked	Traces	x	$$$ ($)
316Ti	12	Row 1	0.80 ±	a	200	N	x	$$
316Ti	12	Row 8	0.58 ±	a	100	N	x	$$
16Mo3	12	Row 8	1.17 ±	b	200	N	x	$$
Alloy 625	12	Row 1	WOL	b	200	Y		$$$$
Alloy 625	12	Row 8	WOL	a	200	Y		$$$$
Alloy 625	24	Row 9	WOL	a+b1	200	Y	x	$$$$
APMT50c	12	Row 8	Coating failure!	x		N	x	$$$$
APMT20c	12	Row 8	Coating failure!	x		N	x	$$$$
CorEr	12	Row 8	Coating failure!	x		N	x	

P15 Händelö

A wide material testing matrix has been performed in Händelö P15 boiler. The material matrix includes conventional steels used today as well as newly developed stainless steels and FeCrAls, both in bulk form and overlay welded. The reference material is alloy 59 overlay welded as it is the material used in the fluidized bed heat exchangers today.

A summary of the results presented below. Figure 62 shows the different

Table 16 shows a summary of the results and observations of the materials exposed at P15 boiler in Händelö after 6 and 12 months of exposure.

Table 16. Summary of the most important findings of the material analysis in the waste-fired boiler P15, Händelö

Material	Exposure time (months)	Material loss (mm/year), $\bar{x}$	Corrosion type	Oxide depth (mm)	Deposit left	Nitridation	Price
EF101	6	0.09 ± 0.06	c	100	Y	High	$$$
EF101	12	0.41 ± 0.43	c	100	Traces	Medium	$$$
EF100	6	0.13 ± 0.09	c	200	Y	Medium	$$$
EF100	12	0.19 ± 0.09	c	100	N	Medium	$$$
APMT	6	0.26 ± 0.18	c	70	N	High	$$$$
APMT	12	0.36 ± 0.21	c	200	N	High	$$$$
SX	6	0.01 ± 0.02	a	100	Y	x	$$$$
SX	12	0.23 ± 0.05	a	400	Y	x	$$$$
Sanicro 69	6	0.04 ± 0.05	a+b1	400	Y	x	$$$$
Sanicro 69	12	1.02 ± 0.59	b1	500	N	x	$$$$
27Cr33Ni3Mo	12	0.33 ± 0.45	a+b1	>300	N	x	R&D
Esshete 1250	6	0.76 ± 0.24	a	300	N	x	$$$
Esshete 1250	12	0.90 ± 0.11	a	300	N	x	$$$
316Ti	6	0.69 ± 0.09	a	250 cracked	N	x	$$
316Ti	12	1.15 ± 0.17	a	300 cracked	N	x	$$
CorER	6	Coating failure!	x	x		x	

Alloy 59	12	WOL	b1	500	N	x	$$$$
EF101 WOL	6	WOL	c	40	Y	Low	$$$
EF101 WOL	12	Lost sample	x	x	x	x	$$$
EF100 WOL	6	WOL	c	450 cracked	N	Low/ medium	$$$
EF100 WOL	12	WOL	c	>300 cracked	N	Medium	$$$
APMT WOL	6	WOL	c	200	Y	Medium	$$$$
APMT WOL	12	Lost sample	x	x	x	x	$$$$
Alloy 625	6	WOL	b1	170	Y	x	$$$$

The first block of materials analyzed is the FeCrAls, marked in green in the

Table 16. As seen in the table, all the FeCrAl materials (bulk and overlay welded) present nitridation in a certain way. As explained above, it is important to clarify that the thickness of the nitridation zone is not included in the material loss calculation.

The behavior of the FeCrAl materials in P15 boiler at Händelö matches the results obtained at P6 in Högdalen presented above. The most promising materials are EF101 and EF100. Both present low material loss and the oxide depth does not exceed 200 μm for any of the exposure times. In the P6 boiler at Högdalen, the EF101 performed slightly better than EF100 after 24 months of exposure, having a very low material loss. At P15 in Händelö, only 6- and 12-months exposures were performed so it is not possible to make an evaluation of the behavior of those materials for longer exposures. Nevertheless, the behavior after 6 months exposure is very similar for both materials. After 12 months, the average material loss is 0.19 mm/year for EF100 vs 0.41 mm/year in EF101, the oxide depth being the same for both the materials after the 12 hours exposure.

The APMT material presents higher material loss both at 6 and 12 months exposure and, just as in P6 Högdalen, the APMT samples are almost totally nitridated. As this material is more expensive than both EF101 and EF100 it is not a good competitor for the fluidized bed heat exchangers in P15 Händelö.
The next group of materials, marked in yellow in

Table 16, is the austenitic stainless steels. Matching the results in P6 Högdalen boiler, the most promising material is the SX. After 6 months exposure it presents a protective Si-rich oxide both on the top of the sample and in the grain boundaries. The material loss is only 0.01 mm/year after 6 months exposure and 0.23 mm/year after 12 months exposure. Sanicro 69, which is in the same price range, does not perform as good as SX, presenting higher material loss both at 6 and 12 months exposure. The depth of the attack is also higher for both exposure times. Alloy 27Cr33Ni3Mo presents less material loss than Sanicro 69 after 12 months, the average value being 0.33 mm/year. This material loss value is in the same range as the SX material after 12 months (0.23 mm/year), but 27Cr33Ni3Mo presents an accumulation of metal chlorides in the grain boundaries. The same effect, which is observed for Sanicro 69 in the P6 Högdalen boiler. This may result in poor scale adhesion after prolonged exposure, which may enhance the diffusion rate of corrosive species to the metal/oxide interface and thus further increase the corrosion rate of the material [11]

Considering these results and P6 Högdalen results, the SX is the most promising material of this group. Compared to Sanicro 69 and 27Cr33Ni3Mo, the SX alloy contains a higher amount of Si. The presence of Si in high-temperature materials has been reported to have a beneficial effect on corrosion protection [8-10] . Increased corrosion resistance and the formation of a SiO_2 layer was also observed for an Fe-20Cr and an Fe-20Cr-20Ni alloy upon addition of silicon in Ar-20CO_2 and Ar-20CO_2-20H_2O at 650 °C [13]. In more corrosive environments (in the presence of KCl) modification of Fe-15Cr alloys by addition of aluminum/silicon showed positive synergistic effects on the corrosion behavior when exposed to air at 650 °C [13, 14] .

The two conventional austenitic stainless steels, 316Ti and Esshete 1250, were subjected to a large degree of intergranular corrosion and the severity of the corrosion attack was increased as a function of time exposed to the present environment. None of them has deposit left over the surface and the 316Ti material presents low quality cracked oxides after both 6 and 12 months exposure. In mild environments, austenitic stainless steels are expected to form a chromium-rich and protective oxide [15] . In environments rich in alkali chlorides, these materials are readily attacked by both alkali and chlorine, forming alkali chromates and metal with a corrosion product layer often consisting of an outward-growing hematite (Fe_2O_3) and an inward-growing (mixed) spinel oxide layer (Me_3O_4) [16] . In this study, only the inward-growing spinel oxide (rich in Cr and Ni) remains on the sample, whereas the outward-growing hematite as well as the deposited layer, have been lost. It is expected that the presence of alkali in the environment has destroyed the protective properties of the initial chromium-rich oxide [17, 18] . Furthermore, a grain boundary attack can be seen. In a recent study, the attack is associated with small levels of chlorine in the grain boundaries, where chlorine is suggested to increase the diffusivity at the grain boundaries and thereby causing accelerated corrosion [19] . This type of behavior is expected to be detrimental to the material over time, either by continuing the attack to spread laterally or by losing whole steel grains, as the attack decreases the mechanical stability of the material.
The last group of samples, marked in blue in

Table 16, are coated materials. Being overlay welded materials, it is not possible to calculate a reliable material loss to compare with the rest of the exposed materials. The corrosion behavior is evaluated by means of SEM images and the depth of the oxide. The reference material is alloy 59, which presents a smooth surface after 12 months of exposure but a very thick oxide (around 500 µm) which is more than 10 times the thickness of the attack at the FeCrAl EF101 overlay weld for the 6 months exposure time. Due to the high thickness of the alloy 59 welded material, there is still much untouched material after the exposure, even having such a thick oxide layer on top. The attack in the alloy 59 is severe so the material "lost" in favor of the oxide still more than for the EF101 overlay weld material. That makes the EF101 WOL very promising for this application. The nitridation level for the EF101 WOL is very low at 6 months exposure too. Unfortunately, the 12 months exposure EF101 sample was lost during the exposure and was not possible to recover for analysis.

The EF100 overlay weld samples do not perform as well as EF100 bulk material for any of the exposure times. Both at 6 and 12 months exposure the overlay weld material presents cracked oxides, which lead to significant local diffusion of oxygen throughout the sample. At 6-month exposure the thickness of the oxide on EF100 is 10 times higher than on EF101. In addition, the oxide formed on EF101 is very smooth and well adherent, not presenting any cracks or detachment from the surface of the sample. The deposit is still present over the EF101 overlay weld.

The APMT overlay weld sample performs well at 6 months exposure presenting a smooth 200 µm oxide. The nitridation in this case is local, presenting zones with very thick nitridation and zones where it is not nitridation at all. Unfortunately, the 12 months exposure APMT WOL sample was lost during the exposure.

The Alloy 625 overlay weld sample presents a 170 µm thick oxide, which is well adherent to the metal surface, but it presents several deep cracks on its own surface, which can lead to local diffusion of oxygen.

Finally, the CorER sample was lost during exposure so no results can be presented in this report.

5.3 REVIEW OF POTENTIAL CORROSION ISSUES USING OCAC

Fluidized bed (FB) boilers are the preferred type of boiler for fuel flexible green heat and power production. FB boilers can burn a wide range of biomass and waste fuels with high efficiency and low emissions. This boiler type relies on a bed of particles that are being fluidized by a gas, typically air. When combusting biomass or waste, the bed particles conventionally use sand. Sand particles are becoming well mixed with fuel particles, which leads to improved combustion of the fuel particles in the presence of the fluidizing air. Besides enabling a good mixing capability, the sand bed is also the bearer of heat to the combustion process of the fuel particles. The main drawback with using sand high in silica as bed material is its agglomeration tendencies [20, 21] .Specially when combusting fuels containing alkali, the silica sand reacts with alkali to form low melting point alkali silicates and/or alkali alumina silicates. Furthermore, from a material degradation point of view, silica particles may possess erosive properties when fluidized.

Despite these drawbacks with sand high in silica, the cost has been fairly low, and it is the most used bed material for FB boilers. However, there has been some research and tests with other types of bed materials, e.g., olivine [22] or dolomite [23] .Besides achieving good heat transfer properties, the bed material can achieve other valuable properties such as e.g., resistance towards agglomeration or the ability to capture SO_2.

During recent years, a new bed material, Ilmenite [24-26] has been presented. Ilmenite is a part of a group of bed materials that possess oxygen carrier properties. This means that the bed material can take up and release oxygen depending on the surroundings. Components of natural sand, e.g., silica (SiO_2) and feldspar (aluminosilicates) do not have this property. During combustion of the fuel particles in FB boilers using a sand bed, additional oxygen is necessary and is supplied via the fluidizing air (or in secondary air inlet). However, by utilizing a bed with bed particles having oxygen carrier abilities there is no necessity for additional oxygen supply at oxygen lean locations as the oxygen carrier particles transport oxygen from oxygen-rich to oxygen-lean locations. Thus, there is an even distribution of heat and oxygen within the reactor. This type of combustion is denoted as OCAC (Oxygen Carrier Aided Combustion) [27] .With OCAC, the surplus of air to the boiler can be decreased without risking poor combustion properties, e.g., high emissions of CO. Bed materials with oxygen carrier abilities are also a key aspect when designing the next generation of FB boilers where CCS (Carbon, Capture & Storage) is integrated (the so-called CLC (Chemical Looping Combustion) plant [28]

One of this project's aims was to investigate how the material degradation (corrosion and/or erosion) may be affected by changing the bed material from sand to Ilmenite (an oxygen carrier material). The initial plan was to conduct corrosion exposures at the FBHE-tubes in the two boilers included in this project. However, due to delays emerging from the COVID pandemic and thereby renewed commercial considerations there has not been any possibility to perform such planned exposures. Instead, this section has been focusing on literature studies in order to estimate potential material degradation. Furthermore, there has been a dialogue and sharing of results between this project and another Biokraft project "46450-1 Syrebärarstödd förbränning för effektivare bränsleomvandling I FB-pannor med samtidig återvinning av alkaliföreningar" regarding the use of ilmenite as bed material. Some of which are summarized below.

Ilmenite is an ore consisting mainly of titanium-iron oxide with formula $FeTiO_3$. It is a weakly magnetic ore and is today mostly used to produce titanium dioxide, for use in paints, plastics, paper, sunscreen and food. It is the presence of iron (Fe) that gives Ilmenite its oxygen carrier properties as iron can switch between its two oxidation states (Fe^{2+} and Fe^{3+}). Ilmenite is, like SiO_2 in sand, readily reacting with alkali at higher temperatures. However, in contrast to alkali silicates, the alkali titanates that form have a much higher melting point. Thus, the ilmenite has compared to sand rich in silica a much lower risk of forming low melting point compounds that will make the particles stick together. As a consequence, the agglomeration risk is considerably lower for ilmenite compared to many varieties of natural sand.

The use of ilmenite as bed material in FB boilers is a rather new experience, however tests have been conducted in industrial scaled boilers in the size from 12 – 400 MW_{th} [29] .The majority of the work has been connected to its oxygen carrier ability, agglomeration tendencies and alkali uptake. From the corrosion point of view, the ability to take up alkali from the fuel and the ability to decrease local "hot-spots" high temperature zones within the furnace are probably the most important parameters.

For superheaters, either placed in the convective pass or in the fluidized bed, the uptake of alkali in the bed is important. Because the alkali not captured by the bed is potentially ending up as corrosive alkali compounds, e.g., KCl or NaCl, on the superheater tubes, causing an accelerated corrosion attack. The use of ilmenite as bed material in CFB boilers has been investigated earlier in literature, however, the published data on utilizing an Ilmenite bed in connection to corrosion is scarce. Thus, the full scale testing investigating the effect of changing bed material to Ilmenite is not fully elucidated. As mentioned above, knowing the mass balance of alkali in the boiler will be of uttermost importance. Recent studies in lab/pilot scale suggest however that the Ilmenite bed will act perfectly as an alkali getter. According to Lu at al. [30] the ilmenite captured about 40-65% of the alkali (K) during a 5h exposure. The formed alkali titanate was KTi_8O_{16}. The potassium uptake with Ilmenite was similar to olivine.

Based on the laboratory and pilot studies using Ilmenite, it shows good ability to capture alkali (with considerably less risk of agglomeration), comparatively to silica sand. However, the release of alkali to the flue gases will be dependent on several operational parameters where the most important will probably be the rate of bed renewal. For natural sand based beds, the renewal rate is usually in the order of 1-3 kg/MWh for biomass fuels and 6 kg/MWh for waste fuels. The total bed inventory differs but can be roughly 60 tons for a FB-boiler in the thermal size of 75 MW. The long-term experiences reached so far with using Ilmenite as bed material, the renewal rate have been decreased with a factor of 8 compared to a silica sand bed. Even though the material performance of e.g., superheater tubes have not been studied in detail, successful operation with an Ilmenite bed for 12 000 hours have been demonstrated [31] . Based on the alkali uptake capability of Ilmenite and long term successful operation, it is anticipated that the corrosion of superheater tube will not increase if changing the bed material from silica sand to Ilmenite. However, this needs to be investigated in depth and primarily in full scale exposures, i.e., in operating commercial plants.

6 Goal fulfillment

This project addresses two problem areas related to material wastage that today limits availability and fuel flexibility of biomass and waste fired power plants, corrosion/erosion of heat exchangers and water walls. The project's goal is to improve plant economy of plants using renewable fuels and increase the competitiveness towards fossil fueled plants by targeting these two problem areas in the (fluidized bed) boilers. Below the different goals are specified in detail and if the goal has been reached or not.

- Reduce the total cost of water walls and/or fluidized bed superheaters by enabling new materials and/or by mitigating the corrosive environment by changing bed material or optimized design. The total cost can be reduced by improving the material lifetime or by lowering the cost.

This project aimed at improving the plant economy for plants using renewable fuels and thereby increasing the competitiveness towards fossil fueled plants by targeting areas in the plants where material issues are of concern. A key parameter in increasing the plant economy is to decrease the maintenance cost. The replacement of failing heat exchanger materials inside the plant is a larger contributor to the maintenance costs. By optimizing the materials, in such a way that the most cost-effective materials are used, the overall maintenance can be decreased. We have performed a substantial number of material testing campaigns including a wide palette of materials for two positions in the boiler, which has high degradation rates when burning challenging fuels: the water walls and fluidized bed superheaters. From a material perspective, almost 20 types of material including low alloyed steels, stainless steels, nickel-based alloys and FeCrAl alloys have been investigated. Furthermore, the material selection has included both commercial alloys and newly developed alloys, in the form of bulk material as well as weld overlay coatings and metallic spray coatings.

The main aim of this goal has been to provide reliable data on the material performance of the abovementioned materials and thereby enable more accurate cost calculations to be done by the industry. As such, the material selection of boiler components can be optimized, and the maintenance cost be decreased. The exact cost of the materials is unfortunately not open to the public and furthermore, the material cost is changing constantly due to the price of alloying elements, etc. However, in order to provide an estimate about the cost difference between different materials (which is fairly stable over time), Table 15 and

Table 16 was provided in chapter 5 “Analysis of the results”. Hereby, the reader can get a rough idea about the material cost, which can be combined with their performance.

This goal is considered as fulfilled.

- Increase the knowledge of material degradation mechanisms and environmental parameters at play in fluidized bed superheaters.

Overall, the large exposure matrix together with a wide and in-depth microstructural analysis had provided the material community with valuable information relevant for corrosion performance. This for two positions in the power plants that today are subject to high material wastage rates.

For the FBHE tubes, there was a special interest in deducing if the material wastage was primarily driven by erosion or by corrosion. The collective analysis of all the clamp samples that have been exposed on top of the tubes within the FBHE section indicates that it is a combination of erosive and corrosive forces that causes the degradation. In many cases, the samples were covered by a deposit, which suggests that erosive forces have been mild. In other cases, the deposit layer was minimal or non-existent leading to the conclusion that erosive forces were at play. Furthermore, it is probable that corrosion and erosion influence each other synergistically, leading to higher material wastages. The results showed signs of steel grain boundary attacks (on several occasions in combination with the presence of Cl) and it is expected that a material suffering from steel GB attack is also more susceptible to erosion.

This goal is considered as fulfilled.

- Investigate the properties of newly developed alloys together with commercially available materials for water walls. Both thermal spray coating and overlay welding will be investigated.

As above, the material matrix executed in the exposures has been wide, covering both materials that are used today and newly developed steels, FeCrAls and coatings. The corrosion analysis has primarily been performed by means of material loss determination and cross-sectional SEM/EDX analysis. Special focus has been put towards the newly developed materials (EF100 and EF101) in order to investigate their potential use for both water walls and for tubes to be used as FBHE material. The results show that the newly developed FeCrAl alloys (EF100 and EF101) are potential candidates as boiler materials, taking a corrosion/erosion perspective. However, both these types of materials suffered from nitridation, which needs to be further studied. It is not clear how the nitridation process affects the corrosion performance on a longer perspective than one year. Furthermore, as these materials are not classed as pressure bearing materials, they cannot be used as monotubes. Instead, their initial use would be as corrosion/erosion resistant coatings and/or co-extruded tubes. The new insights in the performance of these alloys were presented in journal article.

This goal is considered as fulfilled.

- Publish 1 scientific article, present the results at two conferences and complete two academic theses within the project.

Within this project the following have been achieved within the sub-goals:

Publish 1 scientific article.

- A material degradation study of novel FeCrAl alloys, stainless steels and nickel base alloy in fluidized bed heat exchangers of a waste fired CFB boiler

Hampus Lindmark, Julien Phother, Maria Dolores Paz Olausson, Johanna Nockert, Fredrik Lind, Anna Jonasson, Vesna Barišić, Kyösti Vänskä, Laura Rioja-Monllor and Jesper Liske

Fuel 338, 127299, 2023

Present the results at two conferences.

- **Investigating the performance of novel FeCrAl alloys in a fluidized bed heat exchanger application of a waste fired CFB boiler**
  Hampus Lindmark, Julien Phother, Maria Dolores Paz Olausson, Johanna Nockert, Fredrik Lind, Anna Jonasson, Vesna Barišić, Kyösti Vänskä, Laura Rioja-Monllor and Jesper Liske

Oral presentation at the 24th Fluidized bed conversion conference, FBC-24, May 2022, Gothenburg Sweden

- **HTC/KME conference 2019**
  KME 803: New materials and Oxygen Carrier Aided Combustion for improved competitiveness of FB plants using renewable fuels

Oral presentation by Julien Phother and Jesper Liske, Gothenburg 12-13 March 2019

- **HTC/KME conference 2020**
  KME 803: New materials and Oxygen Carrier Aided Combustion for improved competitiveness of FB plants using renewable fuels

Oral presentation by Julien Phother and Jesper Liske, Digital conference, 4-5 November 2020

- **KME conference/workshop (planned 6th March 2023)**
  KME 803: New materials and Oxygen Carrier Aided Combustion for improved competitiveness of FB plants using renewable fuels

Oral presentation by Hampus Lindmark and Maria Dolores Paz

Complete two academic theses

- **Julien Phother Ph.D. thesis**
  High Temperature Corrosion Behavior in Biomass- and Waste-Fired Boilers - Insights into catastrophic corrosion and corrosion mitigation techniques
  Ph. D. thesis, Chalmers, 2020

- **Hampus Lindmark, Licentiate thesis**
  Title to be decided
  Lic. Thesis planned for fall 2023

This goal is considered as fulfilled. This includes a planned licentiate thesis to be presented in the fall 2023, based on the results and conclusions obtained within this project. The other subgoals (publishing one journal article and two conference presentations) are reached within the project's timeframe.

7 Summary and conclusions

The project has successfully conducted several corrosion tests in two commercially operated boilers; the waste-fired P15 boiler at Händelö and the waste-fired P6 boiler in Högdalen. The corrosion tests were carried out at two different positions in the boiler; the water wall region and the fluidized bed heat exchanger region. The water wall tests were carried out in the P6 boiler in Högdalen and lasted for 1 week while the fluidized bed heat exchanger tests were carried out both in Högdalen and Händelö with an exposure time ranging from 6 to 24 months. A wide range of materials, ranging from low alloyed steels, stainless steels, Ni-base alloys, FeCrAl alloys and different coating techniques including overlay weld materials has been investigated. The following conclusions can be made from the findings:

Water wall exposures:

- Oxide formation was only observed for the low alloyed steel (16Mo3) after 1 week of exposure in the water wall region of the waste fired P6 boiler in Högdalen. High concentration of chlorine was observed close to the metal/oxide interface suggesting that Cl diffusion through the oxide plays an important role in the material degradation rate.
- Neither Ni-base steel nor stainless steel showed any indication of material degradation, and no accumulation of Cl was observed at the metal/deposit interface for these samples.
- Both conventional and newly developed FeCrAl alloy showed promising results as their performance was on par with the Ni-base and stainless-steel samples.

Fluidized bed heat exchangers:

- The newly developed FeCrAl EF101 showed the most promising results after 12 and 24 months of exposure in Händelö and Högdalen, respectively, obtaining a material loss significantly lower than conventional stainless steels and Ni-base alloys.
- Nitridation zones were observed on all FeCrAl alloys regardless of boiler type with the following severity ranked: APMT > EF100 > EF101. It is not known how nitridation affects the corrosion behavior. In the present project the material presented an increase of thickness of the nitridated zone without an increase in the material loss, so it is unclear how nitridation affects corrosion in this particular application or if it affects at all.
- EF101 WOL is the most promising material from the overlay weld samples at Händelö. It performs better than all the other coatings at 6 months. It performs better than the EF101 bulk material for the same exposure time.

No sample could be recovered from the P15 boiler in Händelö after 12 months exposure.

- The most promising material from the austenitic stainless-steel block is the alloy SX. It experienced the lowest material loss regardless of boiler type and time. A Si-rich/Cr-rich oxide was observed in the grain boundaries at the corrosion front of the material. It is suggested that Si oxide may improve the resistance towards both corrosion and erosion mechanisms.
- Both HVAF and CorEr coating failed after 12 months of exposure regardless of boiler type. The oxide formation on the underlaying bulk material indicate that the failure occurred at an early stage of the exposure.

8 References

[1] H. Kinnunen, M. Hedman, M. Engblom, D. Lindberg, M. Uusitalo, S. Enestam and P. Yrjas. The influence of flue gas temperature on lead chloride induced high temperature corrosion. Fuel, 2017; 196:241-251

[2] A. Persdotter, M. Sattari, E. Larsson, M. A. O. Ogaz, J. Liske and T. Jonsson. Oxidation of Fe-2.25Cr-1Mo in presence of KCl(s) at 400 degrees C - Crack formation and its influence on oxidation kinetics. Corrosion Science, 2020; 163:

[3] M. A. Olivas-Ogaz, J. Eklund, A. Persdotter, M. Sattari, J. Liske, J. E. Svensson and T. Jonsson. The Influence of Oxide-Scale Microstructure on KCl(s)-Induced Corrosion of Low-Alloyed Steel at 400 degrees C. Oxidation of Metals, 2019; 91:291-310

[4] N. Folkeson, T. Jonsson, M. Halvarsson, L. G. Johansson and J. E. Svensson. The influence of small amounts of KCl(s) on the high temperature corrosion of a Fe-2.25Cr-1Mo steel at 400 and 500°C. Materials and Corrosion, 2011; 62:606-615

[5] H. Kinnunen, M. Hedman, D. Lindberg, S. Enestam and P. Yrjas. Corrosion in Recycled Wood Combustion-Reasons, Consequences, and Solutions. Energy & Fuels, 2019; 33:5859-5866

[6] Y. Alipour and P. Henderson. Corrosion of furnace wall materials in waste-wood fired power plant. Corrosion Engineering Science and Technology, 2015; 50:355-363

[7] J. Eklund, M. D. Paz, B. Jönsson, J. Liske, J. E. Svensson and T. Jonsson. Field exposure of FeCrAl model alloys in a waste-fired boiler at 600°C: The influence of Cr and Si on the corrosion behaviour. Materials and Corrosion, 2019; 70:1476-1485

[8] V. Asokan, J. Eklund, S. Bigdeli and T. Jonsson. The influence of Si on the primary protection of lean FeCrAl model alloys in O2 and O2+H2O at 600 °C—A microstructural investigation. Corrosion Science, 2021; 179:

[9] J. Eklund, I. Hanif, S. Bigdeli and T. Jonsson. High temperature corrosion behavior of FeCrAlSi model alloys in the presence of water vapor and KCl at 600 °C – The influence of Cr content. Corrosion Science, 2022; 198:

[10] T. Sand, A. Edgren, C. Geers, V. Asokan, J. Eklund, T. Helander, J. E. Svensson and L. G. Johansson. Exploring the Effect of Silicon on the High Temperature Corrosion of Lean FeCrAl Alloys in Humid Air. Oxidation of Metals, 2021; 95:221-238

[11] M. D. Paz. Increased steam temperature with Steamboost superheater in grate-fired boilers- Linking deposit formation and high temperature corrosion. Impacts of Fuel Quality on Power Production, Prague 2016

[12] D. M. Rishel, F. S. Pettit and N. Birks. Some Principal Mechanisms in the Simultaneous Erosion and Corrosion Attack of Metals at High-Temperatures. Materials Science and Engineering a-Structural Materials Properties Microstructure and Processing, 1991; 143:197-211

[13] Y. S. Li, Y. Niu and M. Spiegel. High temperature interaction of Al/Si-modified Fe-Cr alloys with KCl. Corrosion Science, 2007; 49:1799-1815

[14] Y. S. Li, M. Spiegel and S. Shimada. Effect of Al/Si addition on KCl induced corrosion of 9% Cr steel. Materials Letters, 2004; 58:3787-3791

[15] J. Pettersson, J. E. Svensson and L. G. Johansson. KCl-induced corrosion of a 304-type austenitic stainless steel in O 2 and in O 2 + H 2O environment: The influence of temperature. Oxidation of Metals, 2009; 72:159-177

[16] A. Persdotter, J. Eklund, J. Liske and T. Jonsson. Beyond breakaway corrosion – Influence of chromium, nickel and aluminum on corrosion of iron-based alloys at 600 °C. Corrosion Science, 2020; 177:108961

[17] T. Jonsson, J. Froitzheim, J. Pettersson, J. E. Svensson, L. G. Johansson and M. Halvarsson. The influence of KCl on the corrosion of an Austenitic stainless steel (304L) in oxidizing humid conditions at 600°C: A microstructural study. Oxidation of Metals, 2009; 72:213-239

[18] J. Pettersson, H. Asteman, J. E. Svensson and L. G. Johansson. KCl induced corrosion of a 304-type austenitic stainless steel at 600°C; the role of potassium. Oxidation of Metals, 2005; 64:23-41

[19] J. Phother-Simon, I. Hanif, J. Liske and T. Jonsson. The influence of a KCl-rich environment on the corrosion attack of 304 L: 3D FIB/SEM and TEM investigations. Corrosion Science, 2021; 183:109315

[20] M. Zevenhoven-Onderwater, M. Ohman, B. J. Skrifvars, R. Backman, A. Nordin and M. Hupa. Bed agglomeration characteristics of wood-derived fuels in FBC. Energy & Fuels, 2006; 20:818-824

[21] H. B. He, D. Bostrom and M. Ohman. Time Dependence of Bed Particle Layer Formation in Fluidized Quartz Bed Combustion of Wood-Derived Fuels. Energy & Fuels, 2014; 28:3841-3848

[22] R. Faust, K. Fürsatz, P. Aonsamang, M. Sandberg, M. Kuba, N. Skoglund and P. Knutsson. Early layer formation on K-feldspar during fluidized bed combustion with phosphorus-rich fuel. Fuel, 2023; 331:

[23] P. Ninduangdee and V. I. Kuprianov. Combustion of oil palm shells in a fluidized-bed combustor using dolomite as the bed material to prevent bed agglomeration. 2013 International Conference on Alternative Energy in Developing Countries and Emerging Economies (2013 Aedcee), 2014; 52:399-409

[24] H. Leion, A. Lyngfelt, M. Johansson, E. Jerndal and T. Mattisson. The use of ilmenite as an oxygen carrier in chemical-looping combustion. Chemical Engineering Research & Design, 2008; 86:1017-1026

[25] A. Corcoran, P. Knutsson, F. Lind and H. Thunman. Mechanism for Migration and Layer Growth of Biomass Ash on Ilmenite Used for Oxygen Carrier Aided Combustion. Energy & Fuels, 2018; 32:8845-8856

[26] R. Faust, I. Lamarca, A. Schaefer, F. Lind and P. Knutsson. Magnetic properties of ilmenite used for oxygen carrier aided combustion. Fuel, 2023; 340:

[27] F. Lind, A. Corcoran and H. Thunman. Validation of the oxygen buffering ability of bed materials used for OCAC in a large scale CFB boiler. Powder Technology, 2017; 316:462-468

[28] A. Lyngfelt, B. Leckner and T. Mattisson. A fluidized-bed combustion process with inherent CO2 separation; application of chemical-looping combustion. Chemical Engineering Science, 2001; 56:3101-3113

[29] F. Storner, F. Lind and M. Ryden. Oxygen Carrier Aided Combustion in Fluidized Bed Boilers in Sweden-Review and Future Outlook with Respect to Affordable Bed Materials. Applied Sciences-Basel, 2021; 11:

[30] D. Y. Lu, Y. Tan, M. A. Duchesne and D. McCalden. Potassium capture by ilmenite ore as the bed material during fluidized bed conversion. Fuel, 2023; 335:

[31] F. Lind, A. Corcoran, B. Å. Andersson and H. Thunman. 12,000 hours of operation with oxygen-carriers in industrially relevant scale. VGB PowerTech, 2017

[32] P. Kofstad. High Temperature Corrosion. 1988

[33] H. Nielsen, F. Frandsen, K. Dam-Johansen and L. Baxter. The implications of chlorine-associated corrosion on the operation of biomass-fired boilers. Progress in energy and combustion science, 2000; 26:283-298

[34] H. P. Nielsen, F. J. Frandsen and K. Dam-Johansen. Lab-scale investigations of high-temperature corrosion phenomena in straw-fired boilers. Energy & Fuels, 1999; 13:1114-1121

[35] M. Sánchez Pastén and M. Spiegel. High temperature corrosion of metallic materials in simulated waste incineration environments at 300–600° C. Materials and corrosion, 2006; 57:192-195

[36] Y. Shinata. Accelerated oxidation rate of chromium induced by sodium chloride. Oxidation of Metals, 1987; 27:315-332

[37] M. Spiegel. Salt melt induced corrosion of metallic materials in waste incineration plants. Materials and corrosion, 1999; 50:373-393

[38] A. Ruh and M. Spiegel. Thermodynamic and kinetic consideration on the corrosion of Fe, Ni and Cr beneath a molten KCl–ZnCl2 mixture. Corrosion science, 2006; 48:679-695

[39] H. Kinnunen, D. Lindberg, T. Lauren, M. Uusitalo, D. Bankiewicz, S. Enestam and P. Yrjas. High-temperature corrosion due to lead chloride mixtures simulating fireside deposits in boilers firing recycled wood. Fuel processing technology, 2017; 167:306-313

[40] D. Bankiewicz, S. Enestam, P. Yrjas and M. Hupa. Experimental studies of Zn and Pb induced high temperature corrosion of two commercial boiler steels. Fuel processing technology, 2013; 105:89-97

[41] D. Bankiewicz, P. Yrjas, D. Lindberg and M. Hupa. Determination of the corrosivity of Pb-containing salt mixtures. Corrosion science, 2013; 66:225-232

[42] A. Talus, R. Norling, L. Wickstrom and A. Hjornhede. Effect of Lead Content in Used Wood Fuel on Furnace Wall Corrosion of 16Mo3, 304L and Alloy 625. Oxidation of Metals, 2017; 87:813-824

[43] B. J. Skrifvars, R. Backman, M. Hupa, K. Salmenoja and E. Vakkilainen. Corrosion of superheater steel materials under alkali salt deposits - Part 1: The effect of salt deposit composition and temperature. Corrosion science, 2008; 50:1274-1282

[44] Y. Alipour. Furnace Wall Corrosion in a Wood-fired Boiler. KTH Royal Institute of Technology 2015; 2015:52:xx, 73

[45] R. F. A. Pettersson, J. Storesund and M. Nordling. Corrosion of overlay weld cladding in waterwalls of waste fired CFB boiler. Corrosion Engineering, Science and Technology, 2009; 44:218-226

[46] P. Henderson, P. Ljung, P. Kallner and J. Tollin. 2000;

[47] P. Henderson, J. Högberg and M. Mattsson. 2002; II:883-892

[48] C. T. Kang, F. S. Pettit and N. Birks. Mechanisms in the Simultaneous Erosion-Oxidation Attack of Nickel and Cobalt at High-Temperature. Metallurgical Transactions a-Physical Metallurgy and Materials Science, 1987; 18:1785-1803

[49] R. Norling and I. Olefjord. Erosion-corrosion of Fe- and Ni-based alloys at 550 degrees C. Wear, 2003; 254:173-184

[50] A. Nafari. Superheater corrosion in the loop seal of a wood-fired CFB boiler. Chalmers University of Technology 2003; Licenciate of Philosophy:

[51] A. Nafari and A. Nylund. Field study on superheater tubes in the loop seal of a wood fired CFB plant. Materials and Corrosion-Werkstoffe Und Korrosion, 2004; 55:909-920

[52] A. Ekström. Förutsättningar för ökad livslängd av sandlåsöverhettare. Uppsala Universitet 2018; Master:

9 Appendix: LITERATURE Review

In order to reduce the net emission of CO_2, biomass and waste are being used as fuel instead of fossil fuels for power plants and combined heat and power plants (CHPs). This change in fuel is environmentally friendly as biomass and waste, considered as renewable fuels, have a lower net emission of CO_2 compared to fossil fuels.

However, the share of fossil fuels in heat and power production in the world is about 70-75% whereas the share of renewable fuels is minor. In order to increase the share of renewables, on the expense of fossil fuels, the competitiveness of boilers using renewable fuels needs to increase. One of the main reasons why using renewable fuels is more expensive than fossil fuels is the maintenance cost. The combustion of biomass and waste leads to a more corrosive environment for the superheaters and water walls. In particular, superheater tubes placed in the loop seal suffer from extensive material degradation. This results in both, planned and unplanned revision stops and leading to direct costs (replacing tubes, building scaffolding, etc.) as well as loss of revenue.

Thus, in order to increase the share of renewable fuels, it is necessary to enhance the competitiveness of plants using renewable fuels. This can be achieved by three different ways:

- Increase the revenue by enhancing the efficiency of the production.
- Reduce the cost by minimizing the maintenance of the plant.
- Reduce the cost by using cheaper fuels.

Work package 1: Water walls

Introduction

Water walls of boilers using renewable fuels are commonly made from low-alloyed steels with a material temperature reaching up to 400 °C and with a flue gas temperature of 750 - 1000 °C. However, the water walls experience accelerated corrosion due to the presence of corrosive species in the deposit and flue gas. The deposits are often reported to contain molten species, which is expected to accelerate the corrosion attack. The temperatures of the material and the flue gas facilitate the deposit to be fully or partly molten. Furthermore, the melting points of the deposits can also be lowered if there is a specific composition of the deposit so that a eutectic melting point could occur between two (or more) mixed salts. The melting point of some salts resulting in a compound/mixture with a lower melting point than each individual salt is listed in Table 17. The presence of e.g. lead (Pb) and zinc (Zn) compounds are usually pointed out as harmful compounds since their melting points are particular low. The presence of lead and zinc compounds is often detected in recycled waste wood and other waste fuels from industry.

In order to reduce the corrosion attack, overlay weldings or coatings are applied onto the water walls to protect the low alloyed-steels. By using a more corrosion-resistant materials, such as e.g. nickel-based alloys, the overall lifetime of the water wall could be prolonged. However, the use of nickel-based materials leads to high costs since nickel-based materials are expensive and the application of the welding/coating needs to be performed during a revision stop of the boiler. Thus, to increase the overall plant economy of boilers using renewable fuels, it is necessary to explore the possibilities of using cheaper materials (having at least as long lifetime as nickel-based materials) or using materials with longer lifetime (and still manageable costs).

Table 17.Salts and mixture with their respective melting temperature

Salt and mixture	Melting point (°C)
$ZnCl_2$	318
$PbCl_2$	489
KCl	772
NaCl	801
$FeCl_2$	673
KCl-$ZnCl_2$	230
KCl-$PbCl_2$	412
KCl-$FeCl_2$	355
NaCl-$ZnCl_2$	262
NaCl-$PbCl_2$	415
NaCl-$FeCl_2$	375

Corrosion mechanisms

The majority of the corrosion mechanisms regarding water walls in biomass- and waste-fired boilers presented in the literature are connected towards a melted deposit and/or corrosion product [32-39] . Kofstad [32] has suggested several reasons for the corrosiveness of melted/liquid phases. First, the liquid itself provides fast transport of ions. Second, a liquid phase provides an electrolyte that can act as a pathway for ionic charge transfer for an electrochemical attack. Thirdly, the melt can dissolve the protective oxide, which exposes the metal to the environment.

In waste-fired boilers, the presence of zinc and lead compounds has also been suggested to account for severe corrosion by lowering the melting point of the deposits [37] .

Ruh, et al have shown using thermodynamic calculations that $FeCl_2$ is soluble in molten KCl-$ZnCl_2$ near eutectic compositions [38] . In this manner, the outward diffusion of $FeCl_2$ is favored and diffuses easily to the outer part of the salt melt layer. As $FeCl_2$ reaches the outer part of the salt melt, $FeCl_2$ will be oxidized due to the high partial pressure of oxygen. The authors have concluded that the solubility of metal chlorides in molten KCl-$ZnCl_2$ leads to higher diffusion rate and subsequently to higher oxidation rate. Thus, the solubility of metal chlorides in molten salts influences the corrosion. A suggested mechanism for the chloride melt-induced dissolution of the steel can be seen in Figure 63.

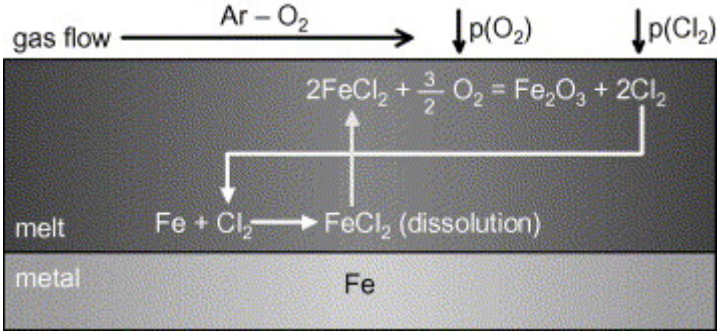

Figure 63. Schematic model of chloride melt induced high temperature corrosion process, showing the transport of gas species and chemical reactions forming iron oxide and iron chloride [38] .

The overall corrosive effect of $ZnCl_2$ and $PbCl_2$ has been studied in several papers [39-42] . The results showed for instance that $PbCl_2$ is more corrosive compared to $ZnCl_2$ [40] . Also, severe corrosion attack could be observed already below the melting point of $PbCl_2$ containing salt mixtures (with KCl or K_2SO_4) on low-alloyed steels such as T22 [39, 41] . Thus, the presence of 100% melted phase is not necessary in order to obtain an accelerated corrosion attack. The terms of sub-T-0 corrosion, indicating corrosion taking place below any melting of the deposit and (2) super-T-0 corrosion, indicating corrosion taking place when the deposit contains melt have been introduced [43] .

In general, the eutectic composition, forming the melt in the deposit, is hard to prove with analytical tools used (primarily SEM/EDX and XRD). The eutectic point

between two salts, of which the phase is 100% in liquid form, is seldom confirmed by the EDX data. This could be due to unavoidable fact that the analysis is always performed post-exposure and at room temperature.

Field exposures

- Furnace Wall Corrosion in a Wood-fired Boiler [44]

The investigation was performed in the Idbäcken power plant of Vattenfall AB in Nyköping, Sweden. The 97.5 MW boiler in which investigations took place is of a BFB type. The steam temperature is 540 °C at 140 bar. The fuel used is 100 % waste wood.

The water walls are made of 16Mo3 which corrodes rapidly when burning waste wood. The cause of the corrosion attack was suggested to be due to chlorides leading to the formation of a continuous but thin layer of iron chloride under a thick iron oxide. Similar corrosion rates were measured from tests lasting 1 000 and 20 000 hours, respectively, indicating a linear corrosion rate. The corrosion mechanism is described as active oxidation by HCl and H_2O where HCl plays a catalytic role in the process rather than Cl_2. The partial pressure of Cl_2 (g) was calculated to be less than 0.1 ppm in this type of boiler environment.

The deposition of KCl and the corrosion rate of 16Mo3 increases with increasing temperature in the furnace walls area of a wood-fired boiler. The corrosion mechanism was found to be similar at low and high temperature. Even at a low metal temperature (285 °C) the corrosion rate of the furnace wall exceeded 0.5 mm per firing season which implied 16Mo3 without a coating is not a suitable material for water walls when burning waste wood. Testing different coating materials showed:

- Nickel-base alloy 625 can reduce the corrosion rate drastically. However, some corrosion attack could still be seen, and the Alloy 625 samples were attacked by a combination of potassium and lead leading to the formation of non-protective potassium lead chromate.
- FeCrAl alloy APMT also showed a very low corrosion rate. APMT samples were mainly attacked by K and Cl. Pb was not found in the corrosion product of APMT.
- Stainless steel 310S showed a moderate corrosion rate and could be a less-expensive alternative to nickel-based alloys. Stainless steel 310S was suggested to be corroded by two mechanisms, a combination of K-Pb and chloride-induced corrosion.

- Corrosion of overlay weld cladding in water walls of waste fired CFB boiler [45]

The investigation was performed in a 75MW CFB boiler in Händelö, Sweden. The steam temperature is 470 °C at 65 bar. During the study the fuel consisted of 50 % household waste and 50 % industrial waste. Test panels were welded on the front wall of the boiler using six different materials:

- Alloy 625
- Alloy 625mod (3 wt-% W)
- Alloy 59
- Alloy 650
- Alloy 22
- Alloy 310

The panels were inspected after 3 827 hours and again after a total of 7 727 hours.

The following statements were made:

- The exposure of overlay welded test water wall panels in a CFB waste fired boiler showed that conditions were extremely corrosive, with metal losses of 0.3 – 1.1 mm measured with an *in-situ* thickness gauge during the 7 727 hours exposure period.
- Extensive pitting occurred on all five of the nickel-based alloys tested. The maximum pit depth measured on specimens removed from the panels was roughly 1 mm. The pit depth was often significantly larger than the metal loss estimated from thickness gauge measurements. This means that there is a danger that the latter underestimates local metal wastage which can lead to premature tube failure
- There was no clear differentiation between the alloying strategies for nickel-based alloys of adding niobium (in alloy 625), tungsten (in alloy 22 and a modified alloy 625 type) or increasing the molybdenum content (in alloy 59). However, alloy 650, which is a cheaper alternative by virtue of its higher iron content of 14% showed a higher corrosion rate and developed the deepest pits.
- The austenitic stainless steel 310 appears to be an attractive alternative to the more expensive nickel-based alloys. This steel exhibited uniform corrosion but no pitting, with the result that metal wastage is predictable and easy to monitor. The uniform metal loss was on a par with the pit depth seen for the nickel-based alloy 650.
- Analysis of the deposits and corrosion products indicated predominant presence of alkali chlorides, also significant amounts of copper, zinc, lead and mercury. The corrosion mechanism was considered to be fluxing or dissolution of the otherwise protective oxide by a complex molten salt.

Work package 2: Fluidized bed heat exchangers

Introduction

In a Circulating Fluidized Bed (CFB) boiler the fuel is combusted in a fluidized sand bed. The sand particles are separated from the produced flue gases in a cyclone and the hot flue gases are subsequently passing superheaters, that are located in the convective pass. However, this position is often rather corrosive and in order to avoid too high corrosion rates the steam temperatures, and thereby also the material temperatures, are kept low. In newer CFB boilers, superheaters have also been mounted in the loop seal, the position of the boiler where the sand is recirculated back into the combustion chamber after been separated from the flue gases in the cyclone. In this position, the heat is transferred to the superheaters from the hot sand, instead of the hot flue gases. By installing a superheater in the loop seal the electrical efficiency of the boiler can be increased. This since higher steam temperatures can be utilized in this, in comparison, mild environment. Also, the heat transfer coefficient between the sand and the superheater tubes is very large resulting in a higher heat transfer per unit area of tube surface compared to the superheaters situated in the convective pass [46, 47] .

The loop seal superheaters are however suffering from material wastages. The supposed mild environment is probably harsher than anticipated due to a combination of corrosive species brought in by contaminated sand particles and erosion. However, little of this problem has been studied in literature.

Corrosion/material degradation mechanisms

The few published works about corrosion in the loop seal points out the erosion corrosion as the main degradation mechanism. This mechanism is especially pronounced at higher temperatures and it is due to the synergism between erosion and corrosion. High temperature erosion-corrosion has been described according to four categories [12, 48]

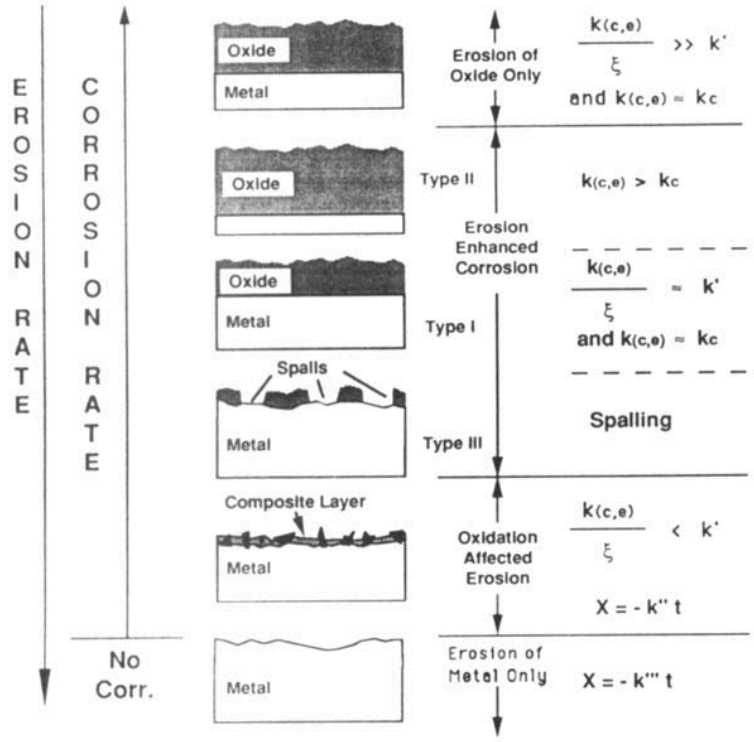

Figure 64. Erosion-corrosion interaction regimes, incorporating three types of erosion enhanced-corrosion behavior [12]

1. *Pure corrosion*. In this regime the effect of erosion is confined to erosion of the oxide layer and is negligible compared with corrosion. The rate of scale thickening can be described by a parabolic relationship (assuming a diffusion-controlled process).
2. *Erosion enhanced-corrosion*. The erosion process does not alter the scale growth mechanism but simply modifies the way in which the scale thickness varies with time and, therefore, influences the variation of the oxidation rate with time. As occurring when erosion thinned the oxide scale such that the oxidation rate increased to balance the erosion rate and a constant steady state scale thickness resulted. Owing to erosive thinning of the scale, the rate of corrosion is increased or enhanced--hence the term erosion-enhanced oxidation. This kind of erosion-corrosion is divided in three types (Figure 64):
    a. Type I occurs if the oxide is eroded to the degree that it is thinner than in the case of pure oxidation. Compare to pure oxidation the material wastage is larger
    b. Type II. The oxide is thicker than in the case of pure oxidation. Formation of cracks in the oxide layer creates short circuit diffusion paths for the reacting species, thereby increasing the corrosion rate [49] . The mechanism is illustrated in Figure 65.
    c. Type III. In the case when the oxide layer has partially spalled due to the thermal and mechanical stresses is no longer protective

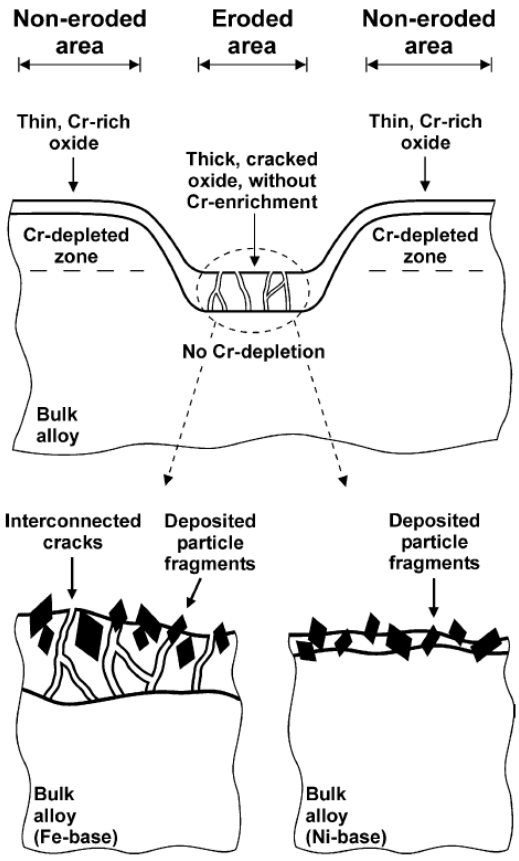

Figure 65. Model illustrating the oxide formation during oxidation and erosion-corrosion at 550°C

3. *Oxidation affected erosion*. It is considered the most serious with a high wastage rate. For this regime, it is no longer meaningful to describe degradation in terms of a corrosion product layer; instead it is necessary to consider the metal or alloy to be covered with a composite layer composed of deformed metal, corrosion products and embedded erodent particles.
4. *Erosion of pure metal*. No oxidation takes place at all. This requires conditions of very high erosion rates or a non-oxidizing surface/atmosphere which are usually not of importance in real applications [50] .

Materials and plants

Very few field tests in the loop seal area have been published. The tests have been performed in two boilers:

1. CFB plant in Nässjö, Sweden. The boiler produces heat and electricity with an efficiency of
   26 MW and 9 MW, respectively. The working temperature in the

combustion chamber is about 850 °C. The plant is fired with wood chips by full or half load depending on the demand and outside temperature. The incoming water vapour at full load is 300 °C and 8 bar in the combustion chamber and 480 °C and 8 bar after the superheaters. The fluidizing sand has a mean particle diameter of 0.25 mm and consists of 91% quartz with no additives. The sintering temperature is about 1225 °C.

The superheater tubes in the tube bundle were welded together from smaller 50 cm long tubes. The tube bundle consists of 4 loops with an incoming steam temperature of 475 °C and an outlet temperature of 538 °C. The corresponding material were measured to be about 510 °C and 550 °C, respectively.
The materials tested were commercially available high temperature austenitic and ferritic steels as well as coatings.
The tested materials were:

- 347H
- AC66
- Esshete 1250
- X10

The results show:

- The corrosion products usually consist in two layers: An outer Fe oxide and an inner mix oxide of Fe and Cr
- The degree of internal corrosion is largest on the alloy with the highest Cr content, AC66
- The corrosion rate is higher on the tubes subjected to a higher temperature
- The oxide growth kinetics in the loop seal environment is non-linear, after initial attack it stabilizes at an approximate constant thickness. [50]

In addition to the solid monotubes presented above, also coatings (primarily thermal sprayed) were tested:

- Alloy 625
- Kanthal 2 (Fe25Cr6Al)
- Stellit 21
- Hastelloy 276
- Metco 8222
- Alloy800
- SS 928L
- Metco12782
- Metco12782+80Ni20Al
- Metco 8443
- 80Ni20Al
- Metcoloy 2
- Metcoloy 2 + 80Ni20Al
- Metco 3006
- Metco 3007

The results show:

- The material degradation on most of the materials tested is very low due to the non-aggressive environmental conditions in the loop seal.
- The oxide growth kinetics is non-linear suggesting pure corrosion and only a minor degree of erosion-corrosion.
- The material wastage increases with increasing steam temperature.
- The corrosion layers on the uncoated steel tubes are composed of one outer iron rich oxide and one internal iron/ chromium oxide.
- Generally, the austenitic steels are subjected to a larger degree of internal and grain boundary corrosion, which is most pronounced in the tube area with the thinnest deposit layers.
- Eight out of 17 tested coating qualities are unaffected by the exposure. These are above all the nickel and high alloyed iron-based coatings.
- Thicker corrosion layers are only developed on the Metcoloy 2, Metcoloy 2 fl 80Ni20Al and Hastelloy 276 coatings.
- Carbide containing coatings are subjected to oxidation and a large degree of delamination. [51]

2. P15 CBF boiler in Händelöverket, Norrköping, Sweden. The thermal capacity is 85 MW supplied by former Sumitomo SHI FW. The boiler produces steam, primarily used for production of electricity, industrial process steam and district heating. The loop seal, which is a feature of the CFB process, offers a location of the final superheater (SH) for two reasons:
   - The heat transfer coefficient in the bubbling bed is 5 to 10 times higher than in the back pass. Hence, the SH area required is reduced by 80 to 90%.
   - The gaseous atmosphere in the loop seal contains less of chlorine and water vapor since the chlorine and water released during the combustion of the RDF is in a gaseous form in the cyclone and therefore follows the flue gas to the back pass. Only the particles separated by the cyclone reach the loop seal.

   The materials used in this boiler were:
   - TP310H (2010-2012)
   - 347H (2012-2014)
   - Base material 316L(N) + overlay welded alloy 59 (2016 -)

A test of the installed material, tube shield and deposit, was performed in 2017-2018 [52] . The results show that the dominant mechanism for material loss in the loop seal superheater is erosion. Overall, all analyses showed low levels of corrosive substances, however, there was a certain corrosion tendency, which indicates that the material loss at the loop seal can also be caused by corrosion-assisted erosion. Erosion is also considerably greater in the cooler loop seal superheater and at its highest on the top rows, which is probably due to a lower sand level around the loop seal superheater two compared to superheater three. In addition, it was seen that at a lower material temperature of the loop seal superheater a higher degree of condensation of the corrosive alkali chlorides NaCl and KCl occurs. This has probably accelerated erosion in the superheater two.

However, the tube shield on the top row is something that proved to be good to minimize the material loss and the erosive load on the tubes.

References

[1] H. Kinnunen, M. Hedman, M. Engblom, D. Lindberg, M. Uusitalo, S. Enestam and P. Yrjas. The influence of flue gas temperature on lead chloride induced high temperature corrosion. Fuel, 2017; 196:241-251
[2] A. Persdotter, M. Sattari, E. Larsson, M. A. O. Ogaz, J. Liske and T. Jonsson. Oxidation of Fe-2.25Cr-1Mo in presence of KCl(s) at 400 degrees C - Crack formation and its influence on oxidation kinetics. Corrosion Science, 2020; 163:
[3] M. A. Olivas-Ogaz, J. Eklund, A. Persdotter, M. Sattari, J. Liske, J. E. Svensson and T. Jonsson. The Influence of Oxide-Scale Microstructure on KCl(s)-Induced Corrosion of Low-Alloyed Steel at 400 degrees C. Oxidation of Metals, 2019; 91:291-310
[4] N. Folkeson, T. Jonsson, M. Halvarsson, L. G. Johansson and J. E. Svensson. The influence of small amounts of KCl(s) on the high temperature corrosion of a Fe-2.25Cr-1Mo steel at 400 and 500°C. Materials and Corrosion, 2011; 62:606-615
[5] H. Kinnunen, M. Hedman, D. Lindberg, S. Enestam and P. Yrjas. Corrosion in Recycled Wood Combustion-Reasons, Consequences, and Solutions. Energy & Fuels, 2019; 33:5859-5866
[6] Y. Alipour and P. Henderson. Corrosion of furnace wall materials in waste-wood fired power plant. Corrosion Engineering Science and Technology, 2015; 50:355-363
[7] J. Eklund, M. D. Paz, B. Jönsson, J. Liske, J. E. Svensson and T. Jonsson. Field exposure of FeCrAl model alloys in a waste-fired boiler at 600°C: The influence of Cr and Si on the corrosion behaviour. Materials and Corrosion, 2019; 70:1476-1485
[8] V. Asokan, J. Eklund, S. Bigdeli and T. Jonsson. The influence of Si on the primary protection of lean FeCrAl model alloys in O2 and O2+H2O at 600 °C—A microstructural investigation. Corrosion Science, 2021; 179:
[9] J. Eklund, I. Hanif, S. Bigdeli and T. Jonsson. High temperature corrosion behavior of FeCrAlSi model alloys in the presence of water vapor and KCl at 600 °C – The influence of Cr content. Corrosion Science, 2022; 198:
[10] T. Sand, A. Edgren, C. Geers, V. Asokan, J. Eklund, T. Helander, J. E. Svensson and L. G. Johansson. Exploring the Effect of Silicon on the High Temperature Corrosion of Lean FeCrAl Alloys in Humid Air. Oxidation of Metals, 2021; 95:221-238
[11] M. D. Paz. Increased steam temperature with Steamboost superheater in grate-fired boilers- Linking deposit formation and high temperature corrosion. Impacts of Fuel Quality on Power Production, Prague 2016
[12] D. M. Rishel, F. S. Pettit and N. Birks. Some Principal Mechanisms in the Simultaneous Erosion and Corrosion Attack of Metals at High-Temperatures. Materials Science and Engineering a-Structural Materials Properties Microstructure and Processing, 1991; 143:197-211
[13] Y. S. Li, Y. Niu and M. Spiegel. High temperature interaction of Al/Si-modified Fe-Cr alloys with KCl. Corrosion Science, 2007; 49:1799-1815
[14] Y. S. Li, M. Spiegel and S. Shimada. Effect of Al/Si addition on KCl induced corrosion of 9% Cr steel. Materials Letters, 2004; 58:3787-3791
[15] J. Pettersson, J. E. Svensson and L. G. Johansson. KCl-induced corrosion of a 304-type austenitic stainless steel in O 2 and in O 2 + H 2O environment: The influence of temperature. Oxidation of Metals, 2009; 72:159-177
[16] A. Persdotter, J. Eklund, J. Liske and T. Jonsson. Beyond breakaway corrosion – Influence of chromium, nickel and aluminum on corrosion of iron-based alloys at 600 °C. Corrosion Science, 2020; 177:108961

[17] T. Jonsson, J. Froitzheim, J. Pettersson, J. E. Svensson, L. G. Johansson and M. Halvarsson. The influence of KCl on the corrosion of an Austenitic stainless steel (304L) in oxidizing humid conditions at 600°C: A microstructural study. Oxidation of Metals, 2009; 72:213-239
[18] J. Pettersson, H. Asteman, J. E. Svensson and L. G. Johansson. KCl induced corrosion of a 304-type austenitic stainless steel at 600°C; the role of potassium. Oxidation of Metals, 2005; 64:23-41
[19] J. Phother-Simon, I. Hanif, J. Liske and T. Jonsson. The influence of a KCl-rich environment on the corrosion attack of 304 L: 3D FIB/SEM and TEM investigations. Corrosion Science, 2021; 183:109315
[20] M. Zevenhoven-Onderwater, M. Ohman, B. J. Skrifvars, R. Backman, A. Nordin and M. Hupa. Bed agglomeration characteristics of wood-derived fuels in FBC. Energy & Fuels, 2006; 20:818-824
[21] H. B. He, D. Bostrom and M. Ohman. Time Dependence of Bed Particle Layer Formation in Fluidized Quartz Bed Combustion of Wood-Derived Fuels. Energy & Fuels, 2014; 28:3841-3848
[22] R. Faust, K. Fürsatz, P. Aonsamang, M. Sandberg, M. Kuba, N. Skoglund and P. Knutsson. Early layer formation on K-feldspar during fluidized bed combustion with phosphorus-rich fuel. Fuel, 2023; 331:
[23] P. Ninduangdee and V. I. Kuprianov. Combustion of oil palm shells in a fluidized-bed combustor using dolomite as the bed material to prevent bed agglomeration. 2013 International Conference on Alternative Energy in Developing Countries and Emerging Economies (2013 Aedcee), 2014; 52:399-409
[24] H. Leion, A. Lyngfelt, M. Johansson, E. Jerndal and T. Mattisson. The use of ilmenite as an oxygen carrier in chemical-looping combustion. Chemical Engineering Research & Design, 2008; 86:1017-1026
[25] A. Corcoran, P. Knutsson, F. Lind and H. Thunman. Mechanism for Migration and Layer Growth of Biomass Ash on Ilmenite Used for Oxygen Carrier Aided Combustion. Energy & Fuels, 2018; 32:8845-8856
[26] R. Faust, I. Lamarca, A. Schaefer, F. Lind and P. Knutsson. Magnetic properties of ilmenite used for oxygen carrier aided combustion. Fuel, 2023; 340:
[27] F. Lind, A. Corcoran and H. Thunman. Validation of the oxygen buffering ability of bed materials used for OCAC in a large scale CFB boiler. Powder Technology, 2017; 316:462-468
[28] A. Lyngfelt, B. Leckner and T. Mattisson. A fluidized-bed combustion process with inherent CO2 separation; application of chemical-looping combustion. Chemical Engineering Science, 2001; 56:3101-3113
[29] F. Storner, F. Lind and M. Ryden. Oxygen Carrier Aided Combustion in Fluidized Bed Boilers in Sweden-Review and Future Outlook with Respect to Affordable Bed Materials. Applied Sciences-Basel, 2021; 11:
[30] D. Y. Lu, Y. Tan, M. A. Duchesne and D. McCalden. Potassium capture by ilmenite ore as the bed material during fluidized bed conversion. Fuel, 2023; 335:
[31] F. Lind, A. Corcoran, B. Å. Andersson and H. Thunman. 12,000 hours of operation with oxygen-carriers in industrially relevant scale. VGB PowerTech, 2017
[32] P. Kofstad. High Temperature Corrosion. 1988
[33] H. Nielsen, F. Frandsen, K. Dam-Johansen and L. Baxter. The implications of chlorine-associated corrosion on the operation of biomass-fired boilers. Progress in energy and combustion science, 2000; 26:283-298
[34] H. P. Nielsen, F. J. Frandsen and K. Dam-Johansen. Lab-scale investigations of high-temperature corrosion phenomena in straw-fired boilers. Energy & Fuels, 1999; 13:1114-1121
[35] M. Sánchez Pastén and M. Spiegel. High temperature corrosion of metallic materials in simulated waste incineration environments at 300–600° C. Materials and corrosion, 2006; 57:192-195
[36] Y. Shinata. Accelerated oxidation rate of chromium induced by sodium chloride. Oxidation of Metals, 1987; 27:315-332

[37] M. Spiegel. Salt melt induced corrosion of metallic materials in waste incineration plants. Materials and corrosion, 1999; 50:373-393
[38] A. Ruh and M. Spiegel. Thermodynamic and kinetic consideration on the corrosion of Fe, Ni and Cr beneath a molten KCl–ZnCl2 mixture. Corrosion science, 2006; 48:679-695
[39] H. Kinnunen, D. Lindberg, T. Lauren, M. Uusitalo, D. Bankiewicz, S. Enestam and P. Yrjas. High-temperature corrosion due to lead chloride mixtures simulating fireside deposits in boilers firing recycled wood. Fuel processing technology, 2017; 167:306-313
[40] D. Bankiewicz, S. Enestam, P. Yrjas and M. Hupa. Experimental studies of Zn and Pb induced high temperature corrosion of two commercial boiler steels. Fuel processing technology, 2013; 105:89-97
[41] D. Bankiewicz, P. Yrjas, D. Lindberg and M. Hupa. Determination of the corrosivity of Pb-containing salt mixtures. Corrosion science, 2013; 66:225-232
[42] A. Talus, R. Norling, L. Wickstrom and A. Hjornhede. Effect of Lead Content in Used Wood Fuel on Furnace Wall Corrosion of 16Mo3, 304L and Alloy 625. Oxidation of Metals, 2017; 87:813-824
[43] B. J. Skrifvars, R. Backman, M. Hupa, K. Salmenoja and E. Vakkilainen. Corrosion of superheater steel materials under alkali salt deposits - Part 1: The effect of salt deposit composition and temperature. Corrosion science, 2008; 50:1274-1282
[44] Y. Alipour. Furnace Wall Corrosion in a Wood-fired Boiler. KTH Royal Institute of Technology 2015; 2015:52:xx, 73
[45] R. F. A. Pettersson, J. Storesund and M. Nordling. Corrosion of overlay weld cladding in waterwalls of waste fired CFB boiler. Corrosion Engineering, Science and Technology, 2009; 44:218-226
[46] P. Henderson, P. Ljung, P. Kallner and J. Tollin. 2000;
[47] P. Henderson, J. Högberg and M. Mattsson. 2002; II:883-892
[48] C. T. Kang, F. S. Pettit and N. Birks. Mechanisms in the Simultaneous Erosion-Oxidation Attack of Nickel and Cobalt at High-Temperature. Metallurgical Transactions a-Physical Metallurgy and Materials Science, 1987; 18:1785-1803
[49] R. Norling and I. Olefjord. Erosion-corrosion of Fe- and Ni-based alloys at 550 degrees C. Wear, 2003; 254:173-184
[50] A. Nafari. Superheater corrosion in the loop seal of a wood-fired CFB boiler. Chalmers University of Technology 2003; Licenciate of Philosophy:
[51] A. Nafari and A. Nylund. Field study on superheater tubes in the loop seal of a wood fired CFB plant. Materials and Corrosion-Werkstoffe Und Korrosion, 2004; 55:909-920
[52] A. Ekström. Förutsättningar för ökad livslängd av sandlåsöverhettare. Uppsala Universitet 2018; Master:

NEW MATERIALS FOR IMPROVED COMPETITIVENESS OF FB PLANTS USING RENEWABLE FUELS

This project addresses two problem areas related to material wastage that today limits availability and fuel flexibility of biomass and waste fired power plants, corrosion/erosion of heat exchangers and water walls. The overall goal of the project is to improve the economy of CHP plants using renewable fuels and thereby increase the competitiveness towards fossil fueled plants by targeting these two problem areas in the (fluidized bed) boilers. The project has successfully conducted several corrosion tests in two commercially operated boilers.

Energiforsk AB | Org.nr 556974-2116 | Telefon: 08-677 25 30 | Fax: 08-677 25 30 | E-post: kontakt@energiforsk.se
Besök: Olof Palmes gata 31, Stockholm. | Post: 101 53 Stockholm | www.energiforsk.se